

This is to certify that the
dissertation entitled

EFFECT OF HEAVY MULTI-AXLE TRUCKS ON FLEXIBLE
PAVEMENT RUTTING

presented by

Hassan Kamal Salama

has been accepted towards fulfillment
of the requirements for the

Ph. D. degree in Civil and Environmental
Engineering



Major Professor's Signature

9/19/2005

Date

PLACE IN RETURN BOX to remove this checkout from your record.
TO AVOID FINES return on or before date due.
MAY BE RECALLED with earlier due date if requested.

DATE DUE	DATE DUE	DATE DUE

**EFFECT OF HEAVY MULTI-AXLE TRUCKS ON FLEXIBLE
PAVEMENT RUTTING**

**By
Hassan Kamal Salama**

A DISSERTATION

**Submitted to
Michigan State University
in partial fulfillment of requirements
for the degree of**

**DOCTOR OF PHILOSOPHY
Department of Civil and Environmental Engineering
2005**

ABSTRACT

Effect of Heavy Multi-Axle Trucks on Flexible Pavement Rutting

By

Hassan Kamal Salama

In this study, heavy axle and truck configurations were investigated to determine their influence on flexible pavement rutting. Several approaches were considered: 1) analysis of State of Michigan, in-service pavement data to investigate the effect of multi-axle trucks on total pavement rutting damage; 2) laboratory simulation of multiple axle and truck configurations to study their effects on asphalt concrete rutting; and 3) mechanistic analysis of rutting damage due to multiple axle and truck configurations using a newly calibrated mechanistic-empirical rutting model.

The analysis of in-service pavement data showed that damage caused by multiple-axle truck configurations is more significant, showing higher β values than single- and tandem-axle truck configurations. This indicates that rutting is most influenced by axle/truck gross weight. In calibrating the VESYS rutting model, time-series, in-service pavement data were used from the SPS-1 experiment. This important methodological improvement over previous studies permits more accurate determination of the permanent deformation parameters (PDP) that lead to better agreement with results from accelerated loading facilities. Analyses of layer rutting contribution of in-service pavement data showed that, on average, the total amount of rutting breaks down as follows: 57% HMA rutting, 27% base rutting, and 16% subgrade rutting. These results

suggest that accounting for subgrade rutting only is no longer valid for designing flexible pavements.

The laboratory investigation indicates that the rutting damage due to different axle configurations is approximately proportional to the number of axles. Calculating truck rutting damage by simply summing the vertical permanent deformation corresponding to its constituent axle groups result in erroneous predictions. Using Miner's rule to determine truck rutting damage from its constituent axles does improve the prediction, although there are still variations among the damage values corresponding to different axle and truck configurations.

The results from mechanistic analyses showed that there is little to no interaction between axles in the vertical strain within the HMA layer. For the vertical strain within the base layer, the interaction between axles increases with increasing HMA layer thickness. On the other hand, there is always high interaction between axles in the subgrade layer (vertical strains). Despite the interaction between axles, the mechanistic analysis in this study confirmed the laboratory findings related to the proportionality of axle and truck factors for the HMA layer. Moreover, it extended this same result to include both the base and subgrade layers.

This dissertation is dedicated to my country

Egypt

ACKNOWLEDGEMENT

Thanks to Allah Almighty for providing me with the opportunity to undertake and complete this task. Special thanks to my advisor Dr. Karim Chatti for his constant guidance and encouragement throughout this research study. Many thanks for the doctoral committee members: Dr. Gilbert Y. Baladi, Dr. Neeraj J. Buch, Dr. Ghassan Abu-Lebdeh, and Dr. Dennis Gilliland.

I would like to extend thanks to the Egyptian Ministry of Higher Education for sponsoring me and my family during this study. Special thanks to the Michigan Department of Transportation, MDOT for funding this research study.

I offer my special thanks to Steven Forbes Tuckey in the Writing Center at Michigan State University for editing this dissertation and his proof-reading. I am grateful to him for the countless hours of constructive discussion and his informative revisions of my work.

I would like to thank my colleagues at Michigan State University, especially Syed Waqar Haider and Hung Suk Lee for their help during this research. Also, many thanks go to the laboratory manager Siavosh Ravanbakhsh and the equipment technologist James C. (JC) Brenton for assisting me during the experimental work.

Last but not the least, many thanks go to my parents who keep praying for me, my wife (Mona Zhran), without whose love, care, encouragement and continuous support I could not complete this work.

TABLE OF CONTENTS

TABLE OF CONTENT.....	vi
LIST OF FIGURES.....	x
LIST OF TABLES.....	xii
CHAPTER 1 – INTRODUCTION	1
1.1 INTRODUCTION	1
1.2 PROBLEM STATEMENT.....	3
1.3 RESEARCH OBJECTIVES	3
1.4 RESEARCH APPROACH	4
1.4.1 Analysis of in service data	4
1.4.2 Laboratory experiment.....	5
1.4.3 Mechanistic analysis	5
1.5 THESIS STRUCTURE.....	7
CHAPTER 2 – LITERATURE REVIEW	8
2.1 INTRODUCTION	8
2.2 ANALYSIS OF IN-SERVICE PAVEMENT DATA	8
2.3 LABORATORY STUDIES.....	10
2.3.1 Fatigue.....	10
2.3.2 Rutting.....	15
2.4 MECHANISTIC ANALYSIS	17
2.4.1 Fatigue.....	17
2.4.2 Rutting.....	19
2.5 SUMMARY	31
2.5.1 Analysis of in-service pavements	31
2.5.2 Laboratory investigations.....	32
2.5.3 Mechanistic analysis	32
CHAPTER 3- ANALYSIS OF FLEXIBLE PAVEMENT RUTTING FROM IN-SERVICE DATA	34

3.1 INTRODUCTION	34
3.2 SITE SELECTION PROCEDURES	34
3.3 PERFORMANCE DATA	36
3.4 TRAFFIC DATA	37
3.4.1 Vehicle Travel Information System, VTRIS	40
3.4.2 Raw Traffic Data.....	41
3.5 ANALYSIS.....	47
3.5.1 Regression Analysis.....	47
3.5.2 Standardized Regression Coefficients	50
3.5.3 Multicollinearity	52
3.5.4 Remedies for the Multicollinearity Problem.....	52
3.6 RESULTS AND DISCUSSION	56

CHAPTER 4 - CALIBRATION OF MECHANISTIC-EMPIRICAL

RUTTING MODEL.....	59
4.1 INTRODUCTION	59
4.2 SPS-1 EXPERIMENT	60
4.2.1 SPS-1 data used in the analysis.....	61
4.3 VESYS MODEL.....	62
4.4 BACKCALCULATION OF PAVEMENT LAYER MODULI.....	63
4.4.1 MICHBACK computer program	63
4.4.2 Quality control of the backcalculation procedures	65
4.4.3 Combination /separation of pavement layers.....	69
4.4.4 Modulus variation in the longitudinal direction.....	72
4.4.5 Summary of the backcalculation procedure.....	72
4.4.6 HMA modulus temperature correction	74
4.5 FORWARD ANALYSIS.....	75
4.6 MESURED RUT DATA FROM IN-SERVICE (SPS-1) PAVEMENTS	77
4.6.1 Filtering the measured rut data	77
4.7 BACKCALCULATION OF PERMANENT DEFORMATION PARAMETERS	78

4.7.1 Backcalculation parameters constraints.....	81
4.7.2 Transverse surface profile.....	82
4.7.3 Transverse surface profile analysis criteria.....	85
4.7.4 Unique solution for backcalculation of permanent deformation parameters...	86
4.7.5 Advantages of using backcalculated parameters	89
4.7.6 Summary statistics for backcalculation of permanent deformation parameters	90
4.7.7 Comparison of obtained α , μ , and rutting percentage with previous work	96
4.8 PREDICTION OF PERMANENT DEFORMATION PARAMETERS.....	98
4.8.1 Available material properties	98
4.8.2 Regression analysis.....	101
4.8.3 HMA layer regression analysis.....	102
4.8.4 Base layer regression analysis	110
4.8.5 Subgrade regression analysis	119
4.9 SUMMARY	126
4.9.1 Conclusion	128
4.9.2 Future research.....	129
CHAPTER 5- LABORATORY INVESTIGATION.....	130
5.1 INTRODUCTION	130
5.2 SAMPLE PREPARATION	131
5.2.1 Samples coring, sawing, and capping.....	134
5.2.2 Air voids before and after coring.....	136
5.3 UNCONFINED UNIAXIAL COMPRESSION STRENGTH TEST.....	137
5.4 UNCONFINED CYCLIC COMPRESSION LOAD TEST	138
5.5 TESTING PROCEDURES.....	140
5.5.1 Typical test results	142
5.6 EXPERIMENTAL TEST RESULTS	145
5.6.1 Effect of interaction level.....	145
5.6.2 Axle Factors	147
5.6.3 Truck factors	149
5.7 PERMANENT DEFORMATION DAMAGE CURVES.....	157

5.7.1 Last peak strain curve	159
5.7.2 Dissipated energy-based curve	161
5.7.3 Strain area-based curve	163
5.7.4 Stress-based curve.....	165
5.8 CALIBRATION OF PERMANENT DEFORMATION DAMAGE MODELS..	166
5.8.1 Peak method.....	166
5.8.2 Peak-midway method.....	168
5.8.3 Integration method	169
5.8.4 Strain rate method	171
5.9 PREDICTION OF PERMANENT STRAIN.....	174
5.10 CONCLUSION.....	178
5.11 FUTURE RESEARCH	179
CHAPTER 6 – MECHANISTIC ANALYSIS.....	180
6.1 INTRODUCTION	180
6.2 FORWARD ANALYSIS.....	181
6.3 RELATIVE COMPARISON OF RUTTING DAMAGE CAUSED BY MULTIPLE AXLES.....	184
6.3.1 Calibrated mechanistic-empirical rutting model.....	184
6.4 RESULTS AND DISCUSSIONS.....	186
6.4.1 Rutting prediction using the new mechanistic-empirical design guide	192
CHAPTER 7 – CONCLUSIONS AND RECOMMENDATIONS.....	195
7.1 CONCLUSIONS.....	195
7.2 RECOMMENDATIONS FOR FUTURE RESEARCH.....	198
APPENDIX.....	200
REFERENCES.....	209

LIST OF TABLES

Table 1-1 Michigan truck configurations	2
Table 2-1 Comparison of applicable test methods for flexible pavement fatigue (Mathews et. al., 1993)	14
Table 2-2 Candidate test methods and responses for the SPT (Witczak <i>et al.</i> , 2002)	16
Table 2-3 Permanent deformation parameters	22
Table 2-4 Field calibration factors for the new mechanistic-empirical design guide.....	23
Table 2-5 Percent layer distribution of rutting (Ullidtz, 1987).....	24
Table 2- 6 Limitations of the existing flexible pavement rutting models.....	25
Table 2-7 Variables affecting the permanent deformation parameters.....	28
Table 2-8 Independent variables included in different models (Simpson <i>et. al.</i> , 1995) ...	30
Table 3-1 Descriptive statistics of rut depth and pavement age	39
Table 3-2 Axle/Truck Count and Weight for Station Number 26183049 East Direction (Michigan Road, M-61)	45
Table 3-3 Proportions and Average Weights for FHWA Truck Classes.....	46
Table 3-4 Number of weigh stations and projects	47
Table3-5 Regression coefficients and collinearity statistics for all truck classes.....	53
Table 3-6 Regression coefficients and collinearity statistics for all truck classes excluding truck class 9.....	54
Table 3-7 Total variance explained by each component	54
Table 3-8 Component matrix	55
Table 3-9 Effect of different truck/axle configurations on pavement rutting.....	58
Table 4-1 Descriptive statistics for SPS-1 experiment (LTPP database release 18)	61
Table 4-2 Descriptive statistics for final backcalculation procedures (109 sections).....	74
Table 4-3 Backcalculation of PDPs using different seed values for section 1-0105	83
Table 4- 4 Number of point locations with corresponding failed layer-section 1-0105 ...	88
Table 4-5 descriptive statistics of PDPs and rutting percentage.....	92
Table 4-6 Climatic variables considered.....	100
Table 4-7 ANOVA for α_{HMA} and μ_{HMA}	104
Table 4- 8 Model Summary for α_{HMA} and μ_{HMA}	104

Table 4-9 Model coefficients for α_{HMA} and μ_{HMA}	105
Table 4-10 Descriptive statistics of α_{HMA} , μ_{HMA} , and their independent variables	110
Table 4-11 ANOVA for α_{base} and μ_{base}	113
Table 4-12 Model summary for α_{base} and μ_{base}	113
Table 4-13 Model coefficients for α_{base} and μ_{base}	114
Table 4-14 Descriptive statistics of α_{base} , μ_{base} , and their independent variables	117
Table 4-15 ANOVA for α_{SG} and μ_{SG}	120
Table 4-16 Model summary for α_{SG} and μ_{SG}	120
Table 4-17 Model Coefficients for α_{SG} and μ_{SG}	121
Table 4-18 Descriptive statistics of α_{SG} , μ_{SG} , and the independent variables	124
Table 5-1 Aggregate gradation of the mix	131
Table 5-2 Volumetric properties of the asphalt mix	131
Table 5-3 Gyratory compactor setup	132
Table 5-4 experimental test factorial for axle configurations	139
Table 5-5 experimental test factorial for axle configurations	140
Table 5-6 Possible combinations of the truck damage from its constituent axles	155
Table 5-7 Experimental test results	158
Table 6-1 Pavement cross-sections and moduli	181
Table 6-2 Calculated permanent deformation parameters	185

LIST OF FIGURES

Figure 1-1 Flow diagram of research plan	6
Figure 2-1 Transverse strain versus time for different truck configurations	12
Figure 2-2 Fatigue curve for multi-axle configurations (El Mohtar, 2003).....	13
Figure 2-3 Axle factors per tonnage for different interaction levels (El Mohtar, 2003) ..	13
Figure 2-4 Transverse surface profile for various rut mechanism (Simpson <i>et al.</i> , 1995)	27
Figure 3-1 Variation of the traffic along CS # 18024.....	35
Figure 3-2 No variation of the traffic along two consecutive control sections (CS # 22023 and 55021)	36
Figure 3-3 Rutting versus Time.....	37
Figure 3-4 FHWA vehicle class definitions.....	42
Figure 3-5 Comparison between 2001 and 2002 total average daily truck traffic.....	43
Figure 3-6 Axle/truck configurations extracted from raw data	44
Figure 3-7 Weight and percentage of FHWA truck classes	44
Figure 3-8 Normality plot.....	48
Figure 3-9 Predicted versus residual plot.....	49
Figure 3-10 Cook's distance	49
Figure 3-11 Ridge trace	56
Figure 4-1 Location of the SPS-1 sites	61
Figure 4-2 Flow chart of calibration of mechanistic-empirical rutting model (VESYS) using SPS-1 experiment.....	64
Figure 4-3 Distribution of RMS (%) for all point locations within SPS-1 experiment ...	66
Figure 4- 4 Equivalent pavement modulus versus the distance from the center of the load at different point locations within the section.....	68
Figure 4-5 Pavement layer thicknesses for conventional pavement.....	70
Figure 4-6 pavement layer thicknesses for full depth asphalt.....	71
Figure 4-7 Modulus variations for the pavement layers along the longitudinal direction	73
Figure 4-8 Division of the subgrade layer into several sub-layers	76
Figure 4-9 Strain at the middle of pavement layers for 5 different SPS-1 sections.....	76
Figure 4-10 Rutting with time for SPS-1 pavements - All sections	77
Figure 4-11 Measured time series rutting data for section 1-0105	79

Figure 4-12 Transverse surface profile for HMA layer rutting— Section 31-0113	84
Figure 4-13 Transverse surface profile for base rutting—Section 20-0102	84
Figure 4-14 Transverse surface profile for subgrade rutting—Section 32-0110	85
Figure 4-15 Definition of positive and negative area in transverse surface profile.....	86
Figure 4-16 Definition of maximum rut depth (White, et al., 2002)	86
Figure 4-17 Transverse profile section 1-0105	89
Figure 4-18 measured versus predicted rut depth for sections used in the backcalculated PDPs.....	89
Figure 4-19 time series rutting data for three layers system.....	91
Figure 4-20 α -value histograms	93
Figure 4-21 μ -value histograms	94
Figure 4-22 Rutting percentage histograms	95
Figure 4-23 Comparison of permanent deformation parameters	97
Figure 4-24 Comparison of rutting contribution of pavement layer.....	98
Figure 4-25 Ranking the importance of the independent variables for α_{HMA} and μ_{HMA} .	106
Figure 4-26 Relationship of α_{HMA} versus strain at the middle of the HMA, % passing sieve number 10, VFA% and Max AT	107
Figure 4-27 Relationship of μ_{HMA} versus α_{HMA} and FI	108
Figure 4-28 Actual versus predicted α and μ for HMA layer	109
Figure 4-29 Sieve analysis of HMA layer	111
Figure 4-30 Sieve analysis of base layer.....	111
Figure 4-31 Relationship between α_{base} and base modulus, base thickness, % passing sieve number 200, and GI	115
Figure 4-32 Relationship between μ_{base} and α_{base} , base thickness, and base strain	116
Figure 4-33 Ranking the importance of the independent variables for α_{base} and μ_{base} ...	117
Figure 4-34 Actual versus predicted α and μ for base layer.....	118
Figure 4-35 Sieve analysis of subgrade layer	119
Figure 4-36 Relationship between α_{SG} and strain at the middle of the top 40 inches of SG, GI, PI, and D32	123
Figure 4-37 Relationship between α_{SG} and FI and wet days	124

Figure 4-38 Relationship between μ_{SG} and modulus, strain at the middle of the top 40 inches of SG, GI, and PI	125
Figure 4-39 Ranking the importance of the independent variables for α_{base} and μ_{base} ...	126
Figure 4-40 Actual versus predicted α and μ for subgrade layer	127
Figure 4-41 Measured, calculated, and predicted total rut depth for section 50113.....	128
Figure 5-1 Compacted test specimen (6-inch diameter, 7-inch height).....	133
Figure 5-2 Coring of test specimens	135
Figure 5-3 Sawing operation.....	135
Figure 5-4 Cored sample.....	136
Figure 5-5 Air voids before and after coring	137
Figure 5-6 Stress versus strain for unconfined compression strength tests at 100°F.....	138
Figure 5-7 Loading and unloading time for axle and truck configurations	141
Figure 5-8 Unconfined cyclic compression load test set up	142
Figure 5-9 Typical experimental results from uniaxial cyclic compression load tests (single axle-sample number 10).....	144
Figure 5-10 Distribution of wheel load (Deen, <i>et al.</i> , 1980).....	145
Figure 5-11 Interaction levels for the quad axle configuration.....	146
Figure 5-12 Effect of the interaction level of different axle configuration on pavement rutting.....	146
Figure 5-13 Axle factors for different axle configurations and interaction levels.....	148
Figure 5-14 Rut damage per axle for two replications of each axle configuration/interaction level pair.....	149
Figure 5-15 Truck factor vs. total number of axles within truck	150
Figure 5-16 Relationship between total number of truck axles, maximum axle group, and truck factor (two replications each)	151
Figure 5-17 Prediction of the truck rutting damage from its constituent axle configurations	152
Figure 5-18 Damage distribution for different truck configurations	156
Figure 5-19 Average and standard deviation of the rutting damage for different truck configurations	157
Figure 5-20 Examples of the last peak of the initial strain pulse.....	160

Figure 5-21 Last peak strain rutting curve.....	161
Figure 5-22 Example of Dissipated energy versus number of load repetitions for one sample (two LVDT).....	162
Figure 5-23 Dissipated energy-based rutting damage curve.....	163
Figure 5-24 Strain area-based rutting damage curve	164
Figure 5-25 Stress level versus number of cycles to failure (S-N curve) for single and tridem axles.....	165
Figure 5-26 Peak and peak midway strain for 4-axle group.....	167
Figure 5-27 Axle factor from calibrated peak method versus laboratory axle factor	168
Figure 5-28 Axle factor from calibrated peak-midway method versus laboratory axle factor values	169
Figure 5-29 Axle factor from the integration method versus laboratory axle factor values	171
Figure 5-30 Depiction of variables from strain rate method.....	172
Figure 5-31 Axle factor from strain rate method versus laboratory axle factor values ..	173
Figure 5-32 Summary of the developed and calibrated rutting damage methods	174
Figure 5-33 Example of normalized cumulative strain with the initial last peak strain versus number of cycles.....	177
Figure 5-34 Values of μ and α for all tested axle and truck configurations	178
Figure 6-1 Vertical compression strain at the middle of each pavement layer due to an 8- axle group on thick pavement (profile 1).....	182
Figure 6-2 Vertical compression strain at the middle of each pavement layer due to an 8- axle group on thin pavement (profile 2)	183
Figure 6-3 Strain values underneath and outside the axle group	186
Figure 6-4 Rut depth for pavement layers and their axle factors at one million repetitions – procedure 1.....	188
Figure 6-5 Rut depth for pavement layers and their truck factors at one million repetitions – procedure 1.....	189
Figure 6-6 Rut depth for pavement layers and their axle factors at one million repetitions – procedure 2.....	190

Figure 6-7 Rut depth for pavement layers and their truck factors at one million repetitions – procedure 2.....	191
Figure 6-8 Rut depth for single and tandem axles and tandem axle factor using new ME guide.....	194

CHAPTER 1 – INTRODUCTION










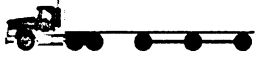


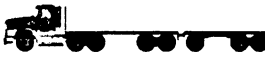



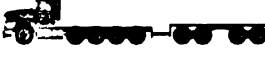



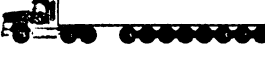
1.1 INTRODUCTION

Truck traffic is a major factor in pavement design because truck loads are the primary cause of pavement distresses. Different truck types with varying axle configurations may contribute differently to pavement distresses. The American Association of State Highway Transportation Officials (AASHTO) pavement design guide converts different axle load configurations into a standard axle load (where one Equivalent Single Axle Load, or ESAL, is 18 kips) using the Load Equivalency Factor (LEF) concept. These LEFs are based on decreases in the Pavement Serviceability Index (PSI), and were developed for a limited number of pavement cross-sections, load magnitudes, load repetitions, and for a single subgrade and climate. The PSI is based on the limited “functional” performance of the road surface, and accounts only to a low degree for other key performance measures such as fatigue and rutting for flexible pavements.

Moreover, the AASHTO procedure for pavement design only accounts for single and tandem axle types based on AASHO road test results, and uses extrapolation to estimate the damage due to tridem axles. Truck axle configurations and truck weights have significantly changed since the AASHO road study was conducted in 1962. There remain concerns about the effect of newer axle configurations on pavement damage, which still are unaccounted for in the AASHTO procedure. Several researchers have investigated the pavement damage resulting from different axle and truck configurations, yet these researches were limited only to single, tandem, and tridem axles. The state of Michigan is unique in permitting several heavy truck axle configurations that are

composed of up to 11 axles, sometimes with as many as 8 axles within one axle group, as shown in Table 1-1. Thus, there is a need to identify the relative pavement damage resulting from these multiple axle trucks, which are unaccounted for in current pavement design. This thesis is concerned with only rutting as a pavement distress.

Table 1-1 Michigan truck configurations

1		2	
3		4	
5		6	
7		8	
9		10	
11		12	
13		14	
15		16	
17		18	
19		20	
21			

1.2 PROBLEM STATEMENT

The state of Michigan hosts several trucks that have unusual axle configurations, up to eleven axles and 164 kips in gross weight and 8 axles within an axle group. The relationship between these trucks and flexible pavement rutting has not been determined, since previous research did not address the damage caused by multiple axle/truck configurations. Therefore, there is a need to examine the relative effect of these heavy vehicles on pavement rutting using field data from in-service pavements, laboratory experimentation, and mechanistic analyses.

The Michigan Department of Transportation (MDOT) has very comprehensive pavement surface distress data files. MDOT also has been collecting rutting data, as well as traffic count and weight data, along its road network. The traffic and weight data collection was recently upgraded by using new weigh-in-motion (WIM) technology. This will allow for a more accurate representation of the distribution of truck axle weights and configurations along MDOT's trunk-lines. In addition to in-service data, simulating the effect of these Michigan multiple axle trucks using mechanistic analysis and in the laboratory will farther explain their relative effect on rutting damage. The conclusions and recommendations of this research can be accomplished by combining the findings using in-service data with those from mechanistic analysis and the laboratory experiment.

1.3 RESEARCH OBJECTIVES

The overall objective of this research study is to investigate the relative effects of different axle/truck configurations on flexible pavement rutting. Several axle

configurations including single, tandem, tridem, quad, 5-axles, 7-axles, and 8-axles as well as twenty different truck configurations are considered in this study, as shown in Table 1-1. This research will also address the following items:

- Developing a Load Equivalency Factor (LEF), and Axle and Truck Factor (AF, TF) for rutting using laboratory data.
- Calibrating a mechanistic-empirical rutting model (VESYS) for flexible pavements using field data from the SPS-1 experiment.
- Developing regression equations to predict permanent deformation parameters based on pavement cross-section, material properties, and climatic condition.
- Comparison the finding from the statistical analysis of in –service data, laboratory test results, and mechanistic analysis.

1.4 RESEARCH APPROACH

The research problem was approached from three different angles 1) field investigation, 2) laboratory experimentation, and 3) mechanistic analysis. Figure 1-1 shows the Flow diagram of research plan for the three different research approaches. A brief description of each approach follows:

1.4.1 Analysis of in service data

The field investigation relates different axle/truck configurations that are common in the state of Michigan (Table 1-1) to rutting. Several regression analyses were performed to examine the relative effect of these axle/truck configurations on flexible pavement rutting.

1.4.2 Laboratory experiment

The unconfined compression cyclic load test with loading cycle that simulate different axle/truck configurations was used to examine their relative effect on permanent deformation of an asphalt mixture. The specimens were prepared according the new procedure from the simple performance test for permanent deformation. Five different axle configurations and five different truck configurations were studied.

1.4.3 Mechanistic analysis

In this analysis, the KENPAVE computer program was used to calculate the vertical compression strain at the middle of each pavement layer caused by various axle and truck configurations for different pavement cross-sections. The mechanistic-empirical rutting model (VESYS), calibrated using field data from SPS-1 experiment, was used to predict the rutting in the various layers within the pavement structure.

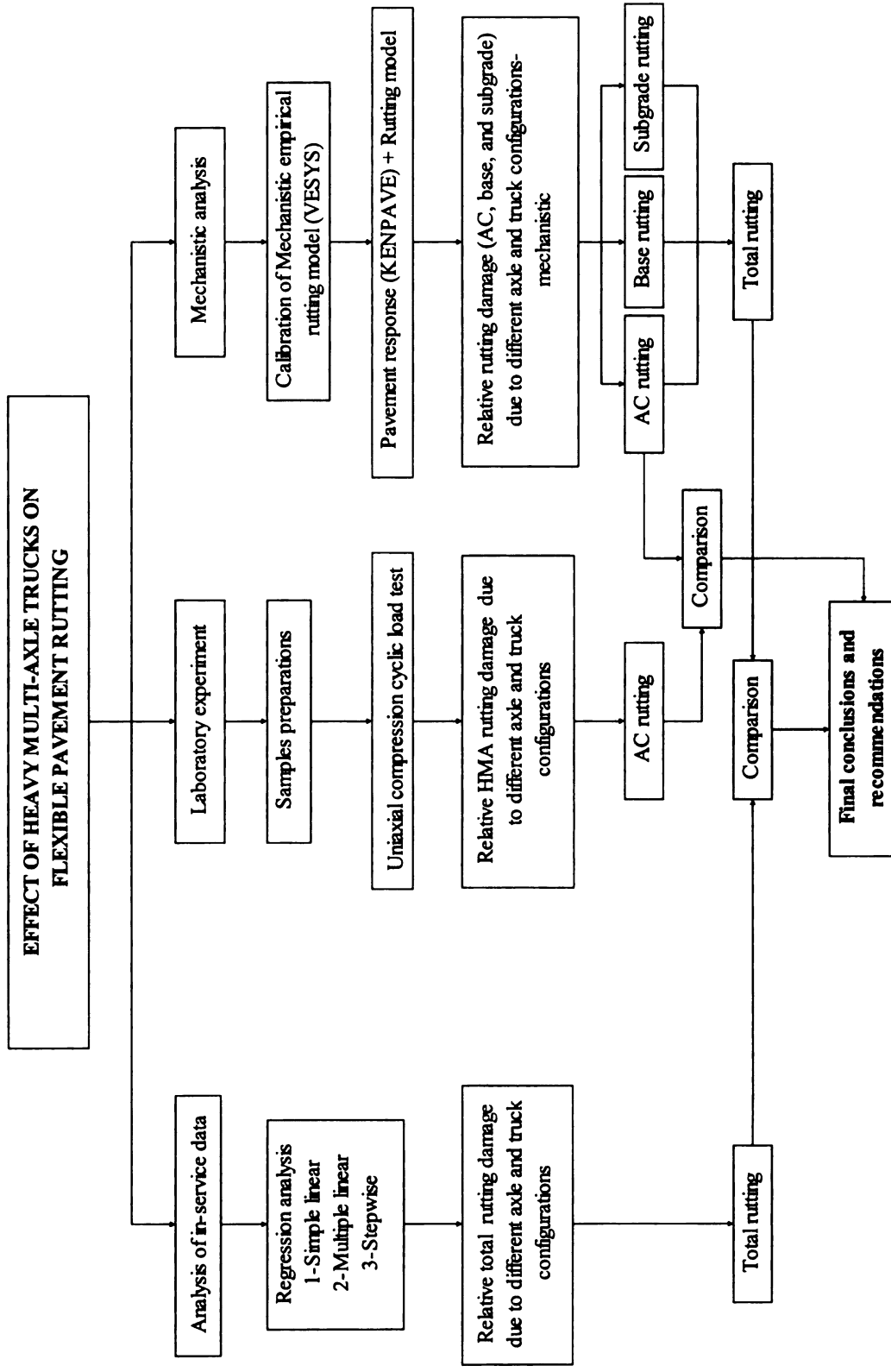


Figure 1-1 Flow diagram of research plan

1.5 THESIS STRUCTURE

This thesis is divided into seven chapters including this introductory chapter. Chapter 2 highlights the most relevant literature related to this research. Chapter 3 details the field investigation of truck traffic and flexible pavement rutting. In this chapter, several regression analyses are performed to examine the relative effect of different axle/truck configurations on the total pavement rutting. Due to the lack of information on permanent deformation parameters in the literature, chapter 4 addresses the calibration of a mechanistic empirical rutting model. Chapter 5 outlines the laboratory experiment designed to study the relative effect of different axle/truck configurations on permanent deformation of an asphalt mixture. This chapter describes the sample preparation as well as the results of unconfined compression cyclic load tests due to different axle/truck configurations. Chapter 6 employs the calibrated rutting model along with the laboratory results to facilitate the mechanistic analysis of the effect of different axle/truck configurations on pavement rutting. Chapter 7 provides the conclusions and recommendations for future research.

CHAPTER 2 – LITERATURE REVIEW

2.1 INTRODUCTION

Several factors such as traffic, environment, material and design considerations affect pavement damage over time. Traffic loads play a key role in pavement deterioration. This deterioration can take several forms of distress in flexible pavements, such as fatigue (alligator cracking), and rutting. In the past, a small number of researchers investigated the effect of some truck configurations on pavement damage empirically (using field and laboratory data) and mechanistically (using theoretical models) (Ilves and Majidzadeh 1991, Saraf and Ilves 1995, Witczak *et al.* 2002, Gillespie *et al.* 1993, and Hajek and Agarwal 1990). The majority of these previous works used one approach to investigate a single type of damage caused by a limited number of axle/truck configurations. This chapter establishes the connection between the three different approaches and emphasizes the need for a more inclusive study of multiple damage forms caused by several axle/truck configurations.

2.2 ANALYSIS OF IN-SERVICE PAVEMENT DATA

Analysis of in-service pavements is crucial since it represents the actual behavior of the pavement, while laboratory and mechanistic investigations are simulations of the real world. There were minimal field investigations related to the relative effect of multi-axle trucks on pavement rutting. Chatti *et al.*, 2004 used field data from the General Pavement Study (GPS-1) in the Long Term Pavement Performance (LTTP) program to investigate the relative damage (fatigue and rutting) to asphalt pavements by various axle and truck

configurations. There were no conclusive results from the analysis about the effect of axle/truck configurations on fatigue and rutting damage.

In examining their special overload permits, the Ohio Department of Transportation (ODOT) recognized that trucks traveling from Michigan to northern Ohio cities were substantially heavier than those in Ohio (Ilves and Majidzadeh, 1991, Saraf and Ilves, 1995). Therefore, a field study was conducted to investigate the effect of Michigan heavy vehicle weights on pavement performance. The following field data were collected for this study: traffic, rutting, faulting, cracking, roughness, and deflection measurements. Regression analysis of rutting data produced the following equation:

$$RUTF = 0.035 + 0.984 (C13) + 0.03(B + C) + 0.0007 (\text{months}) \quad (2-1)$$

where RUTF is rutting (in inches) in flexible pavement,

C13 is the number of FHWA class 13 vehicles in the lane per day in thousands,

B is the total number of trucks in FHWA classes 8-12 in thousands,

C is the total number of trucks in FHWA classes 4-7 in thousands,

months is the number of months of testing with January 1986 as month =1.

They concluded that heavy axle loads affected rutting of flexible and composite pavements; however, the field traffic and performance data used in the study were from only four roads linking Ohio and Michigan. In addition, the analysis did not compare the relative damage resulting from various axle/truck configurations.

2.3 LABORATORY STUDIES

2.3.1 Fatigue

Several methodologies exist to measure the fatigue life of flexible pavements such as the repeated flexural test, direct tension test, diametral repeated load test (Indirect Tensile Cyclic Load Test, ITCLT), dissipated energy method, fracture mechanics test, repeated tension or tension and compression test, triaxial repeated tension and compression test, and wheel track test (Rao *et al.*, 1990 and Matthews *et al.*, 1993). Matthews *et al.*, 1993 ranked these methods, incorporating the advantages, disadvantages and limitations, as shown in Table 2-1. They also listed the laboratory fatigue tests (simple fracture, support fracture, direct axial, diametral, triaxial, fracture tests, and wheel tracking tests) and the basic concept of each test. Some of these tests were stresses-controlled while others were strain-controlled. However, all of these tests have been performed using either a single pulse with rest period or a continuous sinusoidal load. When a vehicle travels over the pavement, a given point in the pavement is subjected to multiple pulses depending on the trucks and their axle configurations as shown in Figure 2-1. To determine the fatigue life under multiple axle loads, Miner's hypothesis is commonly applied to accumulate the damage resulting from the different axles within an axle group. This relation is given by (Miner, 1945).

$$\frac{n_1}{N_{1f}} + \frac{n_2}{N_{2f}} + \frac{n_3}{N_{3f}} + \dots + \frac{n_i}{N_{if}} + \dots + \frac{n_m}{N_{mf}} \leq 1 \quad (2-2)$$

where “i” is the i^{th} level of applied strain/stress at the point under consideration. “ n_i ” is the actual number of applications at strain level “i” that is anticipated, and “ N_{if} ” is

the number of applications at strain level “i” expected to cause fatigue failure if applied separately.

Hence, the actual fatigue life of flexible pavements resulting from multiple axle/truck loads has not been considered directly. Recently, Chatti and El Mohtar, 2004 studied the fatigue life of an asphalt mixture in the laboratory under different truck axle configurations (single to 8-axles) using the ITCLT by applying load pulses that are equivalent to the passage of an entire axle group or truck. A unique fatigue curve relating the number of repetitions to cause failure in the laboratory, and the initial dissipated energy for various axle configurations was found (see figure 2-2). The results indicated that multiple-axle groups were less damaging in fatigue per tonnage carried as compared to single axles (see Figure 2-3). The increased number of axles carrying the same load resulted in less damage due to the decreased, evenly distributed weight at any given point on the pavement. This decrease in damage was found to be more significant between single, tandem and tridem axles, while it starts to level off at higher axle numbers, as shown in Figure 2-3. Similar results were obtained for trucks with larger axle groups, which had lower truck factors per tonnage than those with single and tandem axles.

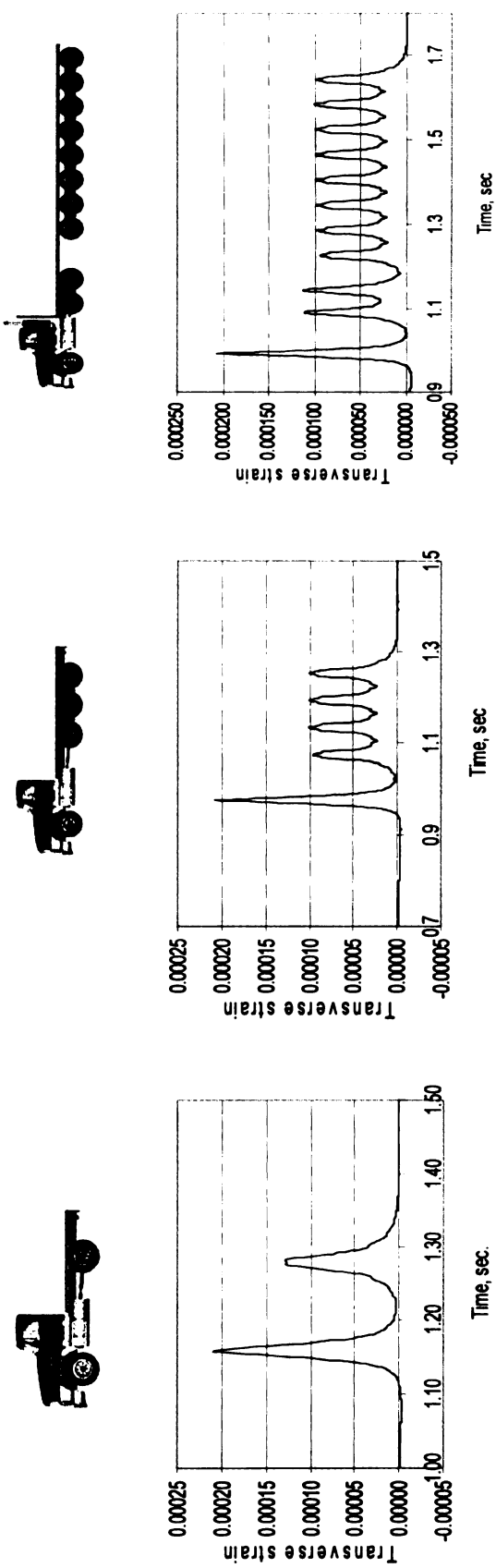


Figure 2-1 Transverse strain versus time for different truck configurations

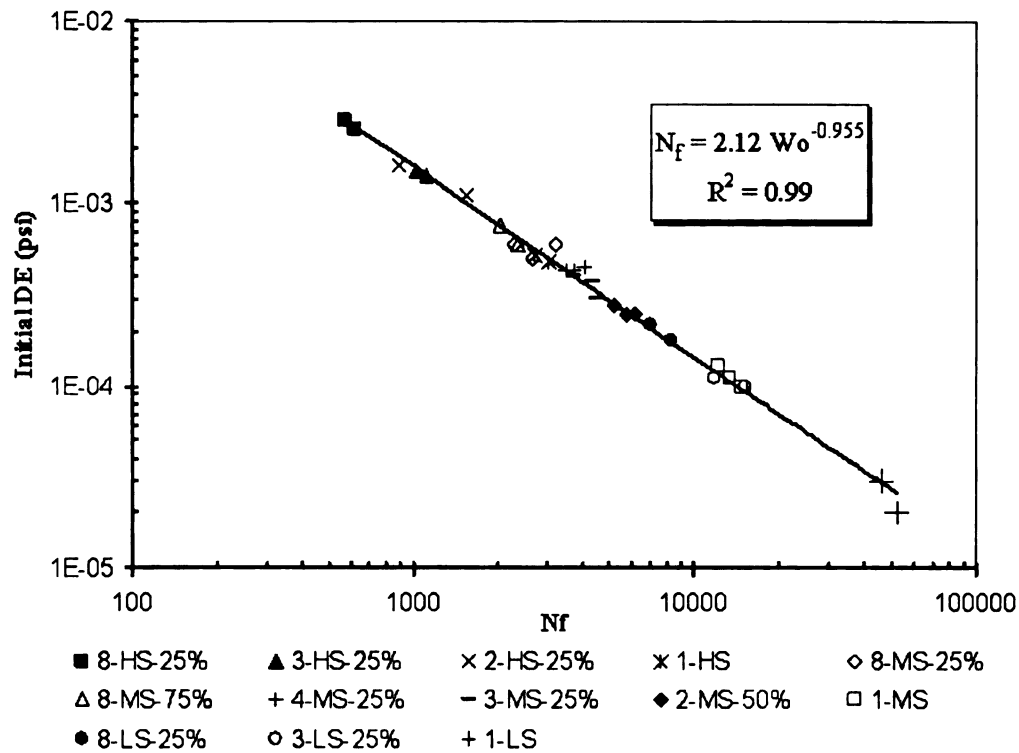


Figure 2-2 Fatigue curve for multi-axle configurations (El Mohtar, 2003)

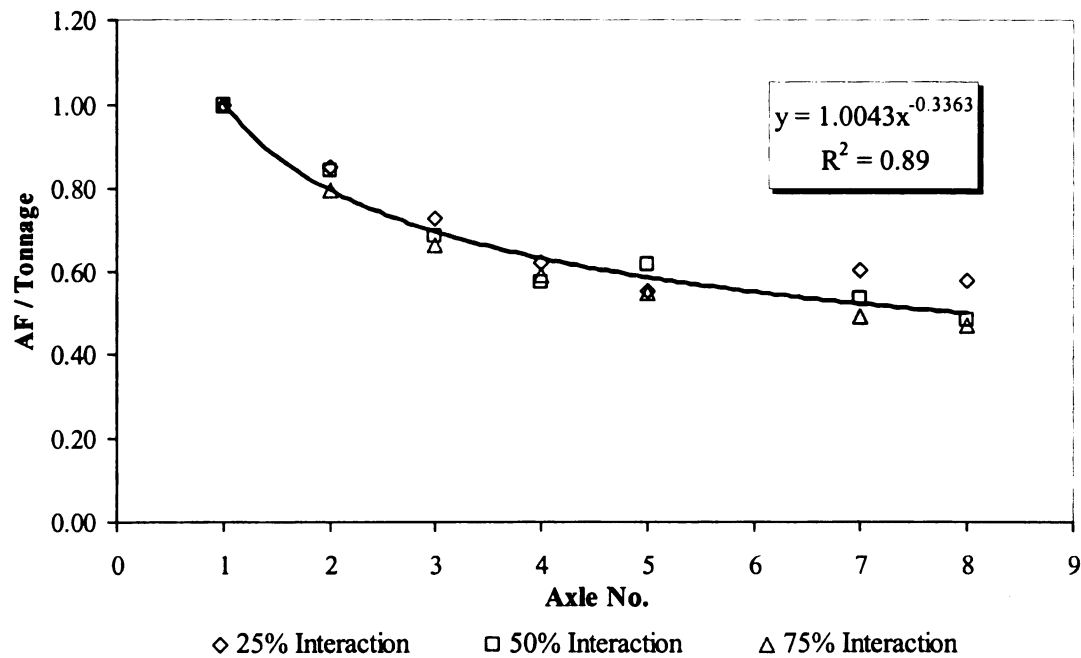


Figure 2-3 Axle factors per tonnage for different interaction levels (El Mohtar, 2003)

Table 2-1 Comparison of applicable test methods for flexible pavement fatigue (Mathews et. al., 1993)

Method	Test Response	Advantages	Disadvantages and limitations	1	2	3
Repeated flexure test	σ_b or ϵ_b , S_{mix}	Well known and widespread in usage Basic technique can be used for different concepts Results can be used directly in design Options of controlled stress or strain	Costly, time consuming, specialized equipment needed	4	4	I
Direct tension test	(Through Correlation) σ_b or ϵ_b , S_{mix}	Eliminates need for conducting additional fatigue tests Direct correlation with existing fatigue test results	In the LCPC methodology: The correlation is based on one million repetitions; at a temperature of 10°C use of EQI (thickness of bituminous layer) for one million repetitions only	9	1	I
Diametral repeated load test	$4\sigma_b$ and S_{mix}	Simple in nature Same equipment can be used for other tests Allows the prediction of cracking	Biaxial stress state Underestimates fatigue life	6	2	II
Dissipated energy method	ϕ , ψ , S_{mix} and σ_b or ϵ_b	Based on physical phenomenon Unique relation between dissipated energy and N	Accurate prediction requires extensive fatigue test data Simplified procedures provide only a general indication of the magnitude of the fatigue life	5	5	III
Fracture mechanics test	K_{I1} , S_{mix} curve ($a/h-N$); calibration function (also k_{I1})	Strong theory for low temperature In principle eliminates the need for conducting fatigue tests	At high temperatures, K_{I1} is not a material constant Large amount of experiment data needed K11 (shear mode) data needed. Link between K1 and K11 to predict fatigue life remains to be established Accounts for only stable crack propagation	7	8	IV
Repeated tension or tension and compression	σ_b or ϵ_b , S_{mix}	Need for flexure test eliminated	Compared to direct tension test, this is time consuming, costly, and special equipment required	8	3	-
Triaxial repeated tension and compression test	σ_b or σ_c , S_{mix}	Relatively better simulation of field conditions	Costly, time consuming and special equipment needed Imposition of shear strains required	2	6	-
Repeated flexure test on elastic foundation	σ_b or ϵ_b , S_{mix}	Better simulation of field conditions Tests can be conducted at higher temperatures since specimens are fully supported	Costly, time consuming and special equipment needed	3	7	-
Wheel tract test (lab)	σ_b or ϵ_b	Good simulation of field conditions	For low S_{max} fatigue is affected by rutting due to lack of lateral wandering effects Special equipment required	1	9	-
Wheel track test (field)	σ_b or ϵ_b	Direct determination of fatigue response under actual wheel loads	Extensive, time consuming Relatively few materials can be evaluated at one time Special equipment required	1	10	-

Simulation of field conditions Simplicity Overall ranking

2.3.2 Rutting

Similar to pavement fatigue, several trials have been made to predict pavement rutting based on laboratory experiments (Leahy, 1989, Ayres, 2002, and Kaloush and Witczak, 2000); however all of these trials were based on single load pulse. In reality, the pavement is subjected to multiple load pulses due to the passage of large axle groups as shown before in Figure 2-1. The permanent deformation parameters can be predicted from laboratory experimental data. Qi and Witczak, 1998 used the unconfined cyclic creep load test to develop a permanent deformation model that considered not only the effects of stress level and temperature but also that of loading time and rest period for asphalt mixtures. They developed predictive equations for the permanent deformation parameters α as a function of loading time and rest period and μ as a function of loading time, rest period, temperature and stress level as follows:

$$\mu = 0.00237082 * t_l^{0.0651478} * t_d^{-0.107480} * T^{1.01843} * \sigma^{0.320862} \quad (2-3)$$

$$\alpha = 0.751629 + 0.0438023 * \log(t_l) - 0.0231006 * \log(t_d) \quad (2-4)$$

where

$$\begin{array}{ll} t_l = \text{loading time (sec)} & t_d = \text{rest period (sec)} \\ T = \text{test temperature (}^\circ\text{F)} & \sigma = \text{stress (psi)} \end{array}$$

Even though these equations were based on a reasonable number of samples (72) they were only for a single asphalt mixture. Moreover, this laboratory investigation did not account for different load configurations (single, tandem, tridem, ect.).

Recently, the National Cooperative Highway Research Program (NCHRP) sponsored a study to identify a simple test for confirming key performance characteristics of Superpave volumetric mix designs (Witczak *et al.*, 2002 and Bonaquist *et al.*, 2003). In

this study, candidate simple performance tests for permanent deformation, fatigue cracking, and low-temperature cracking were identified and validated. Table 2-2 identifies the test methods and the response variables measured in each test that was evaluated for their correlation to permanent deformation performance.

The principal selection criteria for these candidate tests were 1) accuracy 2) reliability 3) ease of use, and 4) reasonable equipment cost. The confined or unconfined repeated load test was one of the recommended candidate tests as a simple performance test for characterizing the permanent deformation.

Table 2-2 Candidate test methods and responses for the SPT (Witczak *et al.*, 2002)

Test method	Mixture response parameters
Dynamic modulus test	Dynamic modulus
	Phase angle
SST shear modulus	Dynamic modulus
	Phase angle
Quasi-Direct shear (field shear test)	Dynamic modulus
	Phase angle
Triaxial repeated load	Slope and intercept of accumulated permanent and total strains
	Plastic to resilient strain ratio
	Resilient modulus, total and instantaneous
	Plastic and resilient strains
	Number of cycles to plastic flow
SST repeated shear, constant-height	Slope and intercept of accumulated permanent and total shear strains
	Plastic to resilient strain ratio
	Resilient shear modulus, total and instantaneous
	Plastic and resilient shear strains
	Number of cycles to plastic flow
Triaxial and uniaxial creep	Angle of internal friction
	Cohesion
	Compressive strength
	Percent strain recovery
Triaxial compressive strength	Angle of internal friction
	Cohesion
	Compressive strength
	Fracture energy

2.4 MECHANISTIC ANALYSIS

Heavy trucks have been recognized as a source of pavement damage due to the stresses and strains imposed by heavy multi-axle loads. Analytical models have been used to calculate generalized pavement response. These responses ultimately cause the major pavement damage manifestations such as fatigue and rutting.

2.4.1 Fatigue

Fatigue is one of the main distress types in flexible pavements. Numerous fatigue models have been formulated based on laboratory testing and calibrated with the field performance and accelerated pavement testing. Some of the well-known equations include those developed by Asphalt Institute (AI) and Shell:

$$N_f = 0.0796 * \epsilon_t^{-3.291} * E_{ac}^{-0.854} \quad (\text{AI}) \quad (\text{Shook, 1982}) \quad (2-5)$$

$$N_f = 0.0685 * \epsilon_t^{-5.671} * E_{ac}^{-2.364} \quad (\text{Shell}) \quad (\text{Claussen, 1977}) \quad (2-6)$$

where

N_f = the number of load repetitions to failure,

ϵ_t = the horizontal tensile strain at the bottom of the HMA layer,

E_{ac} = the dynamic modulus of elasticity of asphalt concrete.

For the future mechanistic-empirical design procedure being developed under the NCHRP 1-37A project the following equation is proposed:

$$N_f = \beta_{f1} F^{10} K_{1\sigma} \left[\frac{1}{\epsilon_t} \right]^{5\beta_{f2}} E^{-1.4\beta_{f3}} \quad (\text{SHRP}) \quad (\text{ARA, Inc., 2004}) \quad (2-7)$$

where

N_f = number of repetitions to fatigue cracking,

ϵ_t = tensile strain at the critical location,

E = material stiffness,

$K_{1\sigma}$ = laboratory calibration parameter,

$\beta_1, \beta_2, \beta_3$ = field calibration factors.

Gillespie *et al.*, 1993 provided the most comprehensive mechanistic analysis of heavy trucks within the NCHRP study titled “Effects of Heavy-Vehicle Characteristics on Pavement Response and Performance.” In this study, analytical models of truck and pavement structures were developed to allow a systematic study of the pavement responses to moving, dynamic loads of various truck configurations. The truck characteristics included in this study were:

- Truck type (straight trucks, tractor-semi-trailers, and multiple-trailer configurations),
- Axle loads,
- Number of axles,
- Spacing between axles,
- Suspension type (single axle with leaf and air spring and tandem axle with leaf spring, air spring, and walking beams), and
- Tire parameters (single/dual configurations, radial/bias construction, and inflation pressure).

The response was determined in both rigid and flexible pavements for various designs and properties, with variations in road roughness and vehicle speed. Pavement responses (stresses, strains, and deflections) were evaluated throughout the pavement. The main conclusions of the study were:

- Static axle load was found to be the unique vehicle factor that has a significant effect on fatigue damage.
- Fatigue in flexible pavements vary in a ratio of 1:20 over a range of axle loads from 10 to 22 kips because fatigue damage is related to the fourth power of the loads.
- Fatigue damage was not directly related to vehicle gross weight but varied with maximum axle loads on each vehicle configuration.

- Axle spacing has little effect on flexible pavement fatigue.
- Static load sharing in multiple axle groups has a moderate effect on the fatigue of flexible pavements.
- Flexible pavement fatigue remained fairly constant with vehicle speed.

Hajek and Agarwal, 1990 highlighted the factors to be considered in calculating the LEFs of various axle configurations for flexible pavements and developed factors using different strain criteria. It was concluded that pavement response parameters such as deflections and strains have considerable influence on LEFs. Moreover, axle weight and their spacing also contribute to the flexible pavement fatigue damage significantly.

Sebaaly and Tabatabaee, 1992 studied the effect of tire parameters on flexible pavement damage and LEFs. They compared single and tandem axles of similar per-axle load levels, and concluded that the passage of one tandem axle produced less fatigue damage than the passage of two single axles. Chatti and Lee, 2004 studied the effects of various truck and axle configurations on flexible pavement fatigue using different summation methods (peak strain, peak-midway strain, and dissipated energy) to calculate the fatigue damage. The results indicate that the peak-midway strain method agrees reasonably well with the dissipated energy method. Moreover, Chatti and Lee recommend using the dissipated energy method because it captures the totality of the stress-strain response during the passage of the loads.

2.4.2 Rutting

Rutting is a major failure mode for flexible pavements. Two mechanistic modeling approaches have been developed to predict rutting. The first approach is referred to as the subgrade strain model, while the second approach considers permanent deformation within each pavement layer.

The two most widely used equations related to the subgrade strain model are the Asphalt Institute (AI) model (Shook, 1982) and the Shell Petroleum model (Claussen, 1977).

$$N_p = 1.365 * 10^{-9} * \epsilon_c^{-4.477} \quad (\text{AI}) \quad (2-8)$$

$$N_p = 6.15 * 10^{-7} * \epsilon_c^{-4} \quad (\text{Shell}) \quad (2-9)$$

where

N_p = Number of load repetitions to failure

ϵ_c = Vertical compressive strain at the top of subgrade.

Failure is defined as the development of 13-19 mm (0.5 to 0.75 in) rut depth in the AI model and 13 mm (0.5 in) rut depth in the Shell model.

Kim (1999) developed a rutting model related to the second approach—permanent deformation within each layer—which accounts for the total rutting in all pavement layers as follows:

$$RD = \left(-0.016H_{AC} + 0.033 \ln(SD) + 0.011T_{annual} - 0.01 \ln(KV) \right) * \left(-2.703 + 0.657(\epsilon_{v,base})^{0.097} + 0.271(\epsilon_{v,SG})^{0.883} + 0.258 \ln(N_{ESAL}) - 0.034 \ln\left(\frac{E_{AC}}{E_{SG}}\right) \right) \quad (2-10)$$

where:

- RD = Total rut depth (in)
- SD = Surface deflection (in)
- KV = Kinematic viscosity (centistoke)
- T_{annual} = Average annual ambient temperature (°F)
- H_{AC} = Thickness of asphalt concrete (in)
- N = cumulative traffic volume (ESAL)
- E_{AC} = Resilient modulus of HMA
- E_{SG} = Resilient modulus of subgrade

$\epsilon_{v,base}$ = Vertical compressive strain at the top of the base (10^{-3})

$\epsilon_{v,SG}$ = Vertical compressive strain at the top of the subgrade (10^{-3})

This model is limited to using the ESAL, and therefore can not handle different axle configurations. Also, the model was calibrated for specific sections in the state of Michigan (50 sections).

The VESYS rutting model (Moavenzadeh, 1974) was derived so that each term of the equation corresponds to one pavement layer with two unique permanent deformation parameters (α and μ). The form of the model is more applicable for use in this research as shown below [Ali and Tayabji, 2000 and Ali *et al.* 1998].

$$\rho_p = h_{AC} \frac{\mu_{AC}}{1-\alpha_{AC}} \left(\sum_{i=1}^K (n_i)^{1-\alpha_{AC}} (\epsilon_{ei,AC}) \right) + h_{base} \frac{\mu_{base}}{1-\alpha_{base}} \left(\sum_{i=1}^K (n_i)^{1-\alpha_{base}} (\epsilon_{ei,base}) \right) + h_{SG} \frac{\mu_{SG}}{1-\alpha_{SG}} \left(\sum_{i=1}^K (n_i)^{1-\alpha_{SG}} (\epsilon_{ei,SG}) \right) \quad (2-11)$$

where:

- ρ_p = total cumulative rut depth (in the same units as the layer thickness),
- i = subscript denoting axle group,
- K = number of axle group,
- h = layer thickness for HMA layer, combined base layer, and subgrade layer, respectively,
- n = number of load applications,
- ϵ_e = compression vertical elastic strain at the middle of the layers,
- μ = permanent deformation parameter representing the constant of proportionality between plastic and elastic strain, and
- α = permanent deformation parameter indicating the rate of change in rutting as the number of load applications increases.

Moreover, Ali *et al.*, 1998 calibrated the new form of the model using 61 sections from the Long Term Pavement Performance (LTPP) General Pavement Study 1 (GPS-1) by backcalculating the permanent deformation parameters for each layer. Ali and Tayabji,

2000 also proposed using a transverse profile to backcalculate permanent deformation parameters, and reported one set of values obtained from only one LTPP section (see Table 2-3).

Kenis (1997) used the Accelerated Pavement Tests (APT) performance data to validate and calibrate the two flexible pavement-rutting models used in VESYS 5. In their study, they suggested a range for the permanent deformation parameters for the pavement layers as shown in Table 2-3.

Table 2-3 Permanent deformation parameters
(Ali *et al.*, 1998, Ali and Tayabji, 2000, Kenis, 1997, and Bonaquist, 1996)

Calibration	Pavement layer	μ	α
LTPP (Ali <i>et al.</i> , 1998)	HMA	0.701	0.7
	Base	0.442	0.537
	Subbase	0.333	0.451
	Subgrade	0.021	0.752
Transverse profile (Ali and Tayabji, 2000)	HMA	0.000103	0.1
	Base	1.163	0.95
	Subgrade	0.0008	0.644
APT (Kenis and Wang, 1997)	HMA	0.6 to 1.0	0.5 to 0.75
	Base	0.3 to 0.5	0.64 to 0.75
	Subgrade	0.01 to 0.04	0.75
APT (Bonaquist, 1996)	Asphalt concrete	0.1 to 0.5	0.45 to 0.9
	Granular base/subbase	0.1 to 0.4	0.85 to 0.95
	Sandy soil	0.05 to 0.1	0.8 to 0.95
	Clay soil	0.05 to 0.1	0.6 to 0.9

The future mechanistic-empirical design procedure being developed under NCHRP 1-37A (ARA, Inc., ERES division, 2004) provides a rutting model for the HMA layer (equation 2-12) as well as unbounded layers (equation 2-13).

$$\frac{\varepsilon_p}{\varepsilon_r} = 0.0007 \beta_r T^{1.734} \beta_{r2} N^{0.39937} \beta_{r3} \quad (2-12)$$

where:

\mathcal{E}_p	= plastic strain	\mathcal{E}_r	= resilient strain
T	= layer temperature	N	= number of load repetitions
$\beta_{r1}, \beta_{r2}, \beta_{r3}$	= field calibration factors		

$$\delta_a(N) = \beta_{s1} \varepsilon_v h \left(\frac{\varepsilon_o}{\varepsilon_r} \right) \left[e^{-\left(\frac{\rho}{N} \right)^\beta} \right] \quad (2-13)$$

where:

δ_a	= permanent deformation for the layer	N	= number of load repetitions
ε_v	= average vertical strain	h	= thickness of the layer
$\varepsilon_o, \rho, \beta$	= material parameters	ε_r	= resilient strain
β_{sl}	= field calibration factor		

The field calibration factors for those two models are shown in Table 2-4.

Table 2-4 Field calibration factors for the new mechanistic-empirical design guide

Optimization	β_{r1}	β_{r2}	β_{r3}	β_{GB}	β_{SG}
Method one	0.551	0.900	1.200	1.050	1.350
Method two	0.509	0.900	1.200	1.673	1.350

As mentioned previously, there are several rutting models available in the literature (more literature in Kim, 1999). However, each rutting model has specific limitations, as

listed in Table 2-6. Ullidtz's, 1987 literature review shows that the subgrade strain models (AI and Shell models) are based on unreasonable assumptions, since they only account for subgrade rutting while neglecting upper pavement layer rutting. He also, reported that the subgrade rutting in the AASHO road test was only 9% of the total rutting as shown in Table 2-5.

Table 2-5 Percent layer distribution of rutting (Ullidtz, 1987)

Pavement layer	Percent observed rutting
Asphalt concrete	32
Base	14
Subbase	45
Subgrade	9

The rutting model form of Ali *et al.* (1998) is more appropriate to apply in this study; however the calibration of the permanent deformation parameters is the weakest point. The previous calibration process of that model has several limitations as shown in Table 2-6. Hence, a calibration procedure for this model is suggested in this study using the LTPP Special Pavement Study-1 (SPS-1) data. This experiment provides rut data for various combinations of layer thickness and base types with fine as well as coarse grained subgrade soils and for different climatic zones (Hanna *et al.*, 1994).

Table 2- 6 Limitations of the existing flexible pavement rutting models

Model #	Model name	Authors	Limitations
1	AI and Shell	Shook 1982; Claussen 1977	<ul style="list-style-type: none"> ➤ These models account only for subgrade rutting and neglect the rutting from other layers. ➤ These models did not account for rate hardening as the number of load applications increase. ➤ The relationship between observed rutting and rutting damage ratio did not follow the expected S-shape.
2	MSU	Kim 1999	<ul style="list-style-type: none"> ➤ Traffic has to be in ESALs ➤ While the model predicts the total rutting, it does not predict rutting within each layer ➤ This model was calibrated for Michigan sections only.
3	VESYS	Ali et al. 1998	<ul style="list-style-type: none"> ➤ Large scatter between predicted and measured rut depths. ➤ Using this model outside the calibrated data yielded inaccurate predictions. ➤ The calibration procedure was only for the latest rut depth rather than time series data.
4	VESYS	Ali and Tayabji 2000	<ul style="list-style-type: none"> ➤ The calibration process was only for one section, which exhibited large amount of rutting. ➤ Using this model for different sections gives unreasonable rut prediction. ➤ The calibrated permanent deformation parameters were completely different from those using the maximum rut values. ➤ These parameters can only be used for the same pavement or for similar materials under similar conditions.
5	VESYS	Kenis, 1997	<ul style="list-style-type: none"> ➤ Wide range of the permanent deformation parameters, however some of these parameters are very sensitive because they used as power in the model.
6	ME design guide (NCHRP 1-37A)	Witczak et al., 2004	<ul style="list-style-type: none"> ➤ Fixed contribution of base and subgrade rutting

2.4.2.1 Contribution of pavement layers to rutting

Rutting is the load-induced permanent deformation of a flexible pavement. According to the magnitude of the load and the relative strength of the pavement layers, permanent deformation can occur in the subgrade, the base, or hot mix asphalt (HMA) layers.

Susceptibility of pavement layers to rutting varies according to pavement material properties and climatic conditions. For example, rutting of HMA layers is more common during hot summer seasons than it is during the winter, and permanent deformation is more likely in unbound sub-layers during wet spring seasons. Suitable rehabilitation of existing rutting requires knowledge of the relative contributions of the layers (i.e., subgrade, base, and HMA) to the total permanent deformation in the pavement. There are two main ways to identify the layers primarily responsible for the rutting of a flexible pavement: 1) trenches and 2) transverse surface profile. The rut depth measurements are not precise in the trenched unbounded layers (base, subbase, and subgrade) due to the inconsistency of layer thicknesses and noise caused by individual particles at the surface. Moreover, digging trenches is expensive and difficult to maintain. On the other hand, measuring a transverse surface profile is easier, less hazardous, and far less costly than cutting a transverse trench to examine underlying layers. Therefore, great effort has been made to investigate and analyze the transverse surface profile in order to determine rutting within the pavement layers (White *et al.*, 2002, Harvey and Popescu, 2000, and Chen *et al.*, 2003).

Simpson *et al.*, 1995 introduced a technique in which the area under the transverse surface profile can be used to determine whether rutting can be attributed to the effect of heave, or changes in the subgrade, base, or asphalt layer. This technique is based on a

linear elastic model to predict the shape of the surface profile. A single line, representing the original pavement surface, was drawn between the two end points of the profile. They used the total area bounded by the original and the current road surfaces and the ratio between the amount of area above and below the original pavement line to determine the possible main contributing layer to rutting. Figure 2-4 shows the variation of transverse profile shapes and indicates for each where the rutting originated within the pavement structure based on the area technique.

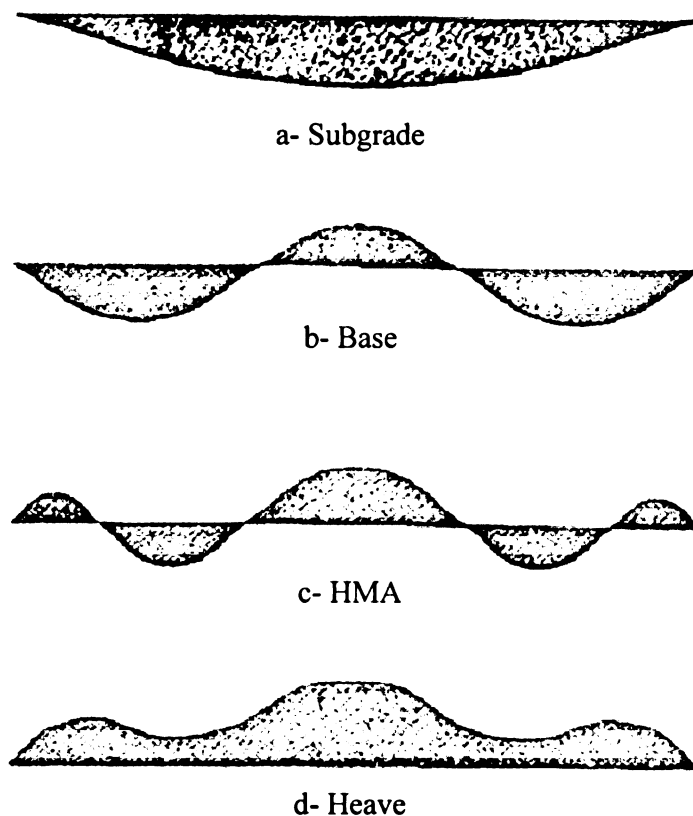


Figure 2-4 Transverse surface profile for various rut mechanism (Simpson *et al.*, 1995)

White *et al.* (2002) indicated that Simpson's technique did not accurately differentiate rutting caused by asphalt or base layers. Their argument suggests that the discrepancies were created because Simpson used a linear elastic theory to estimate the shape of the

surface profiles. White has extended Simpson's method using a nonlinear visco-elastic finite element model to predict pavement deformation. The FEM analysis matched Simpson's predictions and in addition, it was able to separate the effects of the base from those of the HMA layer. However, the authors noted that the rut depths on all of the sections analyzed in their research were greater than 5 mm (0.2 in). The rut depth has to be well defined to accurately determine the reference line between the two end points of the surface profile. White's procedure required that the transverse profile measurements be greater than 3.6 meters (12 ft), especially when a shoulder was present in the section.

2.4.2.2 Variables affecting permanent deformation parameters

There are several variables affecting permanent deformation parameters α and μ (see equation 2-11) . These variables can be divided into four groups 1) environmental, 2) material properties, 3) cross sections, and 4) construction quality. Simpson *et al.*, 1994 developed a rutting model to predict the total rut depth for LTPP data (GPS-1 and GPS-2). The model uses a multiplicative regression equation and includes several variables as shown in Table 2-7.

Table 2-7 Variables affecting the permanent deformation parameters
(Simpson *et al.*, 1994)

Environmental	Material properties	Cross sections	Construction quality
Freeze index	Air voids in HMA	HMA thickness	Base compaction
Annual precipitation	% passing sieve 200 in subgrade	Base thickness	
Average annual minimum temperature	% passing sieve 4 in HMA		
Number of days above 90 °F	Asphalt viscosity		

In a further study, Simpson *et al.*, 1995 distinguished the rutting contribution from each pavement layer using the same LTPP data. A general model for the total surface rutting, subgrade rutting, base rutting, HMA rutting, and heave was generated using neural network analysis. The variables that were considered in each model are listed in Table 2-8.

Table 2-8 Independent variables included in different models (Simpson *et. al.*, 1995)

Total surface rutting	Subgrade rutting	Base rutting	HMA rutting	Heave
HMA thickness	Annual precipitation	Annual precipitation	HMA thickness	Annual precipitation
Air voids percentage	Number of days above 90°F	Number of days above 90°F	Asphalt content	Freeze thaw cycles
Asphalt viscosity @140°F	Freeze thaw cycles	Base thickness	Air voids percentage	Plasticity Index
Annual precipitation	Plasticity Index	Base compaction	% passing # 4 in HMA	Subgrade moisture
Number of days above 90°F	Subgrade moisture	ESALs	Asphalt viscosity @140°F	% passing # 200 in subgrade
Freeze thaw cycles	% passing # 200 in subgrade		Number of days above 90°F	ESALs
Plasticity Index	ESALs		ESALs	
Subgrade moisture				
% passing # 200 in subgrade				
Base thickness				
ESALs				

2.5 SUMMARY

The main goal of this research is to investigate the relative effects of different axle/truck configurations on rutting of flexible pavements. Although some research has been conducted on the subject, there is still a need to extend this research to include new, heavy, multi-axle trucks. This section will detail the research approach based on the literature review presented above for analysis of in-service pavements, laboratory investigation and mechanistic analysis.

2.5.1 Analysis of in-service pavements

It appears that previous field investigations were very limited and did not answer the research question. Therefore, in the present study, actual field data from the state of Michigan were analyzed to study the effects of various axle and truck configurations on rutting. The Michigan Department of Transportation (MDOT) has very comprehensive pavement performance data as part of their Pavement Management System (PMS). MDOT also collects rutting and roughness data, as well as traffic count and weight data, throughout its network. Collection of traffic and weight data has been recently upgraded by using new Weigh In Motion (WIM) technology. This allows for a more accurate representation of the distribution of truck axle weights and configurations along MDOT's trunk-lines. The details of the truck traffic and pavement rutting data, as well as the analyses conducted, are explained in the following chapter.

2.5.2 Laboratory investigations

2.5.2.1 Fatigue

The relative effect of different axle/truck configurations on fatigue cracking has been extensively investigated in the laboratory at Michigan State University (Chatti and El Mohtar, 2004).

2.5.2.2 Rutting

Based on the literature review, the most suitable rutting test that can characterize the relative permanent deformation damage for asphalt mixture was the unconfined cyclic creep test. The unconfined cyclic creep test will be utilized according to the new procedure for sample preparations (coring, sawing, and capping). Different axle/truck load configurations will be simulated as a series of different load pulses, and the cumulative permanent strain and flow number will be used for relative comparisons.

2.5.3 Mechanistic analysis

The mechanistic analysis will consider the relative effect of different axle/truck configurations on the entire pavement system (HMA, base, and subgrade layers). This analysis will be compared with the field investigations.

2.5.3.1 Fatigue

The relative effect of different axle/truck configurations on fatigue cracking has been extensively investigated mechanistically by Gillespie *et al.*, 1993 and Chatti and Lee, 2004. Based on the results, fatigue is greatly affected by individual axles (as opposed to gross weight of the truck), and large axle groups cause less damage per tonnage carried than smaller axle group.

2.5.3.2 Rutting

The study of relative effects of different axle/truck configurations on permanent deformation was limited to single and tandem axles only. Based on the literature review, the most suitable rutting model for calculating the permanent deformation in each pavement layer due to different axle/truck configurations is the VESYS model. Even though several trials have been made to backcalculate the permanent deformation parameters, they yield a wide range for these parameters. Therefore, this research will consider calibration of the VESYS rutting model using in-service data from the LTPP SPS-1 experiment.

CHAPTER 3- ANALYSIS OF FLEXIBLE PAVEMENT RUTTING FROM IN-SERVICE DATA

3.1 INTRODUCTION

The Michigan Department of Transportation (MDOT) has very comprehensive pavement surface distress data files. The data include flexible pavement rutting as well as traffic count and weight data. Therefore, these data can be utilized to investigate the relative effect of Michigan multi-axle trucks on actual pavement rutting. In addition, investigating the relationship between truck traffic and pavement rutting from in-service pavements can be used to verify mechanistic and laboratory findings.

3.2 SITE SELECTION PROCEDURE

The following summarizes the steps that have been done for the site selection:

- Extract the stations rut data that have available traffic for the years 2000 and 2001 from the FHWA program (VTRIS).
- Match those stations rut data with the control sections using the Permanent Traffic Recorder, PTR, file provided by MDOT.
- Locate the stations in each county using the control section in the 2001 Physical Reference/Control Section, PR/CS atlas and determine exactly the location of the weigh stations on the control sections.
- Traffic data in the sufficiency rating book and Michigan annual average 24-hour commercial traffic volumes maps were used to examine the variation of the traffic

relative to the weigh station segment. The variation on the considered length of the control section was limited to a maximum of 10%.

- In some cases, the truck traffic data were valid only for a small portion of the control section (the weigh station segment), especially when there are several main exits and entrances on the road as shown in figure 3-1.
- In other cases, the traffic data were valid for two consecutive control sections where there are no main exits or entrances on the road as shown in Figure 3-2.

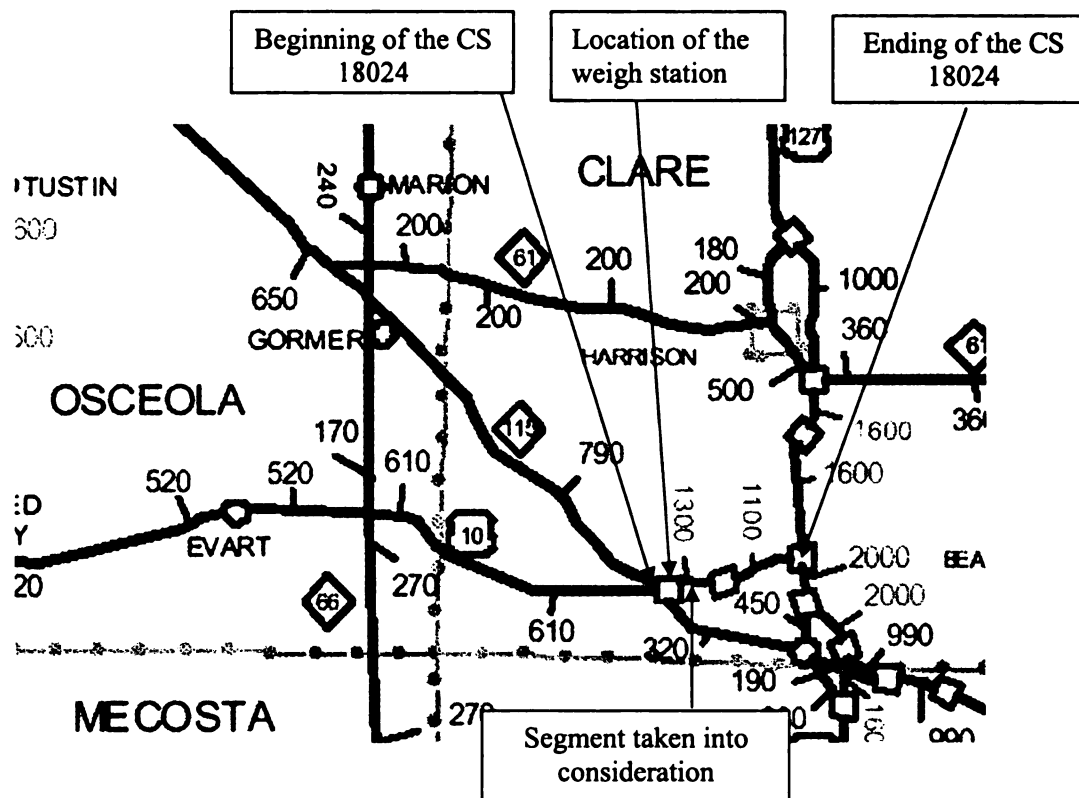


Figure 3-1 Variation of the traffic along CS # 18024

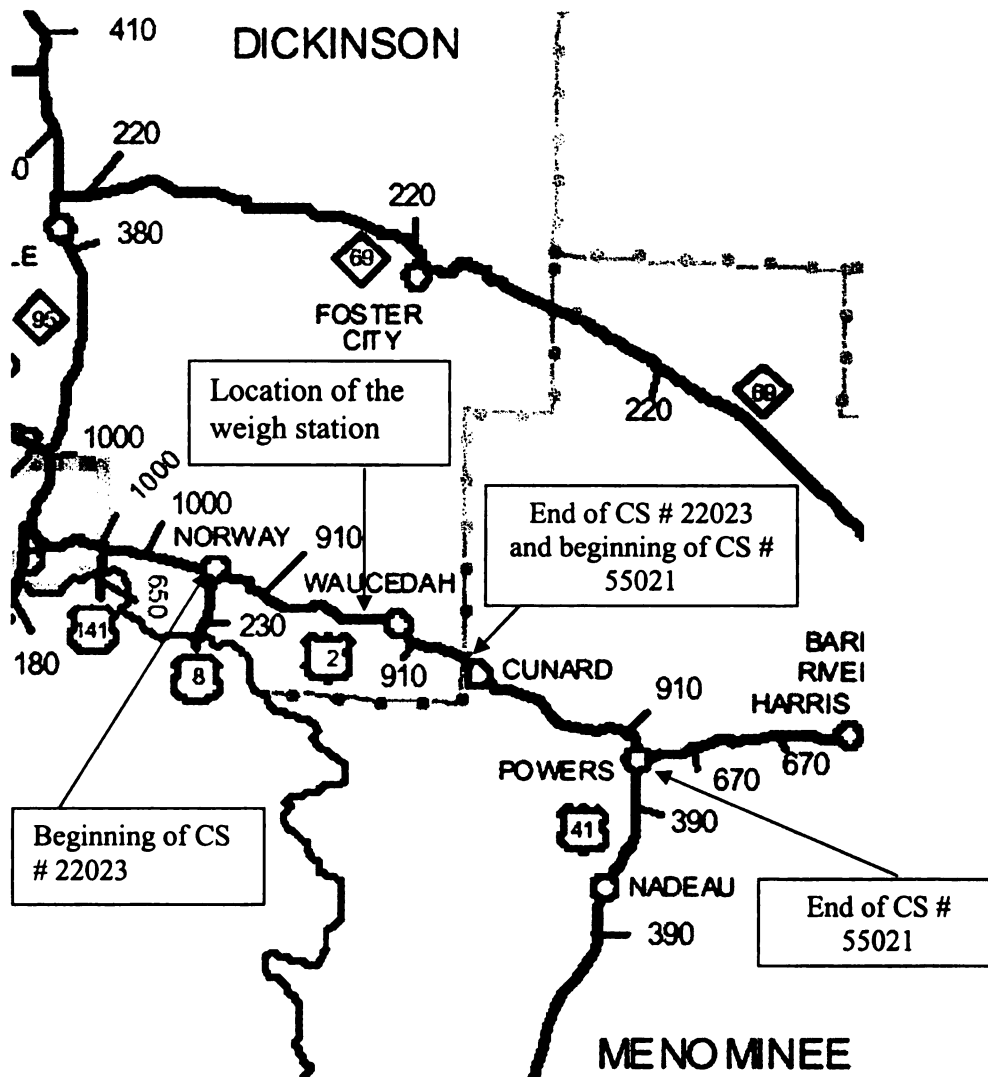


Figure 3-2 No variation of the traffic along two consecutive control sections (CS # 22023 and 55021)

3.3 PERFORMANCE DATA

Great effort has gone into selecting sections with different pavement type, age, cross-sectional design, and traffic loading. The same control section was divided into several sections that have similar Average Daily Truck Traffic (ADTT) so that if pavement age varies, the cumulative control section traffic will reflect each subsection's age. MDOT

surveys flexible pavement rutting for half of their network every year. The distress survey includes only outside (slow) lane where most trucks travel.

Rutting is a main load-related distress in flexible pavements. It is the permanent deformation in the transverse profile under the wheel path, starting at zero rut depth and increasing with the number of heavy load repetitions. Rutting is cumulative over time unless major rehabilitation is applied to the pavement. MDOT consider a rutting threshold of 0.5 inch (12 mm) to be the boundary for poor pavement conditions as shown in Figure 3-3. Table 1-1 shows the descriptive statistics for rut depth and corresponding age for pavement sections used in the analysis.

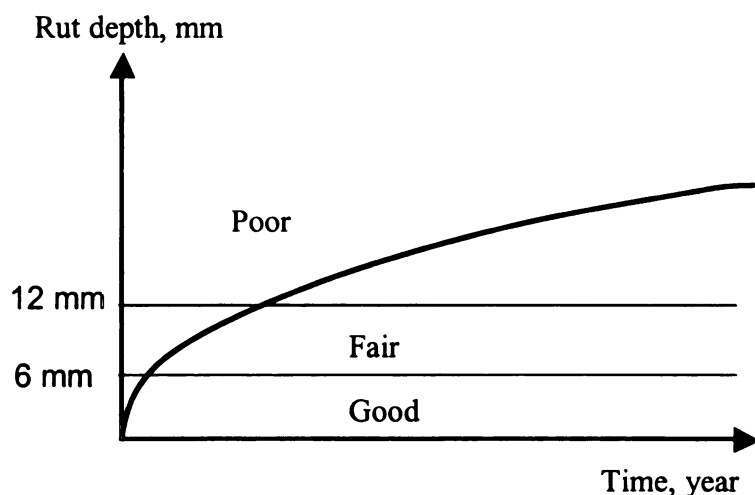


Figure 3-3 Rutting versus Time

3.4 TRAFFIC DATA

The Federal Highway Administration (FHWA) assembles highway traffic information all over the United States and provides it in its Vehicle Travel Information System (VTRIS), which is available as public domain software. The FHWA classifies truck traffic into nine categories according to the number of axles and number/type of truck units. Most of the

truck categories include different truck configurations. The program provides the count of each FHWA truck class without differentiating between different configurations or providing the proportion of each configuration under a given category. Not all needed traffic counts/proportions and the average weights of each truck configuration are available in the VTRIS program. It was therefore necessary to analyze raw traffic data provided by MDOT in order to extract all essential truck information.

Table 3-1 Descriptive statistics of rut depth and pavement age

Type of traffic data *	Pavement type	Number of projects	Rutting				Age			
			Min.	Max.	Average	Std. Dev.	Min.	Max.	Average	Std. Dev.
VITRS	Overall	52	0.04	0.46	0.20	0.09	0	30	6	6
	Interstate	9	0.17	0.36	0.25	0.08	1	7	4	3
	US-roads	23	0.16	0.46	0.25	0.07	0	24	5	5
	Michigan roads	20	0.04	0.31	0.12	0.06	1	30	9	8
Raw traffic data	Overall	29	0.14	0.46	0.23	0.08	0	24	5	4
	Interstate	9	0.17	0.36	0.25	0.08	1	7	4	3
	US-roads	13	0.16	0.46	0.26	0.08	0	24	5	6
	Michigan roads	7	0.14	0.19	0.16	0.02	1	8	6	3

* Explained in details in the following section

3.4.1 Vehicle Travel Information System, VTRIS

The FHWA traffic data are classified into 13 classes. Classes 5 to 13 are for truck traffic, reported as the ADTT count per class type. Figure 3-4 shows the class definition, axle groups (number of axles within an axle group), and examples of truck configurations for classes 5 through 13. Axle spectra are also available from FHWA data but only for single, tandem, tridem, and quad axles (FHWA website). The program does not have the count for large (≥ 5) axle groups, which are of interest in this research. Using the FHWA data (from “W-2” tables at the website), the ADTT for classes 5 through 13 were extracted for the control sections corresponding to the outside lane. The improvement year of the control section was also obtained from MDOT’s sufficiency-rating books. The improvement year represents the most recent year the segment received significant work that improved the pavement condition or extended the life of the pavement. The Cumulative Truck Traffic, (CTT) for classes 5 through 13 was calculated as follows:

$$\text{CTT of class} = \text{ADTT of class} \times \text{pavement age} \times 365 \quad (3-1)$$

where:

ADTT = average daily truck traffic of a given class

Pavement age = year of improvement – distress survey year.

The consistency of weigh station traffic data from year to year was examined for total ADTT and individual truck classes. Figure 3-5 shows a comparison of ADTT in 2001 and 2002 traffic data for all weigh stations in the State of Michigan. No significant change can be seen in the traffic data. Therefore, the 2001 traffic data were used for truck classes’ analysis.

3.4.2 Raw Traffic Data

Since VTRIS does not provide some essential data needed for this research, raw truck traffic data for 2000 were analyzed to determine the distribution of axle and truck configurations for all axle groups including those with a large number of axles for each weigh station. Trucks were categorized according to their largest axle group. For example, a quad axle is an axle group that has four axles that share the same weight, so that trucks with a quad-axle are all trucks that have quad axle as the largest axle group. Figure 3-6 shows the axle and truck categories used in the analysis. Table 3-2 shows an example of the extracted axle/truck information. The analysis of raw traffic data also allowed for determining the proportions of each truck type within each FHWA truck class. Table 3-3 shows the proportions, average truck weight, and the percentage of truck configurations within each class. FHWA truck class 13, which is the heaviest truck class, includes many different configurations with most having very small numbers. Figure 3-7 shows that truck classes 7 and 12 have very small percentages (less than 0.4 %) and truck class 5 has the lowest overall average weight (6.0 tons). These trucks will not significantly contribute in explaining the pavement damage; therefore they were excluded from the analysis.

Table 3-4 shows the number of weigh stations for raw traffic and VTRIS analysis as well as the number of projects corresponding to each one of them. A more details information about where these stations located on the roads, the beginning and ending, the length of each project can be found in Table A-1 (appendix). Also, rut depth and traffic count for each project are shown in Table A-2 (appendix).







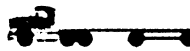
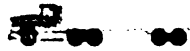
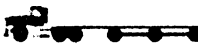

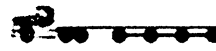
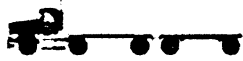
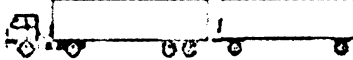








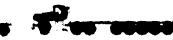
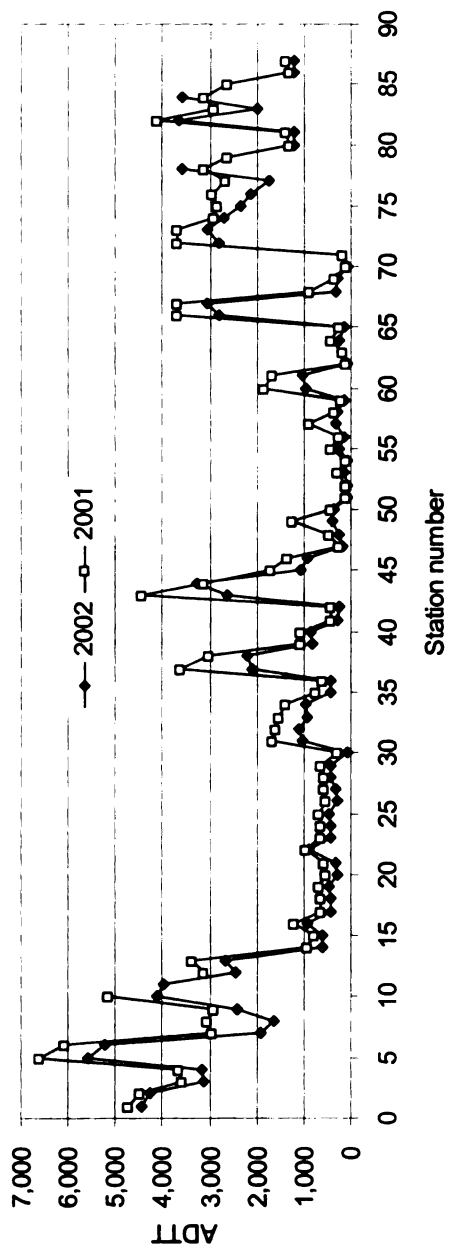
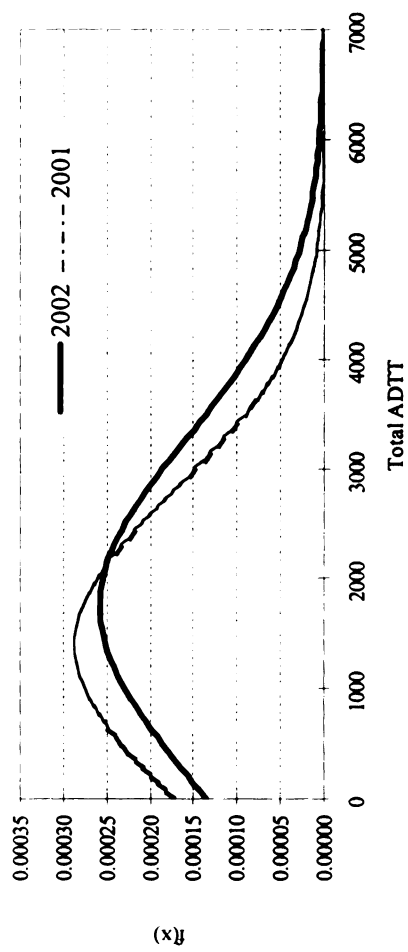
FHWA Class Type	Class Definition	Axle Group	Example truck configurations
5	Two-axle, six-tire, single-unit trucks	1	
6	Three-axle single- unit trucks	1 and 2	
7	Four or more axle single-unit trucks	1, 3 and 4	 
8	Four or fewer axle single-trailer trucks	1 and 2	 
9	Five-axle single- trailer trucks	1 and 2	 
10	Six or more axle single-trailer trucks	1, 2, 7 and 8	  
11	Five or fewer axle multi-trailer trucks	1	
12	Six-axle multi- trailer trucks	1 and 2	
13	Seven or more axle multi-trailer trucks	1, 2, 3, 4, 5, 7 and 8	        

Figure 3-4 FHWA vehicle class definitions



(a) One to one station



(b) Distribution of the traffic

Figure 3-5 Comparison between 2001 and 2002 total average daily truck traffic

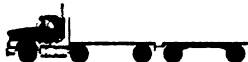







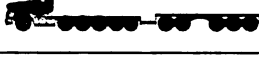

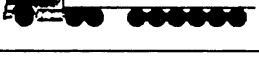





Axle/truck	Example truck configurations	Axle configurations
Single		
Tandem		
Tridem		
Quad		
Five		
Six		
Seven		
Eight		

Figure 3-6 Axle/truck configurations extracted from raw data

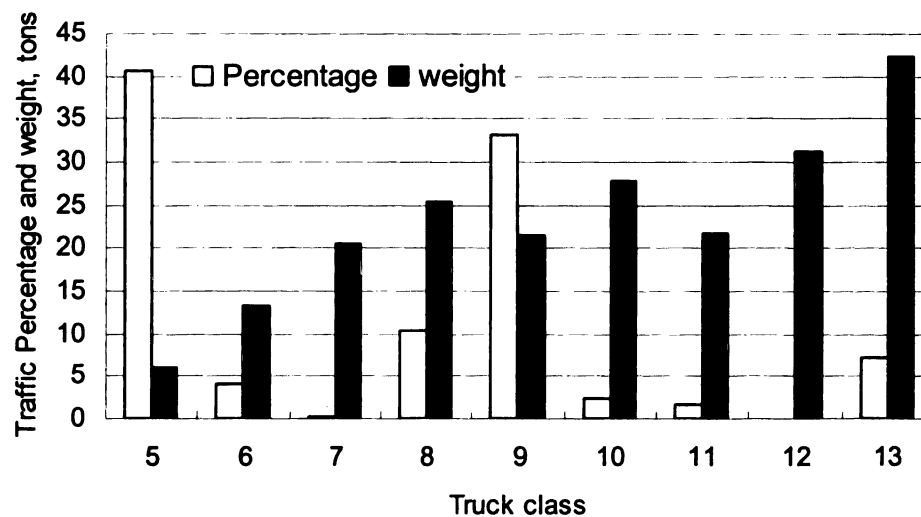


Figure 3-7 Weight and percentage of FHWA truck classes

Table 3-2 Axle/Truck Count and Weight for Station Number 26183049 East Direction (Michigan Road, M-61)

Type	Configuration	Count	Average weight (tons)	Min. weight (tons)	Max. Weight (tons)	St. dev. of the weight (tons)
Axles	Front	23772	4.5	1.8	27.2	9.6
	Single	14312	4.1	0.3	27.1	8.6
	Tandem	16382	7.6	0.6	37.4	10.2
	Tridem	3305	10.2	0.9	26.4	13.9
	Quad	1267	13.1	2.3	32.3	18.1
	5-Axle	652	18.3	3.5	40.4	23.3
	6-Axle	90	24.4	7.7	37.6	11.8
	7-Axle	317	29.9	6.0	45.2	19.5
	8-Axle	214	30.7	4.7	44.6	25.3
	1-axle	10283	8.6	3.6	105.0	19.0
Trucks	2-axle	8103	15.8	5.5	82.7	20.5
	3-axle	2708	22.0	5.6	64.3	29.6
	4-axle	1265	28.8	7.2	70.6	39.6
	5-axle	652	42.9	11.5	78.3	50.8
	6-Axle	90	51.1	17.7	81.4	21.5
	7-Axle	317	48.2	19.4	71.5	28.9
	8-Axle	214	46.6	13.3	64.9	35.4

Table 3-3 Proportions and Average Weights for FHWA Truck Classes

FHWA class	Truck configuration	Truck count	Total count	Proportions, %	Average truck weight, tons
5	5F1*	892451	905700	98.5	6.0
	5F12	10635		1.2	7.0
	5F11	1405		0.2	6.8
	5F111	1209		0.1	7.7
6	6F2	91657	91657	100.0	13.3
7	7F3	6096	6975	87.4	19.8
	7F21	879		12.6	25.6
8	8F11	149141	229718	64.9	30.7
	8F12	65798		28.6	15.3
	8F21	7880		3.4	16.1
	8F111	6899		3.0	14.6
9	9F22	631743	738310	85.6	21.4
	9F211	106567		14.4	23.0
10	10F23	35972	51930	69.3	24.4
	10F2111	10657		20.5	37.1
	10F212**	5234		10.1	32.6
	10F221	67		0.1	29.2
11	11F1111	37790	37790	100.0	21.8
12	12F2111	1323	1323	100.0	31.2
13	Trucks with 8-axle***	6987	158305	4.4	58.3
	Trucks with 7-axle	5753		3.6	68.7
	Trucks with 6-axle	4284		2.7	66.5
	Trucks with 5-axle	31383		19.7	61.7
	Trucks with 4-axle	52190		32.8	58.5
	Trucks with 3-axle	33914		21.3	51.1
	Trucks with 2-axle	23794		14.9	53.8

* FHWA class 5 front and single axle

** FHWA class 10 front, tandem, single, and tandem

*** Trucks with 8-axle group as the largest group

Table 3-4 Number of weigh stations and projects

Traffic configuration	Year	Number of weigh stations	Number of projects	Source of the data
Axle type	2000	12	29	Raw traffic data
Truck type	2000	12	29	Raw traffic data
FHWA truck classes	2001	20	52	VTRIS

3.5 ANALYSIS

The analysis was conducted using three different independent variables: 1) axle configuration (29 subsections); 2) truck configuration (29 subsections); and 3) FHWA truck class (52 subsections). The effects of these on pavement rutting were investigated using simple, multiple, and stepwise linear regression.

3.5.1 Regression Analysis

A series of simple univariate linear regressions was used to investigate the effect of each axle/truck configuration on rutting. The simple linear regression provides the value of the slope and the correlation coefficient of the relationship between the independent variables (axle/truck configurations) and dependent variable (rutting). Univariate analysis can only partially explain pavement rutting since it does not account for other variables. It was primarily used to gain insight into the data.

Multiple linear regression takes into account all specified variables at the same time. The multiple linear equations produced herein are not intended to be a universal model to predict pavement rutting. The regression parameter (β), coefficient of determination (R^2), and test statistic (p -values) were utilized to compare the effect of

different axle and truck configurations on pavement rut damage. The analysis included checking the normality assumption (Figure 3-8) and constant variance of the residual (Figure 3-9), as well as deleting the influential points based on Cook's distance as shown in Figure 3-10.

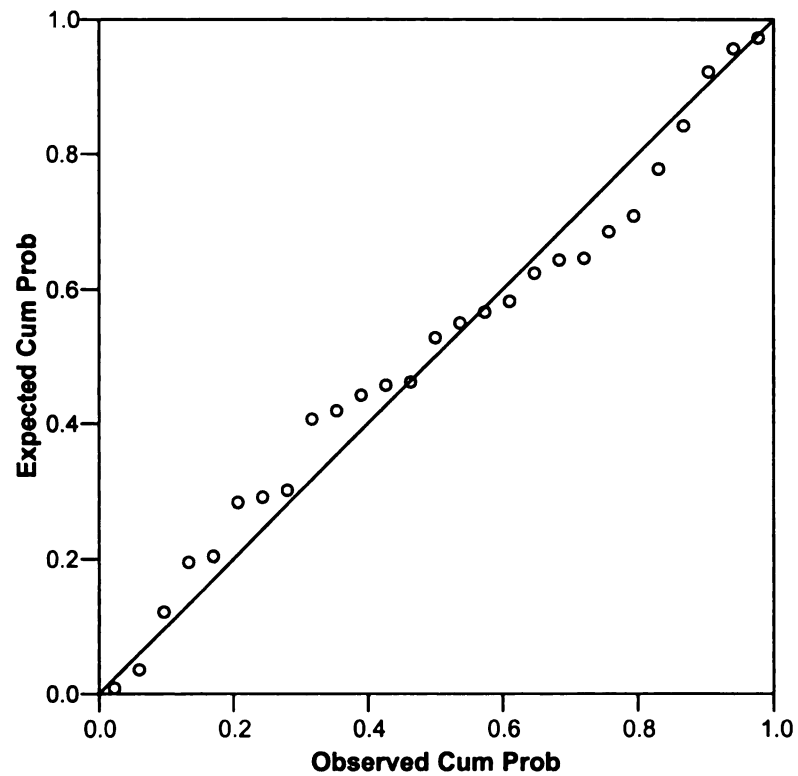


Figure 3-8 Normality plot

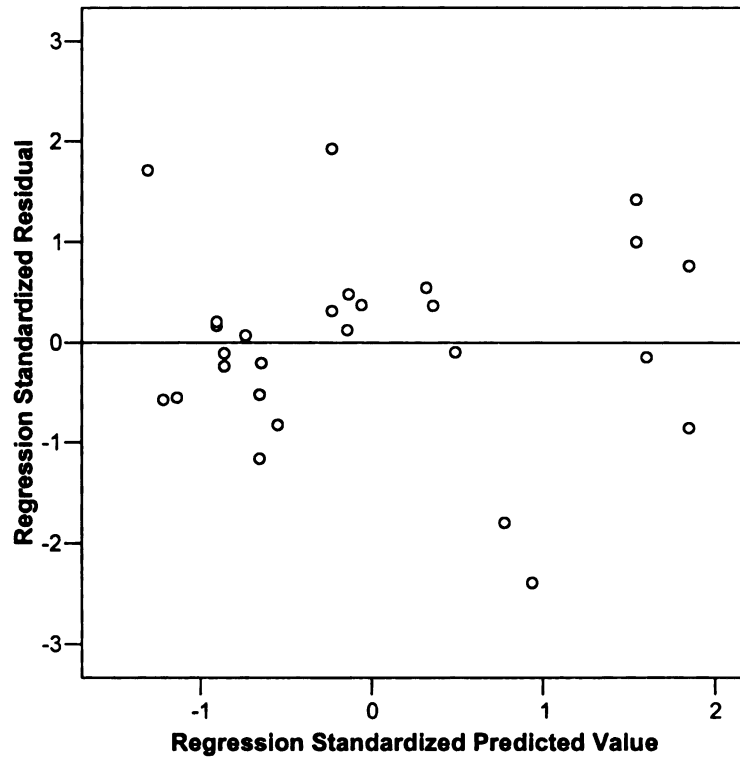


Figure 3-9 Predicted versus residual plot

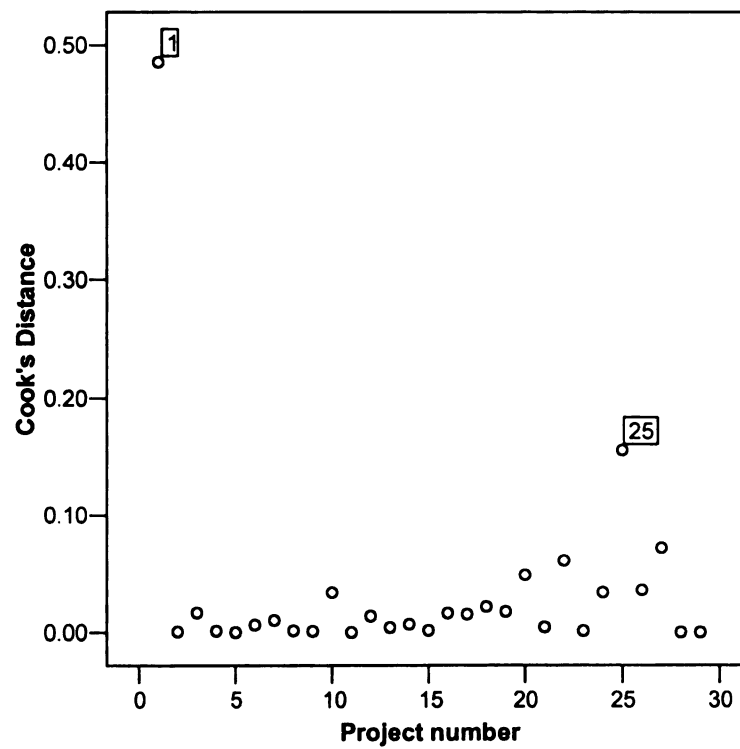


Figure 3-10 Cook's distance

Stepwise regression was also used to confirm the results from simple and multiple linear regressions. Stepwise regression is a technique for choosing the variables to include in a multivariate regression model. Forward stepwise regression starts with no model terms. At each step, it adds the most statistically significant term (the one with the highest F statistic or lowest *p-value*) until the addition of the next variable makes no significant difference. An important assumption behind the method is that some input variables in a multiple regression do not have an important explanatory effect on the response. Stepwise regression keeps only the statistically significant terms in the model.

3.5.2 Standardized Regression Coefficients

The value of the slopes (β s) in simple, multiple, and stepwise linear regression depends on the unit of measurement (number of truck repetitions). This slope represents the change in rutting (dependent variable) due to a unit increase in the number of axle or truck repetitions (independent variables). Axle/truck configurations with fewer repetitions will have a larger slope value, while those axle/truck configurations with more repetitions will have a very small slope value, which does not represent the actual effect regardless of the number of repetitions. Moreover, the intercept for each independent variable will be different from each other, which may not help in comparing the relative effects. The standardized slope has been documented as a measure to compare the relative importance of different independent variables (Dillon, W. and M. Goldstein, 1984, and Allen, J.C., 2001). Standardized slope values are determined by converting all variables (dependent and independent) into Z-scores. Having the variables in Z-score form will convert the distribution mean to zero and standard deviation to one, such that

all variables will have a common measurement scale and one can determine which independent variable is relatively more important. The following equation represents the non-standardized simple linear regression.

$$Y = a + \beta X \quad (3-2)$$

where:

Y = dependent variable (rutting)

a = intercept

β = non-standardized slope

X = independent variable (for example, single-tandem or multiple axle repetitions)

The following equations represent the standardized simple linear regression.

$$Y^* = \beta^* X^* \quad (3-3)$$

$$X^* = Z_x = \frac{\bar{X} - X}{\sigma_x} \quad (3-4)$$

$$Y^* = Z_y = \frac{\bar{Y} - Y}{\sigma_y} \quad (3-5)$$

where:

Y^* = standardized dependent variable,

β^* = standardized slope,

\bar{Y} = average value of dependent variable,

X^* = standardized independent variable, and

\bar{X} = average value of independent variable.

The same procedures were used to standardize the regression coefficient parameters in multiple and stepwise regression. The standardized slope was used to compare the relative effect of the axle/truck configurations in all regression analyses presented in the following sections.

3.5.3 Multicollinearity

In multiple linear regression analysis, having several independent correlated variables in the model will affect the values of the regression coefficients and in some cases cause the signs to switch to counter-intuitive values. There are several outcomes that result from multicollinearity in the data (Neter, and Wasserman, 1996):

1. Disagreement between the F-test in the overall ANOVA table and the marginal t-tests.
2. Inaccurate estimation of the regression parameters (β s) where some of the β values are negative in multiple linear regression while they are positive in simple linear regression.
3. Large standard errors for the regression parameters.
4. A large Variance Inflation Factor (VIF), which measures how much the variance of a coefficient is increased because of multicollinearity. A $VIF \geq 10$ indicates a serious multicollinearity problem.
5. Correlations of the independent variables. An examination of the correlation matrix showed that the weigh station traffic data for different truck types were highly correlated with each other ($\rho > 0.7$).

3.5.4 Remedies for the Multicollinearity Problem

There are several methods suggested in the literature (Belsley, 1980) to remedy the multicollinearity problem. Some of these methods are outlined below:

1. Remove one or several predictor variables from the model in order to reduce the multicollinearity and standard error of the regression parameters as shown in

Table 3-5 and 3-6. These tables show that truck classes 9 and 13 should be excluded from the analysis to reduce the multicollinearity; however truck class 13 is one of the heaviest trucks and truck class 9 represents 33 % of the total truck populations. Therefore, this method is not preferred since keeping all truck classes in the model is desirable.

Table3-5 Regression coefficients and collinearity statistics for all truck classes

Independent Variable	Unstandardized Coefficients		Standardized Coefficients	t	Sig.	Collinearity Statistics	
	B	Std. Error	Beta			Tolerance	VIF
(Constant)	.211829	.021110		10.034	.000		
Class 5	.000000	.000000	-.010	-.060	.953	.522	1.914
Class 6	-.000001	.000001	-.645	-1.996	.052	.134	7.467
Class 7	.000000	.000002	-.024	-.162	.872	.622	1.607
Class 8	-.000002	.000001	-1.603	-2.015	.050	.022	45.300
Class 9	.000001	.000000	3.241	2.508	.016	.008	119.480
Class 10	-.000002	.000001	-.667	-2.367	.023	.176	5.680
Class 11	-.000008	.000004	-1.158	-2.147	.038	.048	20.808
Class 12	-.000124	.000050	-1.432	-2.502	.016	.043	23.441
Class 13	.000001	.000000	1.614	3.138	.003	.053	18.938

Table 3-6 Regression coefficients and collinearity statistics for all truck classes excluding truck class 9

Independent Variable	Unstandardized Coefficients		Standardized Coefficients	t	Sig.	Collinearity Statistics	
	B	Std. Error	Beta			Tolerance	VIF
(Constant)	.1864365	.0196320		9.497	.000		
Class 5	.0000000	.0000000	-.012	-.068	.946	.522	1.914
Class 6	-.0000007	.0000007	-.324	-1.032	.308	.159	6.301
Class 7	-.0000002	.0000019	-.015	-.093	.926	.623	1.605
Class 8	.0000003	.0000004	.247	.781	.439	.157	6.379
Class 10	-.0000008	.0000007	-.306	-1.193	.240	.238	4.202
Class 11	.0000010	.0000011	.139	.850	.400	.589	1.697
Class 12	-.0000163	.0000262	-.188	-.621	.538	.171	5.855
Class 13	.0000006	.0000003	.862	1.947	.058	.080	12.504

2. Principal component analysis can be used to form one or several composite indices based on the highly correlated predictor variables. The principal components method provides combined indices that are uncorrelated. However, this method also is not preferred since it can lump totally dissimilar truck configurations together as shown in Tables 3-7 and 3-8. As can be seen in the tables each component is composed of all truck classes. Also this method is not desirable for meeting the objective of this research.

Table 3-7 Total variance explained by each component

Component	Initial Eigenvalues		
	Total	% of Variance	Cumulative %
1	4.537	64.819	64.819
2	1.303	18.608	83.427
3	0.761	10.870	94.297
4	0.213	3.047	97.343
5	0.119	1.694	99.037
6	0.051	0.724	99.761
7	0.017	0.239	100.000

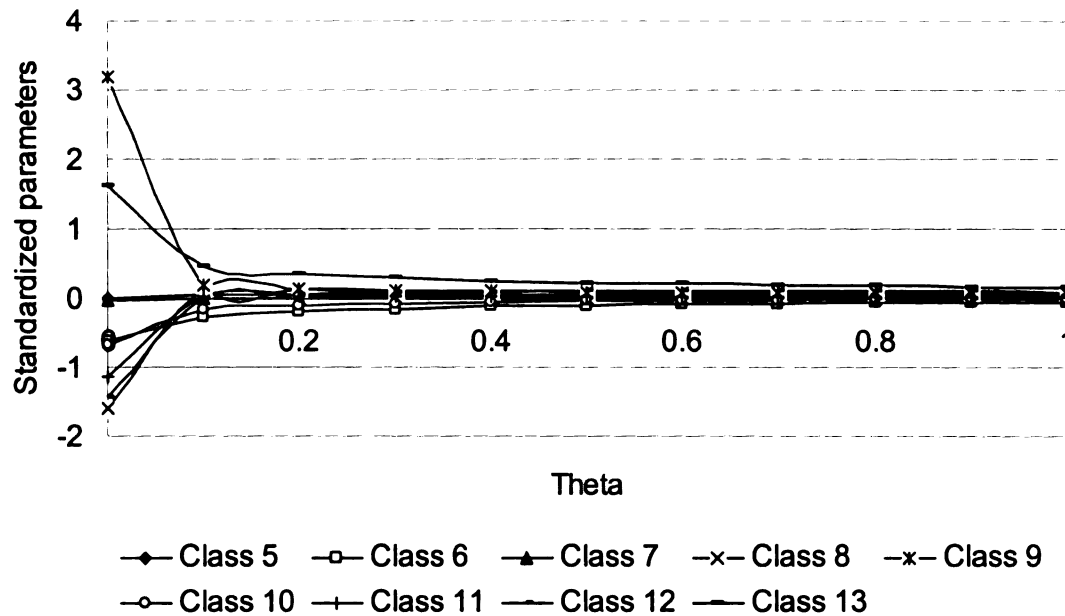
Table 3-8 Component matrix

	Component	
	1	2
Class 6	.886	.350
Class 7	.528	.806
Class 8	.897	.284
Class 9	.953	-.211
Class 10	.870	-.293
Class 11	.694	-.503
Class 13	.721	-.257

- Ridge regression is one of the remedies for such a problem. Ridge regression introduces bias to the diagonal of $X'X$ matrix (where X is $n \times k$ matrix of independent variables, and X' is the inverse of X matrix) for calculating the regression coefficients, shrinks the coefficient values toward zero, and decreases the standard error of the coefficients.

Ridge Regression, RR, has been suggested in the literature as one of the remedy methods that deal with multicollinearity data (Belsley, 1980). RR introduces biasing coefficient, θ , into the regression equation, thereby reducing the estimated coefficient error. The resulting coefficient estimates are biased, but are often more precise than those obtained from standard multiple regression analysis. The desirable θ value can be determined from ridge trace graphs, as shown in Figure 3-11. The appropriate θ value is 0.1 at which the majority of coefficient estimators (β 's) are positive except for classes 6, 10, and 12. The coefficient values cannot be negative since it is impossible to have the total number of trucks increasing while the pavement surface distress decreases. Having the precise regression coefficient estimates will assist in ranking the truck classes/types correctly according to their relative damage to the pavement. However due to the high

collinearity in the data the regression coefficients become positive at higher value of theta which require more bias.



4. Based on engineering judgment, combine similar truck configurations.

The final analysis was done using the last method.

3.6 RESULTS AND DISCUSSION

As mentioned above, the most logical way to compare the effect of different correlated axle/truck configurations and truck classes was to group similar configurations together. Therefore, axles/trucks were categorized into two groups: 1) single-tandem, and 2) multiple axles/trucks. FHWA truck classes have nine different truck types (classes 5 through 13). Classes 7 and 12 were excluded based on their low percentage and class 5 was excluded due to the insignificant effect caused by its light weight. Trucks with single

and tandem axles can be found in classes 6, 8, 9, 10, and 11, while trucks with multiple axles are only in class 13. A given weigh station can be the source of traffic data for several subsections based on their age; while the level of traffic is the same for these subsections, their different ages will make their cumulative traffic different.

The results from the analyses are summarized in Tables 3-9. The results show that multiple axles/trucks are significant and show higher β values than single-tandem axles/trucks, which are not significant. This indicates that rutting is more influenced by heavier loads (axle/truck gross weight), this also agrees with the analytical results of other researchers (Gillespie *et al.*, 1993).

Similar analysis for Distress Index, DI (pavement cracks) and Ride Quality Index, RQI (pavement roughness) are shown in Tables A-3 and A-4 (appendix).

Table 3-9 Effect of different truck/axle configurations on pavement rutting

Axle/Truck Configurations	Independent variables	Simple linear regression			Multiple linear regression			Stepwise regression		
		β	P- value	R ²	β	P- value	R ²	β	P- value	R ²
Axle types	1 and 2	0.399	0.032	0.159	0.059	0.773	0.58	N/S*	NA	0.578
	3, 4, 5, 6, 7, and 8	0.441	0.017	0.194	0.715	0.002		0.790	0.0000	
Truck types	1 and 2	0.283	0.137	0.079	-0.009	0.957	0.584	N/S*	NA	0.584
	3, 4, 5, 6, 7, and 8	0.440	0.017	0.193	0.769	0.0006		0.695	0.0000	
Truck classes	6, 8, 9, 10, and 11	0.395	0.004	0.156	0.073	0.6316	0.412	N/S*	NA	0.409
	13	0.537	0.0004	0.288	0.590	0.0003		0.639	0.0000	

*N/S: not selected by model

CHAPTER 4 - CALIBRATION OF MECHANISTIC-EMPIRICAL RUTTING MODEL

4.1 INTRODUCTION

Since rutting is a major failure mode in flexible pavements, researchers have been trying to predict rut depth for future rehabilitation and budget allocation. There are two main approaches for the prediction of rutting: 1) subgrade strain model (i.e. AI and Shell models) and 2) permanent deformation within each layer. The first approach assumes that most of the rutting results from the subgrade layer only, and is no longer valid based on observations from the field. The second approach considers the rutting contribution from all pavement layers, and is not widely used due to the difficulties of determining the elasto-plastic characteristics of pavement materials. Due to increased tire pressures and new axle configurations as well as observations from the field, researchers began to investigate the rutting contribution from all pavement layers. This approach is also implemented in the new mechanistic-empirical (ME) pavement design guide.

One of the main models related to this approach is the VESYS rutting model that relates the plastic strain to the elastic strain through the permanent deformation parameters (PDPs) μ and α as follows:

$$\varepsilon_p(n) = \mu * \varepsilon_e * n^{-\alpha} \quad (4-1)$$

The most essential task in using this model is to accurately calculate PDPs (μ and α) for each pavement layer within the pavement system. As mentioned earlier in chapter 2 (section 2.4.2), several attempts have been made to estimate these parameters; however agreement between studies varies. Yet, the previous research provides a common, but wide range for these parameters. As can be seen in Equation 4-1, α is an exponent and therefore prediction

of rutting is very sensitive to small changes in the α -value. In this research, PDPs were backcalculated by matching the rut time series data from the SPS-1 experiment in the LTPP program. The most novel aspect of this backcalculation process involved the application of the approach developed in NCHRP 468 (White *et. al.*, 2002), which uses transverse surface profiles to locate the layer causing most of rutting. Using this process, a unique solution for these parameters was attained for each pavement section within the SPS-1 experiment– a result that was empirically unattainable from previous approaches. PDPs were then related to pavement material properties, climatic conditions, and particular pavement cross-sections through regression analysis of SPS-1 experiment data.

4.2 SPS-1 EXPERIMENT

The Specific Pavement Study-1 (SPS-1) experiment includes eighteen sites with twelve pavement sections each, for a total of 216 sections located in all four LTPP climatic regions: Wet Freeze (WF), Wet-No-Freeze (WNF), Dry Freeze (DF), and Dry-No-Freeze (DNF). The locations of SPS-1 sites within the United State are shown in Figure 4-1. The SPS-1 experiment includes a wide range of pavement structures (different HMA/base/subbase thickness and base types) in various site conditions (traffic level, subgrade type and climate). Table 4-1 shows the descriptive statistics for the SPS-1 variables.

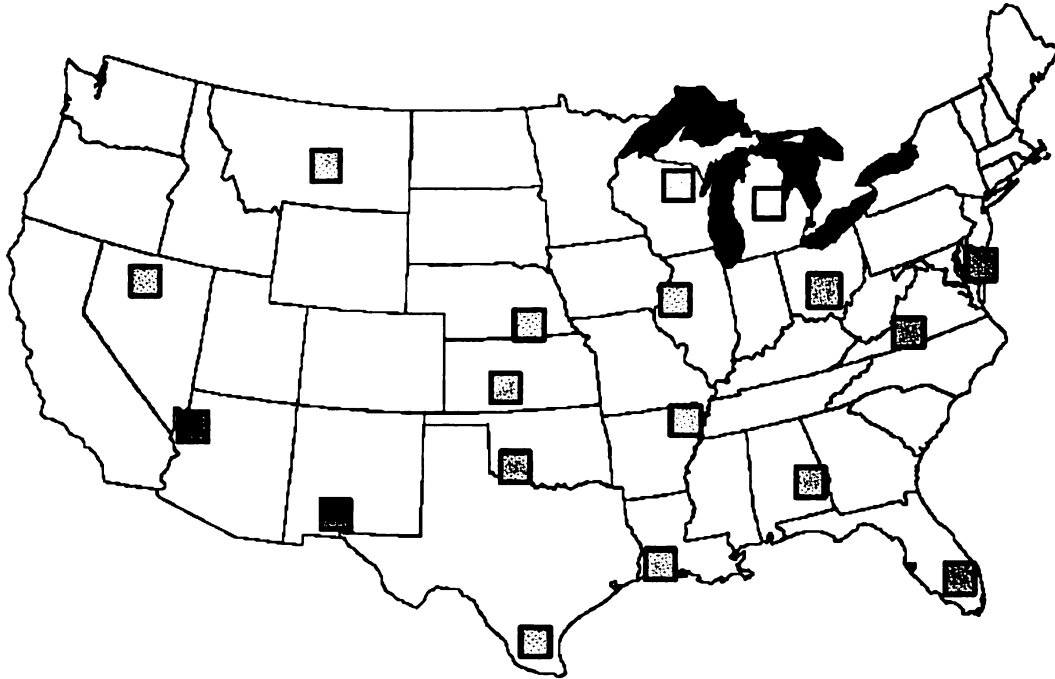


Figure 4-1 Location of the SPS-1 sites

Table 4-1 Descriptive statistics for SPS-1 experiment (LTPP database release 18)

Variables	Minimum	Maximum	Average	St. dev.	COV %
HMA thickness, in	3.4	9.5	5.75	1.5	26
Base thickness, in	7.1	17.9	11.14	2.88	25.8
Rut depth, mm	3	30	8.62	5.31	61.6
KESAL/year	113	524	279	126	45.2
Age, year	0.83	10.2	6.5	2.34	36
FI*, °C-day	0	988	226	276	121.7
AARF**, mm	221	1539	846	402	47.5

* Freezing index

** Average annual rain fall

1 inch = 2.54 cm

4.2.1 SPS-1 data used in the analysis

The SPS-1 data used in this research are as follows:

- Initial Falling Weight Deflectometer (FWD) data for backcalculation of pavement layer moduli,
- Time series rutting data for minimizing the error between predicted and measured rut depth,
- Transverse profile data to locate rutting within individual pavement layers,
- Traffic data for rutting prediction,

- Pavement layer thicknesses for backcalculation of material properties and regression analysis to predict permanent deformation parameters,
- Climatic data for regression analysis to predict permanent deformation parameters, and
- Material properties for regression analysis to predict permanent deformation parameters.

4.3 VESYS MODEL

The original form of VESYS rutting model is based on the assumption that the permanent strain is proportional to the resilient strain so that:

$$\varepsilon_p(n) = \mu \varepsilon_e n^{-\alpha} \quad (4-2)$$

where

- $\varepsilon_p(n)$ = the permanent or plastic strain due to a single load application,
- ε_e = the elastic or resilient strain at 200 repetitions,
- n = the number of load applications,
- α = permanent deformation parameter indicating the rate of decrease in permanent deformation as the number of load applications increases (hardening effect),
- μ = permanent deformation parameter representing the constant of proportionality between plastic and elastic strain.

The total permanent deformation can be obtained by integrating Equation 4-2 as follows:

$$\varepsilon_p = \int_0^n \mu \varepsilon_e n^{-\alpha} dn = \frac{\mu}{1-\alpha} \varepsilon_e n^{1-\alpha} \quad (4-3)$$

The cumulative permanent deformation, ρ_p in all pavement layers from all load groups can be calculated from the following equation:

$$\rho_p = \sum_{j=1}^L h_j \frac{\mu_j}{1-\alpha_j} \left(\sum_{i=1}^k \varepsilon_{e_{i,j}} n_i^{1-\alpha_j} \right) \quad (4-4)$$

where

- $\varepsilon_{e_{i,j}}$ = the vertical compressive strain at the middle of layer j due to load group i ,

α_j and μ_j = PDPs for layer j .

Determining the actual values for the PDPs for each pavement layer is the most challenging task to achieve an accurate rutting prediction. The flow chart in Figure 4-2 shows the process used to predict the values of α and μ from in-service pavements in the SPS-1 experiment.

4.4 BACKCALCULATION OF PAVEMENT LAYER MODULI

In this analysis, the initial layer moduli for each SPS-1 pavement section were backcalculated using Falling Weight Deflectometer (FWD) data obtained after the initial construction of the test sections. The MICHBACK computer program was used for the (static) backcalculation.

4.4.1 MICHBACK computer program

There are several computer programs that can be used for backcalculation of the pavement layer moduli such as MICHBACK, MODCOMP, MODULUS, and EVERCALC.

Backcalculation analysis was performed for two pavement sections, which have known layer moduli (from the forward analysis), using the four backcalculation programs (Svasdisant, 2003). The MICHBACK computer program produced similar, and in some cases better results over other backcalculation programs. Moreover, each SPS-1 section has 11 or more FWD measurements, and each point location requires backcalculation of the layer moduli. The MICHBACK computer program can carry out backcalculation of all these point locations at once, which simplifies the analysis and makes it more efficient.

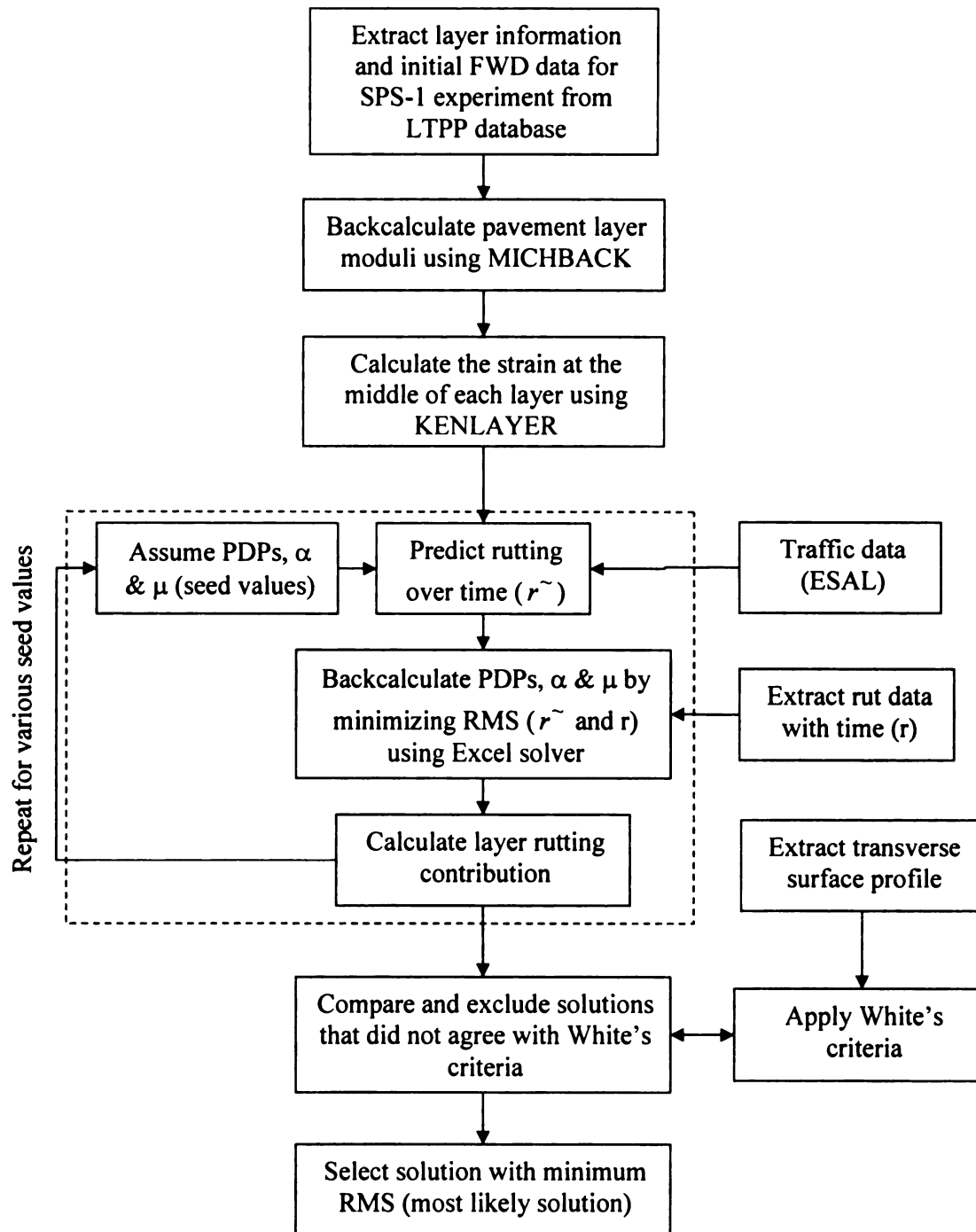


Figure 4-2 Flow chart of calibration of mechanistic-empirical rutting model (VESYS) using SPS-1 experiment

In this study, the backcalculation of layer moduli for all SPS-1 sections was conducted in order to calculate the vertical compressive strain at the middle of each pavement layer. The process of layer moduli backcalculation yields a variety of possible values, some of which are highly improbable (i.e. sub-layers with higher moduli than the HMA layer). Therefore, the following section will highlight the procedures used during the backcalculation to insure accurate estimation of pavement layer moduli.

4.4.2 Quality control of the backcalculation procedures

Several steps were used to ensure accurate and reliable backcalculation of pavement layer moduli as follows (Schorsch, 2003):

- The solutions converge, which means the difference between two consecutive solutions is smaller than a specified tolerance limit. This criterion was used to eliminate any unacceptable results. If the solution did not converge several trials were made to combine or separate (subgrade) layers and/or introduce a stiff layer. The sections with convergent moduli values were used in the later analysis of this research, while all others were eliminated.
- Low RMS values provide high accuracy backcalculation results and assure close matches of the measured and calculated deflection basins. Figure 4-3 shows the distribution of RMS (%) for all point locations within the SPS-1 experiment. Though all data were initially included, later procedural steps eliminated those with unacceptable RMS% values.
- HMA layer moduli > base layer moduli > roadbed soil moduli. This criterion is based on the principles of pavement design which call for decreasing the pavement modulus with depth. This was held as a general rule, but if the solution did not meet this criterion other trials with pavement layer combinations or stiff layers were introduced.
- A roadbed modulus criterion of < 60000 psi was employed to eliminate unreasonable moduli for natural subgrade soil.

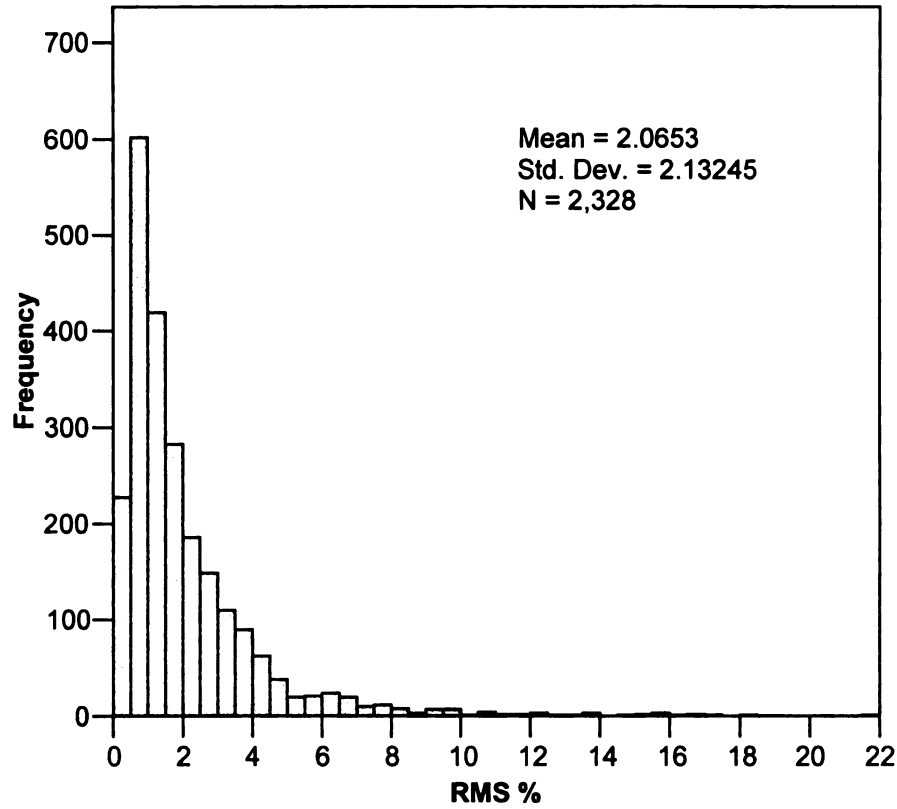


Figure 4-3 Distribution of RMS (%) for all point locations within SPS-1 experiment

In parallel with the above criteria, examining the presence of a stiff layer for each SPS-1 section was taken into consideration to improve the backcalculation procedure. The deflection data can be utilized to calculate the surface modulus which represents the weighted mean modulus of the half space. The surface modulus calculated using Boussinesq's equations [Ullidtz, 1987].

$$E_o(0) = 2 * (1 - \mu^2) * \sigma_o * \frac{a}{d(0)} \quad (4-5)$$

$$E_o(r) = (1 - \mu^2) * \sigma_o * \frac{a^2}{(r * d(r))} \quad (4-6)$$

where

$E_o(r)$ = surface modulus at a distance r from the center of the FWD loading plate

μ = Poisson's ratio

σ_o = contact stress under the loading plate

$d(r)$ = deflection at a distance r

Figure 4-4 shows an example of the relationship between the equivalent modulus and the distance from the center of the FWD loading plate at different point locations within the section. If the equivalent modulus value at the tail of the curve remains constant with increasing distance, it indicates a deep or non-existent stiff layer and linear elastic behavior of subgrade as shown in Figure 4-4 (a) . If the equivalent modulus value at the tail of the curve increases with increasing distance, it indicates the presence of a shallow stiff layer and nonlinear elastic behavior of subgrade as shown in Figure 4-4 (b). If the equivalent modulus value at the tail of the curve decreases with increasing distance, it indicates no presence of stiff layer and nonlinear elastic behavior of subgrade as shown in Figure 4-4 (c). Taking into account an existing stiff layer helps the solution to converge; however the exact depth of the stiff layer was determined by trials according to the minimum RMS. In this study, only linear elastic backcalculation analyses were considered (Ullidtz, 1987).

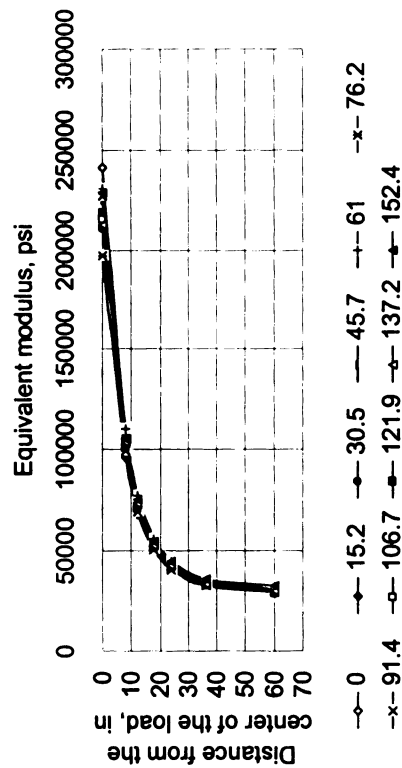
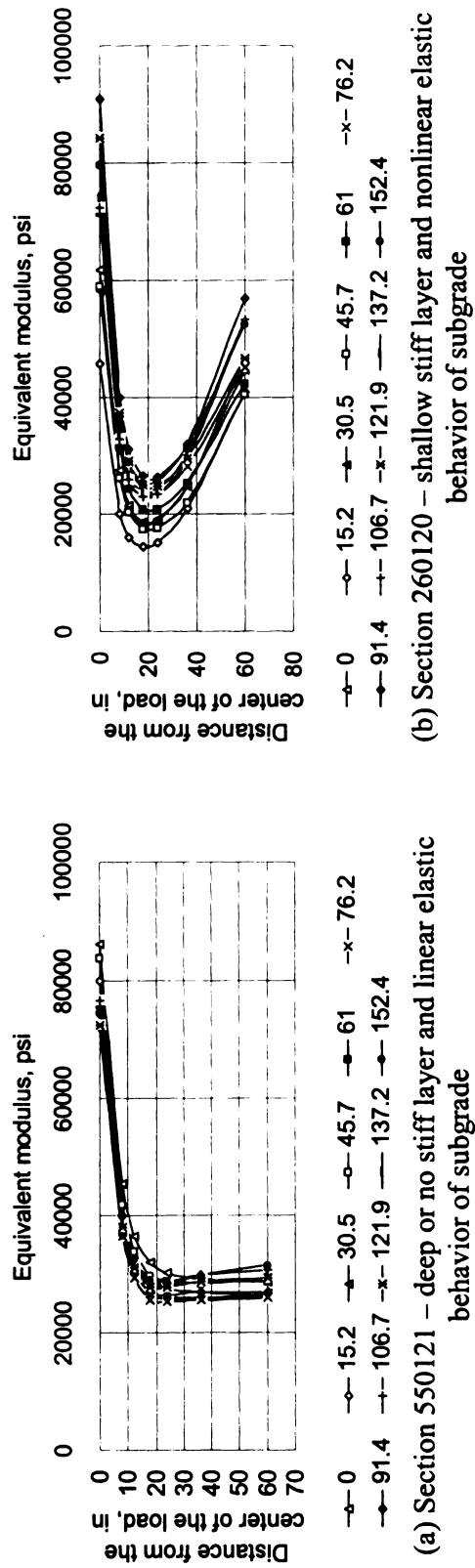
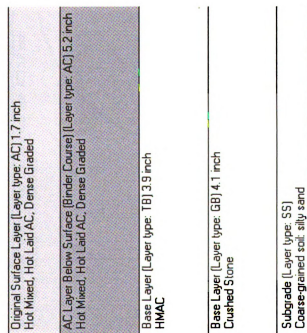


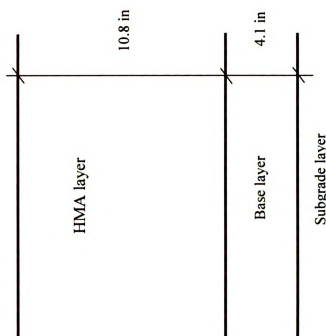
Figure 4- 4 Equivalent pavement modulus versus the distance from the center of the load at different point locations within the section.

4.4.3 Combination /separation of pavement layers

MICHBACK computer program can backcalculate the layer moduli for 3 to 5 layers, however the backcalculation for 5 layers is less accurate. Also, increasing the number of layers will increase the number of PDPs since each layer has two unknown parameters. In most cases, the SPS-1 sections have more than 4 pavement layers. Therefore, the combination of similar pavement layers or division of the subgrade into two layers was taken into consideration in order to treat the pavement structure as a 3- layers system. This allowed the highest accuracy backcalculation and minimized the number of unknown permanent deformation parameters. Figure 4-5 shows an example of pavement section with (a) as constructed layers and (b) pavement layer thicknesses used in the backcalculation procedure. The HMA layers and the treated base layer were combined together as one HMA layer (as shown in Figure 4-5 (b)) and an average modulus was used for forward analysis. On the other hand, when no granular base existed in the design the treated base layer was used as a separate layer in the backcalculation. If this solution did not converge, the treated base was assumed to be part of the overall HMA layer and a 24-inch layer of the subgrade was treated as a base layer, with the rest of the subgrade below considered as the third layer as shown in Figure 4-6.



(a) Section 5-0117

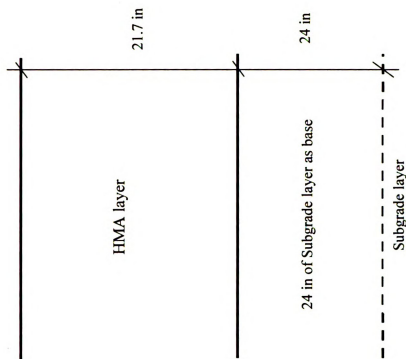


(b) Backcalculated layers

Figure 4-5 Pavement layer thicknesses for conventional pavement

Original Surface Layer (Layer type: AC) 11.3 inch Hot Mixed, Hot Lead AC, Dense Graded
AC Layer Below Surface (Binder Course) (Layer type: AC) 5.6 inch Hot Mixed, Hot Lead AC, Dense Graded
Base Layer (Layer type: B) 11.3 inch HMAC
Base Layer (Layer type: B) 3.5 inch Open Graded, Hot Lead, Central Plant Mix
IndiLayer (Layer type: EF) 0.1 inch Woven Geotextile
Subgrade (Layer type: SS) Coarse Grained Soil, Poorly Graded Sand with Silt

(a) Section 5-0124



(b) Backcalculated layers

Figure 4-6 pavement layer thicknesses for full depth asphalt

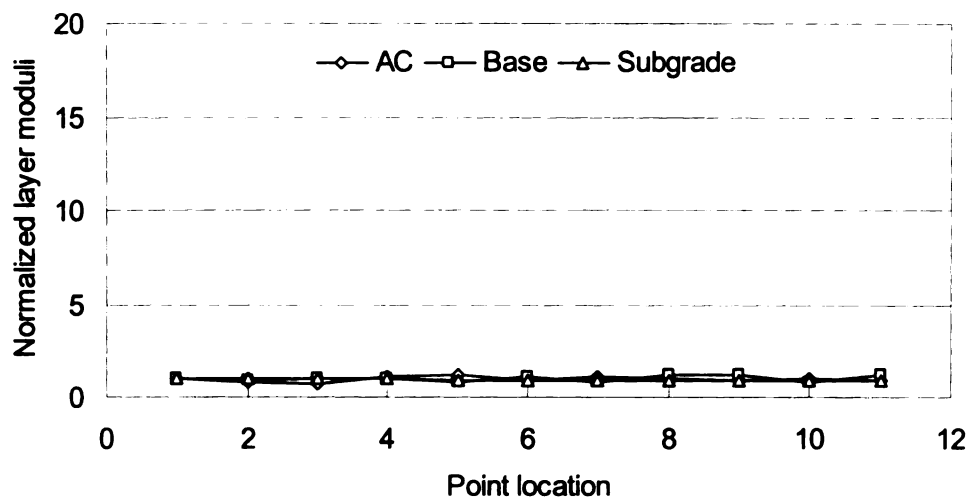
4.4.4 Modulus variation in the longitudinal direction

The length of each SPS-1 pavement section is 500 ft with 11 or more point locations for collecting FWD data. Sometimes, the inconsistency of pavement layer thickness, material variability, and computational quality among other factors cause large variations in the backcalculated moduli between point locations. Hence, the layer moduli variability in the longitudinal direction of each section was tested. All pavement layer (HMA, base, subgrade) moduli were normalized to the first point location, and other point locations were checked against this point for all pavement sections. Figure 4-7 shows two example modulus variations for the pavement layers along the longitudinal direction of two sections. Figure 4-7 (a) shows the modulus variations for section 50113 where there are acceptable modulus variations along the longitudinal direction. Figure 4-7 (b) shows huge variations in the base modulus which might be due to inconsistency in the base thickness.

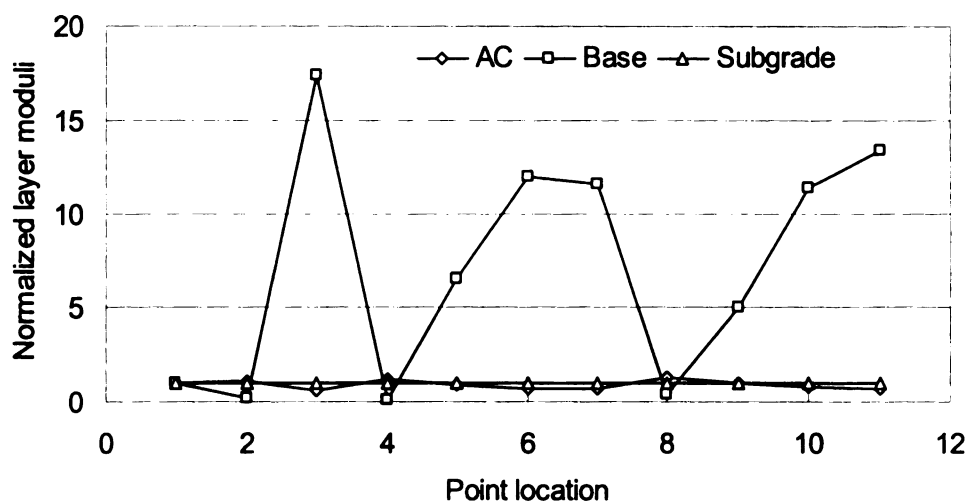
4.4.5 Summary of the backcalculation procedure

As explained above, there are many steps in determining layer moduli that extend beyond the simple backcalculation output. The results of the backcalculation procedure as output from programs often require additional attention and discrimination. Great effort went into the backcalculation procedure through several trials and checking steps to ensure the backcalculated moduli are the most suitable ones. After applying all the quality control steps, the number of sections reduced from 216 to 159 sections. All sections with HMA, granular base, and subgrade layers (conventional pavements) were categorized as one group (120 sections). These sections should have a common set of 6 unknown PDPs (two for each layer). Sections with HMA and subgrade layers (full-depth asphalt pavements) were categorized as another group (39 sections). This group should have a common set of 4 unknown PDPs (2 for the HMA layer and 2 for the subgrade layer). Table 4-2 shows the

descriptive statistics of HMA and base thicknesses as well as layer moduli for the final 109 sections that used for backcalculating the PDPs.



(a) section 5-0113



(b) section 30-0123

Figure 4-7 Modulus variations for the pavement layers along the longitudinal direction

Table 4-2 Descriptive statistics for final backcalculation procedures (109 sections)

Variables	Minimum	Maximum	Average	St. dev.	COV %
HMA thickness, in	4.0	22.2	11.56	4.27	36.94
Base thickness, in	3.5	46.1	18.77	11.62	61.91
HMA modulus, psi	69,201	2,778,015	686,030	567,971	82.79
Base modulus, psi	4,599	2,499,710	118,191	345,501	292.32
Subgrade modulus, psi	15,099	57,984	29,980	8,757	29.21

4.4.6 HMA modulus temperature correction

The FWD test temperature varies with time and space even between point locations within the same section. Therefore, the backcalculated HMA modulus needs to be corrected for the standard temperature of 68°F (20°C). The following equation was used (Park, 2000):

$$CF = 10^{0.0224(T-T_r)} \quad (4-7)$$

where

CF = Temperature correction factor
 T = Mid-depth temperature (°C)
 T_r = Reference temperature of 20°C

The backcalculated HMA modulus is multiplied by CF to normalize the modulus to the reference temperature. Park (2000) developed an empirical equation to predict the temperature at the mid-depth of the HMA layer from the measured surface temperature.

$$T_h = T_{surf} + (-0.3451h - 0.0432h^2 + 0.00196h^3) * \sin(-6.3252t + 5.0967) \quad (4-8)$$

where

T_h = HMA temperature at depth h in °C
 T_{surf} = HMA temperature at the surface in °C
 h = mid-depth of HMA at which temperature is to be determined in cm
 t = time when the HMA surface temperature was measured in days ($0 < t < 1$, e.g., 1:30 pm = $13.5/24 = 0.5625$ days)

4.5 FORWARD ANALYSIS

The VESYS model relates the plastic strain occurring in each pavement layer to the vertical elastic compressive strain in that layer. There are several computer programs for conducting the forward analysis such as ELYSYM5, VESYS, MICH-PAVE, ILLI-PAVE, and DAMA.

The KENLAYER computer program was developed by Huang (1993). He compared the forward analysis of all of these computer programs with KENLAYER results. The solution of the KENLAYER program gave similar or better results for all types of analyses.

Therefore, the KENLAYER computer program was used to calculate the vertical compressive strain at the middle of each pavement layer, assuming that the mid-depth strain represented the average layer strain.

To calculate the total rut depth resulting from all layers, it is essential to calculate the strain in the sub-layers until the strain is no longer detectable. Based on the assumption that there is no deformation beyond a certain depth in the subgrade, the subgrade was divided into six 40-inch layers and the calculation of vertical compressive strain performed until the strain approached zero. Figure 4-8 shows the division of the subgrade layer into six 40-inch sub-layers. Also, Figure 4-9 shows the strain values at the middle of each pavement layer for 5 different SPS-1 sections caused by one standard 18-kips single axle. As shown in the figure the strain at the middle of the sixth layer has a very small value, as expected.

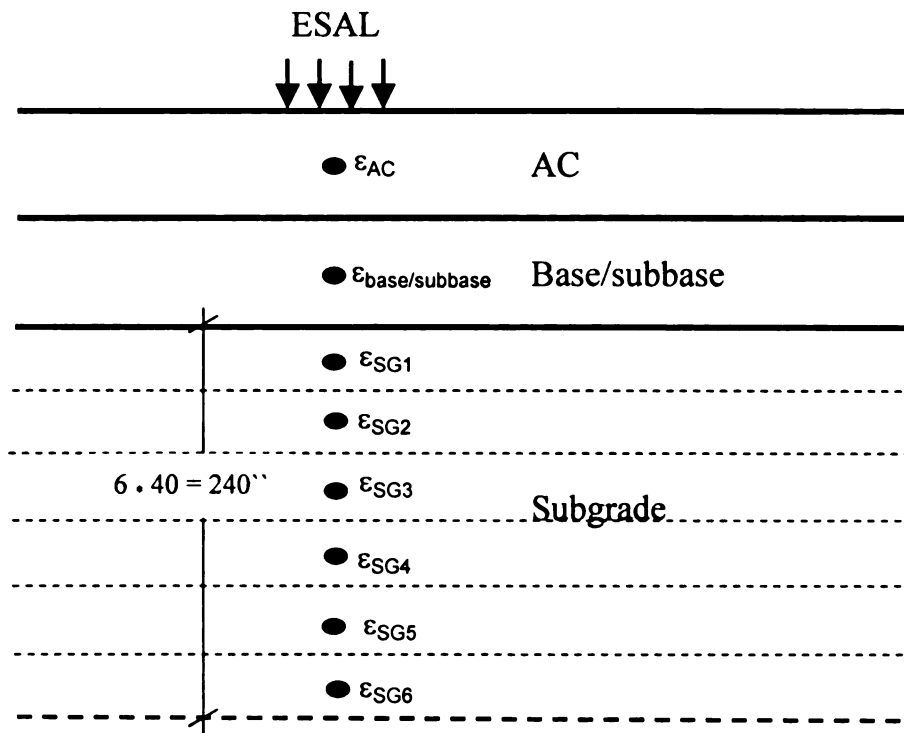


Figure 4-8 Division of the subgrade layer into several sub-layers

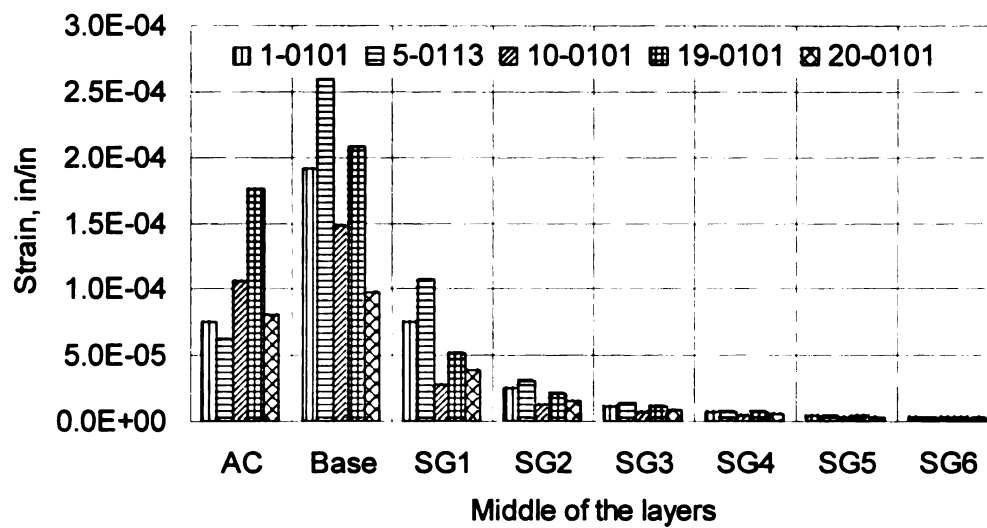


Figure 4-9 Strain at the middle of pavement layers for 5 different SPS-1 sections

4.6 MEASURED RUT DATA FROM IN-SERVICE (SPS-1) PAVEMENTS

The Long Term Pavement Performance (LTPP) database includes time series rutting data for all SPS-1 sections. Figure 4-10 shows the progression of rutting with time for all SPS-1 sections. As shown in the figure some of these sections showed premature rutting due to material- or construction-related problems. These sections were excluded from the proceeding analysis since the VESYS model can not predict premature rutting. More details analysis regarding to premature rutting due to material- or construction-related problems and structure rutting can be found in NCHRP 20-50 (10/160) report (Chatti *et al.*, 2005).

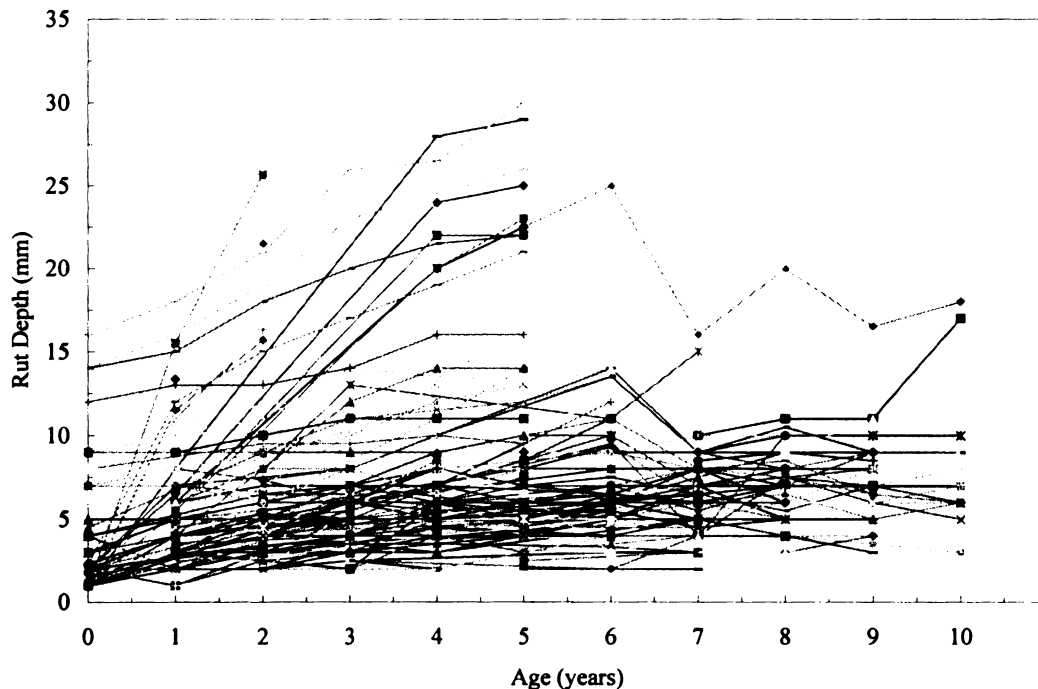


Figure 4-10 Rutting with time for SPS-1 pavements - All sections

4.6.1 Filtering the measured rut data

Due to the inconsistency of field measurements with time, there was some variability of the measured rut depth. Therefore, in order to have a consistent time series trend, the rut depths which were believed to be caused by the measurement variability/error were removed from the original data, especially where no maintenance action was carried out. Making the time

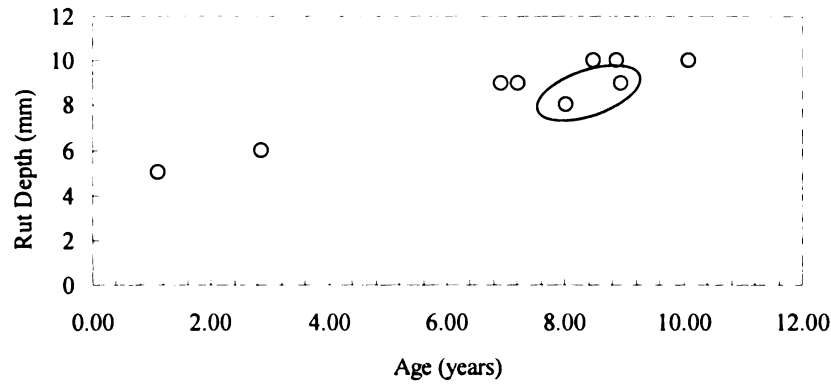
series trend smoother helped in achieving a better optimization (minimizing the RMS between measured and predicted) as explained in the proceeding section. Figure 4-11 (a) shows an example of a pavement section (1-0105) where only two points at year 8 and 10 have shown a lower rut depth compared to the existing time series trend. However, no maintenance was performed at that time; therefore, these two points were considered as faulty measurements and were deleted for this section. Figures 4-11 (b) and (c) show the cleaned rut data with time and load with the time series trend. A similar procedure to clean the time series rut depth data was adopted for all the pavement sections in the SPS-1 experiment. The VESYS rutting model was used to determine the PDPs for each section by minimizing the error between the actual field data and the predictions. This is explained in detail in the following sections.

4.7 BACKCALCULATION OF PERMANENT DEFORMATION PARAMETERS

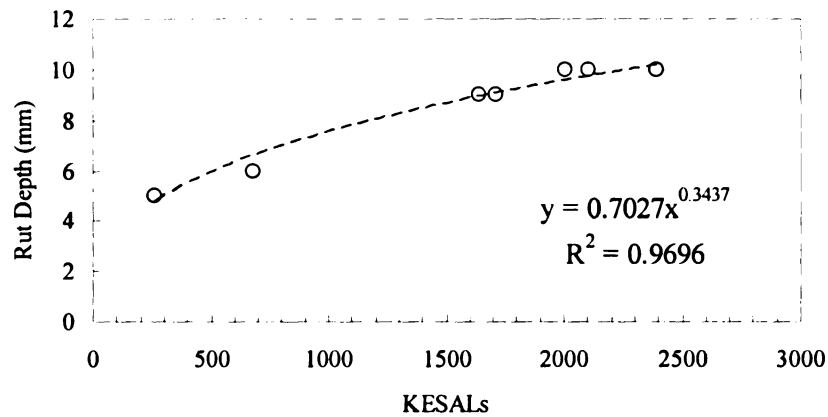
The backcalculation was performed based on three layers, HMA, base, and subgrade. Each layer has two PDPs (α and μ); therefore a total of six parameters need to be backcalculated for each SPS-1 section. The parameter α represents the rate of decrease in permanent deformation as the number of load applications increase (hardening/densification effect).

The parameter μ represents the constant of proportionality between plastic and elastic strain due to the repetition of each load. As shown in equation 4-2, the number of load repetitions (n) is raised to the power $-\alpha$, therefore α is site-specific and has to be backcalculated by changing the number of load repetitions (i.e. using time series rutting data for each section).

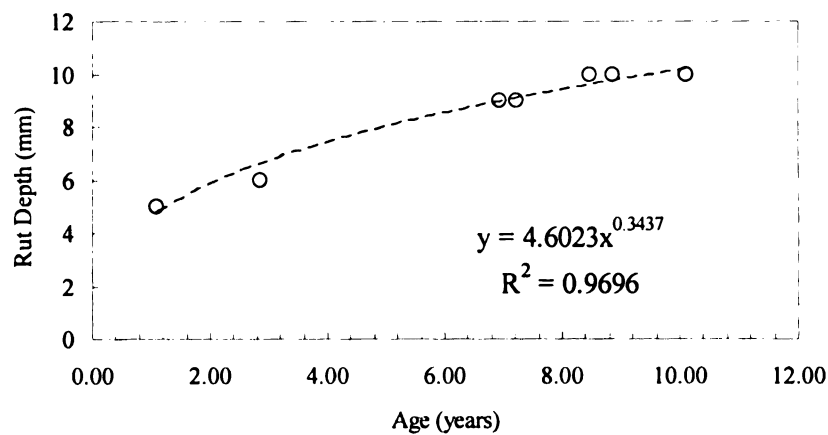
Rutting can be predicted by using seed values for α and μ , such as those provided in Chapter 2 (Table 2-1).



(a) original rut data versus time



(a) cleaned rut data versus load



(b) cleaned rut data versus time

Figure 4-11 Measured time series rutting data for section 1-0105

These six PDPs were backcalculated for each pavement section using Microsoft Excel "Solver," by minimizing the Root Mean Square (RMS) difference between the

measured and the predicted rutting. The following equation shows the optimization procedure:

$$\text{minimize } F = \sum_{i=1}^s (\rho_i - RD_i)^2 \quad (4-9)$$

where:

- F = function to be minimized by changing α and μ ,
- ρ_i = predicted rut depth from equation 4-4,
- RD_i = measured rut depth in the field,
- s = total number of rutting measurements in the field over time.

For backcalculating the six parameters simultaneously, a good agreement (small RMS) between measured and predicted rutting can be achieved; however the solution is not unique. In other words, the backcalculated parameters are dependent on the seed values. This was due to the various possible distributions of rutting throughout the multiple pavement layers which still match the total surface rutting, and yet did not match the actual rutting percentage for each individual layer. Table 4-3 shows the backcalculation of PDPs using different seed values. In the first ten solutions, the same seed values were used for all six parameters, while the remaining solutions have different seed values (according to results from previous research, see Table 2-1) for each parameter. The RMS values, after the third solution, were very small (less than 1%) and close to each other which indicate good agreement between the measured and predicted rut depth. However, each solution gives completely different rut percentage for each pavement layer, yet the total rutting for all layers matches well with the measured surface rutting. The question now is which solution is closest to the actual pavement behavior?

The most logical way to solve this problem involves knowing the rut percentage within each pavement layer, such that only two parameters can be calculated at one time. There are several ways to determine the percent rutting for each pavement layer:

- Assume the percent rutting within each pavement layer based on other studies. However these percentages are section-specific and depend on the pavement material properties, load, and climatic conditions. Therefore, it is not suitable to generalize this assumption for different pavement sections,
- Cut trenches and measure the rutting contribution from each layer. However, the inconsistency of the pavement layer thicknesses along with the noise caused by the erratic sub-layer boundary make the measurement of layer contribution difficult to determine (Chen *et al.*, 2003).
- Install Linear Variable Differential Transformer (LVDT) instruments (e.g., a device such as the Multi-Depth Deflectometer, MDD). However, these instruments are very expensive and not suitable for long-term investigation due to durability issues (they may be suitable for accelerated pavement tests) (Zhou and Scullion, 2002 and Huang, 1993).
- Measure the transverse surface profile of the pavement. Using transverse surface profiles, the contribution of each pavement layer can be identified as a percentage of the total rutting. The required data are available for each section, require less complicated and non-destructive procedures to collect, and can be easily monitored over time while the pavement is in-service. The LTTP database includes transverse surface profile data for all SPS-1 sections as part of the monitoring data. In addition, agencies are increasingly collecting transverse surface profiles instead of measuring only the maximum rut depth. Therefore, this extensive data were used as a means for solving the problem of unique parameter solutions.

Though a method for determining percentage of rutting within each layer is available, there remain constraints on the possible values for each parameter.

4.7.1 Backcalculation parameters constraints

Investigating the VESYS rutting model (Equation 4-4) showed that α represents the rate (progression) of permanent deformation and operates within the exponent of the number of load applications as $(1-\alpha)$. Increasing the number of load applications will increase the

rutting rate, meaning the exponent must be a positive value. So α is constrained to a range of values between 0 and 1. Lower values of α indicate higher rutting rates, and vice versa. The parameter μ represents the constant of proportionality between plastic and elastic strains in Equation 4-4. Since rut depth is defined as a positive value, the value of μ has to be positive. Low values of μ indicate low initial rutting while higher μ values (>1) indicate premature rutting. These constraints were taken into consideration in the optimization procedure that involved choosing seed values from the transverse surface profiles.

4.7.2 Transverse surface profile

Several researchers have analyzed the transverse surface profile (Simpson, *et al.*, 1995, White, *et al.*, 2002 and Villiers, *et al.*, 2005). The shape of the transverse surface profile is a good indication of where the rutting originated within the pavement structure. Simpson, *et al.*, 1995 developed criteria for analyzing the transverse surface profile such that one can locate the individual failed layer (the most probable contributor to the rutting). Furthermore, White *et al.*, 2002 refined these criteria by applying finite element analysis. Based on the refined criteria, Figures 4-12, 4-13, and 4-14 show examples of transverse surface profiles for failed HMA, base, and subgrade layers, respectively. The criteria used for this research are discussed in the following section.

Table 4-3 Backcalculation of PDPs using different seed values for section 1-0105

Solution #	Seed parameter	μ_{HMA}	μ_{Base}	μ_{SG}	α_{HMA}	α_{Base}	α_{SG}	RMS%	HMA rut %	Base rut %	SG rut %
1	0.01	0.010	0.011	0.010	0.346	0.363	0.999	7.860	27%	73%	0%
2	0.1	0.014	0.015	0.011	0.297	0.469	0.646	7.660	68%	26%	6%
3	0.2	0.010	0.113	0.081	0.681	0.544	0.693	1.055	0%	74%	25%
4	0.3	0.303	0.282	0.295	0.597	0.632	0.999	0.713	35%	65%	0%
5	0.4	0.368	0.356	0.412	0.670	0.633	0.999	0.661	18%	82%	0%
6	0.5	0.406	0.391	0.427	0.630	0.657	0.999	0.668	32%	68%	0%
7	0.6	0.515	0.532	0.523	0.584	0.758	0.999	0.642	68%	32%	0%
8	0.7	0.559	0.320	0.010	0.723	0.622	0.842	0.656	16%	84%	1%
9	0.8	0.024	0.010	0.448	0.346	0.999	0.982	0.499	60%	0%	40%
10	0.9	0.010	0.486	0.010	0.904	0.657	0.553	0.658	0%	85%	15%
11	Lower Limits of Kenis and Wang*	0.571	0.185	0.012	0.584	0.688	0.830	0.761	76%	23%	1%
12	Middle limits of Kenis and Wang	0.480	0.199	0.056	0.636	0.609	0.983	0.639	35%	60%	5%
13	Upper limits of Kenis and Wang	0.539	0.301	0.015	0.605	0.680	0.732	0.657	56%	41%	3%
14	Lower Limits of Bonaquist**	0.044	1.582	0.010	0.411	0.838	0.631	0.564	48%	46%	6%
15	Middle limits of Bonaquist	0.218	0.146	0.154	0.583	0.769	0.667	0.671	29%	8%	63%
16	Upper limits of Bonaquist	0.679	0.015	0.134	0.967	0.988	0.619	0.639	5%	1%	94%

* Kenis and Wang, 1997

** Bonaquist, 1996

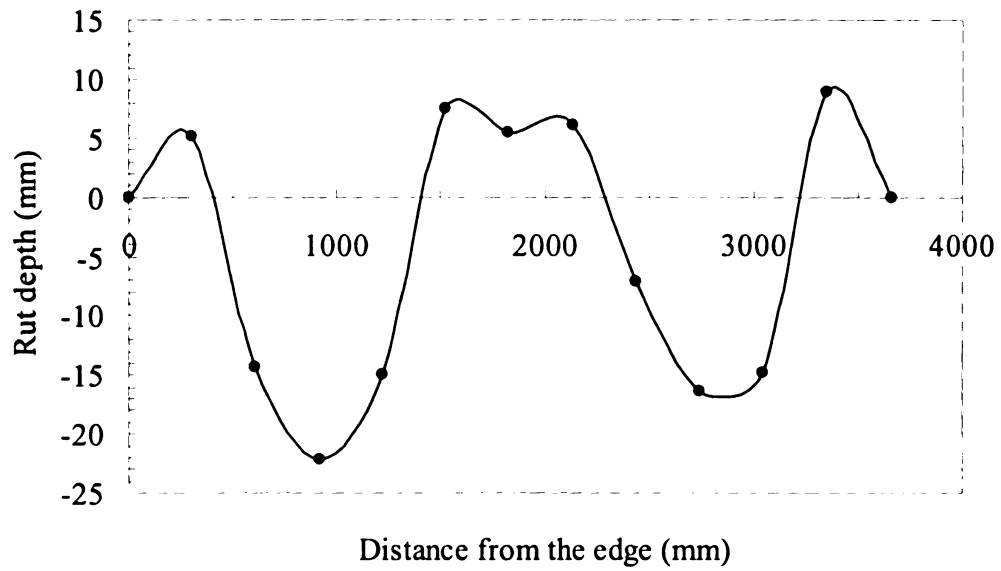


Figure 4-12 Transverse surface profile for HMA layer rutting—Section 31-0113

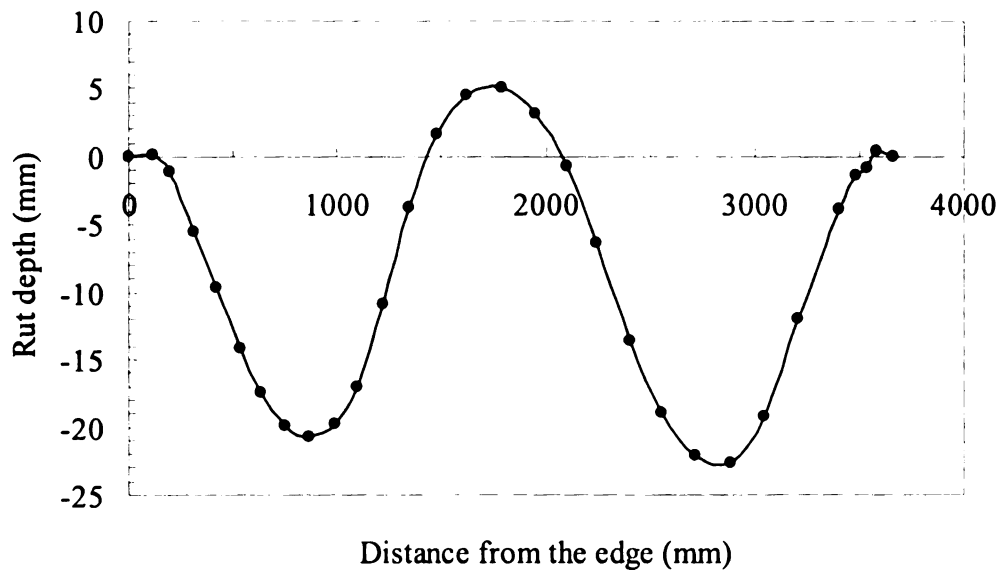


Figure 4-13 Transverse surface profile for base rutting—Section 20-0102

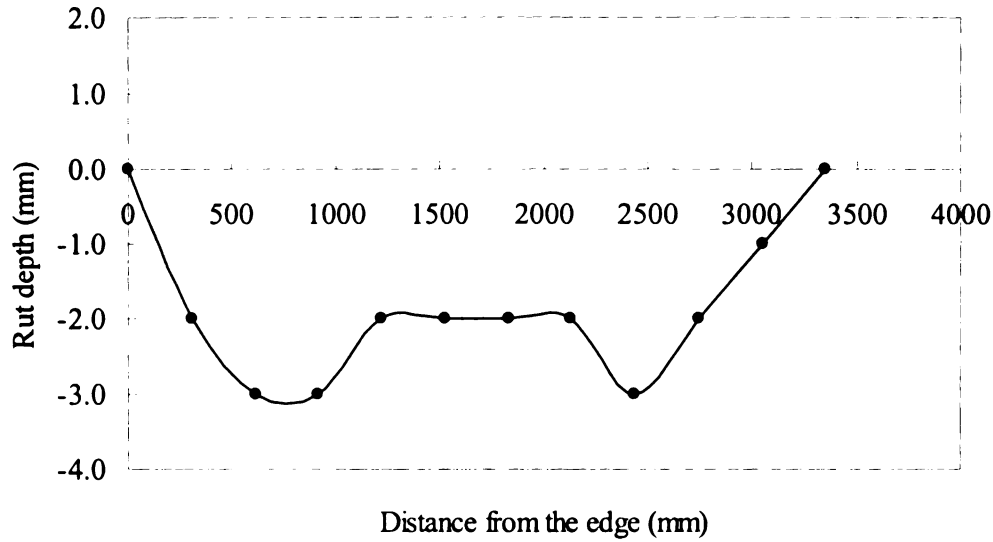


Figure 4-14 Transverse surface profile for subgrade rutting—Section 32-0110

4.7.3 Transverse surface profile analysis criteria

The following equations represent the criteria developed by White, *et. al* to determine the failed layer identity using transverse surface profile data:

$$A = A_p + A_n \quad (4-10)$$

$$R = \left| \frac{A_p}{A_n} \right| \quad (4-11)$$

$$C_1 = (-858.21)D + 667.58 \quad (4-12)$$

$$C_2 = (-1509)D - 287.78 \quad (4-13)$$

$$C_3 = (-2,120.1)D - 407.95 \quad (4-14)$$

where:

A = total area

A_p = positive area (see Figure 4-15)

A_n = negative area (see Figure 4-15)

R = area ratio

C_1 = theoretical average total area for HMA failure, mm^2

C_2 = theoretical average total area for base/subbase failure, mm^2

C_2 = theoretical average total area for subgrade failure, mm^2

D = maximum rut depth, mm (see Figure 4-16)

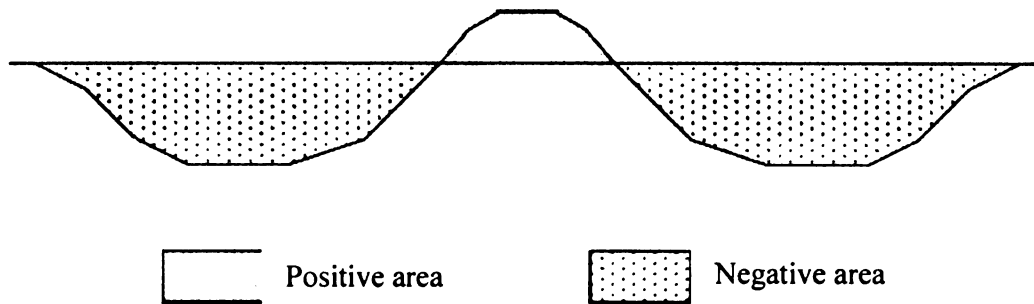


Figure 4-15 Definition of positive and negative area in transverse surface profile
(White, *et al.*, 2002)

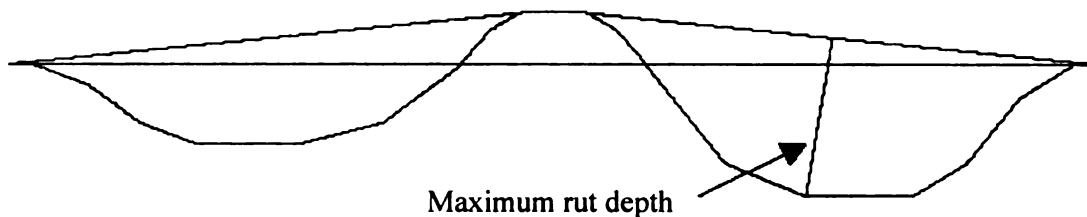


Figure 4-16 Definition of maximum rut depth (White, *et al.*, 2002)

Based on the characteristics of a given surface profile and the criteria described above, the following outcomes can be predicted:

(a) Failure will occur in the HMA layer if:

$$R > 0.05 \quad \text{and} \quad A > (C_1 + C_2)/2$$

(b) Failure will occur in the base/subbase layer if:

$$R < 0.05 \quad \text{and} \quad A > (C_2 + C_3)/2$$

(c) If none of the above criteria are satisfied, that suggests subgrade layer failure.

4.7.4 Unique solution for backcalculation of permanent deformation parameters

The problem of parameter uniqueness described previously can be dealt with by combining backcalculation strategies with transverse surface profile analysis. This combination of procedures overcomes the uniqueness problem for the backcalculation of the PDPs by

limiting the number of realistic candidates. In applying this technique to section 1-0105 (as shown in Table 4-3), the following steps are required:

- Backcalculate the parameters using different typical seed values (as shown in Table 2-2).
- For each solution calculate the RMS error and the percent rutting from each layer as shown in Table 4-3. Since the RMS error is minimized when there is a good match with the field measurement, solutions 1, 2, 3, and 4 are excluded because they have higher RMS compared to other solutions.
- Assume that each layer will share some portion of the total rutting, unless premature rutting occurred due to construction-related issues. Based on this assumption, one can exclude solutions 1, 3, 4, 5, 6, 7, 9 and 10, since they have negligible detected rutting in at least one layer.
- Apply the criteria from section 4.6.3 for available transverse surface profiles at different times (with more consideration for the latest available data) and point locations within the pavement section to determine where the rutting originated. Figure 4-17 shows the transverse surface profile for section 1-0105 at one point location from the latest observation. The shape suggests that the rutting originated in both HMA and base layers (see discussion in section 4.6.3).
- To further verify this initial visual assessment, Table 4-4 shows the frequency of layer failure over 9 years along the 11 point locations (making a total of 99 surface profiles available for analysis). Based on this, solutions 8, 11, 12, 13, and 14 are probable candidates; however the most likely solutions are 13 and 14. This is based on their close agreement with the transverse surface profile analysis and relatively low RMS errors. Furthermore, a solution with minimal RMS error comes closer to representing the actual pavement behavior in the field. In this case, solution number

14 satisfies all of these criteria, and can therefore be considered as the most likely solution for the permanent deformation parameters.

- A point of caution: Any rutting within the pavement will show on the surface, though it is logical that rutting percentages should be in sequential order through the different layers (e.g. if the HMA layer fails, it should have the highest rutting percentage, with the second highest rutting percentage in the base, and the lowest in the subgrade).

This same procedure was applied to the surface profiles for all sections in order to backcalculate the unique permanent deformation parameters; out of 120 three-layer sections, 109 sections (91%) had a most likely solution. In the remaining 11 sections, rutting measurements were too low for layer-identification. Figure 4-18 shows the measured (from the field) versus predicted rut depth for all sections included in the backcalculation of PDPs (109).

The ability to obtain a unique solution for each section's PDPs allows for many advantages in rutting prediction. These will be discussed in the following section.

Table 4- 4 Number of point locations with corresponding failed layer-section 1-0105

Number of surface profiles	Failed layer
56	HMA
37	Base
3	Subgrade
3	NA*

*White's criteria failed to recognize them

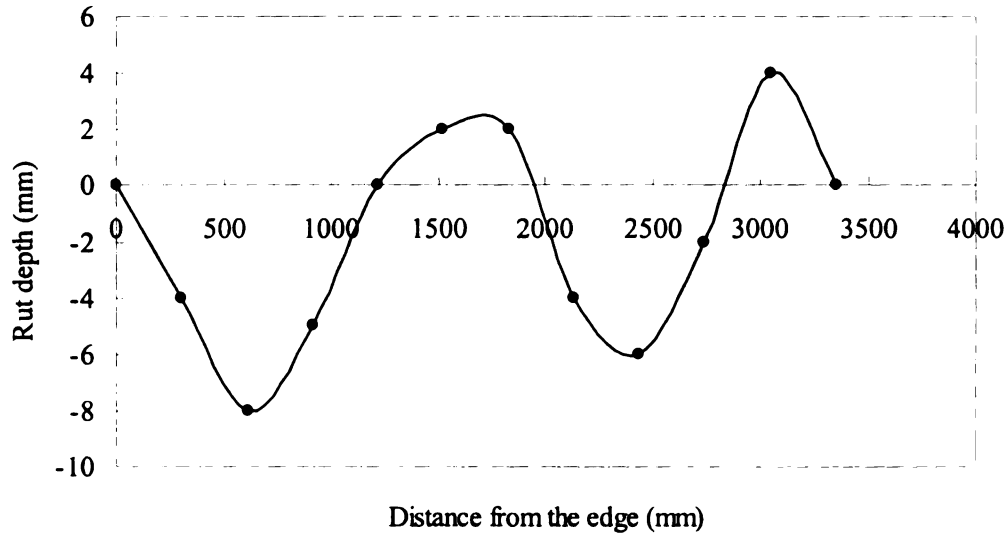


Figure 4-17 Transverse profile section 1-0105

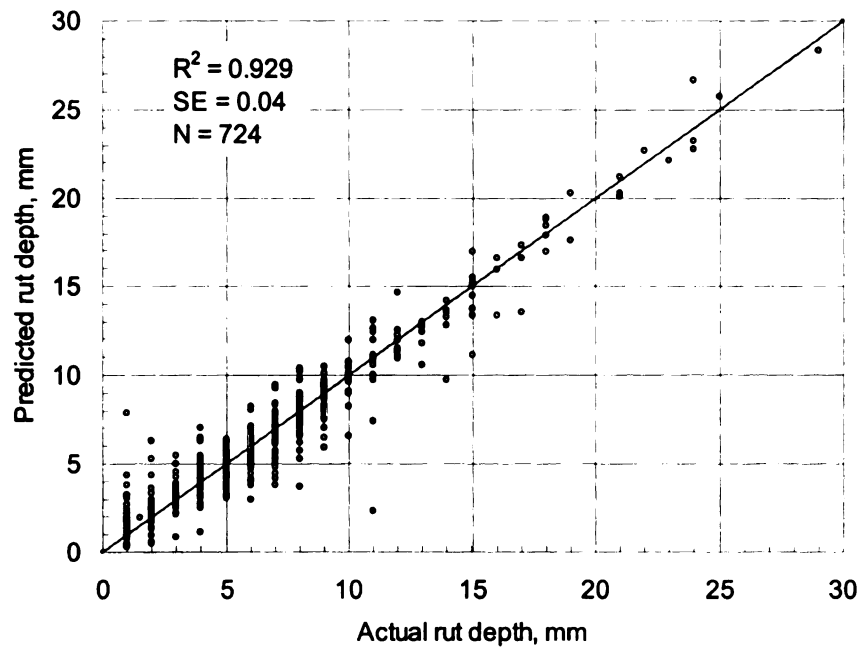


Figure 4-18 Measured versus predicted rut depth for sections used in the backcalculation

4.7.5 Advantages of using backcalculated parameters

There are several advantages of using the obtained PDPs as follows:

- Determine precise parameters for pavement layers, since they are specific for each section,
- Determine the contribution (percentage) of each layer to the total pavement rutting,

- Characterize existing rutting as either premature or structural,
- Based on the above information, a correct remedial action can be taken for pavement rehabilitation,
- These procedures also can be used as diagnostic/prediction tools for rutting,
- Non-destructive rutting test to calculation the layer rutting contribution,
- Compare these parameters as well as the rutting percentage with the previously developed parameters of accelerated loading facilities, ALFs to describe the difference in behavior between the actual field performance and ALFs,
- These parameters can be predicted based on the material parameters, cross sections, environmental conditions (from actual field data) of each section,
- These procedures can be incorporated into a spreadsheet such that from the transverse surface profile data the layer rutting contribution can be calculated in a cost-effective manner.

4.7.6 Summary statistics for backcalculation of permanent deformation parameters

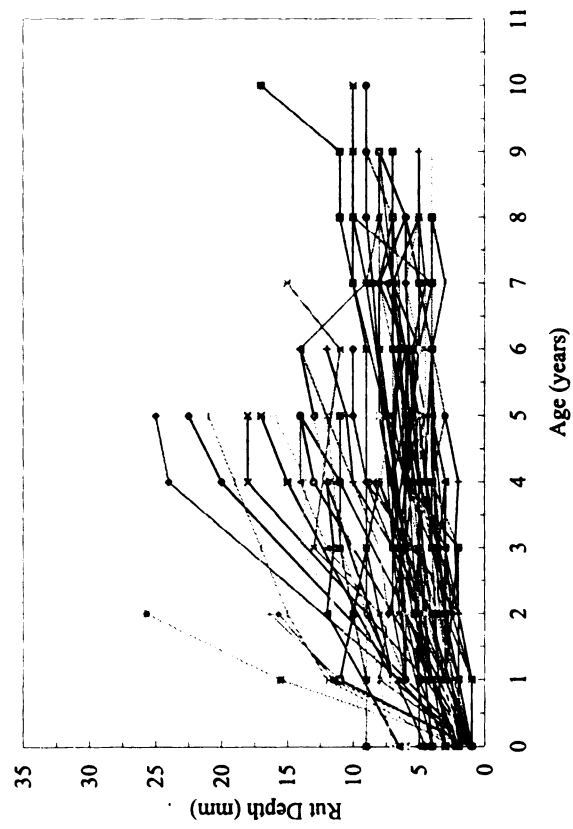
By applying the above procedures to distinguish the most likely solution, the backcalculated PDPs and the rutting contribution of each pavement layer were determined for all (109) sections. Excluding the sections that have:

- $\mu > 1$ which represents high initial rutting (premature rutting),
- $\alpha = 0.99$ which represents no progression of rutting with time because the majority of the rutting occurred at the initial stage,
- 100% of the rutting in the HMA layer, in order to eliminate any rut failure due to specific material problems within the HMA layer,

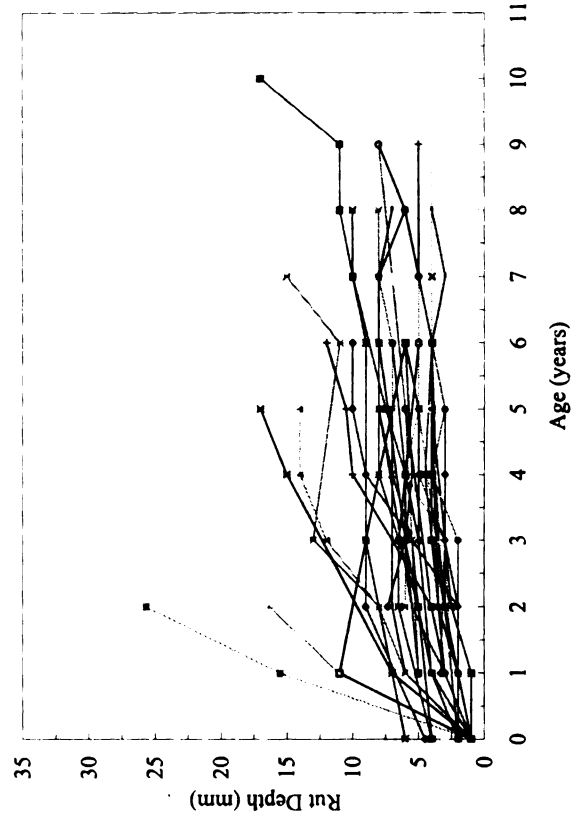
The number of sections with normal structural rutting reduced from 109 to 43 sections.

Figure 4-19 shows the time series rutting data for both categories, and Table 4-5 shows their respective descriptive statistics. Also, the distribution of α and μ as well as the rutting percentages for both categories are shown in Figures 4-20, 4-21, and 4-22, respectively.

Figures 4-20 and 4-22 show that excluding the abnormal sections, α -values and the rutting percentage become normally distributed. On the other hand, μ -values showed either uniform or lognormal distribution even after excluding the abnormal sections.



(a) time series rutting data for 109 sections

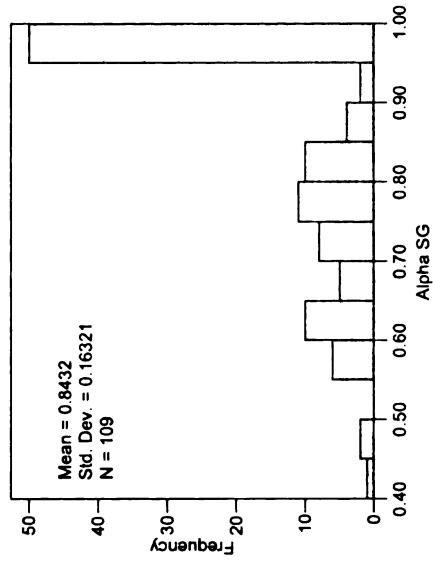
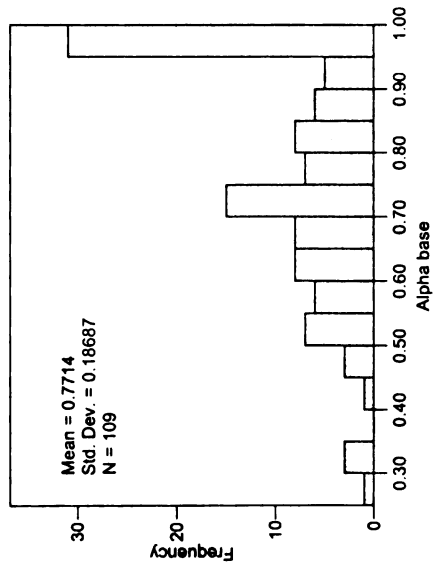
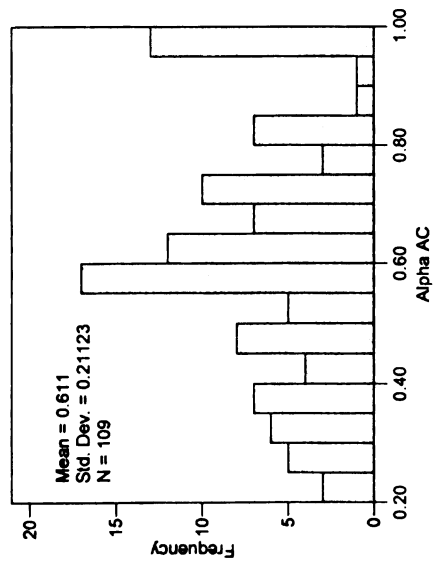


(b) time series rutting data for 43 sections

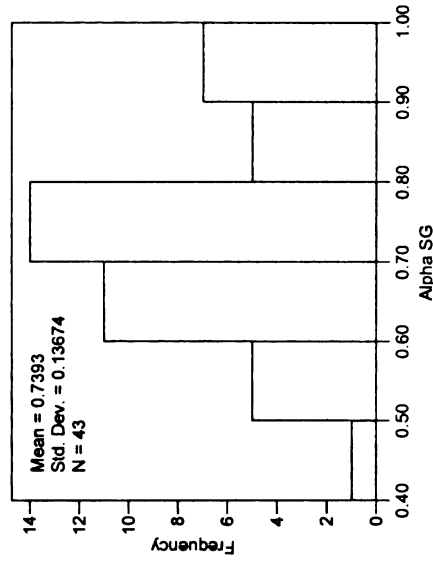
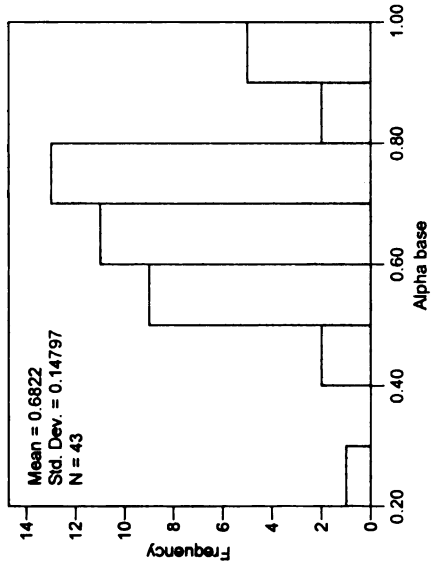
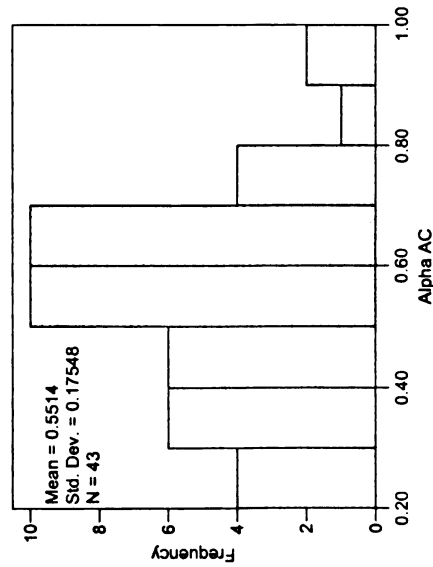
Figure 4-19 time series rutting data for three layers system

Table 4-5 descriptive statistics of PDPs and rutting percentage

Number of sections		α_{HMA}	α_{base}	α_{SG}	μ_{ac}	μ_{base}	μ_{SG}	HMA rut %	Base rut %	SG rut %
109	Minimum	0.207	0.258	0.410	0.010	0.010	0.010	0.0	0.0	0.0
	Maximum	0.999	0.999	0.999	9.962	10.123	2.085	100.0	71.7	99.2
	Average	0.611	0.771	0.843	0.947	0.700	0.302	63.3	25.6	11.2
	St. dev.	0.211	0.187	0.163	1.355	1.473	0.440	24.4	17.1	17.1
	COV	34.57	24.22	19.36	143.06	210.38	145.71	38.59	66.71	152.97
43	Minimum	0.272	0.258	0.410	0.010	0.010	0.010	7.5	02.9	0.5
	Maximum	0.955	0.990	0.986	0.993	0.927	0.824	95.6	66.2	54.6
	Average	0.551	0.682	0.739	0.381	0.245	0.130	57.0	27.5	15.5
	St. dev.	0.175	0.148	0.137	0.340	0.263	0.219	2.0	12.8	15.0
	COV	31.83	21.69	18.49	89.15	107.38	168.70	35.05	46.55	96.75

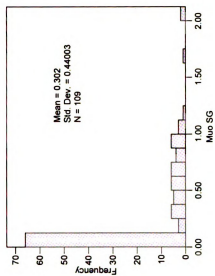
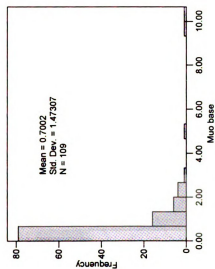
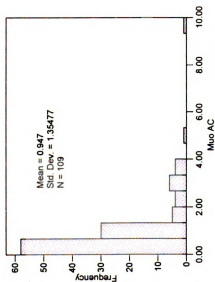


(a) data from all sections

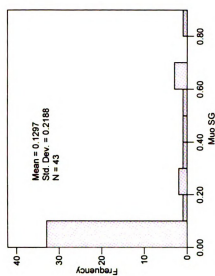
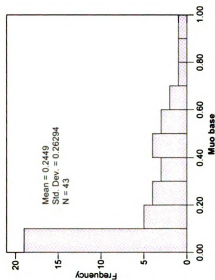
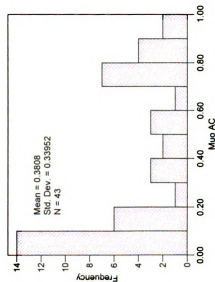


(b) Data from sections with structure rutting

Figure 4-20 α -value histograms

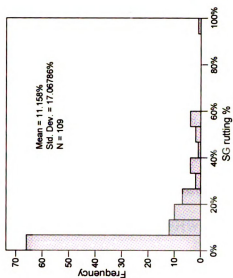
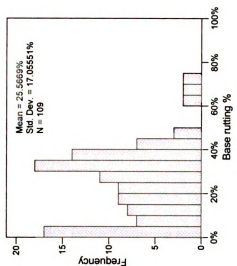
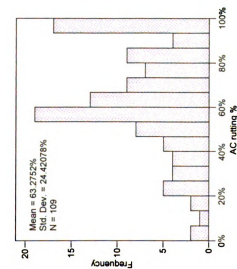


(a) data from all sections

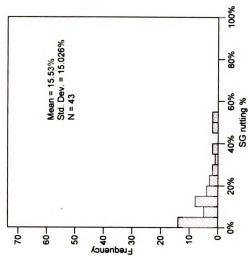
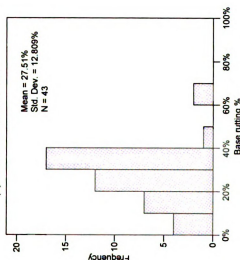
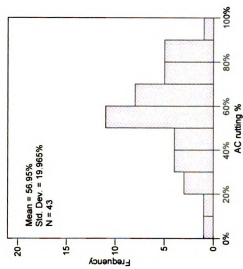


(b) Data from sections with structure rutting

Figure 4-21 μ -value histograms



(a) data from all sections



(b) Data from sections with structure rutting

Figure 4-22 Rutting percentage histograms

4.7.7 Comparison of obtained α , μ , and rutting percentage with previous work

There were several trials in the past to backcalculate the permanent deformation parameters, some of them from field data and the others from ALF. The first study predicted overall average parameters for GPS-1 sections and was not based on time series rutting data to predict the parameters for each section (Ali *et al.*, 1998). The second study predicted the parameters for only one section using the transverse surface profile (Ali and Tayabji, 2000). Other researchers used ALF (FHWA and TxMLS) data to backcalculate the permanent deformation parameters. Figure 4-23 shows comparison of the average predicted PDPs with the previous studies. A good agreement exists between this study's SPS-1 predicted parameters with those of the ALF studies especially the α values.

Also, there were several methods to measure the rutting contribution from each pavement layer. The results from the above developed procedure for predicting the rut percentages from each layer was compared with the measured rut depths from previous studies (AASHO and ALFs). Figure 4-23 shows the average rut percentage of the normal behavior group (43 sections) with AASHO and ALF. The results showed a good agreement between the predicted rutting percentages of the SPS-1 sections and the ALF-TxMLS. It is important to note that the developed procedure (a non-destructive method for analyzing rutting by layer) compares quite favorably with the trenching technique for measuring the same rut layer contribution used in the other studies (Zhou and Scullion, 2002).

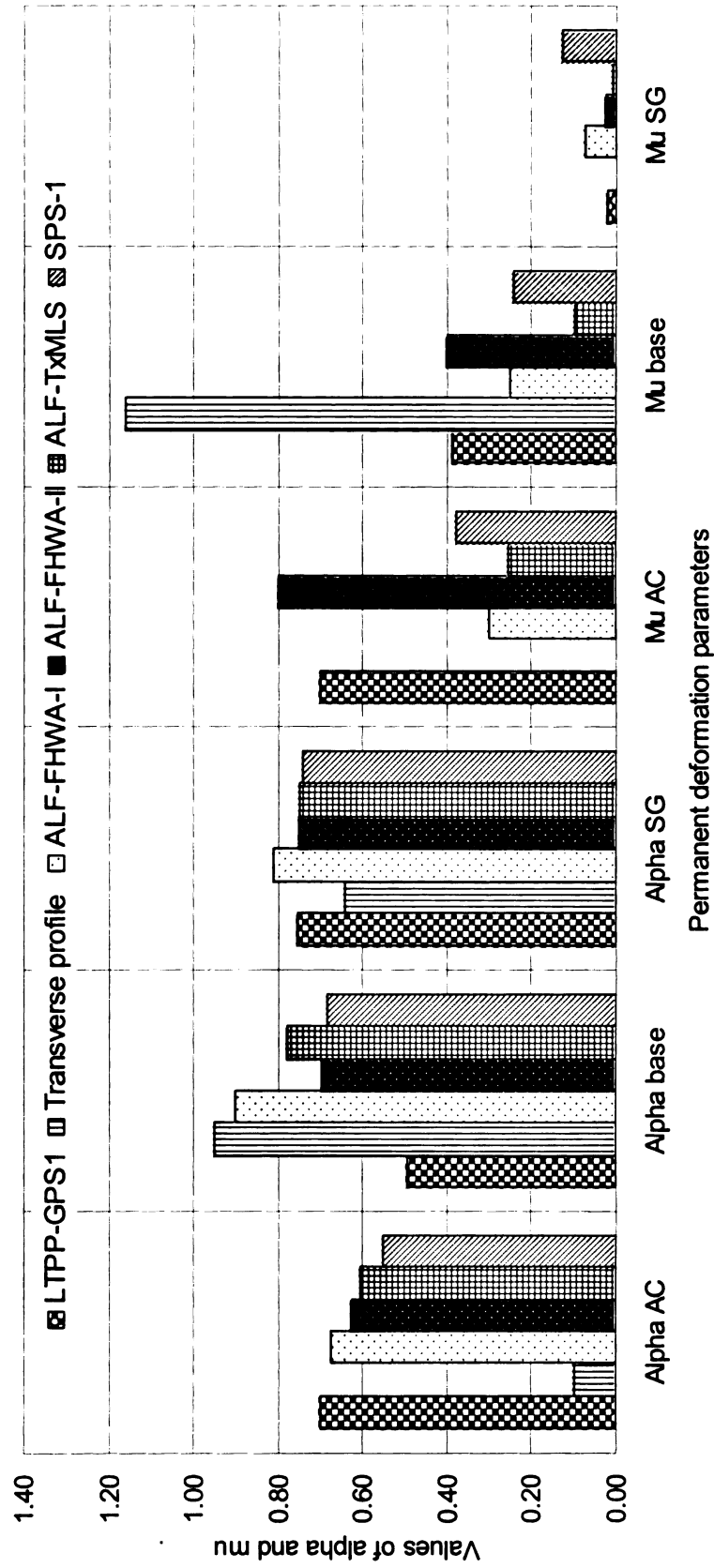


Figure 4-23 Comparison of permanent deformation parameters

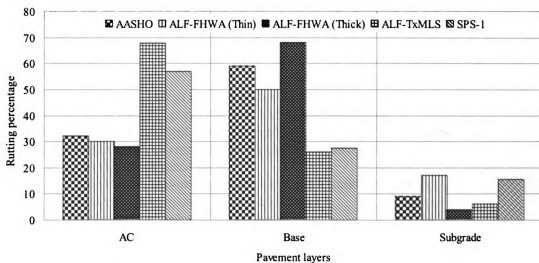


Figure 4-24 Comparison of rutting contribution of pavement layer

4.8 PREDICTION OF PERMANENT DEFORMATION PARAMETERS

A majority of the previous studies give a wide range of values for the permanent deformation parameters. Compared with the multiplicative constant, μ , even slight changes in the exponential constant, α , produce enormous differences in predicted rutting over the lifetime of the pavement (see Equation 4-1). Moreover, these parameters are section-specific according to material properties, layer cross section, and even climatic condition. In the past, there were some trials to predict these parameters in the laboratory for HMA-layer material, yet predicted values need to be shifted to account for actual field behavior. The proceeding sections will explain the regression analysis used to predict the PDPs for in-service pavements (considering material properties, layer cross section, and climatic conditions) in the SPS-1 experiment.

4.8.1 Available material properties

The LTPP database provides information for the pavement layers of all SPS-1 experiment sections, structural, material as well as climatic variables. Several data elements were

extracted for each pavement layer from release 17 of the LTPP database (Datapave.com) as follows:

- HMA layer
 - The gradation of the fine and coarse aggregate,
 - Bulk specific gravity of fine and coarse aggregate,
 - Bulk specific gravity of the asphalt mixture from field cores,
 - Maximum theoretical specific gravity of the mix,
 - HMA binder content,
 - Kinematic and absolute viscosity of the asphalt binder
 - Indirect tensile strength of the mixture,
 - Resilient modulus of the mixture.
- Base layer
 - The gradation of the fine and coarse aggregate.
 - Atterberg limits (liquid and plastic limits)
- Subgrade layer
 - Gradation,
 - Moisture content and dry density,
 - Atterberg limits (liquid and plastic limits)
 - Unconfined strength test.

Using the HMA layer data, the voids in total mix (VTM), voids in mineral aggregate (VMA), and voids filled with asphalt (VFA) were calculated as follow:

$$VTM = \left(1 - \frac{G_{mb}}{G_{mm}} \right) * 100 \quad (4-15)$$

$$VMA = \left[1 - \frac{G_{mb}(1 - P_b)}{G_{sb}} \right] * 100 \quad (4-16)$$

$$VFA = \left(\frac{VMA - VTM}{VMA} \right) * 100 \quad (4-17)$$

Bulk specific gravity of the combined aggregate, G_{sb} , can be calculated from the following equation:

$$G_{sb} = \frac{\frac{P_F + P_C}{\frac{P_F}{G_F} + \frac{P_C}{G_C}}}{\quad} \quad (4-18)$$

where

VTM = voids in total mix
 VMA = voids in mineral aggregates

VFA = voids filled with asphalt
 G_{mb} = bulk specific gravity of the cores
 G_{mm} = maximum theoretical specific gravity
 G_{sb} = aggregate bulk specific gravity
 P_b = percent asphalt content
 P_F = weight percentages of fine aggregates (percent passing sieve # 4)
 P_C = weight percentages of coarse aggregates (1- percent passing sieve # 4)
 G_F = bulk specific gravity of fine aggregate
 G_C = bulk specific gravity of coarse aggregate

Several climatic variables were extracted from the SPS-1 data, and Table 4-6 explains those that are considered in the regression analysis.

Table 4-6 Climatic variables considered

Climatic variables	Description
Mean annual temperature	Average of daily mean air temperatures for year, °C
Maximum annual temperature	Average of daily maximum air temperatures for year, °C
Minimum annual temperature	Average of daily minimum air temperatures for year, °C
Days above 32 °C	Number of days where daily maximum air temperature is above 32.2 °C for year
Days below 0 °C	Number of days where daily minimum air temperature is below 0 °C for year
Freeze index	Calculated freezing index for year
Freeze thaw cycle	Number of freeze/thaw cycles for year.
Total annual precipitation	Total precipitation for year
Wet days	Number of days for which precipitation was greater than 0.25 mm for the month.
Intense precipitation days/year	Number of days for which precipitation was greater than 12.7 mm for year

The pavement layer thicknesses from the backcalculation procedure and the strain at the middle of each pavement layer were considered as independent variables in the regression analysis.

Since the independent variables are many, not all are introduced in the multiple linear regression analysis. Based on the previous studies along with the simple univariate linear regression of each variable, the independent variables that have reasonable relationships with the PDPs were selected and introduced in the model. Additionally, the backward

regression analysis selects the most statistically significant variables for each permanent deformation parameter.

4.8.2 Regression analysis

Possible forms of multiple linear regression models are shown in Equations 4-19 through 4-23. Equation 4-19 shows the general form of multiple regression; Equation 4-20 is a mathematical form for multiple linear regression; Equation 4-21 is similar to Equation 4-20 except that it includes additional interactive effects; Equation 4-22 is a multiplicative form of regression which can consider the non-linear effects of the variables; and Equation 4-23 shows the log-linear regression form for multiple variables.

$$Y = f(x_1, x_2, x_3, \dots) + \varepsilon_{\text{model}} \quad (4-19)$$

$$Y = \beta_0 + \sum_i^n \beta_i x_i + \varepsilon_{\text{model}} \quad (4-20)$$

$$Y = \beta_0 + \sum_i^n \beta_i x_i + \sum_i^n \sum_j^n \beta_{ij} x_i x_j + \varepsilon_{\text{model}} \quad (4-21)$$

$$Y = \beta_0 \prod_i^n x_i^{\beta_i} \varepsilon_{\text{model}} \quad (4-22)$$

$$\log Y = \log \beta_0 + \sum_i^n \beta_i \log x_i + \varepsilon_{\text{model}} \quad (4-23)$$

The multi-linear regression analysis with variable selection offers two major advantages:

- It provides relationships with explicit terms, and
- Allows for accuracy assessment of permanent deformation parameter predictions.

In this study, the multiplicative form of multiple linear regression (Equation 4-22) was utilized to model the nonlinear relationship between the PDPs and the independent variables. Several precautions were taken into consideration to ensure integrity of the model as follows:

- The signs of the multiple linear regression coefficients agree with the signs of the simple linear regression of the individual independent variables,

- The signs of the multiple linear regressions for each independent variable agree with intuitive engineering judgment. For example, higher annual temperature should increase the rate of the rutting in HMA layer, and therefore create more positive values for $(1-\alpha)$ and μ .
- There should be no multicollinearity among the final selected independent variables. For example, two independent variables having the same effect (high bivariate correlation) on the dependent variable should not be included in one model at the same time.
- One of several variable selection algorithms, such as stepwise, forward, and backward regression analyses, is used in regression to eliminate the statistically insignificant independent variables.
- The model is selected with the smallest number of independent variables, minimum standard error, and highest R^2 value.

In addition, after finalizing the model for each permanent deformation parameter, the regression models were tested to ensure there were no assumption violations. These tests are:

- Normality distribution,
- Constant variance,
- Cook's distance.

4.8.3 HMA layer regression analysis

The rutting in the HMA layer is characterized by α_{HMA} and μ_{HMA} . The parameter, α_{HMA} , represents the rate of decrease in HMA rutting as the number of load applications increases (since there is a natural limit to the amount of permanent deformation) and as the material becomes stiffer (the hardening effect due to environmental conditions). The parameter, μ_{HMA} , represents the constant of proportionality between plastic and elastic strain within the HMA layer.

There are several factors affecting HMA rutting. All available material and climatic data used to explain HMA rutting were extracted from the LTPP database (section 4.7.1), as per the existing literature (see chapter 2, section 2.2.1.3). Using simple linear regression,

these independent variables were regressed on α_{HMA} and μ_{HMA} . The variables that have reasonable relationships (relatively higher R^2) were introduced into the multiple linear regression models. The backward regression analysis was utilized to select the statistically significant variables for the final model. A total of 15 sections were used for predicting α_{HMA} and μ_{HMA} . This is due to the limited amount of available data to calculate VTM, VFA, and VMA, which are important for explaining the rate of the HMA rutting. Equations 4-24 and 4-25 show the final model for α_{HMA} and μ_{HMA} .

$$\alpha_{HMA} = 5105.124 * (Strain)^{0.555} * P_{10}^{-1.013} * (VFA)^{-0.58} * (Max AT)^{0.732} \quad (4-24)$$

$$\mu_{HMA} = 6.746 * \alpha_{AC}^{4.102} * FI^{-0.213} \quad (4-25)$$

where:

- Strain* = strain at the middle of HMA layer due to ESAL
- P₁₀* = % passing sieve number 10 of the most upper HMA layer
- VFA* = % voids filled with asphalt of the most upper HMA layer
- Max A T* = Average of daily maximum air temperatures for year, °C
- FI* = freezing index

It can be seen from the equations that α_{HMA} is a function of P_{10} and VFA (both material-related properties), *strain* (structure-related), and Max AT (environment-related), while μ_{HMA} is a function of α_{HMA} (rate of rutting) and FI (environment-related). This implies that, in order to predict μ_{HMA} , an estimate for α_{HMA} must be predicted first. Attempts were made to predict μ_{HMA} from variables other than α_{HMA} (mainly those listed below Equations 4-24 and 4-25), but all alternatives to using α_{HMA} were found to have much lower R^2 values. Figures 4-26 and 4-27 show the individual relationship between these independent variables and α_{HMA} and μ_{HMA} , respectively. Table 4-7 shows the analysis of variance of the multiple linear regression of α_{HMA} and μ_{HMA} . The results show that the overall models for α and μ are statistically significant. Table 4-8 shows that 90% and 79 % of the variance for α_{HMA} and μ_{HMA} , respectively, is explained by the independent variable.

Table 4-7 ANOVA for α_{HMA} and μ_{HMA}

Variable		Sum of Squares	df	Mean Square	F	Sig.
α	Regression	1.675	4	.419	33.604	0.000
	Residual	0.125	10	0.012	-	-
	Total	1.800	14	-	-	-
μ	Regression	16.675	2	8.338	26.065	0.000
	Residual	3.519	11	0.320	-	-
	Total	20.194	13	-	-	-

Table 4- 8 Model Summary for α_{HMA} and μ_{HMA}

Variable	R	R ²	Adjusted R ²	Std. Error of the Estimate
α	0.965	0.931	0.903	0.111641
μ	0.909	0.826	0.794	0.565585

Table 4-9 shows the unstandardized and standardized model coefficients, *t*-test, statistical significance, and collinearity statistics for both α_{HMA} and μ_{HMA} . It can be seen from the table that all independent variables included in the model for both α_{HMA} and μ_{HMA} are statistically significant. Also, there was no concern about the multicollinearity (small VIF). Moreover, there is a good agreement between the multiple linear regression coefficient signs and the univariate relationship of the individual variables as shown in Figures 4-26 and 4-27. The standardized regression coefficients show that:

- The higher the initial strain and/or the yearly average of daily maximum air temperatures, the higher the α_{HMA} value, which means a lower rate of rutting progression with time (the exponent is $1-\alpha_{HMA}$). In other words, if the HMA layer is soft (higher initial strain) or the climatic region is hot (higher temperatures); the majority of the rutting will occur at the initial stage and taper off with the remaining life of the pavement.

- The higher the percent passing sieve number 10 and/or the percent of voids filled with asphalt, the lower the α_{HMA} value, which means a higher rate of rutting progression with time. In other words, rutting will be more pronounced if the HMA layer is composed of a finer mix or it contains more voids.
- The higher the α_{HMA} , the higher the μ_{HMA} , as can be seen in Figure 4-27. This means that pavements with lower initial rutting (lower μ_{HMA} value) will show rutting over a longer period of time (lower α_{HMA} value).
- The higher the freezing index for a region, the lower its μ_{HMA} values. This indicates that unlike hotter regions, pavements constructed in colder regions will show lower initial rutting.

Table 4-9 shows the standardized regression coefficients used to rank the importance of the independent variables to α_{HMA} and μ_{HMA} values, as shown in Figure 4-25.

Table 4-9 Model coefficients for α_{HMA} and μ_{HMA}

Variables		Unstandardized Coefficients		Standardized Coefficients	t	Sig.	Collinearity Statistics	
		Beta	Std. Error	Beta			Tolerance	VIF
α	Constant	8.538	1.220	-	6.997	0.000	-	-
	Strain	0.555	0.071	0.727	7.820	0.000	0.802	1.247
	% passing # 10	-1.013	0.156	-0.611	-6.485	0.000	0.781	1.281
	VFA	-0.580	0.238	-0.213	-2.439	0.035	0.907	1.103
	Max A T	0.732	0.105	0.589	6.951	0.000	0.966	1.036
μ	Constant	1.909	0.419	-	4.550	0.001	-	-
	α_{HMA}	4.102	0.658	0.786	6.229	0.000	0.995	1.005
	FI	-0.213	0.066	-0.406	-3.219	0.008	0.995	1.005

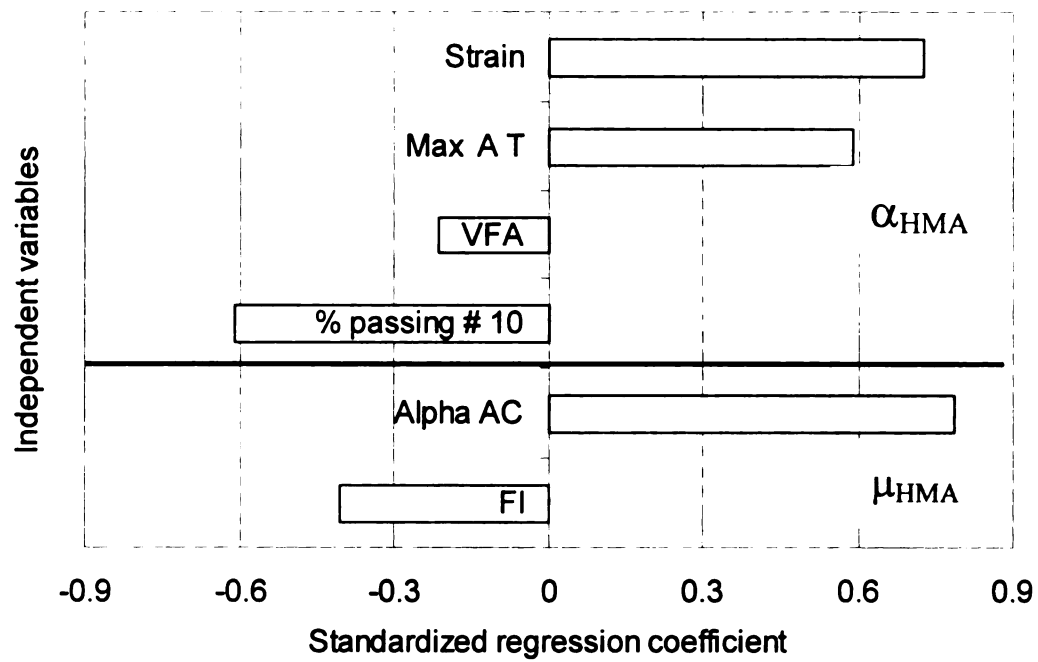


Figure 4-25 Ranking the importance of the independent variables for α_{HMA} and μ_{HMA}

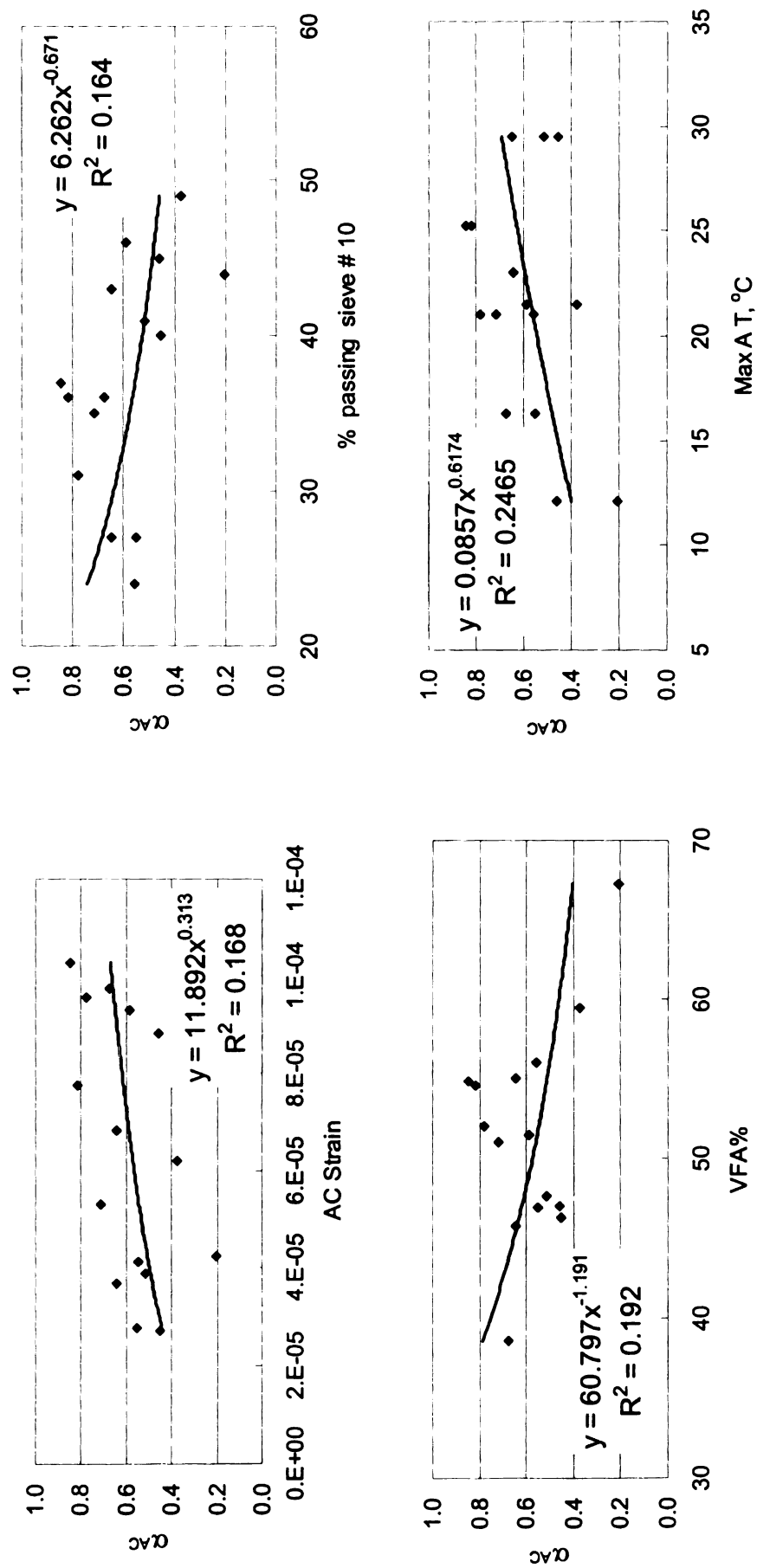


Figure 4-26 Relationship of α_{HMA} versus strain at the middle of the HMA, % passing sieve number 10, VFA% and Max AT

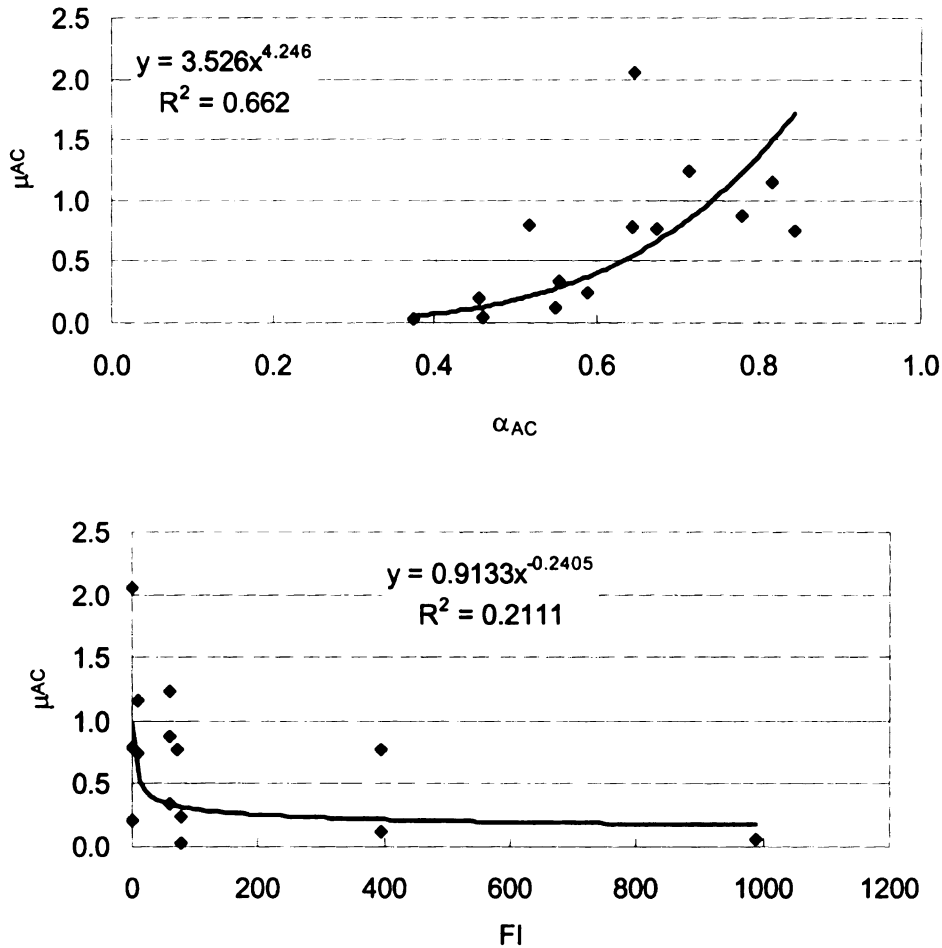
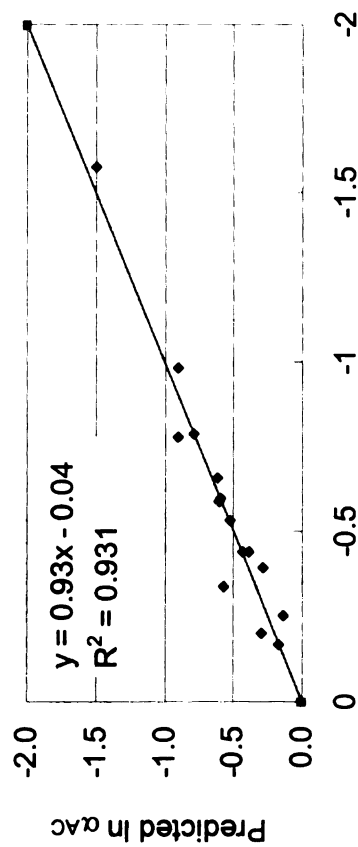


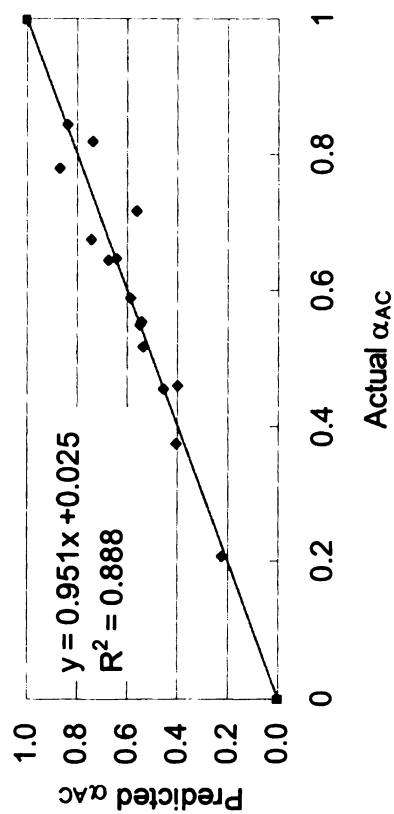
Figure 4-27 Relationship of μ_{HMA} versus α_{HMA} and FI

Figure 4-28 shows a reasonable prediction of α_{HMA} and μ_{HMA} in logarithmic (ln) and arithmetic scales. A reduction in R^2 (small for α_{HMA} and quite large for μ_{HMA}) occurs due to the transformation from logarithmic (ln) to arithmetic scale. This dramatic reduction for μ_{HMA} implies:

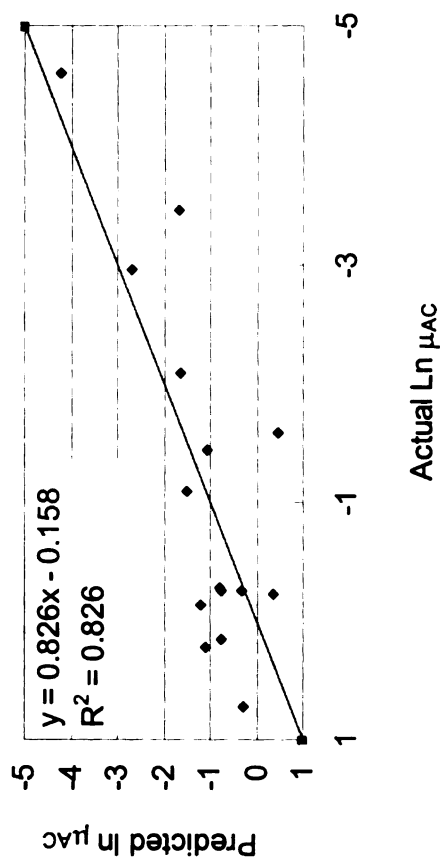
- Prediction of μ_{HMA} is very sensitive to α_{HMA} (standardized $\beta = 0.786$), so small changes in α_{HMA} prediction affect the predicted value of μ_{HMA} to a great degree.
- There is large scatter in the relationship between α_{HMA} and μ_{HMA} (Figure 4-26) especially when μ_{HMA} is greater than 0.7.
- Good prediction of μ_{HMA} at higher values (>1) is not expected since higher μ_{HMA} values represent higher initial HMA rutting due to specific problems (material and/or construction and/or environment).



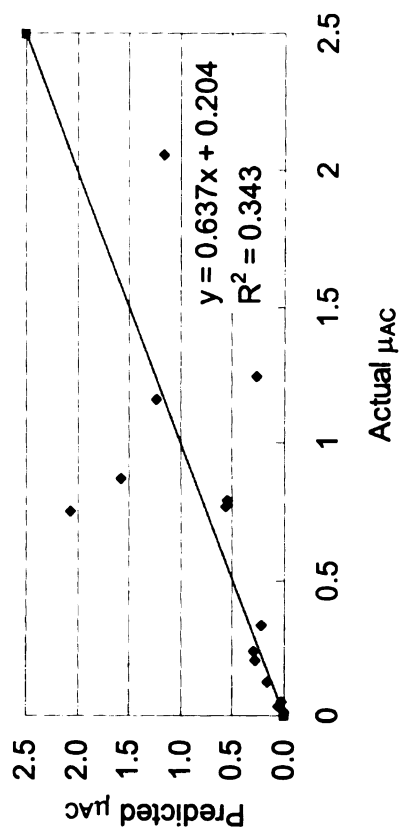
(a) Actual versus predicted α (ln scale)



(b) Actual versus predicted α



(c) Actual versus predicted μ (ln scale)



(d) Actual versus predicted μ

Figure 4-28 Actual versus predicted α and μ for HMA layer

Table 4-10 shows the descriptive statistics for α_{HMA} , μ_{HMA} and their independent variables used in the regression analyses. It should be noted that Equations 4-24 and 4-25 should be used within the range for each variable listed in Table 4-10 in order to obtain reasonable predictions.

Table 4-10 Descriptive statistics of α_{HMA} , μ_{HMA} , and their independent variables

	α_{HMA}	μ_{HMA}	Strain	P ₁₀	VFA	Max AT	FI
Mean	0.589	0.649	6.35E-05	37	51.6	22	158
St. Dev.	0.173	0.675	2.73E-05	8	6.8	6	273
Minimum	0.207	0.010	2.69E-05	24	38.5	12	1
Maximum	0.844	2.059	1.03E-04	49	67.3	29	988

4.8.4 Base layer regression analysis

For base layer, the only data available were the gradation, base thickness used in the backcalculation, and the calculated strain at the middle of the base due to one standard axle. Unlike the HMA layer, in which the materials are highly controlled, the base and subgrade layers of flexible pavements are frequently more dissimilar from one section to another. This becomes evident when examining sieve analyses. Since the content of HMA material is highly controlled, a particular sample can be uniquely identified by an individual sieve measurement, that is, the percent material passing through one particular sieve (see Figure 4-29). This is not the case for the base layer material, since base materials from two different sections might have the same percent passing through one sieve and different gradations for the other sieves, as shown in Figure 4-30. Therefore, a new index termed, Gradation Index (GI) is introduced in this analysis to represent the gradation of the base layer such that using the GI alone or with the percent passing of any given sieve (such as

sieve 4, 10, or 200) will be more representative of an individual base layer's material. The

GI can be calculated from the following equation:

$$GI = \frac{\sum P * \log SS}{\sum \log SS} \quad (4.26)$$

where

p = log % passing of the individual sieve, and
 $\log SS$ = sieve size in mm.

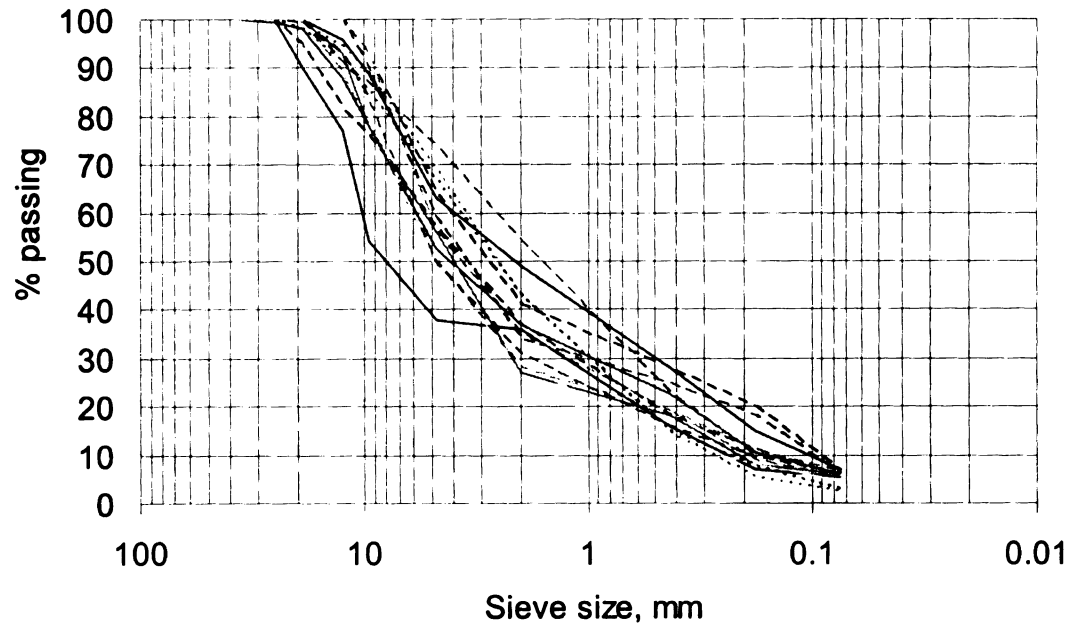


Figure 4-29 Sieve analysis of HMA layer

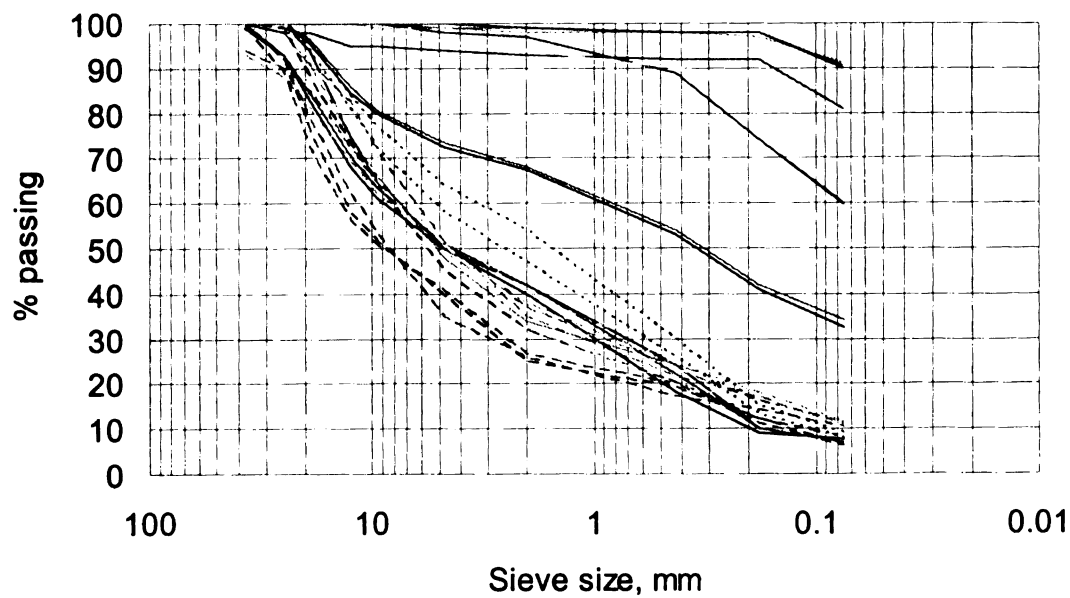


Figure 4-30 Sieve analysis of base layer

For the base regression analysis, only sections that have base rutting of 10 percent or more out of the total surface rutting and available base gradations were considered, these total 27 sections. The final regression equations for predicting the α_{base} and μ_{base} are shown below:

$$\alpha_{base} = 2.724 * 10^{-5} * modulus^{0.102} * Thickness^{0.066} * P_{200}^{-0.098} * GI^{1.982} \quad (4-27)$$

$$\mu_{base} = 7.1977 * 10^{-3} * \alpha^{6.256} * Thickness^{-0.808} * strain^{-0.809} \quad (4-28)$$

where

- Modulus = backcalculated base modulus, psi
- Thickness = Thickness of base layer used in the backcalculation, in
- P_{200} = % passing sieve number 200
- GI = Gradation index
- Strain = Strain at the middle of the base layer due to one standard axle

Table 4-11 shows the analysis of variance of the multiple linear regression for α_{base} and

μ_{base} . The results show that the overall models for α_{base} and μ_{base} are statistically

significant. Table 4-12 shows that 50.6 % and 68.7 % of the variance for α_{base} and μ_{base} , respectively, is explained by the independent variable.

Table 4-13 shows the unstandardized and standardized model coefficients, t -test, statistical significance, and collinearity statistics for both α_{base} and μ_{base} . It can be seen from the table that all independent variables included in the model for both α_{base} and μ_{base} are statistically significant except for the base thickness in the α_{base} model. Excluding the base thickness from the model causes dramatic reduction of R^2 , therefore base thickness was kept in the model. Also, there was no concern about multicollinearity (small VIF). Moreover, there is a good agreement between the multiple linear regression coefficient signs and the univariate relationship of the individual variables as shown in Figures 4-31 and 4-32. The standardized regression coefficients show that:

- The higher the initial modulus, the higher the α_{base} value, which means a lower rate of rutting progression with time (the exponent is $1-\alpha_{\text{base}}$).
- The thicker the base with higher GI (coarser material), the higher the α_{base} , which means a lower rate of base rutting with time.
- The higher the percent passing sieve 200, the lower the α_{base} , which leads to a higher rate of rutting with time.
- Similar to the HMA layer, there is a strong relationship between α_{base} and μ_{base} ($R^2 = 0.5949$); the higher the α_{base} the higher the μ_{base} as can be seen in Figure 4-32. This means that a pavement with lower initial rutting (lower μ_{base} value) will show rutting over a longer period of time (lower α_{base} value).
- The thicker the base layer with higher initial strain value, the lower the μ_{base} , which indicates that rutting will keep progression with time.

Table 4-13 shows the standardized regression coefficients used to rank the importance of the independent variables in the α_{base} and μ_{base} models, as shown in Figure 4-33.

Table 4-11 ANOVA for α_{base} and μ_{base}

Variables		Sum of Squares	df	Mean Square	F	Sig.
α	Regression	0.674	4	0.169	7.653	0.001
	Residual	0.485	22	0.022	-	-
	Total	1.159	26	-	-	-
μ	Regression	59.631	3	19.877	20.000	0.000
	Residual	22.859	23	.994	-	-
	Total	82.490	26	-	-	-

Table 4-12 Model summary for α_{base} and μ_{base}

Variables	R	R ²	Adjusted R ²	Std. Error of the Estimate
α	0.763	0.582	0.506	0.148
μ	0.850	0.723	0.687	0.997

Table 4-13 Model coefficients for α_{base} and μ_{base}

Variables		Unstandardized Coefficients		Standardized Coefficients	t	Sig.	Collinearity Statistics	
		Beta	Std. Error	Beta			Tolerance	VIF
α	Constant	-10.511	3.519	-	-2.987	0.007	-	-
	Modulus	0.102	0.037	0.447	2.751	0.012	0.721	1.387
	Thickness	0.066	0.051	0.205	1.303	0.206	0.771	1.297
	P200	-0.098	0.032	-0.462	-3.094	0.005	0.854	1.172
	GI	1.982	0.715	0.429	2.774	0.011	0.794	1.259
	Constant	-4.934	2.083	-	-2.369	0.027	-	-
μ	α	6.256	0.942	0.742	6.639	0.000	0.966	1.035
	Thickness	-0.808	0.355	-0.298	-2.280	0.032	0.707	1.415
	Strain	-0.809	0.254	-0.417	-3.182	0.004	0.700	1.428

Figure 4-34 shows the prediction of α_{HMA} and μ_{HMA} in logarithmic (ln) and arithmetic scales. Similar to α_{HMA} and μ_{HMA} , the figure shows a reasonable prediction of α_{base} in the actual scale. A reduction in R^2 for μ_{base} occurs due to the transformation from *ln* to actual scale, similar to μ_{HMA} (as mentioned previously).

Table 4-14 shows the descriptive statistics of α_{base} , μ_{base} and their independent variables used in the regression analysis. It should be noted that Equations 4-27 and 4-28 are used within the range of the data in Table 4-14 to obtain reasonable predictions.

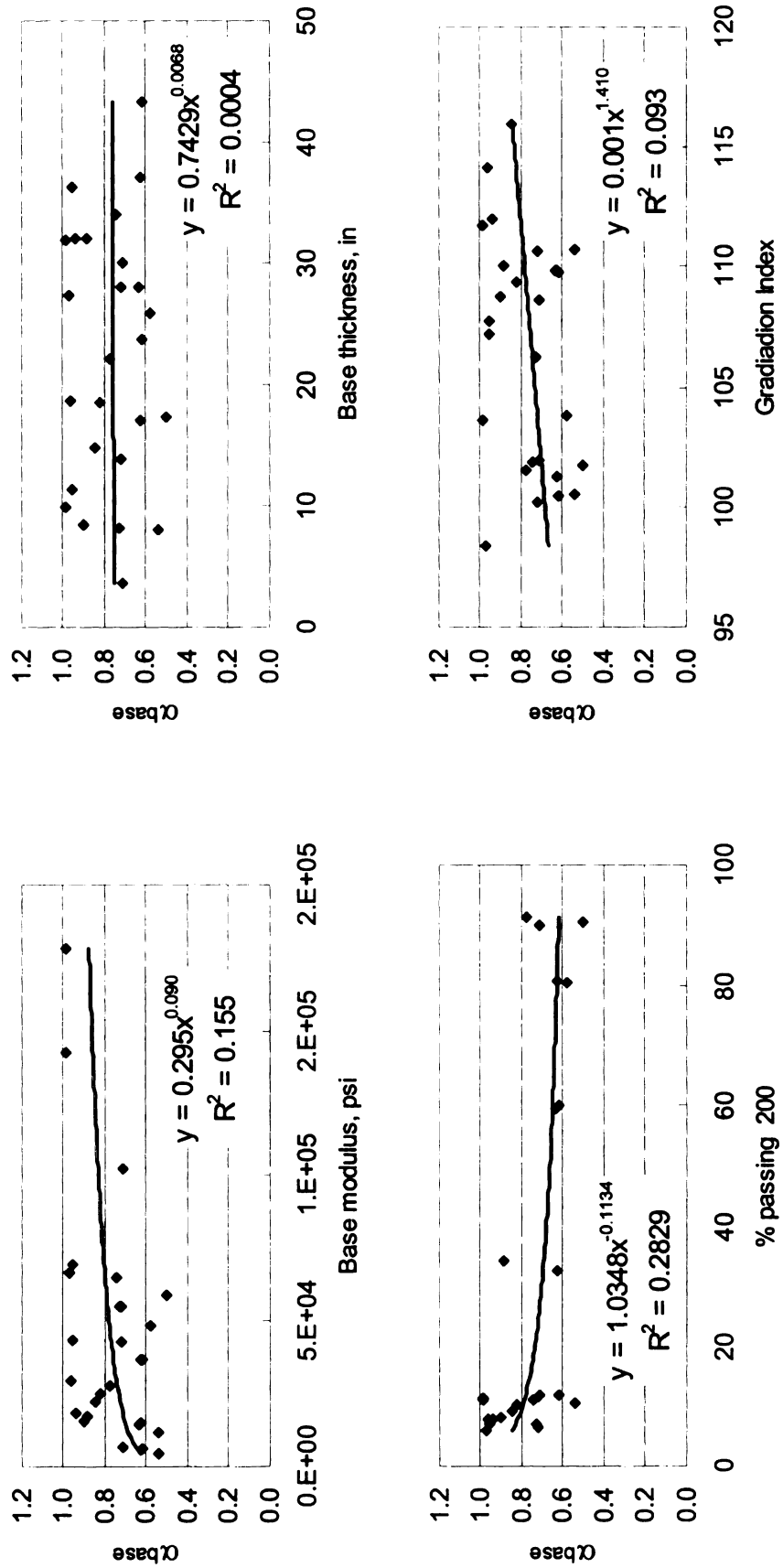


Figure 4-31 Relationship between α_{base} and base modulus, base thickness, % passing sieve number 200, and GI

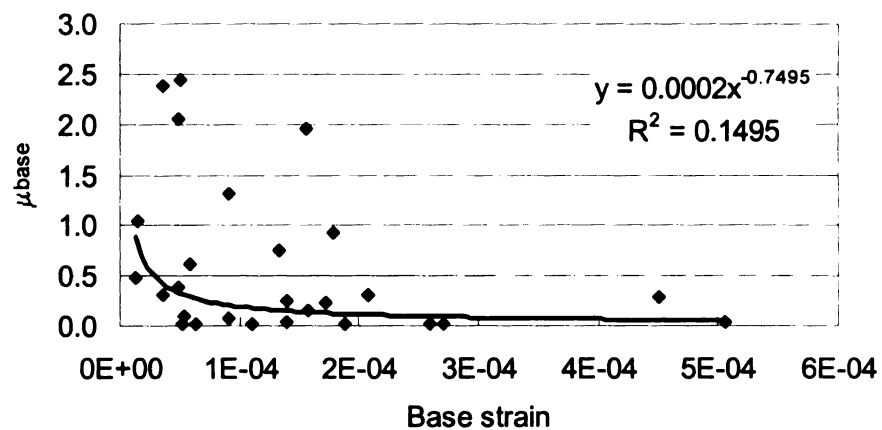
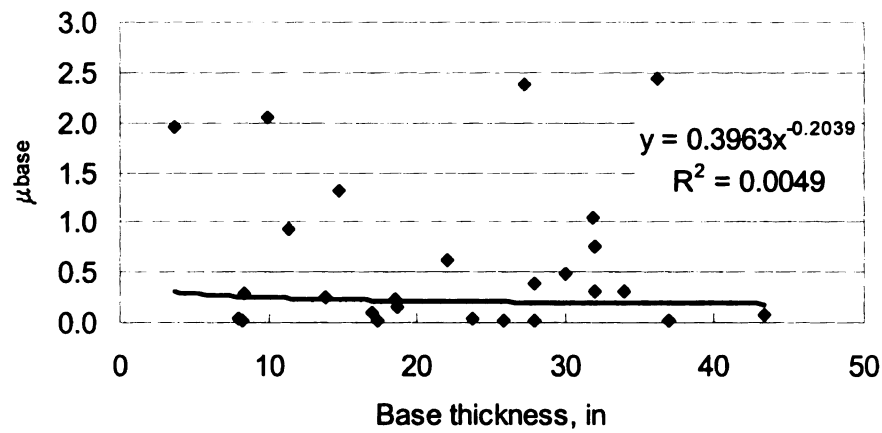
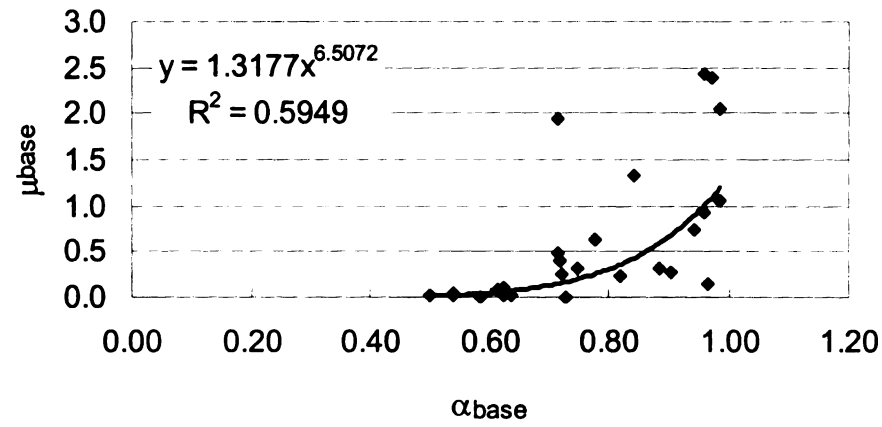


Figure 4-32 Relationship between μ_{base} and α_{base} , base thickness, and base strain

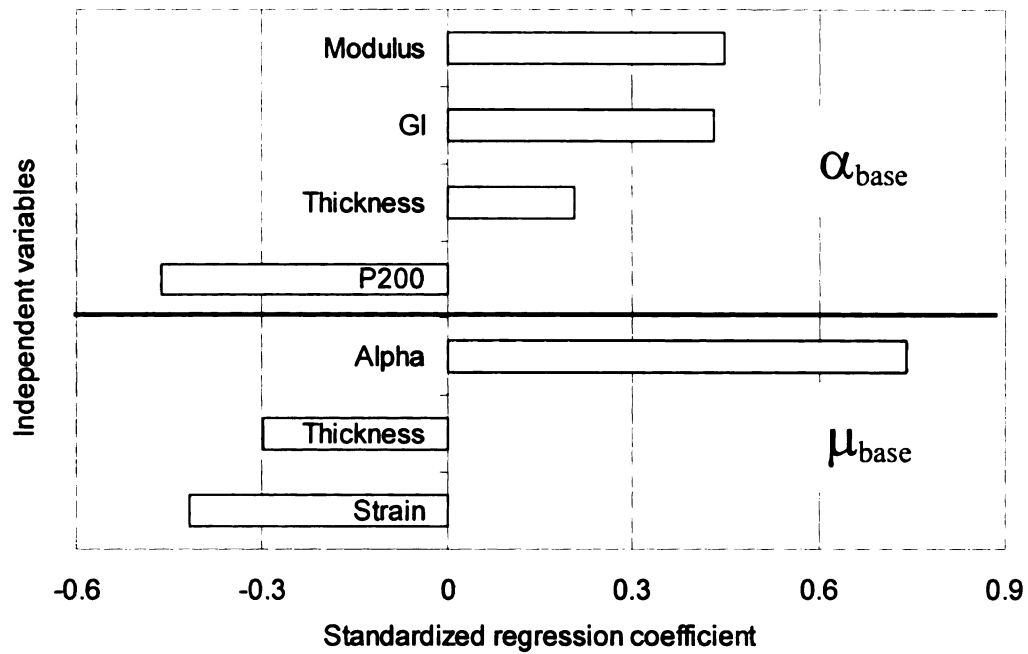
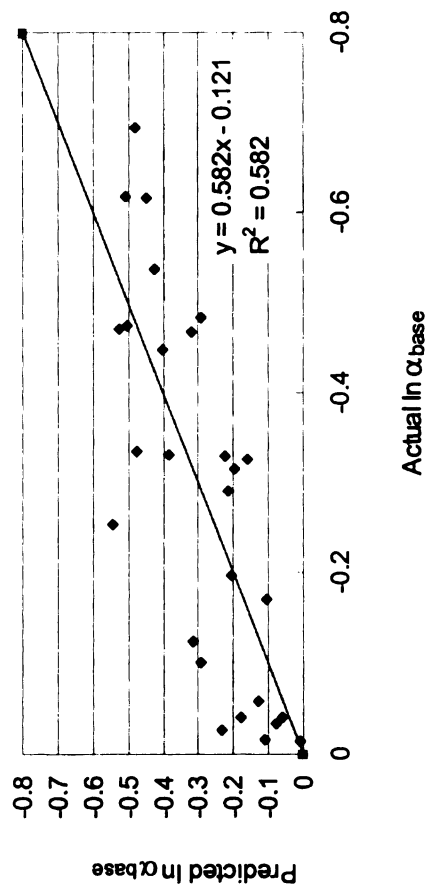


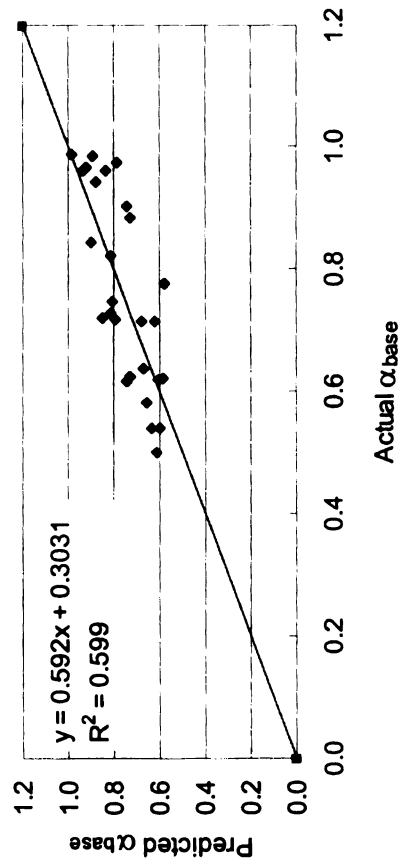
Figure 4-33 Ranking the importance of the independent variables for α_{base} and μ_{base}

Table 4-14 Descriptive statistics of α_{base} , μ_{base} , and their independent variables

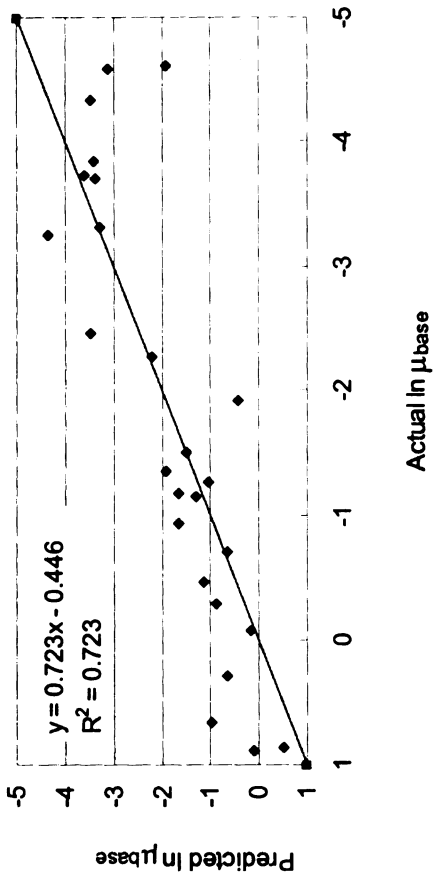
Item	μ_{base}	α_{base}	modulus	thickness	Strain	P ₂₀₀	GI
Mean	0.60	0.76	45058	21.7	1.38E-04	29.1	106.59
ST. DEV.	0.77	0.16	41131	11.0	1.21E-04	31.5	4.86
Minimum	0.01	0.50	4599	3.6	1.29E-05	5.9	98.38
Maximum	2.44	0.99	178098	43.3	5.07E-04	91.3	115.99



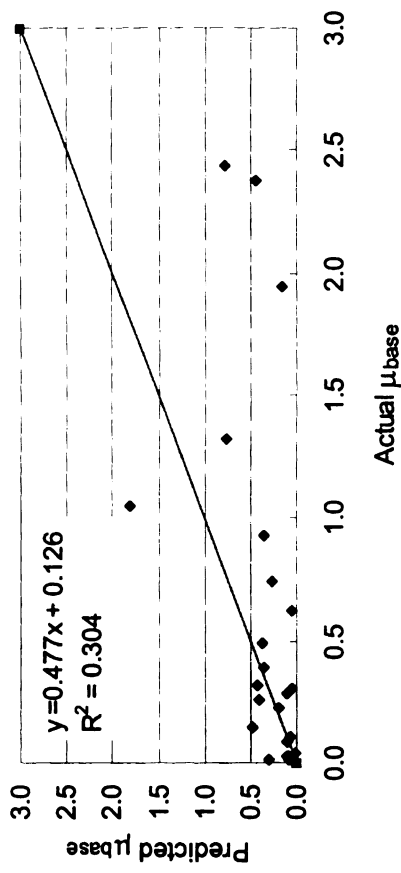
(a) Actual versus predicted α – ln scale



(b) Actual versus predicted α



(c) Actual versus predicted μ – ln scale



(d) Actual versus predicted μ

Figure 4-34 Actual versus predicted α and μ for base layer

4.8.5 Subgrade regression analysis

Similar to the base layer and even more pronounced, the percent subgrade material passing through one sieve is not enough to characterize the subgrade materials, as shown in Figure 4-35. Therefore, the need for the GI (Equation 4-26) is at least as great for the subgrade regression analysis as it was for the base layer.

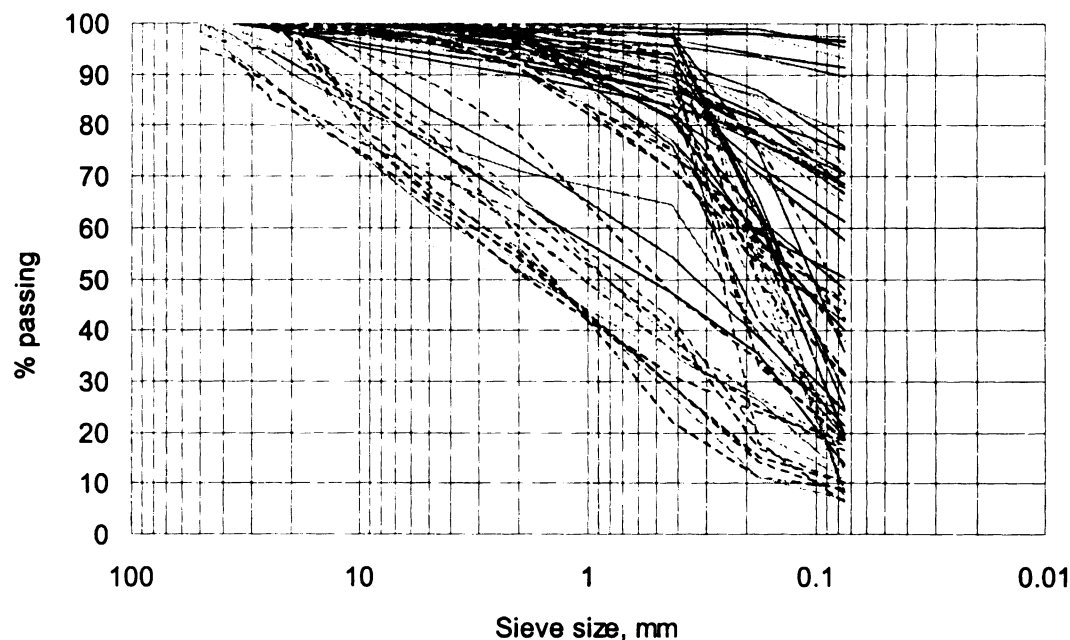


Figure 4-35 Sieve analysis of subgrade layer

For subgrade analysis, only those sections that show rutting in the subgrade and have α_{SG} values less than 0.9 were considered, which totals 17 sections. The final regression equations for predicting the α_{SG} and μ_{SG} are shown below:

$$\alpha_{SG} = 1.385 \times 10^{-5} * strain^{0.043} * GI^{1.89} * PI^{0.116} * D_{32}^{0.14} * FI^{0.036} * wet\ days^{0.326} \quad (4-29)$$

$$\mu_{SG} = 2.575 * 10^{-63} * modulus^{2.41} * strain^{-0.764} * GI^{22.594} * PI^{1.304} \quad (4-30)$$

where

- Strain = Strain at the middle of the first 40 inches of subgrade layer due to one ESAL
- GI = Gradation index (as calculated from equation 4-26)

PI = Plasticity index of subgrade layer
D₃₂ = Number of days where daily maximum air temperature is above 32.2 °C for year
Wet days = Number of days for which precipitation was greater than 0.25 mm for year.
Modulus = backcalculated subgrade modulus, psi

Table 4-15 shows the analysis of variance for α_{SG} and μ_{SG} . The results show that the overall models for α_{SG} and μ_{SG} are statistically significant. Table 4-16 shows that 47.3% and 84.8% of the variance for α_{SG} and μ_{SG} , respectively, is explained by the independent variables.

Table 4-15 ANOVA for α_{SG} and μ_{SG}

Variables		Sum of Squares	df	Mean Square	F	Sig.
α	Regression	0.152	6	0.025	3.389	0.043
	Residual	0.075	10	0.007	-	-
	Total	0.227	16	-	-	-
μ	Regression	33.212	4	8.303	23.344	0.000
	Residual	4.268	12	0.356	-	-
	Total	37.480	16	-	-	-

Table 4-16 Model summary for α_{SG} and μ_{SG}

	R	R ²	Adjusted R ²	Std. Error of the Estimate
α	0.819	0.670	0.473	0.08660
μ	0.941	0.886	0.848	0.59640

Table 4-17 shows the unstandardized and standardized model coefficients, *t*-test, statistical significance, and collinearity statistics for both α_{SG} and μ_{SG} . It can be seen from the table that all independent variables included in the model for both α_{SG} and μ_{SG} are statistically significant except for the strain and FI in the α_{SG} model. Excluding either of these variables from the model causes a dramatic reduction of the R² value, therefore, similar to the base layer, they were kept in the model since the backward regression analysis selects them. Also, there was no concern about multicollinearity (small VIF). Moreover, there is a good agreement between the multiple linear regression coefficient signs and the univariate

relationship of the individual variables as shown in Figures 4-36, 4-37 and 4-38. The standardized regression coefficients as depicted in Figure 4-39 show that:

- The higher the PI, GI, D₃₂, wet days, FI, and vertical compressive strain at the middle of the first 40 in of the subgrade, the higher the α_{SG} , which means a lower rate of rutting progression with time (the exponent is $1-\alpha_{SG}$). This is what the multiple linear regression analysis showed; however the univariate relationship of these variables with α_{SG} supports this result with a weak trend. Hence, the resulting α_{SG} relationships can not be generalized since the statistical evidence is not strong enough.
- The higher the PI, GI, and subgrade modulus, the higher the μ_{SG} , which means a majority of the resulting rutting will occur at the first stage of pavement life with very little progression with time. Similar to the base layer, higher initial strain value in the subgrade indicates that rutting will keep progressing with time.

Table 4-17 Model Coefficients for α_{SG} and μ_{SG}

Variables		Unstandardized Coefficients		Standardized Coefficients	t	Sig.	Collinearity Statistics	
		Beta	Std. Error	Beta			Tolerance	VIF
α	Constant	-11.187	3.965	-	-2.822	0.018	-	-
	Strain	0.043	0.031	0.283	1.391	0.194	0.798	1.252
	GI	1.890	0.805	0.955	2.348	0.041	0.199	5.020
	PI	0.116	0.035	1.271	3.342	0.007	0.228	4.387
	D ₃₂	0.140	0.061	0.914	2.269	0.047	0.203	4.924
	FI	0.036	0.020	0.656	1.796	0.103	0.247	4.047
	Wet days	0.326	0.105	0.853	3.109	0.011	0.438	2.281
μ	Constant	-144.12	21.825	-	-6.603	0.000	-	-
	SG modulus	2.410	0.956	0.403	2.521	0.027	0.371	2.692
	Strain	-0.764	0.274	-0.388	-2.786	0.016	0.490	2.043
	GI	22.594	5.006	0.890	4.513	0.001	0.244	4.096
	PI	1.304	0.211	1.118	6.191	0.000	0.291	3.436

Figure 4-40 shows the prediction of α_{SG} and μ_{SG} in logarithmic (ln) and arithmetic scales.

Table 4-18 shows the descriptive statistics of α_{SG} , μ_{SG} and the independent variables used in the regression analysis. Similar to the HMA and base layers, Equations 4-29 and 4-30 are used within the range of the data in Table 4-18 to obtain reasonable predictions. Figure 4-41 shows the measured (field), calculated (backcalculated PDPs), and predicted (regression equations) rut depth for one of the sections that have data for HMA, base, and subgrade layers (section 50113).

Finally, it should be noted that, as shown in Figure 4-24, a majority of the total rutting occurs within the HMA layer (on average, 57%), followed by the base layer (27.5%), and the subgrade layer (15.5%). The decay in PDP prediction is justifiable when correlated with the decay in successive layers' overall rutting percentages. This is primarily due to two analytical/data factors. First, with a smaller percentage of the total rutting to predict, the base and subgrade models are more constrained by available data and the smaller magnitude of the rutting effect measured within these layers. Secondly, the base and subgrade layers have successively fewer variables available within the predictive models than the HMA layer; therefore, it is more difficult to explain the rutting in these layers with a decreased number of variables. The results of this analysis agree with the expectation that prediction of the PDPs decays as the rutting percentage decreases. HMA regression analysis showed that the overall model for α_{HMA} and μ_{HMA} are statistically significant, as are all variables included. On the other hand, the overall models for α_{base} and μ_{base} are statistically significant, with only one insignificant variable (base thickness). Following the same pattern of decreased significance with decreased rutting percentage, the overall models for α_{SG} and μ_{SG} are statistically significant, yet contain two insignificant variables (strain and FI). This understandable pattern suggests the need for more study and further theorizing of variables to explain rutting within the base and subgrade layers.

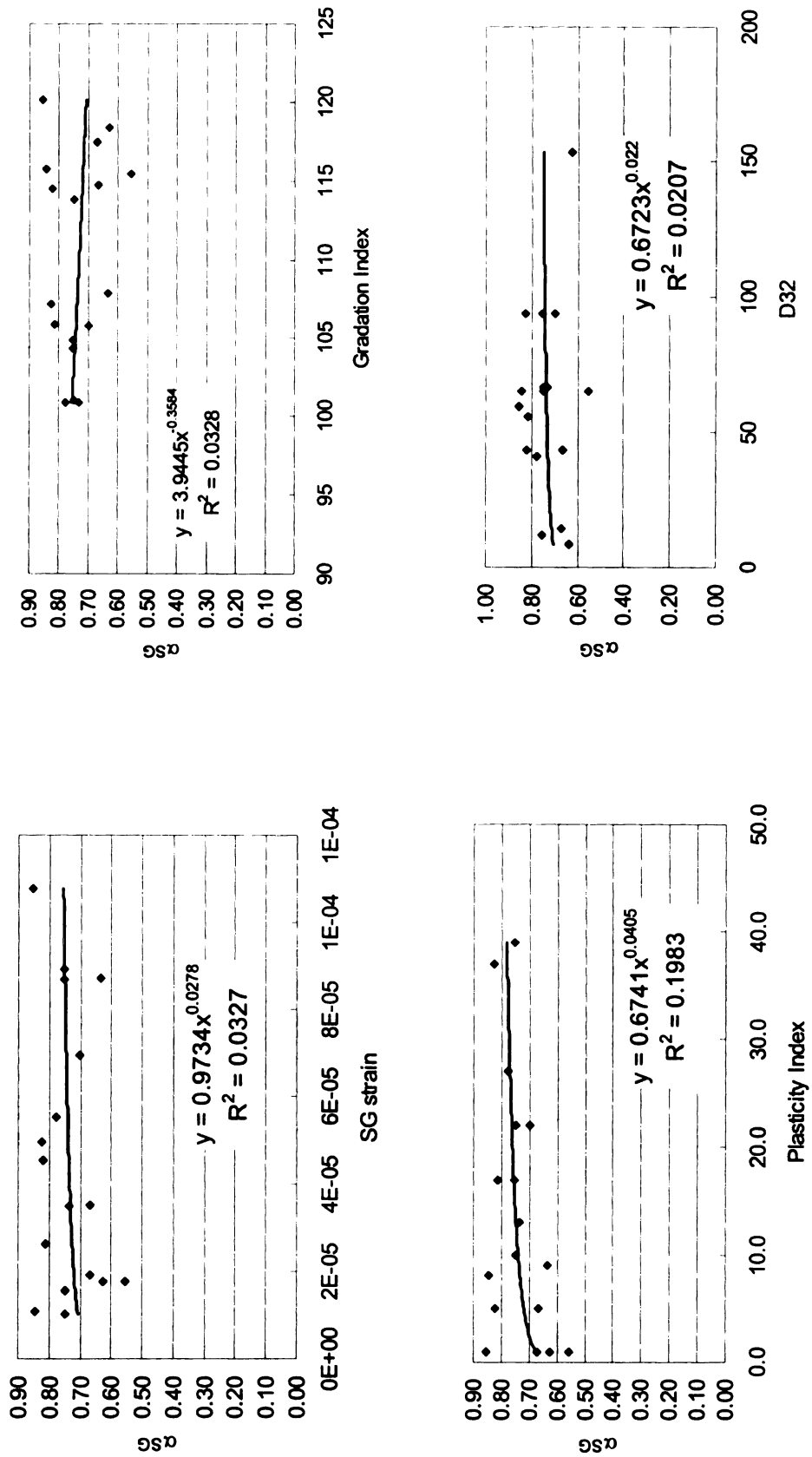


Figure 4-36 Relationship between α_{SG} and strain at the middle of the top 40 inches of SG, GI, PI, and D₃₂

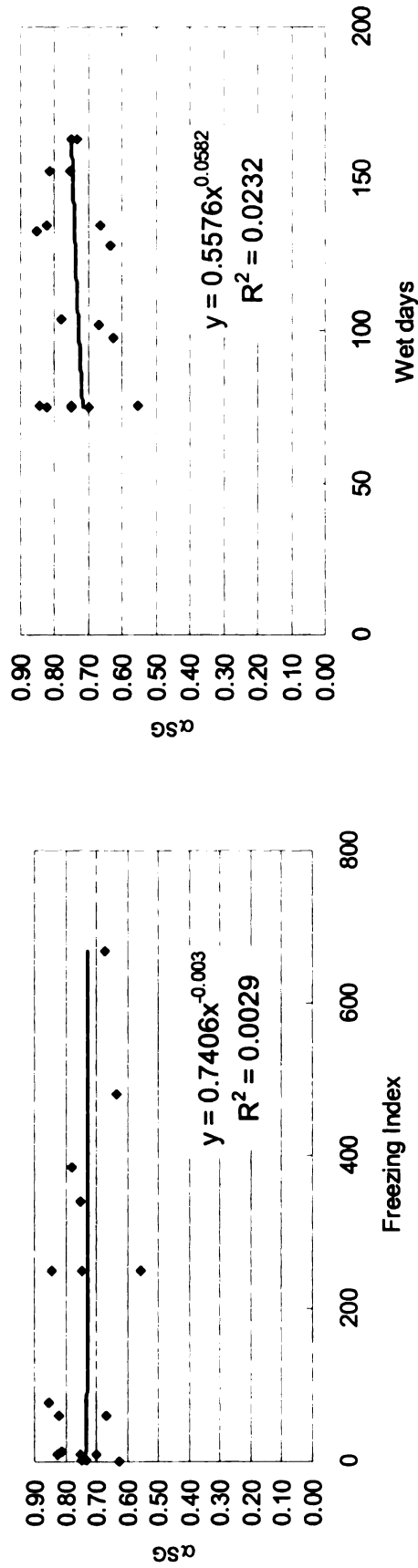


Figure 4-37 Relationship between α_{SG} and FI and wet days

Table 4-18 Descriptive statistics of α_{SG} , μ_{SG} , and the independent variables

	μ_{SG}	α_{SG}	modulus	strain	GI	PI	D32	FI	Wet days
Average	0.22	0.74	31189	4.578E-05	109.94	13.82	61.12	168.31	112.87
Minimum	0.01	0.56	16846	1.014E-05	100.86	1.00	8.43	0.74	75.04
Maximum	1.67	0.85	48495	1.077E-04	120.13	39.00	153.43	667.27	163.43
St. dev.	0.41	0.08	7827	3.171E-05	6.62	12.21	35.66	202.53	34.34
COV	54.55	871.78	398	144.35	1661.89	113.24	171.39	83.10	328.71

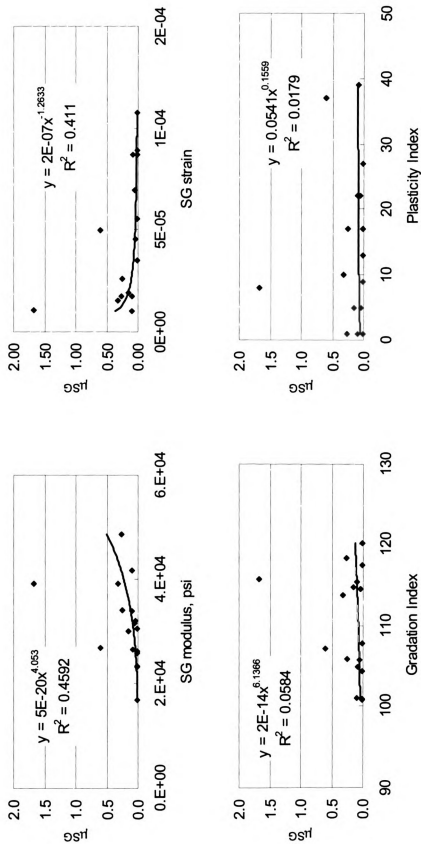


Figure 4-38 Relationship between μ_{SG} and modulus, strain at the middle of the top 40 inches of SG, GI, and PI

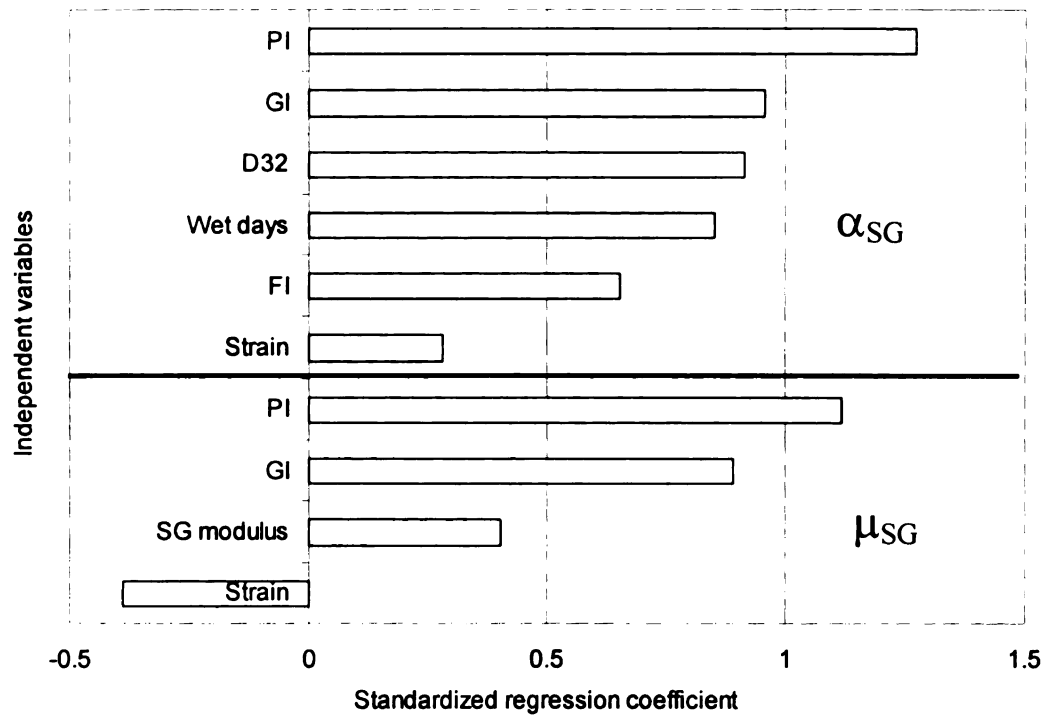
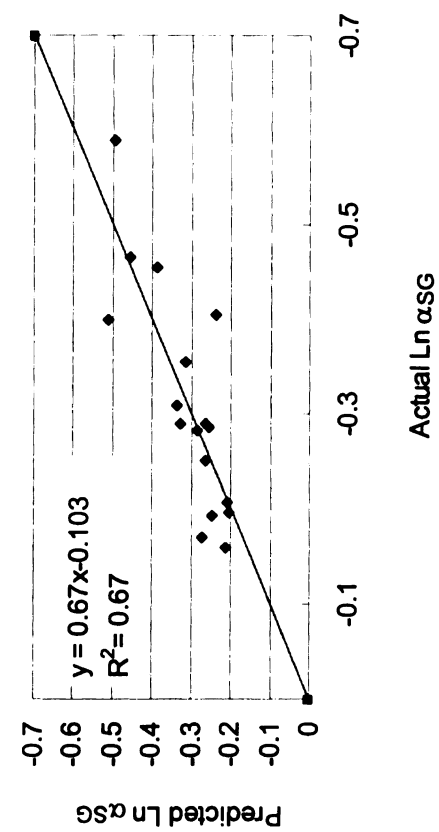


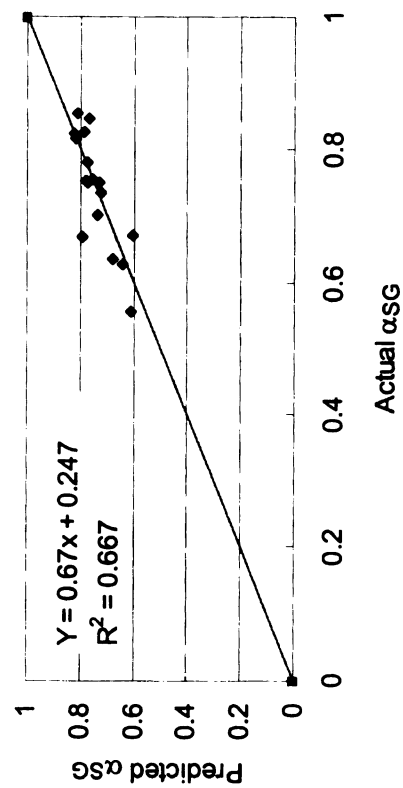
Figure 4-39 Ranking the importance of the independent variables for α_{base} and μ_{base}

4.9 SUMMARY

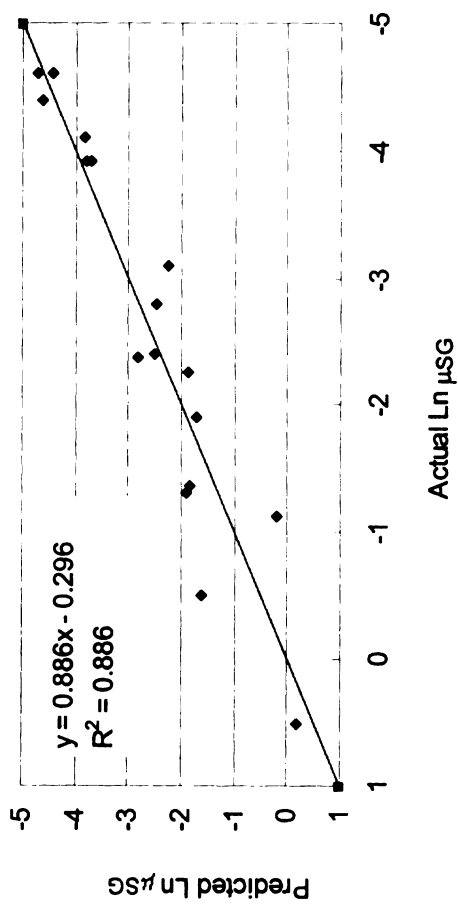
This chapter addresses several procedural difficulties that were major concerns within previous PDP backcalculations such as: 1) PDPs are site specific rather than average values that can be generalized, 2) the backcalculated PDPs are based on time series data of rutting for each section instead of one rutting value, 3) α -values should be backcalculated based on a varying traffic level (α is within the exponent of n , which is the number of load repetitions) rather than one rut value which corresponds to one traffic level, 4) choosing the backcalculated PDP values that match the sectional transverse surface profiles solves the uniqueness problem. The resulting calibrated rutting model will be utilized in the mechanistic analysis (Chapter 6) for relative comparison of different axle/truck configurations and their effects on rutting. The following section summarizes the main conclusions and the recommended future research related to this analysis.



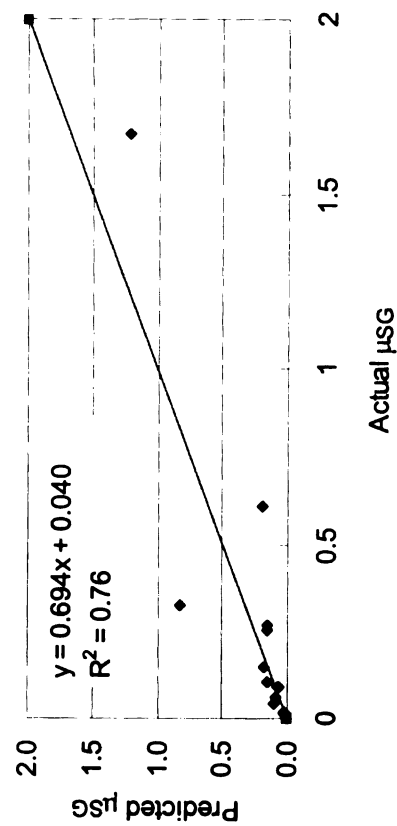
(a) Actual versus predicted α – ln scale



(b) Actual versus predicted α



(c) Actual versus predicted μ – ln scale



(d) Actual versus predicted μ

Figure 4-40 Actual versus predicted α and μ for subgrade layer

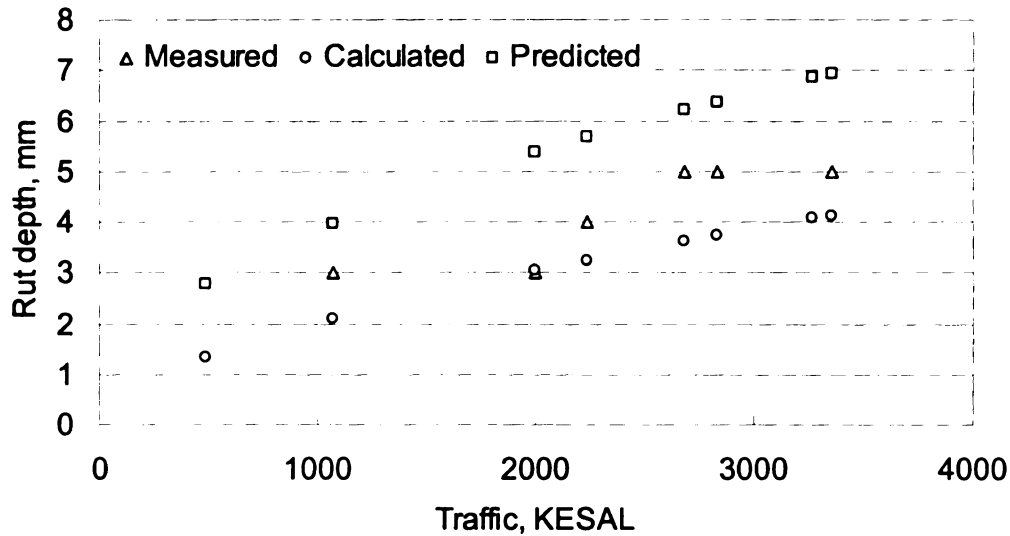


Figure 4-41 Measured, calculated, and predicted total rut depth for section 50113

4.9.1 Conclusion

Within this chapter, the following items were accomplished:

- Backcalculation of the PDPs from in-service pavement rut data;
- A remedy for uniqueness of backcalculation of PDPs was developed by selecting the solution that produces layer rutting percentages matching the individual transverse surface profile;
- A developed procedure allowing for calculation of the layer rutting contribution through non-destructive means, which also can be used as a diagnostic/prediction tool;
- A good agreement between the backcalculated PDPs, as well as layer rutting percentage, with the previously developed parameters of ALFs; and
- Parameters were predicted based on the material properties, cross sections, environmental conditions (actual field data) of each section.

4.9.2 Future research

Though the improved methodology outlined in this chapter yields promising results, there are several areas of the current study open for future improvement.

- The same analysis can be conducted again when there are more material properties available, such as *VTM*, *VMA*, and *VFA* for the HMA layer; compaction data (moisture content and dry density) and unconfined compression strength for the base layer; and more aggregate gradation for all pavement layers.
- The same analysis procedures can be performed for ALFs where more data and more controlled environments are available.
- Further validation of the calibrated rutting model can be conducted using other data sets outside of the SPS-1 experiment, such as GPS-1 and ALFs.
- The rutting model was calibrated based on the calculated strain due to one standard axle; however, either validation or calibration can be done based on axle load spectra to eliminate the error due to converting the actual load distribution to ESALs based on load equivalency factors, LEF.
- In this analysis, the rutting model was calibrated for conventional flexible pavements (three layer system); the amount of the data two-layer systems (full depth pavements) was very small. So, similar procedures for full depth asphalt pavements can be done wherever there are data for two layer pavement systems. Fortunately, the uniqueness problem will be less severe since there will be four PDPs instead of the six values in a three layer system.

CHAPTER 5- LABORATORY INVESTIGATION

5.1 INTRODUCTION

In the past few years, several research studies were conducted to select a fundamental-based laboratory Simple Performance Test (SPT) for permanent deformation. The candidate tests were evaluated and validated using three different experimental sites: 1) the Minnesota Test Road (MnROAD), 2) the Federal Highway Administration's (FHWA) Accelerated Loading Facility (ALF) test sections, and 3) the West Track FHWA test road facility. The candidate test parameters had good to excellent correlation with actual measured rut depths. The test methods and their parameters were ranked as follows: 1) the dynamic modulus measured through triaxial compression tests at high temperature; 2) the flow time measured through triaxial creep tests; 3) the flow number measured through confined or unconfined repeated load tests; and 4) the permanent shear strain measured at 1000 loading cycles using repeated shear load tests (Kaloush and Witczak, 2002).

The main purpose of the experiment in this research study is to investigate the relative rut damage caused by different axle types (single, tandem, tridem, quad etc.) as well as different truck configurations on hot mix asphalt (HMA). For this purpose, the unconfined cyclic load test was used to determine the effect of multiple loading pulses on the rutting performance of an asphalt mixture. The test enables a direct comparison of the effect of axle/truck configurations on rut performance of HMA.

5.2 SAMPLE PREPARATION

This section details the sample preparation procedure including how to determine the exact sample weight for the target air voids and gyratory compaction. Twenty 66-lb asphalt concrete bags of 4E3-MDOT mix (Layer number four from the bottom, three million ESAL repetitions) were obtained during the summer of 2004 from the Spartan Asphalt mix plant (Lansing, Michigan), labeled and stored at room temperature. Table 5-1 shows the aggregate gradation of the mix. The volumetric properties of the mix are shown in Table 5-2.

Table 5-1 Aggregate gradation of the mix

Sieve Number (opening, mm)	% passing
3/4 in (19.00)	100
1/2 in (12.50)	99.5
3/8 in (9.50)	88.6
4 (4.75)	58.7
8 (2.36)	35.2
16 (1.18)	23.7
30 (0.60)	17.3
50 (0.30)	11
100 (0.15)	6.5
200 (0.075)	4.7

Table 5-2 Volumetric properties of the asphalt mix

Property	G_{mm}	G_{mb}	G_{se}	G_{sb}	VMA	VFA	G_b
Value	2.487	2.386	2.714	2.641	14.7%	72.7%	1.028

where:

G_{mm} = maximum theoretical specific gravity	G_{mb} = bulk specific gravity
G_{se} = effective specific gravity of aggregates	G_{sb} = bulk specific gravity of aggregates
VMA = voids in mineral aggregate	VFA = voids filled with asphalt

G_b = specific gravity of the bitumen
 A 6-inch (diameter) by 7-inch (height) cylindrical sample required approximately 15.4 lb of the mixture. Since there is no simple relationship between the sample weight and percent air voids, the required sample weight for the target air voids (5.5 %) was determined through trials. Initial calculations estimated the approximate sample weight to be 15.84 lb. Knowing the target percent air voids ($Va\%$) and the maximum theoretical specific gravity of the asphalt concrete mixture (G_{mm}), the bulk specific gravity of the compacted sample can be calculated using the following equation:

$$G_{mb} = G_{mm}(100 - Va\%) \quad (5-1)$$

Knowing the expected bulk specific gravity and volume of the sample, the approximate required weight of the sample was calculated using the following equation:

$$W = G_{mb} * \rho_w * V \quad (5-2)$$

where:

- W = weight of the sample,
- ρ_w = the density of water, and
- V = the final volume of the compacted specimen.

By using this approximated theoretical weight in the first compaction trial, the number of trials to determine the targeted sample weight was minimized. The Superpave gyratory compactor was used to compact samples in the laboratory with a target air voids content of 5.5 %, as shown in Figure 5-1. Table 5-3 shows the specific gyratory compactor parameters used during the compaction procedures.

Table 5-3 Gyratory compactor setup

Setup	Value
Angle of tilt	1.25°
Loading ram	600 kPa
Rotation speed	30 rpm
Specimen height	7 inch



Figure 5-1 Compacted test specimen (6-inch diameter, 7-inch height)

For each sample, a specific gravity test (ASTM D-2726) was used to determine the actual specific gravity, volume, and air void content. The bulk specific gravity of the mix, G_{mb} , was calculated using the following equation:

$$G_{mb} = \frac{W_{dry\ in\ air}}{(W_{SSD} - W_{Submerged}) * \rho_w} \quad (5-3)$$

where:

- $W_{dry\ in\ air}$ = dry weight of the specimen,
- W_{SSD} = saturated surface dry specimen weight,
- $W_{Submerged}$ = weight of the specimen submerged in water, and
- ρ_w = density of water.

The volume of the specimen and its air voids content were calculated using the following equations:

$$V_{sample} = (W_{SSD} - W_{Submerged}) * \rho_w \quad (5-4)$$

$$Va\% = \frac{G_{mm} - G_{mb}}{G_{mm}} * 100 \quad (5-5)$$

where:

$Va\%$ = the air voids content, and

G_{mm} = the maximum theoretical specific gravity of the asphalt mix.

The air void tolerance for the test specimens was $\pm 0.5\%$ variation from the mean air voids content.

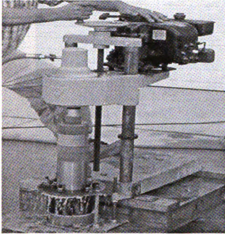
5.2.1 Samples coring, sawing, and capping

After gyratory compaction and the specific gravity test, the samples were cored from the center to produce a 3.7-inch diameter specimen. Figure 5-2 shows the coring device used. The sample holder shown in the figure was fabricated in house and used to restrain the sample during the coring process. A 0.5 inch was trimmed from each side of the cored specimen to achieve 6-inch height sample, using a saw as shown in Figure 5-3. Figure 5-4 shows the final cored and sawed sample. The cored samples were capped with sulfur capping compound according to ASTM 617-98(2003) standard. There are three main reasons for using smaller capped test specimens obtained from larger gyratory specimens in this experiment [Monismith, C.L. *et. al.* 2000 and Leahy, R.B. *et. al.* 1994]:

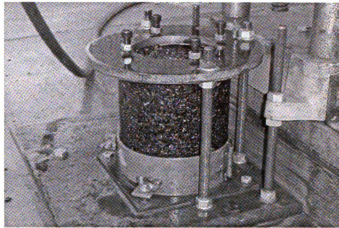
- To obtain an appropriate aspect ratio for the test specimens – A minimum H/L ratio of 1.5 was needed ($6/3.7 = 1.62$) in order to ensure that the response of a tested sample using unconfined uniaxial compression test represents a fundamental engineering property.
- To eliminate areas of high air voids in the gyratory specimens – As numerous studies have illustrated, gyratory compacted specimens of this size typically have

a large degree of non-homogeneity of air voids near the ends and the circumference of the specimen.

- To eliminate end friction and violation of the theoretical boundary effects – Relatively smooth, parallel specimen ends were achieved in the testing.



(a) Coring machine



(b) Sample holder

Figure 5-2 Coring of test specimens

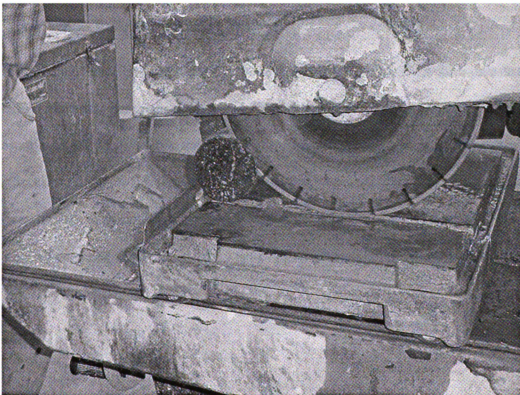


Figure 5-3 Sawing operation

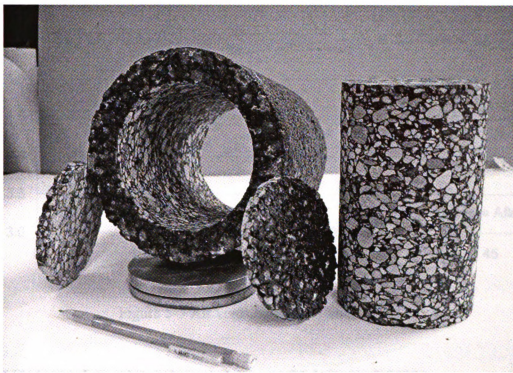


Figure 5-4 Cored sample

5.2.2 Air voids before and after coring

The bulk specific gravities and air void contents for each test specimen were measured before and after the specimens were cored. The air void tolerance used to accept or reject the test specimens was a $\pm 0.5\%$ variation from the mean air voids content for both before and after coring. Figure 5-5 shows the air voids content before and after coring. As shown in the figure the average air voids percentage before coring was 5.47 with standard deviation of 0.09 and after coring 4.22 with standard deviation of 0.15 respectively.

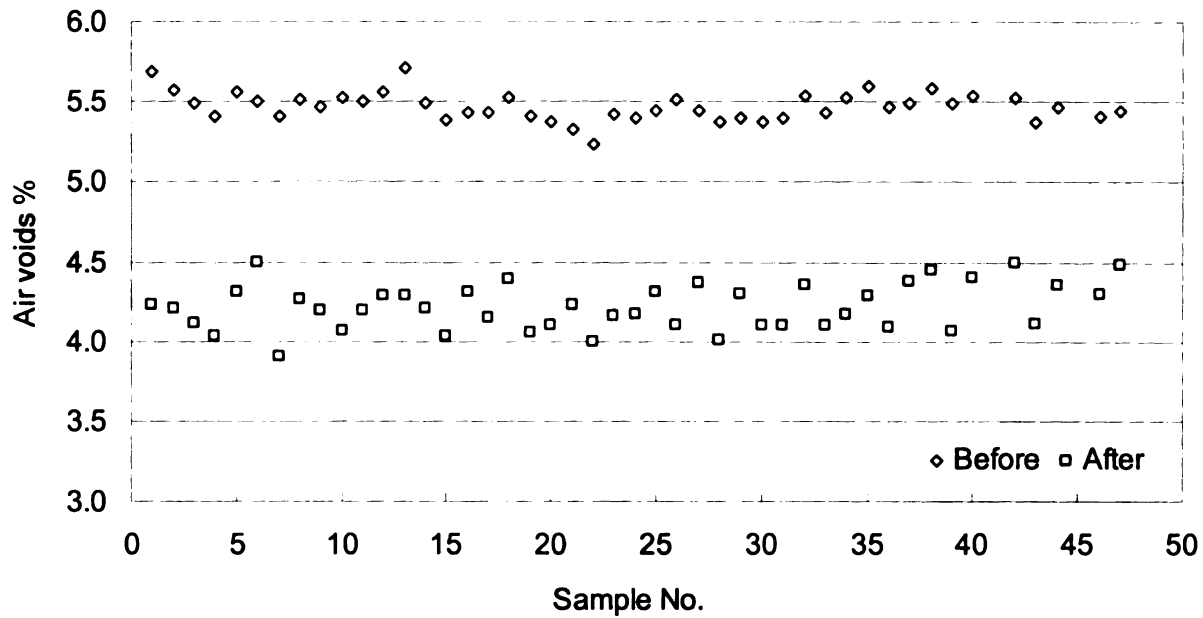


Figure 5-5 Air voids before and after coring

5.3 UNCONFINED UNIAXIAL COMPRESSION STRENGTH TEST

Unconfined uniaxial compression strength tests were conducted, at first, for two samples at 100°F to determine the maximum compression strength of the asphalt concrete cylinder. The vertical load and deformation were recorded during each test. The vertical load applied in the uniaxial cyclic load test should be much lower than the peak vertical force from the compression strength test (stress ratio from 0.3 to 0.1) to ensure that failure is not due to shear. Figure 5-6 shows the relationship between the stress and strain of samples 13 and 35. The maximum unconfined compressive strength at 100°F was 355 and 349 psi for samples 13 and 35, respectively. The stored energy (the area under the stress-strain curve in Figure 5-6) until total failure was 22.16 and 20.98 psi for the samples, respectively.

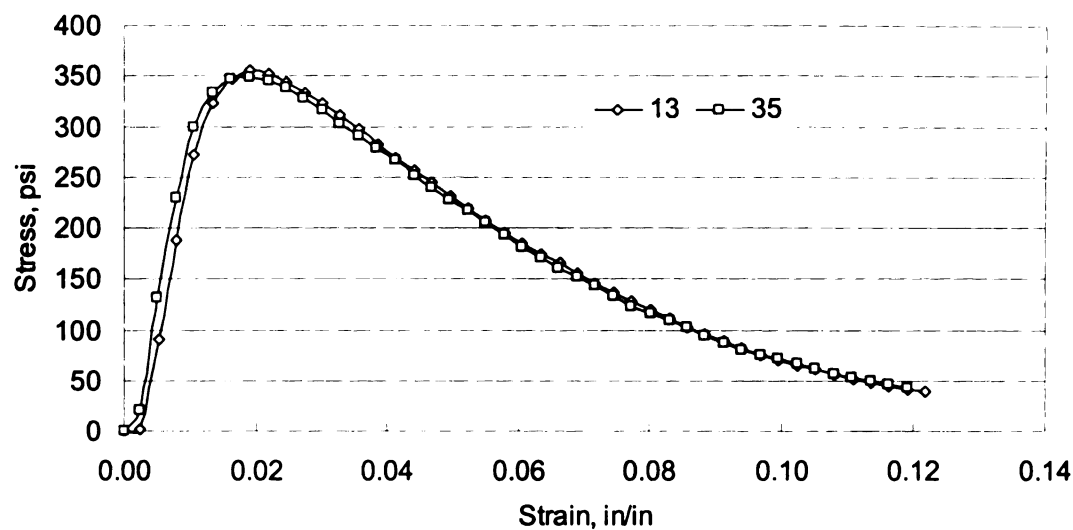


Figure 5-6 Stress versus strain for unconfined compression strength tests at 100°F

5.4 UNCONFINED CYCLIC COMPRESSION LOAD TEST

The objective of this experiment is to investigate the effect of different axle configurations and truck types on the rutting of an asphalt mixture. The results of this experiment provide a relative assessment of HMA rut damage from different axle/truck combinations, and not a (universal) predictive rut model. The specimens were subjected to cyclic pulses in an Unconfined Cyclic Compression Load Test (UCCLT). The series of cyclic uniaxial compression tests were conducted using different multiple load pulses. The pulses were designed to simulate different axle/truck configurations. The ratio of loading/unloading duration to rest period was held constant at (1:9). For single axles (as an example), the loading duration was found to be 0.08 s to simulate a load moving at 30 mph; therefore a rest period of 0.72 s was used. For multiple axle configurations and trucks, the loading time was taken as the time from the beginning of response due to the first axle until the time when the response of the last axle dies as shown in Figure 5-7.

Laboratory testing of both axle and truck configurations were performed at identical temperature (100°F) and average air void (4.22%) levels, and had the same number (2) of replications. The experimental test factorial for axle configurations is shown in Table 5-4. All axle configurations were tested at 25% and 75% interaction levels and at high stress level (corresponding to trucks tire pressure), while single and tridem axles were also tested at the 0% interaction level and the additional stress levels of low and medium (corresponding to passenger cars and light weight trucks tire pressure).

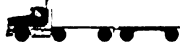




Table 5-4 experimental test factorial for axle configurations

Variable	Level of treatment				
	(1)	(2)	(3)	(4)	(5)
Axles	Single	Tandem	Tridem	Quad	8-axles
Interactions	25% and 75%	25% and 75%	25% and 75%	25% and 75%	25% and 75%
Stress level*	H, M, and L	H	H, M, and L	H	H

* Stress level: H =87.88 psi, M = 60.13psi, L = 32.38 psi

After testing axle configurations at variable interaction levels (25% and 75%), the results (to be discussed in more detail later) showed no significant difference. This influenced the subsequent design of the truck configuration testing. As a result, all truck configurations were tested at the 0% interaction level and at the high stress level (corresponding to truck tire pressure) (see Table 5-5).

Table 5-5 experimental test factorial for axle configurations

Variable	Level of treatment				
	(1)	(2)	(3)	(4)	(5)
Trucks*	S5** 	S1T2 	S1T2Tr2** 	S3T2Q1 	S1T1E1** 
Interactions	0%	0%	0%	0%	0%
Stress level	H	H	H	H	H

* Trucks defined by their axle configuration

** S5 = Truck with five single axles, S1T2Tr2 = Truck with one single axle + 2 tandem axle + 2 tridem axles, and SIT1E1= truck with one single axle + one tandem axle + one eight axle

5.5 TESTING PROCEDURES

The unconfined cyclic compression load tests were conducted using an MTS electro-hydraulic test machine, as shown in Figure 5-8. Since the pavements are more likely to rut at higher temperature, the tests were performed at controlled temperature ($100^{\circ}\text{F} \pm 1$). The samples were raised to a temperature of 100°F inside the test chamber over the course of 12 hours before starting the actual test to insure uniform temperature throughout the mass of the specimen. Two steel plates (one at the top and another at the bottom) were used to distribute the load evenly over the cross-sectional area of the specimen. Two linear variable displacement transducers (LVDTs) were connected to the sample to measure vertical deflection. The samples took from 4 to 5 hours until total failure at high stress level for all axle and truck configurations, 9 to 11 hours at medium stress level, and 45 to 50 hours at low stress level.

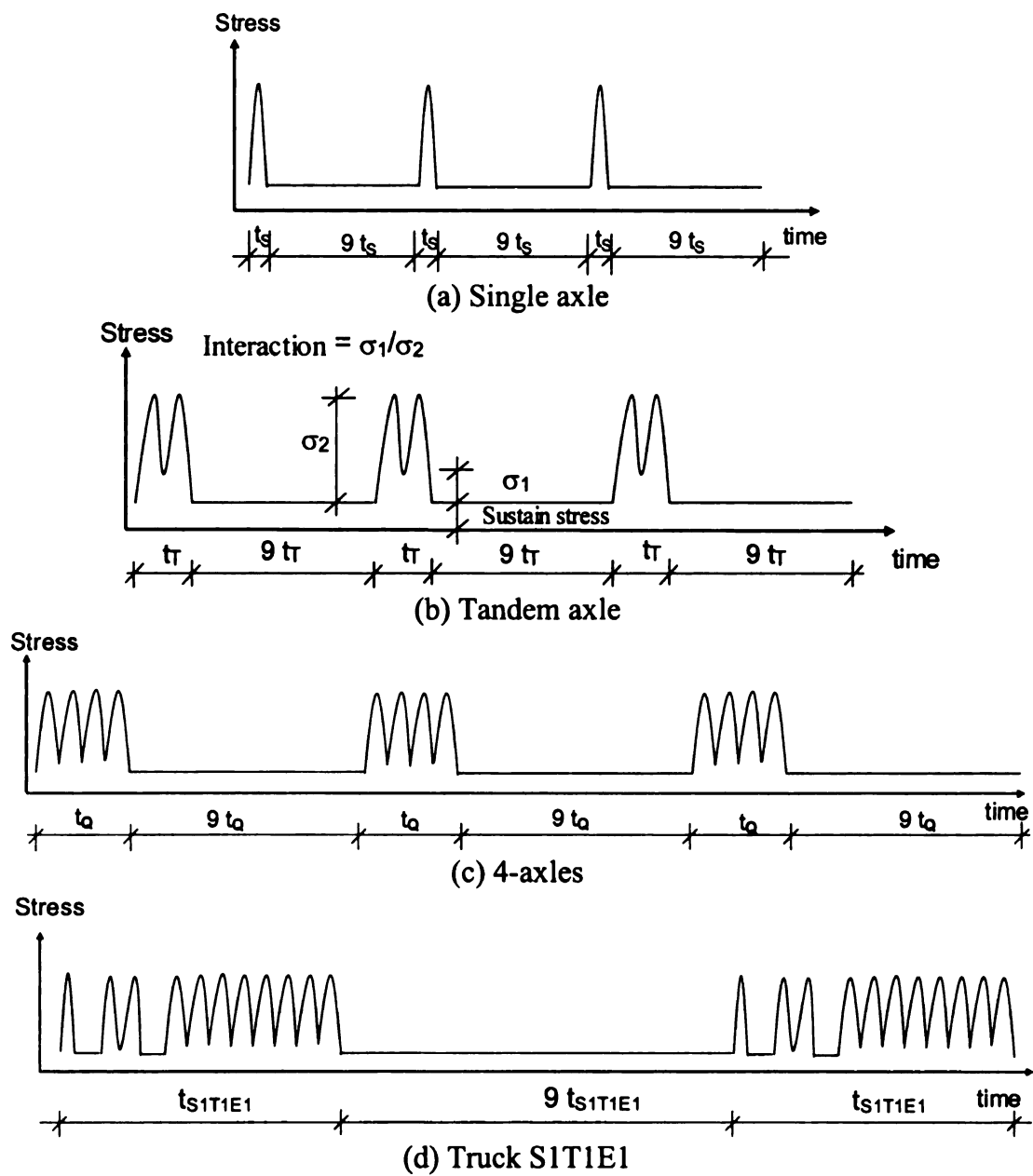


Figure 5-7 Loading and unloading time for axle and truck configurations

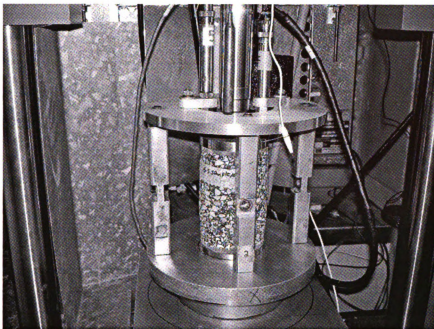


Figure 5-8 Unconfined cyclic compression load test set up

5.5.1 Typical test results

A typical example of uniaxial cyclic compression load tests results is shown in Figure 5-9 (a). As shown in the figure, the cumulative vertical permanent deformation (CVPD) can be divided into three major zones:

- The primary zone—the portion in which the strain rate decreases with loading time;
- The secondary zone—the portion in which the strain rate is constant with loading time; and
- The tertiary flow zone—the portion in which the strain rate increases with loading time.

Ideally, the large increase in compliance occurs at a constant volume within the tertiary zone. The starting point of tertiary deformation is defined as the flow number (N_f), which has been found to be a significant parameter in evaluating an HMA mixture's rutting resistance (Kaloush and Witczak, 2002). The rate of change in *CVPD* was obtained by

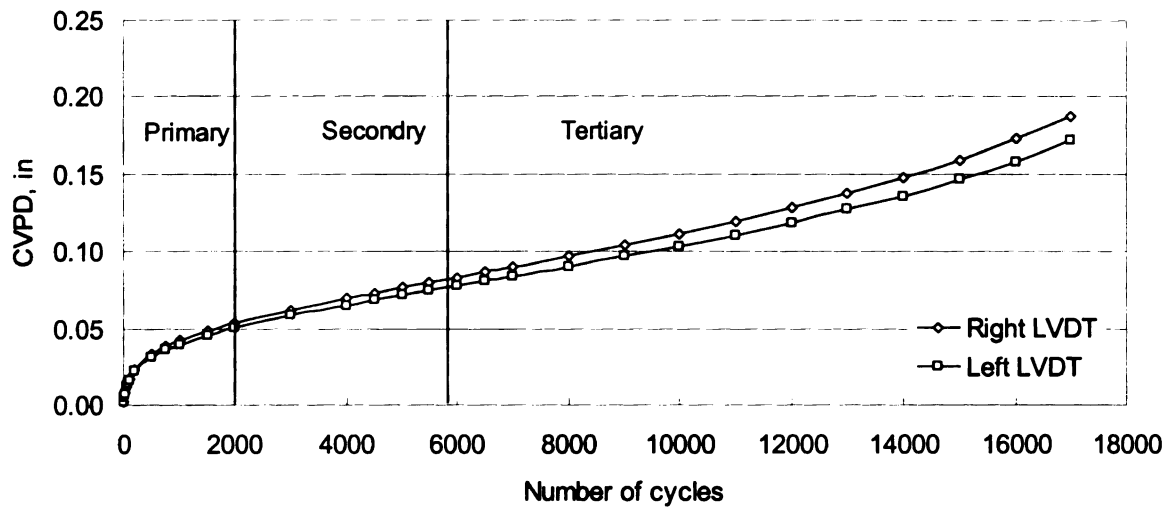
calculating the incremental slope with respect to the number of load repetitions as shown below:

$$\text{Slope} = \frac{\Delta CVPD}{\Delta N} = \frac{(CVPD)_{N_i} - (CVPD)_{N_{i-1}}}{N_i - N_{i-1}} \quad (5-6)$$

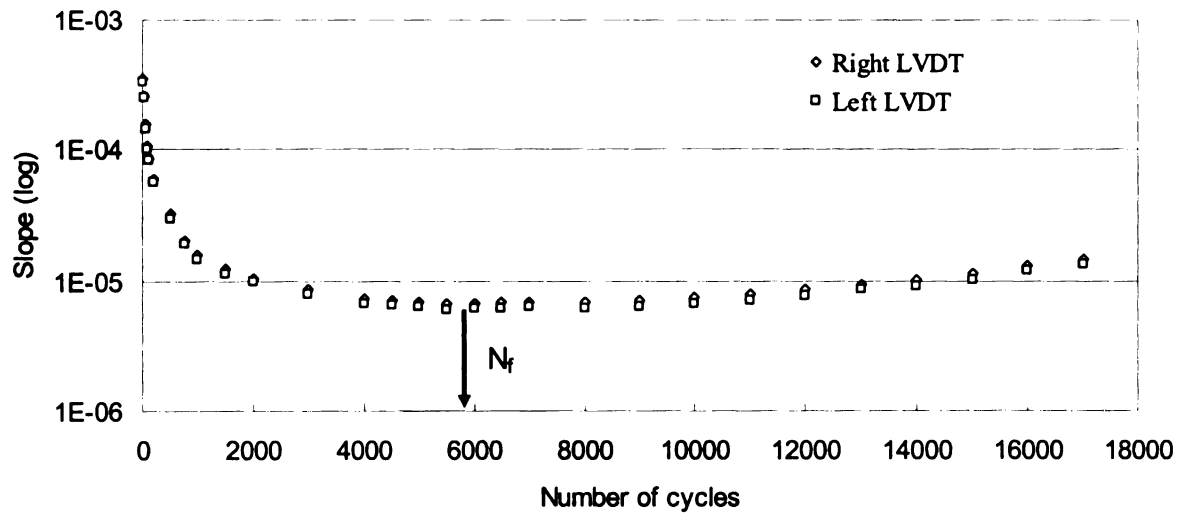
where:

$CVPD$ = cumulative vertical permanent deformation at cycle N_i or N_{i-1}
 N = number of cycles

The slope of the $CVPD$ curve first decreases (primary zone), reaches a valley or plateau (at the end of the secondary zone), and then starts to increase (throughout the tertiary zone). The decrease in the slope at the beginning of the test is due to densification and sample seating. When cracks are initiated, the rate of $CVPD$ increases. Hence, in this procedure, the rutting life of a sample is defined as the number of load repetitions at which the rate of accumulation of $CVPD$ starts to increase, as shown in Figure 5-9 (b).



(a) Relationship between cumulative vertical permanent deformation and number of cycles



(b) Rate of change in cumulative vertical permanent deformation vs. number of cycles

Figure 5-9 Typical experimental results from uniaxial cyclic compression load tests
(single axle-sample number 10)

5.6 EXPERIMENTAL TEST RESULTS

The main objective of this experiment is to study the relative effect of different axle and truck configurations on asphalt pavement rutting. Several factors were included in the experiment, and the following sections discuss these factors and show the experimental results.

5.6.1 Effect of interaction level

The applied load from a truck axle group at the surface of the pavement is distributed downward through the pavement over a triangular pattern, when viewed along a longitudinal cross-section. At the tire-pavement interface, the stress is close to the tire pressure value and there is no interaction between the responses caused by the individual axles. The load from the axle tire is distributed over a larger area at increasing depth within the pavement as shown in Figure 5-10. The amount of the interaction level depends on the thickness and the stiffness of the asphalt concrete layer, among other factors.

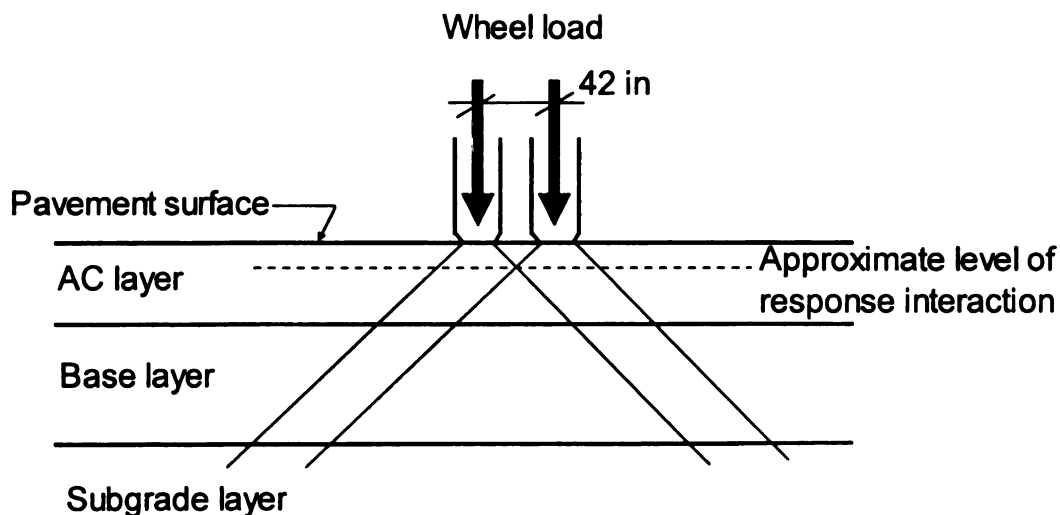


Figure 5-10 Distribution of wheel load (Deen, *et al.*, 1980)

All axle configurations used in this experiment were simulated at 25% and 75% interactions. Figure 5-11 shows an example of the interaction levels for the quad axle configurations. The number of cycles to failure (N_f) for all tested axles configurations were determined. Figure 5-12 shows the effect of the interaction level of different axle configuration on pavement rutting. The results show that there is no significant effect of the interaction level on the number of cycles to rutting failure for different axle configurations. These results indicate that the most important two factors that characterize the sample failure are the stress level and the loading pulse duration.

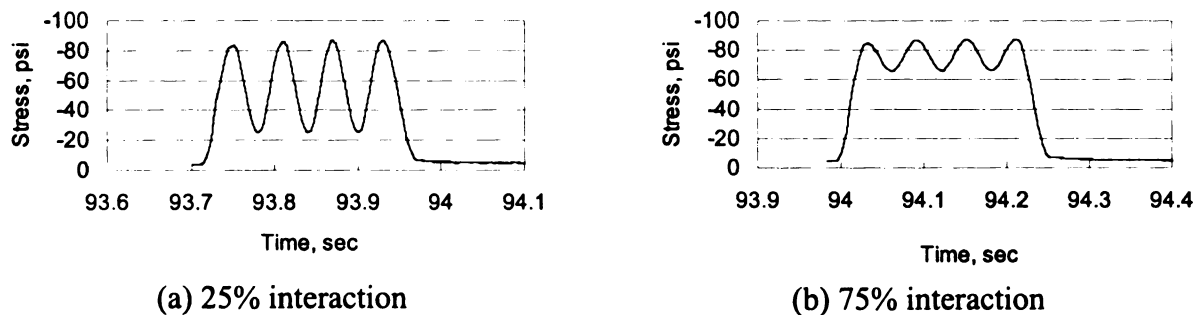


Figure 5-11 Interaction levels for the quad axle configuration

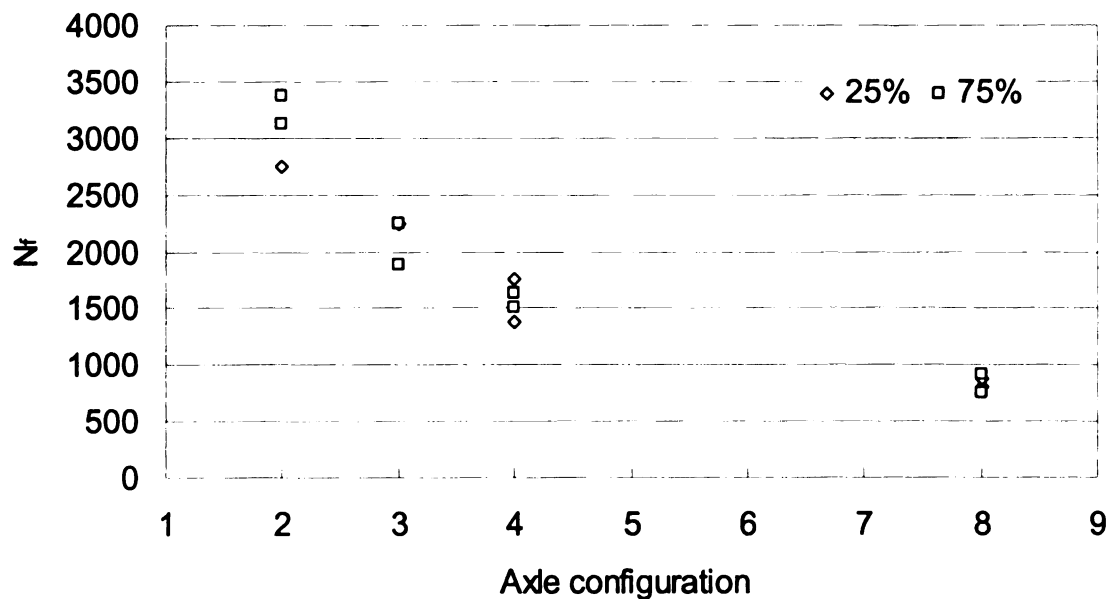


Figure 5-12 Effect of the interaction level of different axle configuration on pavement rutting

5.6.2 Axle Factors

The axle factor (AF) is defined as the damage of an axle group normalized to that of a single axle carrying the same load as any of the individual axles within the axle group.

The AF can be calculated from the following equation:

$$AF = \frac{\text{Damage of the axle group}}{\text{Damage of the single axle}} = \frac{\frac{1}{N_f \text{ axle group}}}{\frac{1}{N_f \text{ single axle}}} = \frac{N_f \text{ single axle}}{N_f \text{ axle group}} \quad (5-7)$$

Figure 5-13 shows the AF s for different axle configurations (single, tandem, tridem, quad, and 8-axles). The results show that the AF s are approximately in proportion to the number of axles within an axle group. In other words, rutting damage is proportional to axle load. A similar mechanistic finding for rutting damage was reported by Gillespie *et al*, 1993; however, the study was done for limited axle configurations. As a confirmation of this finding, the rutting damage normalized per axle load is shown in Figure 5-14. The results show that the rut damage per axle is constant for both interaction levels.

The results from this experiment provide evidence that multiple axles cause rutting at the same relative rate as single axles. They produce similar or even slightly less (the 8-axle result is 7.07 times the damage of a single axle) rutting damage than single axle loads. Additionally, comparing AF s that were previously developed for fatigue damage due to the same axle configurations at Michigan State University (El Mohtar, 2003), it appears that the multiple axles impose far less fatigue damage (the 8-axle result is 4.5 times the damage of a single axle) relative to rutting damage. To compare the results obtained from this study with those from the AASHO findings, when compared to the 13-kip single axle configuration, the AF values of the 26-kip tandem and 39-kip

tridem configurations were calculated to be 1.38 and 1.49, respectively. The AF values for the tandem and tridem configurations from this study were found to be 1.97 and 2.74, respectively. It should be noted that the AF s from the AASHO study are based on Pavement Serviceability Index (PSI) values from the AASHO road test and not from laboratory rutting tests; therefore, a significant difference between the two is understandable. The fact that the AASHO AF s fall between the AF s from this study and those of the previously cited fatigue study, suggests that axle factors need to be developed for each pavement distress rather than expecting a single axle factor to speak for all distresses. Furthermore, since pavement fatigue and rutting rarely occur at extreme levels within the same pavement, the environmental conditions of the site (i.e., average yearly temperature, seasonal variation in temperature and precipitation, etc.) must be taken into consideration when selecting the most appropriate AF to use in pavement design.

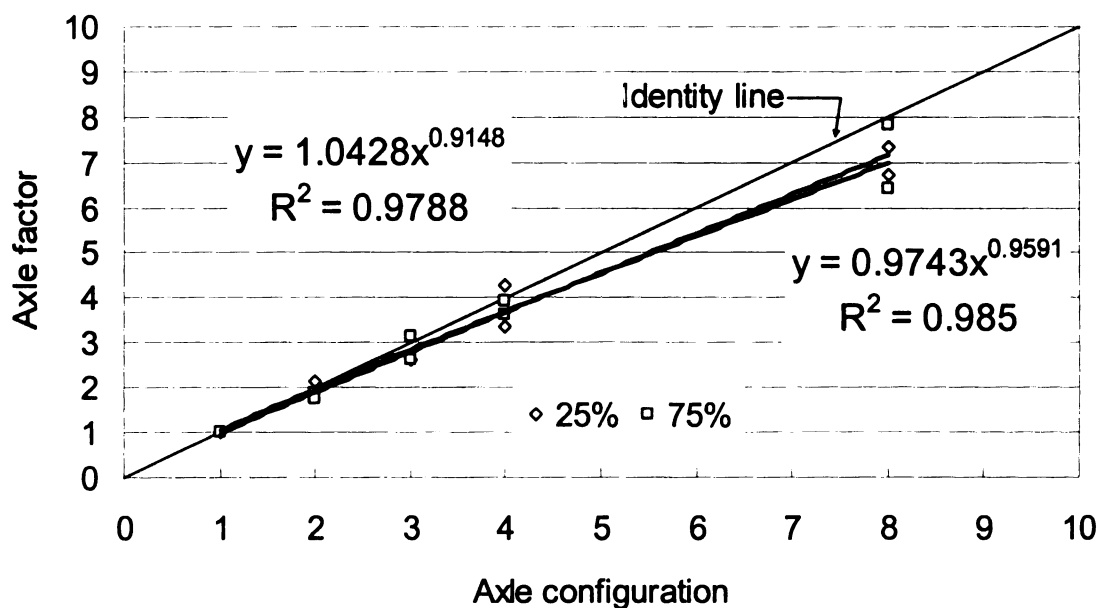


Figure 5-13 Axle factors for different axle configurations and interaction levels

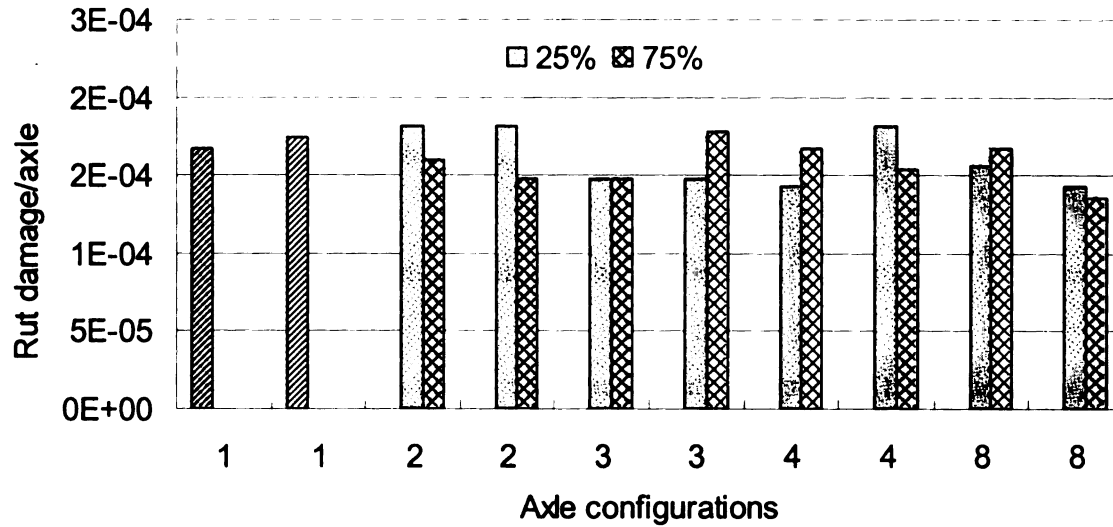


Figure 5-14 Rut damage per axle for two replications of each axle configuration/interaction level pair

5.6.3 Truck factors

As mentioned previously, after testing axle configurations at various interaction levels (25% and 75%), the results showed no significant difference between the two levels.

This influenced the subsequent design of the truck configuration testing. As a result, all truck configurations were tested at 0% interaction and high stress levels. Similar to the axle factor, the truck factor is calculated as follows:

$$TF = \frac{\text{Damage of the truck}}{\text{Damage of the single axle}} = \frac{\frac{1}{N_{f \text{ truck}}}}{\frac{1}{N_{f \text{ single axle}}}} = \frac{N_{f \text{ single axle}}}{N_{f \text{ truck}}} \quad (5-8)$$

Figure 5-15 shows the truck factors for the tested truck configurations. Though there are only two values for the total number of axles, the scatter of the results within both is far

from the direct proportionality observed in the axle factor section. It is important to note that, in both cases (5- and 11-axes), grouping of axles resulted in reduced damage. The most likely reasons for this are:

- The rest period between the truck axles is not the same as the individually tested axles,
- The sequences of the axles are mixed which affects the total sum of the damage.

Rut damage per axle for trucks is not as constant as that axle groups (from Figure 5-13), and a possible trend based on axle groups is detected. The results in Figure 5-16 suggest that as the size of the maximum axle group within truck configuration increases, the amount of rutting damage caused per load carried decreases. This result indicates that larger axle groups cause less damage per axle load when compared to smaller axle groups. It should be noted that the truck that has quad axle as a maximum axle group shows similar or slightly higher *TF* because unlike the other trucks (S1T2Tr2 and S1T1E1) this truck (S3T1Q1) has 3 single axles which create more rutting damage.

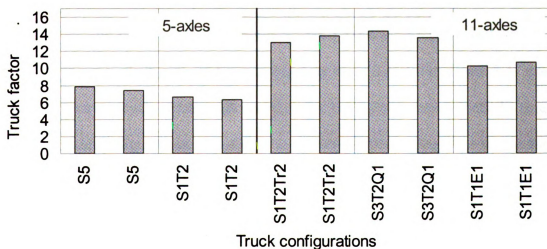


Figure 5-15 Truck factor vs. total number of axles within truck



Figure 5-16 Relationship between total number of truck axles, maximum axle group, and truck factor (two replications each)

Unlike fatigue damage, permanent deformation (rutting damage) can be constantly measured in the laboratory during the testing. Trials have been made to compose a truck's cumulative vertical permanent deformation from the values of its constituent axle configurations; however, such a sum does not match the actual values resulting from the testing of specific truck configurations, as shown for an 11-axle truck in Figure 5-17. This difference is the result of a simple addition of mismatched zone values. For example, the 8-axle configuration and the truck depicted in Figure 5-17 reach the tertiary zone at a cycle number that is well within the primary zone of both the single and tandem axle configurations. Since the vertical deformation taking place within these two zones is qualitatively different, it is unreasonable to consider summing them.

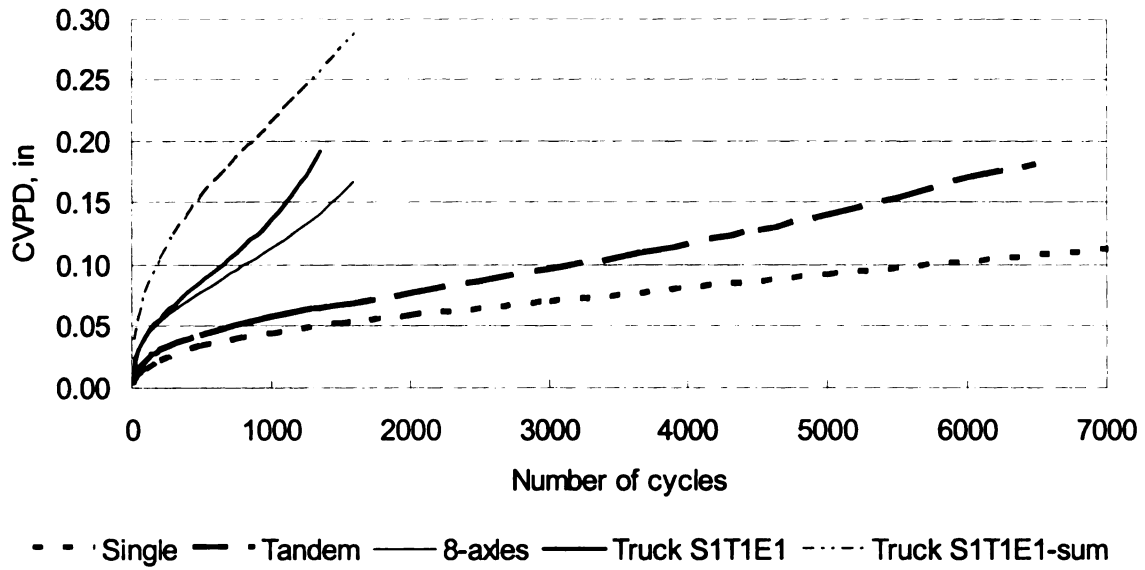


Figure 5-17 Prediction of the truck rutting damage from its constituent axle configurations

Since prediction of the truck damage from the summation of its individual axle rutting damage is erroneous, this study uses the most common method of summing damage for a loading spectrum, Miner's rule (Miner, 1924).

$$D = \sum \frac{n_i}{N_i} \quad (5-9)$$

where:

n_i = Number of cycles to failure for the truck

N_i = Number of cycles to failure for the individual axle

This method is widely understood and easy to implement and is the foundation for many other cumulative damage theories that have been proposed. Ideally, the summation of damage ratios would equal one at failure. The parameter D has been documented in the literature; it is usually found in the range $0.7 < D < 2.2$ with an average value near unity (Shigley and Mischke, 1989). Therefore, the truck damage was calculated from its

constituent axles that were tested separately. The following steps show the calculation for truck S3T2Q1.

- Using Equation 5-9, n_i is the number of cycles to failure for the truck,
- Each truck as well as its constituent axles has a duplicate,
- Table 5-6 shows the possible combinations of summing the truck damage from its constituent axles (from both axle replications); it shows 8 different possible combinations to compose the truck from its axle groupings using the number of cycles to failure from the first truck sample,
- The same equations can be applied using the number of cycles to failure from the second truck sample,
- The above steps are applied at different values of *CVPD* (0.04, 0.05, 0.06, 0.07, 0.08, 0.09, 0.1, 0.11 inch) which are within the secondary zone of permanent deformation,
- These steps produce 8 (possible combinations) * 2 (truck samples) * 8 (values of *CVPD*) = 128 possible combinations,
- It should be noted that these are not all the possible combinations, however the rest will give damage values within the range defined by the considered combinations.

The distribution of the calculated damage for each truck is shown in Figure 5-18. The average value of the damage and the standard deviation is illustrated in Figure 5-19. The results show that damage is underestimated for trucks with smaller axle groups, and as the size of the maximum axle groups increases, the rutting damage increases. The range

of the mean damage is 0.67 for the single axle truck (S5) to 1.075 for the eight-axle truck (S1T1E1); however, the overall mean damage from all truck configurations is close to unity (0.873). The accuracy of Miner's rule in calculating the rutting damage depends on the axle load spectra. In other words, if the axle loads are mixed and have all axle configurations (single to eight axles) the damage predictions will be very close to unity. Where as, if the majority of the axles are small axle groups, the predicted damage will be underestimated. On the other hand, if the majority of the axles are within larger axle groups, the predicted damage will be overestimated. There are two significant drawbacks to using Miner's rule that cause the damage values to have a wide range. First, the influence of the order of application of various axle configurations is not considered. Second, the damage is assumed to accumulate at the same rate (linear) at a given axle configuration (Oh, 1991). Though both of these need further study, developing a non-linear damage model is outside the scope of this study.

Table 5-6 Possible combinations of the truck damage from its constituent axles

1	$D1 = 3 \frac{n_1}{N_{s1}} + 2 \frac{n_1}{N_{T1}} + \frac{n_1}{N_{Q1}}$
2	$D2 = 3 \frac{n_1}{N_{s2}} + 2 \frac{n_1}{N_{T2}} + \frac{n_1}{N_{Q2}}$
3	$D3 = 3 \frac{n_1}{N_{s1}} + 2 \frac{n_1}{N_{T2}} + \frac{n_1}{N_{Q2}}$
4	$D4 = 3 \frac{n_1}{N_{s2}} + 2 \frac{n_1}{N_{T1}} + \frac{n_1}{N_{Q2}}$
5	$D5 = 3 \frac{n_1}{N_{s2}} + 2 \frac{n_1}{N_{T2}} + \frac{n_1}{N_{Q1}}$
6	$D6 = 3 \frac{n_1}{N_{s1}} + 2 \frac{n_1}{N_{T1}} + \frac{n_1}{N_{Q2}}$
7	$D7 = 3 \frac{n_1}{N_{s1}} + 2 \frac{n_1}{N_{T2}} + \frac{n_1}{N_{Q1}}$
8	$D8 = 3 \frac{n_1}{N_{s2}} + 2 \frac{n_1}{N_{T1}} + \frac{n_1}{N_{Q1}}$

where:

n_1 = number of cycles to reach certain *CVPD* for truck S3T1Q1 for the first sample

N_{s1} = number of cycles to reach certain *CVPD* for single axle for the first sample

N_{s2} = number of cycles to reach certain *CVPD* for single axle for the second sample

N_{T1} = number of cycles to reach certain *CVPD* for tandem axle for the first sample

N_{T2} = number of cycles to reach certain *CVPD* for tandem axle for the second sample

N_{Q1} = number of cycles to reach certain *CVPD* for quad axle for the first sample

N_{Q2} = number of cycles to reach certain *CVPD* for quad axle for the second sample

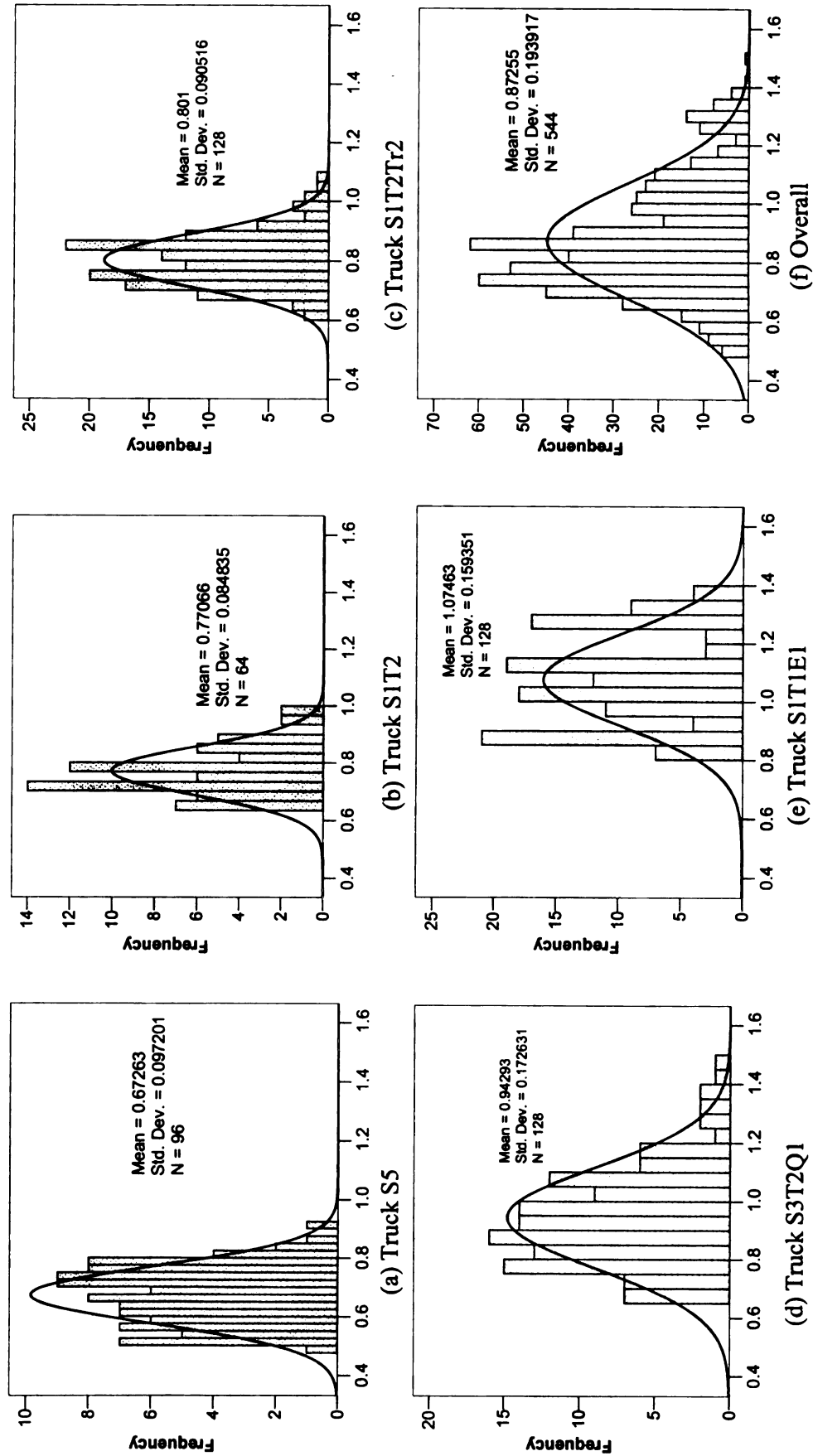


Figure 5-18 Damage distribution for different truck configurations

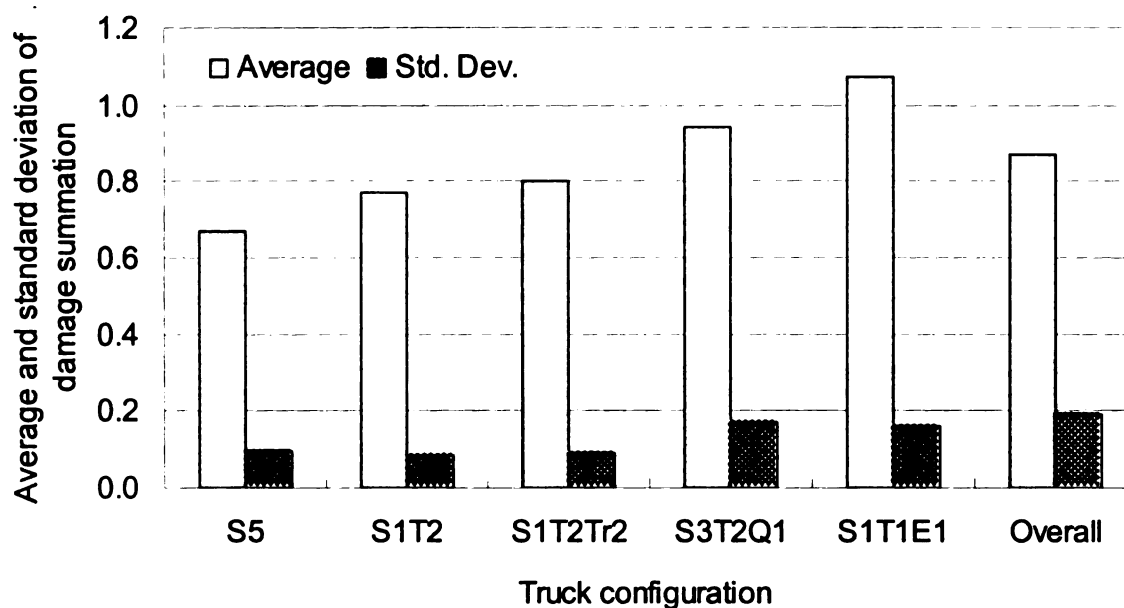


Figure 5-19 Average and standard deviation of the rutting damage for different truck configurations

5.7 PERMANENT DEFORMATION DAMAGE CURVES

Several permanent deformation damage curves were developed in this study based on: (1) last peak strain, (2) dissipated energy, (3) strain area, and (4) S-N rutting curves. The data from which these rutting damage model curves are calculated are represented in Table 5-7.

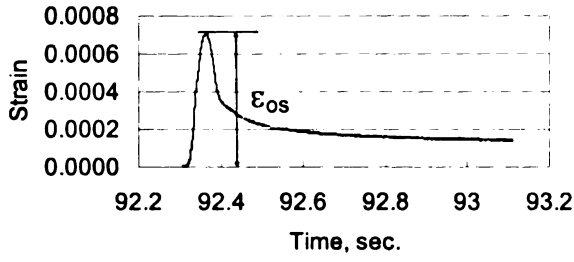
Table 5-7 Experimental test results

Axle configurations	# of Axles	Interaction level	Stress* level	AV %	Flow number (N _f)	IDE, psi	Last Peak Strain (ε _o)	Initial strain area
1-axles	1	NA	H	4.2	6000	0.02572	0.00092	0.00025
1-axles	1			4.07	5750	0.02715	0.00092	0.00025
2-axles	2	25%		4.2	2750	0.04182	0.00118	0.00055
3-axles	3			4.19	2250	0.04950	0.00114	0.00109
4-axles	4			4.23	1750	0.06223	0.00148	0.00145
8-axles	8			4.23	800	0.09877	0.00199	0.00415
2-axles	2			4.35	2750	0.04486	0.00130	0.00068
3-axles	3			4.36	2250	0.05594	0.00146	0.00112
4-axles	4			4.38	1375	0.06852	0.00183	0.00190
8-axles	8			4.39	875	0.09904	0.00203	0.00432
2-axles	2	75%		4.1	3125	0.04836	0.00144	0.00078
3-axles	3			4.11	2250	0.05550	0.00162	0.00128
4-axles	4			4.11	1500	0.06374	0.00188	0.00191
8-axles	8			4.12	750	0.07804	0.00205	0.00409
2-axles	2			4.3	3375	0.04305	0.00127	0.00066
3-axles	3			4.3	1875	0.05999	0.00175	0.00139
4-axles	4			4.31	1624	0.06465	0.00182	0.00196
8-axles	8			4.31	917	0.08345	0.00227	0.00484
1-axle	1	NA	L	4.49	74500	0.00301	0.00028	0.00004
1-axle	1			4.5	57500	0.00351	0.00038	0.00008
1-axle	1		M	4.4	13500	0.01267	0.00063	0.00017
1-axle	1			4.5	10500	0.01420	0.00072	0.00020
1-axle	1			4.45	7500	0.01349	0.00067	0.00016
3-axle	3	0%		4.17	4500	0.02887	0.00098	0.00089
3-axle	3			4.17	3125	0.03050	0.00097	0.00075
3-axle	3	L	4.16	25000	0.00708	0.00049	0.00043	
3-axle	3		4.14	19750	0.00773	0.00052	0.00046	
Truck S1T2	5	0%	H	4.08	933	0.11798	0.00190	0.00662
Truck S1T2	5			4.09	883	0.11086	0.00182	0.00629
Truck S5	5			4.1	800	0.11807	0.00180	0.00495
Truck S5	5			4.1	750	0.14000	0.00162	0.00415
Truck S5	5			4.26	750	0.12449	0.00173	0.00916
Truck S1T2Tr2	11			3.91	450	0.21985	0.00226	0.03430
Truck S1T2Tr2	11			3.99	425	0.22077	0.00257	0.01756
Truck S1T1E1	11			4.01	575	0.18627	0.00208	0.01106
Truck S1T1E1	11			4.03	550	0.18959	0.00230	0.01281
Truck S3T2Q1	11			4.05	411	0.22742	0.00189	0.01573
Truck S3T2Q1	11			4.07	434	0.21491	0.00176	0.01441

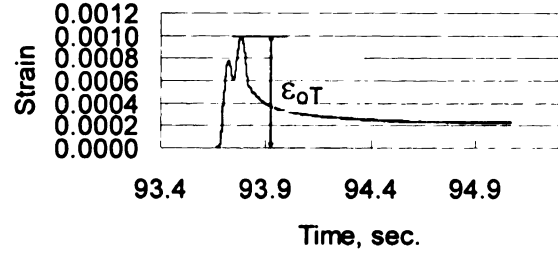
* Stress level: H = 87.88 psi, M = 60.13psi, L = 32.38 psi

5.7.1 Last peak strain curve

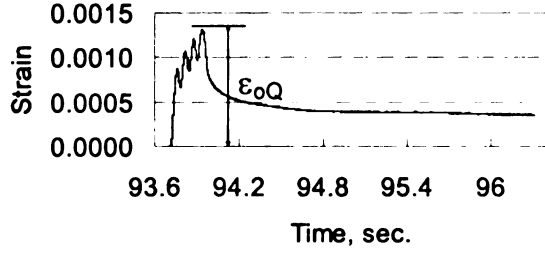
Strain-based damage curves are the most used curves for asphalt concrete. In this study, the uniaxial compression cyclic load test runs in a stress controlled mode. When testing specimens under a multi axle configuration, it was noticed that the strain peak value increased significantly from the first peak, to the subsequent peaks. The last peak strain has the advantage of representing and identifying the tested axle group or truck as shown in Figure 5-20. The last peaks of the initial strains pulses were plotted versus the number of load repetitions to failure. A strain-based rutting curve was generated based on the last strain peak of the initial cycles for all tested axles and truck configurations, as shown in Figure 5-21. The resulting last peak strain of the initial cycles can characterize the axle or truck configuration which overcomes the need for a separate rutting curve for each axle configuration. When considering the last peak strain instead of the first, the number of axles and their spacing is taken into account leading to a unique curve for different axle groups. All the different axle and truck configurations with the different interaction and stress levels are presented in Figure 5-21. Therefore, using this strain-based rutting curve allows for determining the number of repetitions until failure for any axle and truck configuration in one step, without the need to conduct testing until the total failure of the sample.



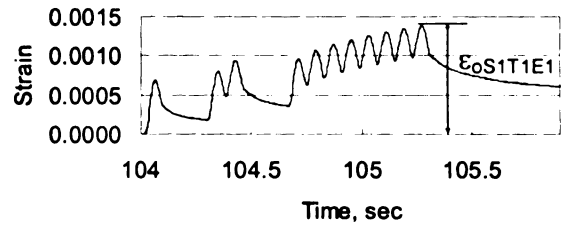
(a) single axle



(b) Tandem axle



(c) Quad axle



(d) Truck S1T1E1

Figure 5-20 Examples of the last peak of the initial strain pulse

The last peak strain rutting damage model is as follows:

$$N_f = 0.00027 \varepsilon_o^{-2.398} \quad (5-10)$$

where:

ε_o = is the last peak strain of the initial cycle, and

N_f = is the number of cycles to failure.

The developed strain-based rutting equation can be used to calculate the axle or truck

factor as follows:

$$AF \text{ or } TF = \frac{\text{Damage of axle or truck}}{\text{Damage of the single axle}} = \frac{N_{f \text{ single axle}}}{N_{f \text{ axle or truck}}} = \left(\frac{\varepsilon_{o \text{ single axle}}}{\varepsilon_{o \text{ axle or truck}}} \right)^{2.398} \quad (5-11)$$

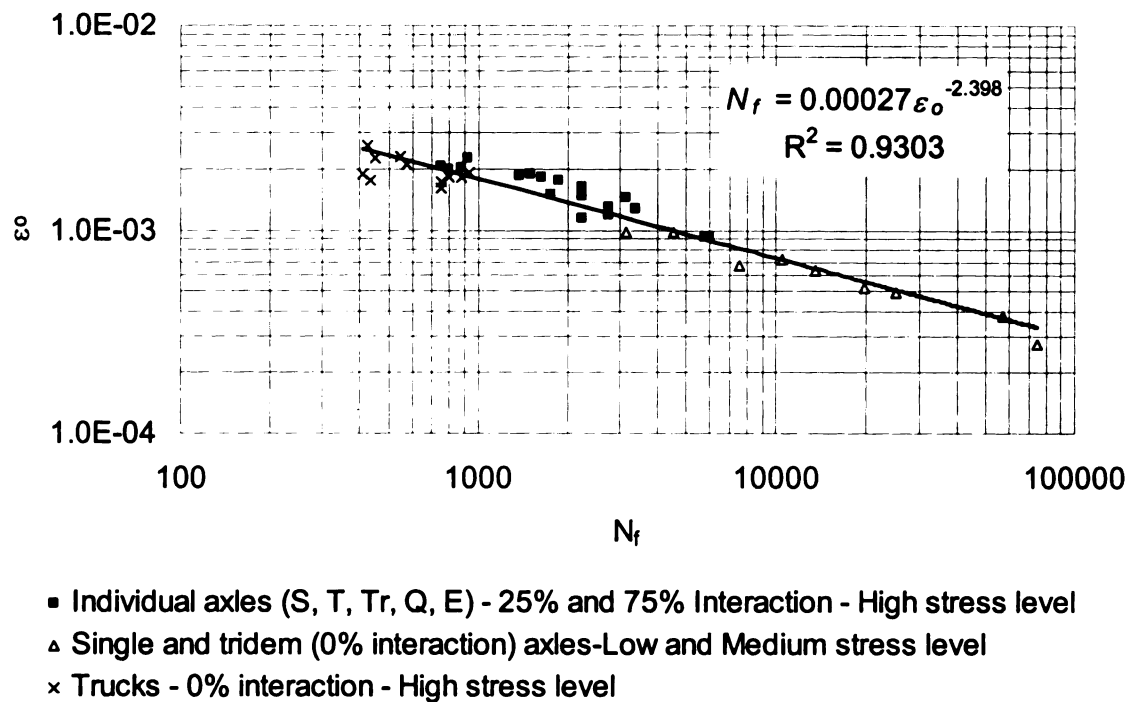


Figure 5-21 Last peak strain rutting curve

5.7.2 Dissipated energy-based curve

The dissipated energy (area within the stress-strain relationship) was calculated for all tested samples as well as the number of cycles to failure (as mentioned earlier, Figure 5-9). Figure 5-22 shows an example of the relationship between the dissipated energy and number of cycles. For the dissipated energy rutting damage curve, the initial dissipated energy density is plotted versus the number of load repetitions to failure. Figure 5-23 shows the dissipated energy rutting curve (for all individual axles, trucks, and individual axles and different stress levels). Similar to the last peak strain rutting curve, the dissipated energy-based curve is unique. All the different axle and truck configurations with the different interaction and stress levels are presented. Therefore, using this rutting curve would allow for determining the number of repetitions until failure for any axle and

truck configuration without conducting testing a sample to failure. In fact, considering the stronger correlation between IDE and N_f , this may be a more precise model for predictive purposes. Yet, the application of the dissipated energy model in mechanistic analyses would require visco-elastic analysis, which is limited by existing software (especially for larger axle groups). The dissipated energy rutting damage model is as follows:

$$N_f = 64.935 \text{ } IDE^{-1.1902} \quad (5-12)$$

where:

IDE = is the initial dissipated energy density in psi of the whole axle or truck group, and

N_f = is the number of cycles to failure.

Equation 5-12 can be used to calculate the axle or truck factors as follow:

$$AF \text{ or } TF = \frac{\text{Damage of axle or truck}}{\text{Damage of the single axle}} = \frac{N_{f \text{ single axle}}}{N_{f \text{ axle or truck}}} = \left(\frac{IDE_{\text{single axle}}}{IDE_{\text{axle or truck}}} \right)^{1.19} \quad (5-13)$$

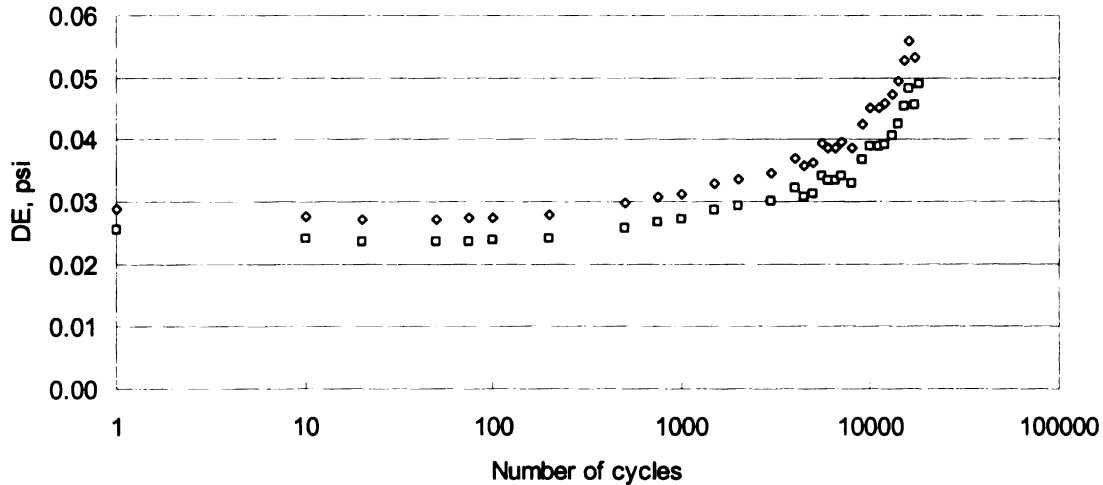


Figure 5-22 Example of Dissipated energy versus number of load repetitions for one sample (two LVDT)

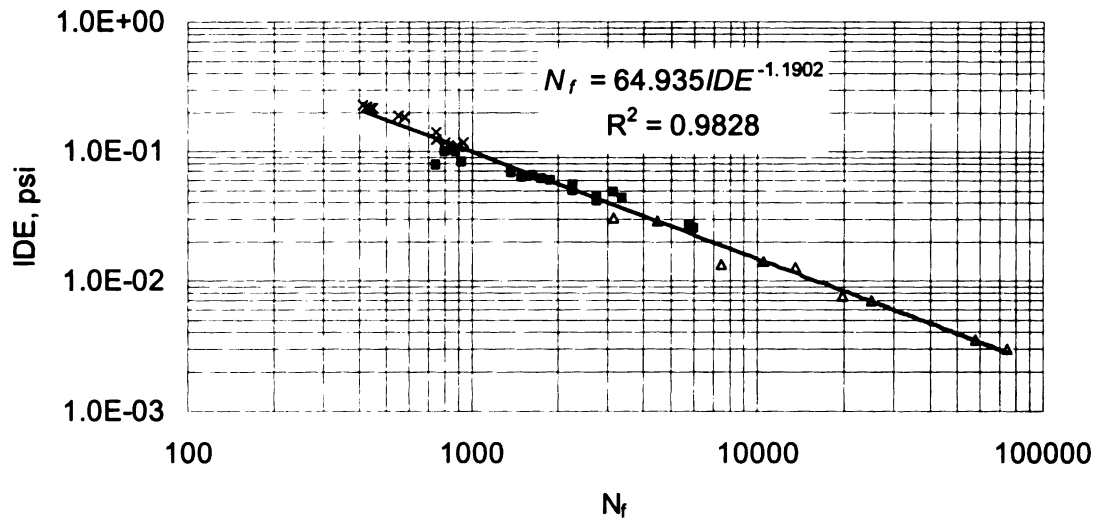


Figure 5-23 Dissipated energy-based rutting damage curve

5.7.3 Strain area-based curve

The area under the initial strain curves (Figure 5-20) were calculated for all tested axle and truck configurations as well as different stress levels, and plotted against the number of cycles to failure, as shown in Figure 5-24. The strain area-based rutting damage model obtained from this procedure is as follows:

$$N_f = 14.857 A_o^{-0.777} \quad (5-14)$$

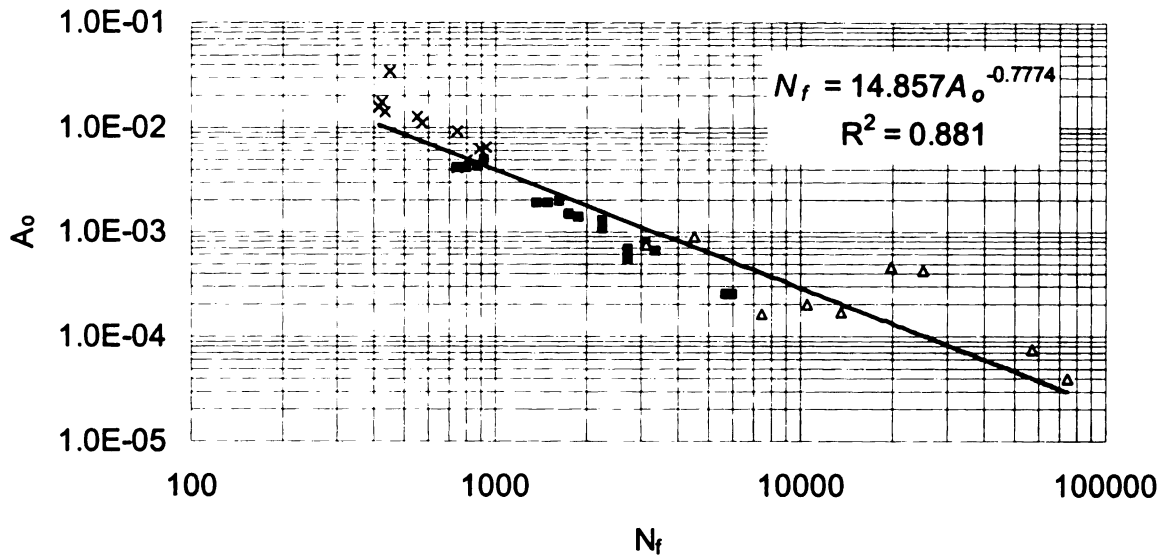
where:

A_o = is the initial area under the strain curve, and

N_f = Number of cycles to failure.

Axle and truck factors can be calculated using the area-based rutting damage as follows:

$$AF \text{ or } TF = \frac{\text{Damage of axle or truck}}{\text{Damage of the single axle}} = \frac{N_f \text{ single axle}}{N_f \text{ axle or truck}} = \left(\frac{A_{o \text{ single axle}}}{A_{o \text{ axle or truck}}} \right)^{0.777} \quad (5-15)$$



- Individual axles (S, T, Tr, Q, E) - 25% and 75% Interaction - High stress level
- △ Single and tridem (0% interaction) axles-Low and Medium stress level
- × Trucks - 0% interaction - High stress level

Figure 5-24 Strain area-based rutting damage curve

The dissipated energy method and the strain area method are recommended for estimating pavement rutting damage, rather than the last peak strain method. This is simply because the initial last peak strain in the laboratory includes not only the effect of the individual axle load, but also the sample's "memory" of previous axle loads within an axle group. Since all peaks are of equal strain value in a mechanistic analysis, especially when elasticity of the pavement system is assumed, a mechanistic application of this method can not adequately represent the system's response to an entire axle group. Since rutting damage depends not only on the discrete strain value, but also the duration of the pulse, the additional advantage of the dissipated energy and strain area methods is that

both utilize a more complete representation of the values and duration of the axle group response.

5.7.4 Stress-based curve

All axles and trucks were tested at high stress level except for single and tridem axles; these were additionally tested at medium and low stress levels. Figure 5-25 shows the relationship between the stress levels (H = 87.88 psi, M = 60.13 psi, L = 32.38 psi) and the number of cycles to failure. The results show that the two relationships for single and tridem are approximately parallel (slope of single = -2.45 and slope of tridem = -2.35) with an average factor of 2.7 for high stress level, 3.2 for medium stress level, and 2.9 for low stress level (overall 2.9) between them. These results confirm the proportionality, even at different stress levels, of rut damage with respect to axle gross weight.

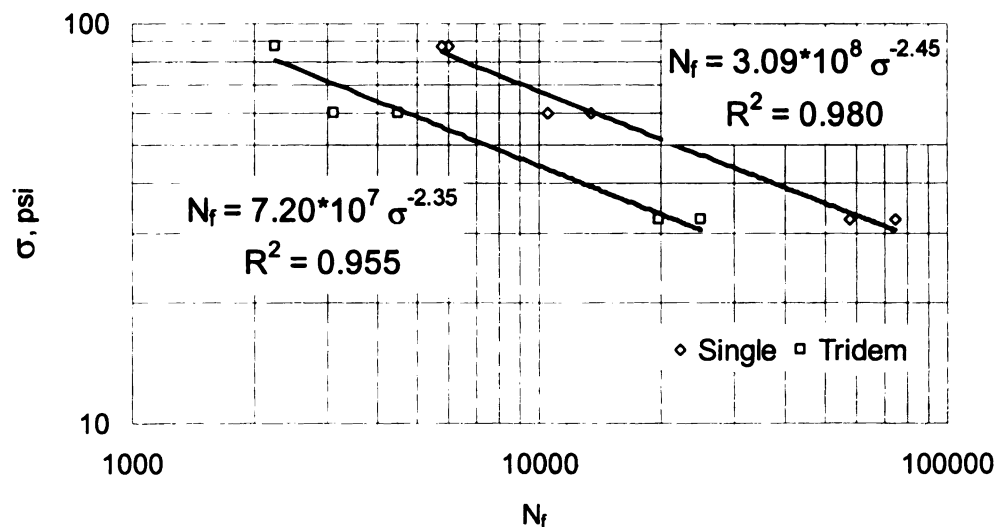


Figure 5-25 Stress level versus number of cycles to failure (S-N curve) for single and tridem axles

5.8 CALIBRATION OF PERMANENT DEFORMATION DAMAGE MODELS

Characterizing the flexible pavement damage caused by multiple axle loads requires quantification and summation of the pavement responses. Two different approaches can be used: (1) discrete methods (Hajek and Agarwal, 1990) and (2) integration (Hajek and Agarwal, 1990) or strain rate methods (Govind, 1988). The discrete methods are applicable only for single pulses, so when it comes to multiple axles their usefulness is debated within the research community since most do not account for the pavement response rate due to the passage of multiple axles. On the other hand, the integration method proposed with an arbitrary exponent, n_i , is incompatible with the other methods. Similarly, the strain rate method was developed for fatigue damage and there is not enough information to apply it to rutting damage. In this research, axle factors for pavement rutting due to multiple axle pulses were developed in the laboratory using Uniaxial Compression Cyclic Load Tests (UCCLT). These axle factor were used to facilitate the calibration of all of these methods in order to determine a suitable exponent for each.

5.8.1 Peak method

This method was developed and used mainly for the mechanistic analysis of asphalt pavement fatigue. This method relates the damage of single or multiple axles and truck configurations to the damage of a standard axle based on peak strains (Figure 5-26) as follows:

$$AF \text{ or } TF = \frac{\text{Damage of axle or truck}}{\text{Damage of the standard axle}} = \frac{N_f \text{ std.}}{N_f \text{ axle or truck}} = \sum_{i=1}^m \left(\frac{\epsilon_{std}}{\epsilon_i} \right)^{n_p} \quad (5-16)$$

where:

- ϵ_{std} = peak strain caused by the standard axle,
- ϵ_i = peak strain from multiple axle or truck,
- M = number of axles in an axle group or truck, and
- n_p = the exponent of the peak method.
- N_f = number of cycles to failure

This method is calibrated by assuming an arbitrary exponent, n_p , and minimizing the sum of the square error between the predicted and the laboratory axle factor using Excel solver. The calibrated exponent (n_p) was 0.2061 with a square error sum of 2.279. Figure 5-27 shows the axle factor from the calibrated peak method versus laboratory axle factor for different axle configurations.

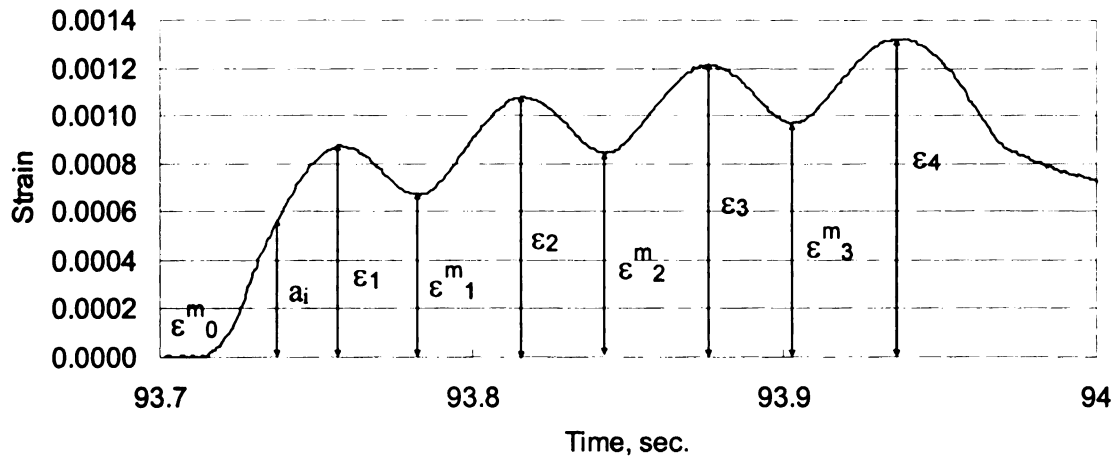


Figure 5-26 Peak and peak midway strain for 4-axle group

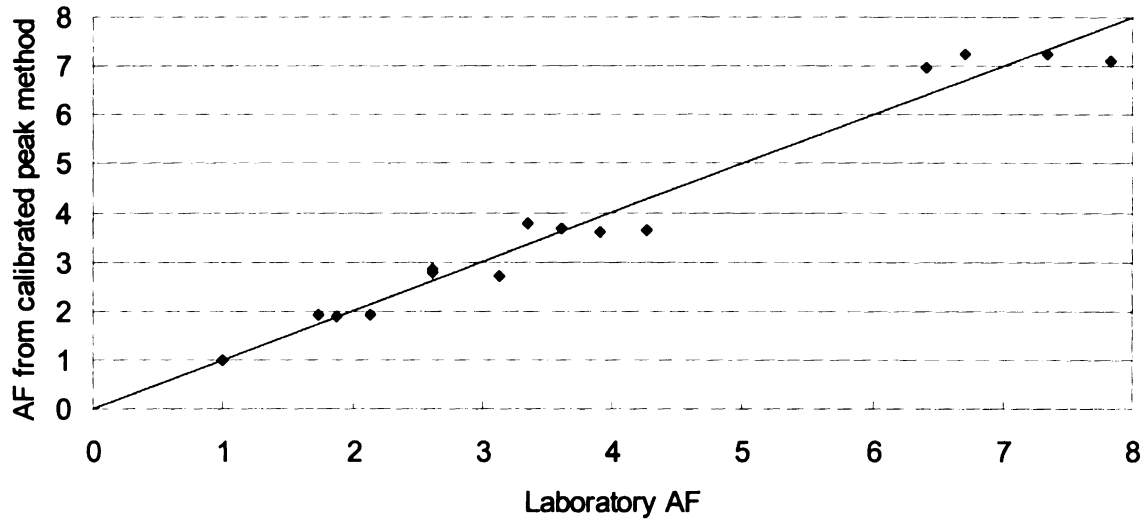


Figure 5-27 Axle factor from calibrated peak method versus laboratory axle factor

5.8.2 Peak-midway method

Similar to the peak method, the peak-midway strain method was developed and used mainly for the mechanistic analysis of asphalt concrete fatigue. This method relates the first peak and the subsequent valley-to-peak difference (Figure 5-26) to the peak of a standard axle raised to the exponent, n_{p-m} , as follows:

$$AF \text{ or } TF = \frac{\text{Damage of axle or truck}}{\text{Damage of the standard axle}} = \frac{N_f \text{ std.}}{N_f \text{ axle or truck}} = \frac{P}{\sum_{i=1}^P} \left(\frac{\epsilon_{std}}{\epsilon_i - \epsilon_{i-1}^m} \right)^{n_{p-m}} \quad (5-17)$$

where:

- ϵ_{std} = peak strain of the standard axle,
- ϵ_i = peak strain of multiple axle or truck,
- ϵ^m = midway strain,
- P = number of axles in an axle group or truck, and
- n_{p-m} = the exponent of the peak-midway method.
- N_f = number of cycles to failure

The peak-midway method was calibrated using the laboratory axle factor values to determine the exponent for rutting damage. The calibrated exponent (n_{p-m}) was -0.1069 with a square error sum of 2.47. Figure 5-28 shows the axle factor of the calibrated peak-midway method versus the laboratory axle factor values for different axle configurations.

Both peak and peak-midway methods do not take into account the duration of the strain pulse since both consider the discrete values of the peak or peak and midway strains. However, rutting damage is highly influenced not only by the strain value but also by the duration of the loading pulse. Therefore, the integration and strain rate methods are examined in the following sections.

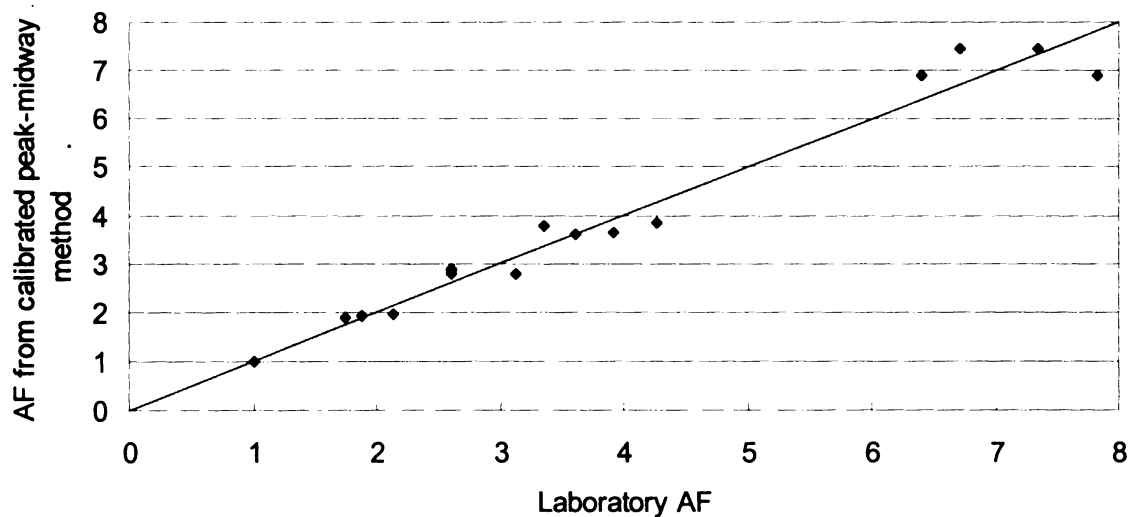


Figure 5-28 Axle factor from calibrated peak-midway method versus laboratory axle factor values

5.8.3 Integration method

The integration method was proposed by Hajek and Agarwal, 1990. Even though the method takes into account both the magnitude and duration of the pavement response due to multiple axles, the arbitrary nature of the exponent, n_i , makes it incompatible with the

other methods. The developed laboratory axle factors facilitate the calibration of this method, and allow for an empirical determination of a suitable exponent. The axle and truck factor can be calculated from the integration method as follows:

$$AF \text{ or } TF = \frac{N_f \text{ std.}}{N_f \text{ axle or truck}} = \frac{\int_0^t |a_i|^{n_i} dt}{\int_0^t |a_s|^{n_i} dt} \quad (5-18)$$

where:

- a_i = the strain values of an axle or truck within the strain time history as shown in Figure 5-26,
- a_s = the strain values of standard axle within the strain time history,
- t = time if the strain is expressed in the time domain and distance if the strain is expressed in the space domain,
- n_i = is the integration method exponent, and
- N_f = number of cycles to failure.

The calibrated exponent for this rutting-oriented application of the integration method is 0.1303, compared to 3.8 for the fatigue discrete methods (peak and peak-midway). The square error sum is 2.387. This large difference can be explained by the following observations:

- The previous exponent (3.8) was not calibrated for the integration method; it was borrowed from the discrete methods.
- The previous exponent (3.8) was based on fatigue, which has a fundamentally different failure mechanism than rutting (0.1303).
- The exponent in the integration method is inside the integrand, which is expected to require, even for fatigue, a dramatically different value due to its location in the equation. Therefore, the usual “power law” explanation does not apply when the exponent is within an integration.

The resulting exponent offers a promising solution to the problem of multi-axle damage prediction, since the integration method accounts for not only the peak values but also for the duration of the strain pulse. Figure 5-29 shows the relationship between the axle factors of the calibrated integration method versus the laboratory axle factor values.

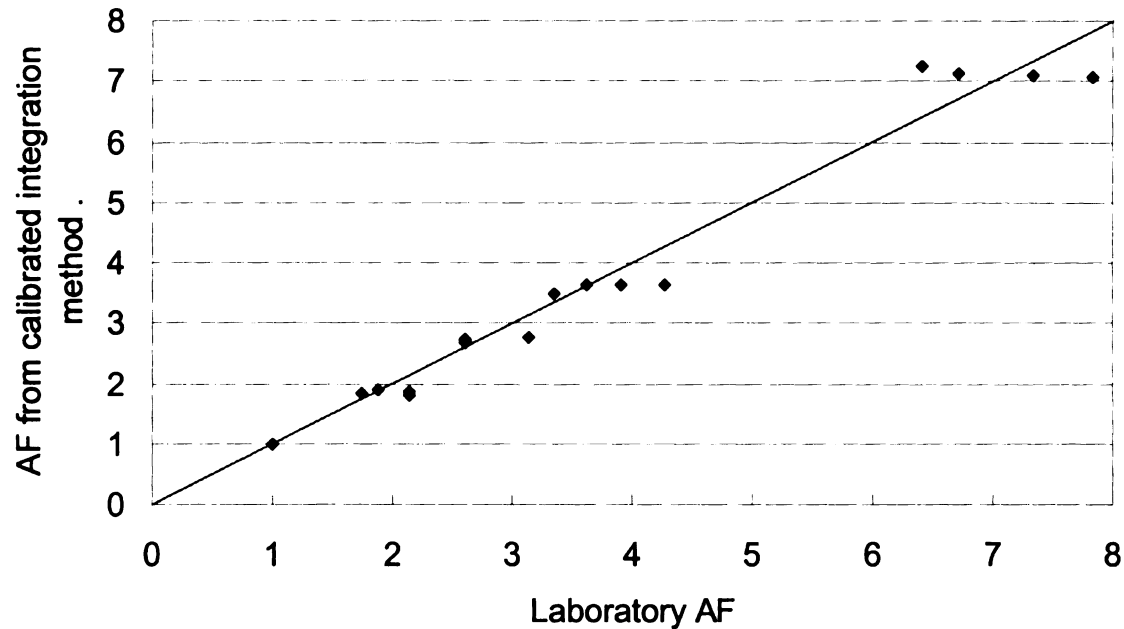


Figure 5-29 Axle factor from the integration method versus laboratory axle factor values

5.8.4 Strain rate method

The strain rate method was developed to determine the damage transform from stress fields as shown in Equation 5-19 (Govind, 1988). The method was developed for fatigue and calibrated using AASHO road test data. The calibration has an excellent agreement with the AASHTO load equivalency factors. The strain rate method is adapted in this study to the strain field as shown in Equation 5-20. Figure 5-30 depicts the elements of the strain rate method.

$$\sum_{i=1}^m D_i^n = \sum_{i=1}^m \left(\frac{1}{t_{i+1} - t_i} \int_{t_i}^{t_{i+1}} \left| \frac{d\sigma}{dt} \right| dt \right)^n \quad (5-19)$$

$$AF \text{ or } TF = \frac{\text{Damage of axle group or truck}}{\text{Damage of single axle}} = \frac{N_f \text{ std.}}{N_f \text{ axle or truck}}$$

$$\begin{aligned} & \sum_{i=1}^m \left(\frac{1}{t_{i+1} - t_i} \sum_{j=1}^p |\epsilon_{j+1} - \epsilon_j| \right)^{n_{s-r}} \\ &= \frac{\sum_{i=1}^m \left(\frac{1}{t_{i+1} - t_i} \sum_{j=1}^p |\epsilon_{j+1} - \epsilon_j| \right)^{n_{s-r}}}{\left(\frac{1}{t_1 - t_0} \sum_{j=1}^p |\epsilon_{j+1} - \epsilon_j| \right)^{n_{s-r}}} \end{aligned} \quad (5-20)$$

where:

m = number of axles (sub-event),

p = number of discrete points within one sub-event,

t_o = the starting time of the sub-event,

t_1 = the ending time of the sub-event 1 and starting time for sub-event 2, and

ϵ = the discrete strain values within the sub-event, and

n_{s-r} = is the exponent for the strain rate method.

N_f = number of cycles to failure

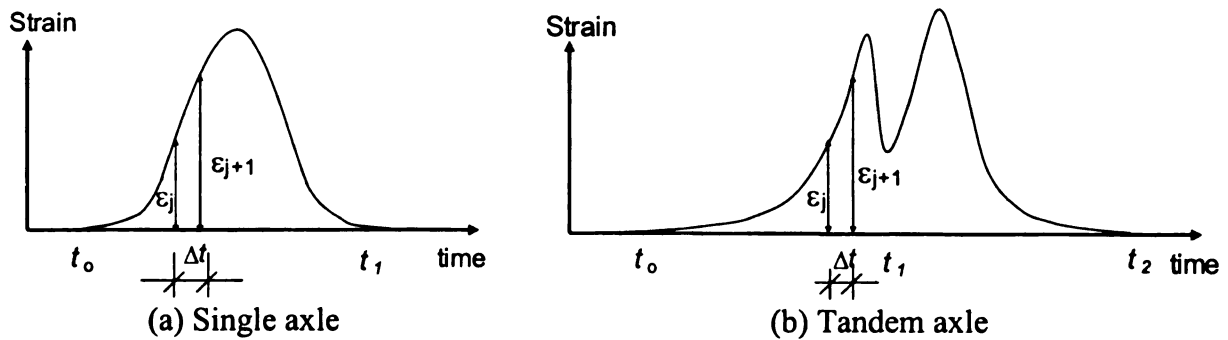


Figure 5-30 Depiction of variables from strain rate method

The laboratory axle factor facilitates the calibration of the strain rate method.

Similar to the integration method, the strain rate method is calibrated by iteration of the square error sum minimization process. Due to its computational complexity, an iterative

approach was used to minimize the difference between the axle factor of the strain rate method and the laboratory axle factor values by changing the exponent n_{s-r} . The calibrated exponent, n_{s-r} , of the strain rate method is 0.8625 with square error sum of 9.032. Figure 5-31 shows the relationship between the calibrated strain rate method axle factors and the laboratory axle factor values.

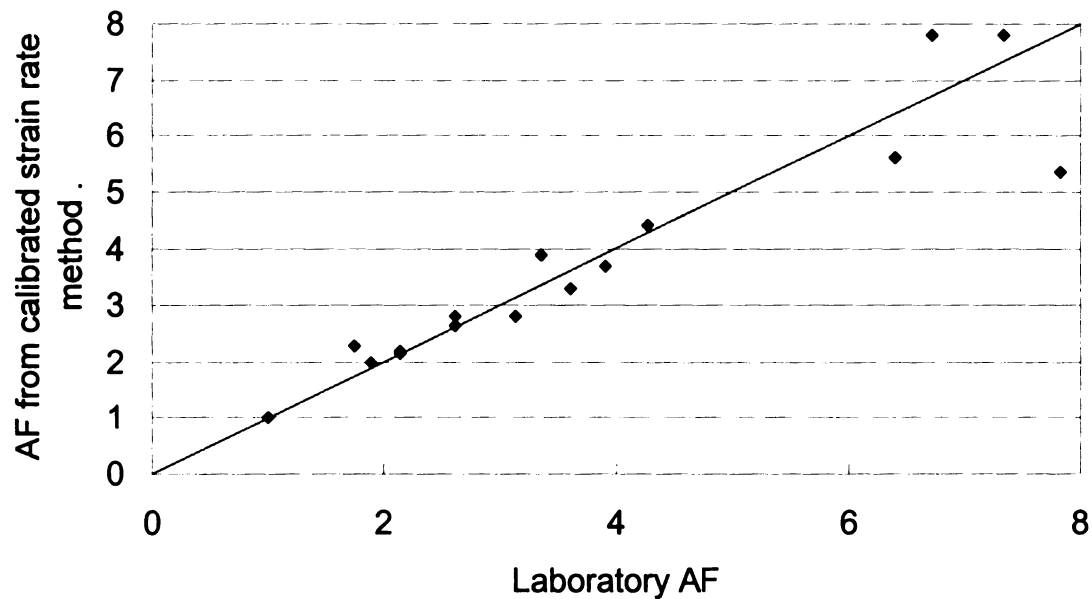
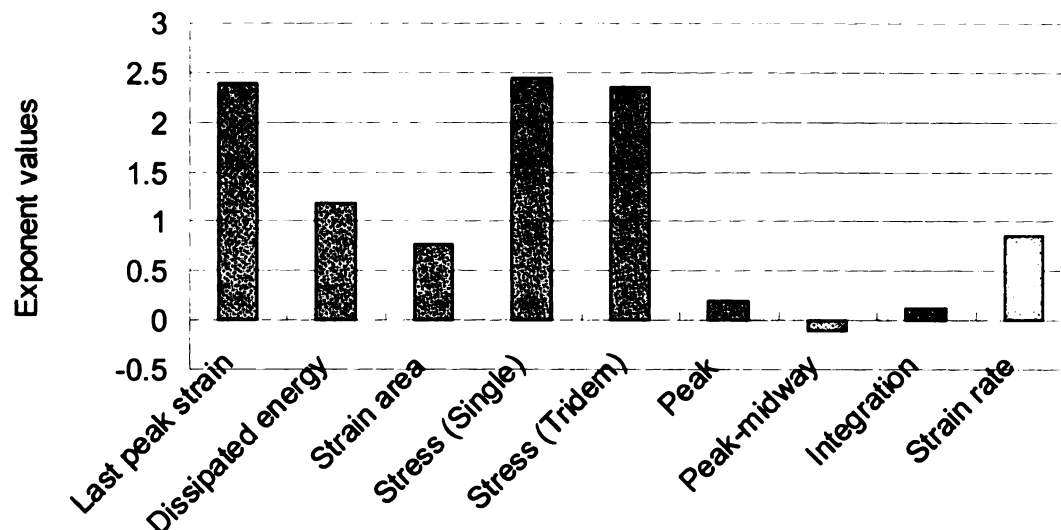


Figure 5-31 Axle factor from strain rate method versus laboratory axle factor values

Figure 5-32 summarize the exponents and the square error sum of all developed rutting damage models and the calibrated methods.



Developed and calibrated methods

Figure 5-32 Summary of the developed and calibrated rutting damage methods

The last peak initial strain, strain area, and dissipated energy methods were calibrated for the laboratory axle factor values, and their exponent values (n 's) were approximately the same as each of the power corresponding to their individual permanent deformation damage curves (section 5.7). The relatively close agreement between these two strategies for calculating each method's n value is evidence of consistency in the calibration procedure. However, the exponent of each permanent deformation damage curve is more reliable, since it is based on a larger, more diverse data set, containing not only all axle configurations but also the truck configurations and stress levels.

5.9 PREDICTION OF PERMANENT STRAIN

It is well known that permanent deformation, whether in the field or in the laboratory, obeys a fractional-power relationship ($0 < \alpha < 1$); however when a laboratory sample

reaches the tertiary zone (failure) this relationship no longer applies ($\alpha > 1$). Therefore, the permanent deformation power function within the first two zones can be expressed as follows:

$$\frac{\varepsilon_p}{\varepsilon_r} = \mu N^\alpha \quad (5-21)$$

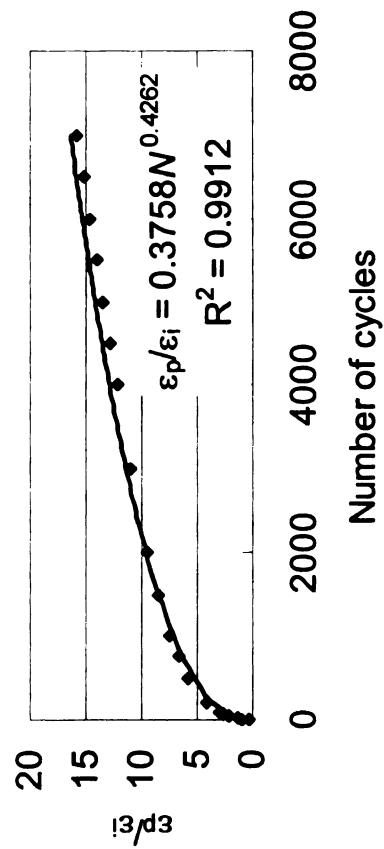
where:

- ε_p = accumulated permanent strain,
- ε_r = resilient strain,
- μ = permanent deformation parameter representing the constant of proportionality between plastic and elastic strain,
- α = permanent deformation parameter indicating the rate of decrease in permanent deformation as the number of load applications increases, and
- N = the number of load applications.

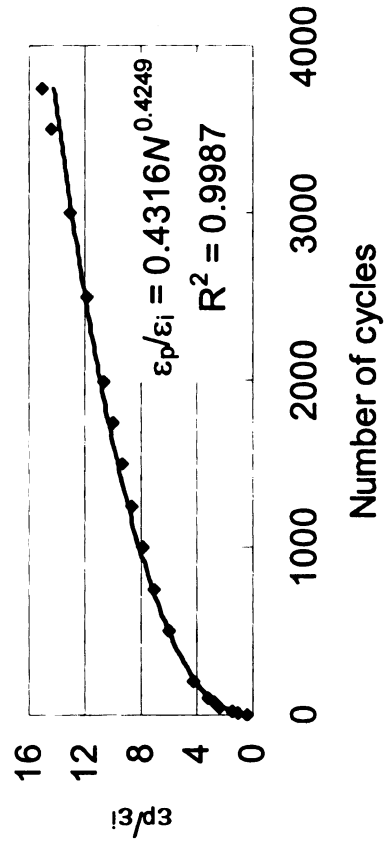
The cumulated vertical permanent strains were normalized with the value of the initial last peak strain (as shown in Figure 5-20). As mentioned earlier, the last peak strain has the advantage of representing and uniquely identifying the tested axle group or truck. The normalized accumulated permanent strains with the values of the initial last peak strain were plotted against the number of load repetitions within the primary and secondary zones only, as shown in Figure 5-33. The figure shows samples of the μ and α values for three different axle configurations and one truck configuration. It should be noted that the initial last peak strain from the laboratory includes the resilient, visco-elastic, and the plastic strain.

The μ and α values for all tested axle and truck configurations were calculated and are displayed in Figure 5-34. As can be seen in the figure the values of α (the rate of change in permanent deformation as the number of load applications increases) cluster tightly in a small range, from 0.35 to 0.61. The values of μ (the proportionality between

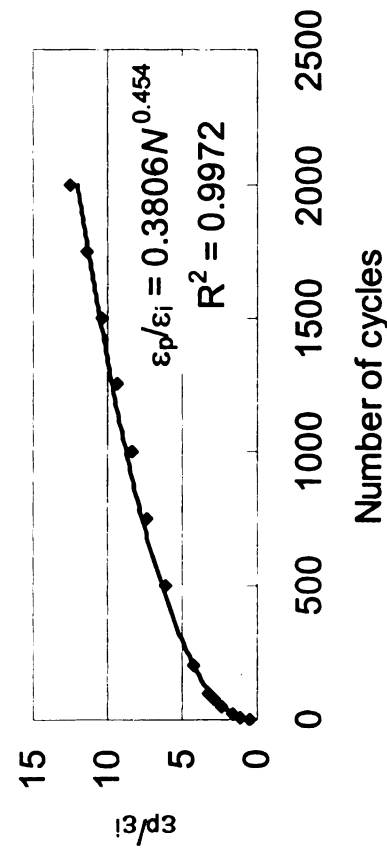
plastic and elastic strain) cluster more loosely in a wider range, from 0.12 to 0.56. This means that once the sample is compacted and the aggregate is seated, the rate of the accumulated plastic strain, when normalized with its initial strain, will be approximately the same regardless of the load configuration. These results indicate that laboratory samples follow a trend that is consistent with the behavior of field performance, but the predictive power of the laboratory values for α and μ depends upon more detailed calibration from field data. Chapter 4 explains one such method that could be used for field calibration of permanent deformation parameters in further detail.



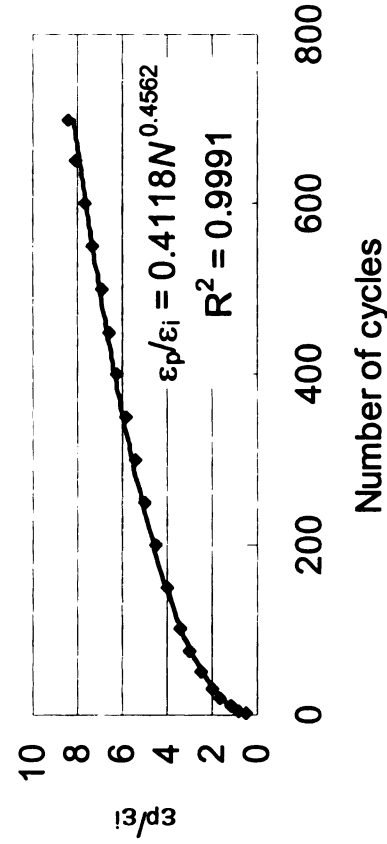
(a) Single axle



(b) Tandem axle



(c) Quad axle



(d) Truck S1T1E1

Figure 5-33 Example of normalized cumulative strain with the initial last peak strain versus number of cycles

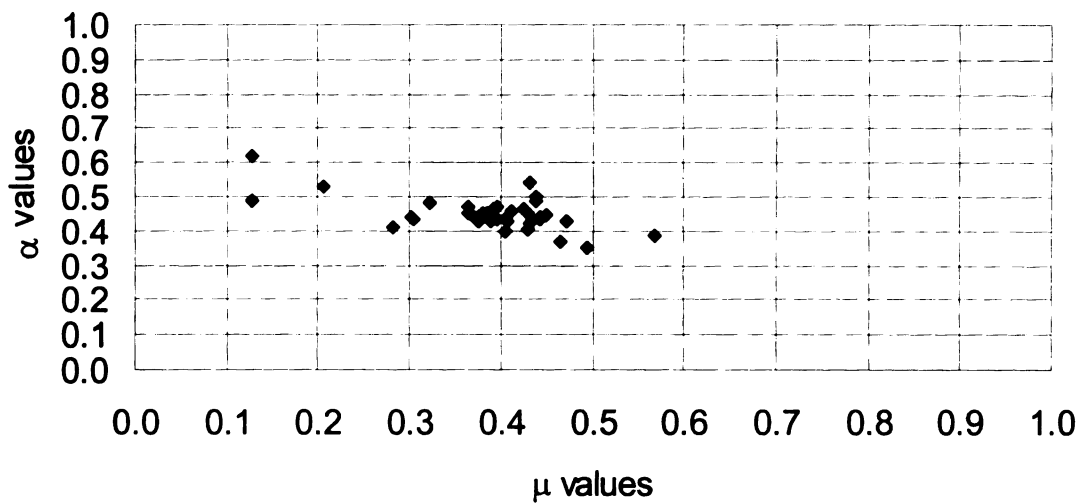


Figure 5-34 Values of μ and α for all tested axle and truck configurations

5.10 CONCLUSION

The main achievements of this laboratory experiment are as follows:

- Axle and truck factors for rutting damage were established based on laboratory data.
- Using Miner's rule to calculate the total damage for each truck by summing the damage caused by its constituent axles is dependant on axle configuration.
- Permanent deformation damage curves were developed using empirical data for the following methods: last-peak strain, dissipated energy, strain area, and peak stress.
- Permanent deformation damage models (peak, peak-midway, integration, and strain rate) were calibrated using laboratory axle factor values.
- The need was established for field calibration of permanent deformation parameters for the purpose of rutting prediction.

5.11 FUTURE RESEARCH

Though this study successfully accomplished its main goals, there is room to improve and expand knowledge. Future studies may focus on the effect of temperature and percent air void on laboratory axle and truck factors. These test variables, though held constant during this experiment, most likely have significant effects on pavement performance, and are therefore worthy of consideration. Further studies may also investigate the effect of axle group on rutting damage using Miner's rule and develop a nonlinear damage model that takes axle grouping within truck configurations into account. With the diversity of truck configurations on today's highways, this further investigation would be quite useful.

CHAPTER 6 – MECHANISTIC ANALYSIS

6.1 INTRODUCTION

In this chapter, the calibrated mechanistic-empirical rutting model (Chapter 4) as well as laboratory results (Chapter 5) will facilitate the relative mechanistic comparison of layer rutting damage for different axle and truck configurations. During the calibration of the VESYS model, an investigation of the contribution of each pavement layer from SPS-1 experiment data showed that, on average, hot mix asphalt concrete (HMA) rutting is 57% of the total, base rutting is 27%, and subgrade rutting is 16% (Figure 4-21). Moreover, the laboratory investigations showed that the axle factors for rutting damage due to different axle configurations follows a trend curve that is slightly below the identity line relating axle factor and the number of axles within an axle group.

The conclusions from the field investigation and the laboratory experiment chapters were further investigated using the mechanistic analysis of axle and truck configuration effects on rutting damage in each individual pavement layer. Since a thick HMA layer will account for a majority of the rutting damage in a pavement system (Chapter 4), and the rutting within such HMA layer is roughly proportional to the number of axles within an axle group (Chapter 5), remaining questions about the effect of axle interaction on the sub-layers are the focus of this chapter. The selection of profiles in this study is designed to further examine the effect of heavy axle trucks on a thick pavement, where there is interaction in the base and subgrade layers (Figure 6-1), and a thin pavement, where there is interaction in the subgrade layer only (Figure 6-2). Table 6-1

shows the layer thicknesses and moduli of the two pavement cross-sections that are used in the mechanistic analysis.

Table 6-1 Pavement cross-sections and moduli

Cross-section #	HMA		Base		Subgrade
	Thickness, in	Modulus, psi	Thickness, in	Modulus, psi	Modulus, psi
1	8	450000	36	30000	10000
2	4.1	551236	8.2	55283	23205

Section 50113 SPS-1 experiment

6.2 FORWARD ANALYSIS

The main goal of this research is to investigate the relative effect of multiple axle and truck configurations on rutting damage. Since there is no available software that can handle larger than tridem axle groups, the KENLAYER (Huang, 1993) elastic analysis program was used with responses due to larger axle groups being calculated by superposition. As shown previously in Figure 4-8, the vertical compression stress and strain due to standard and single axles at the middle of the HMA, base, and six 40-inch subsequent layers of subgrade were calculated. The standard axle load used in this analysis is 18 kips with a tire pressure of 70 psi, while the single axle load is 13 kips with a tire pressure of 100 psi. For the purposes of consistency, the responses of all multiple axle and truck configurations were compiled from the superposition of the appropriate number of single axles. As an example, Figure 6-1 and 6-2 show the vertical compression strain at the middle of the HMA, base, and six subsequent subgrade (SG) layers due to an 8-axle group for cross-sections number 1 and 2.

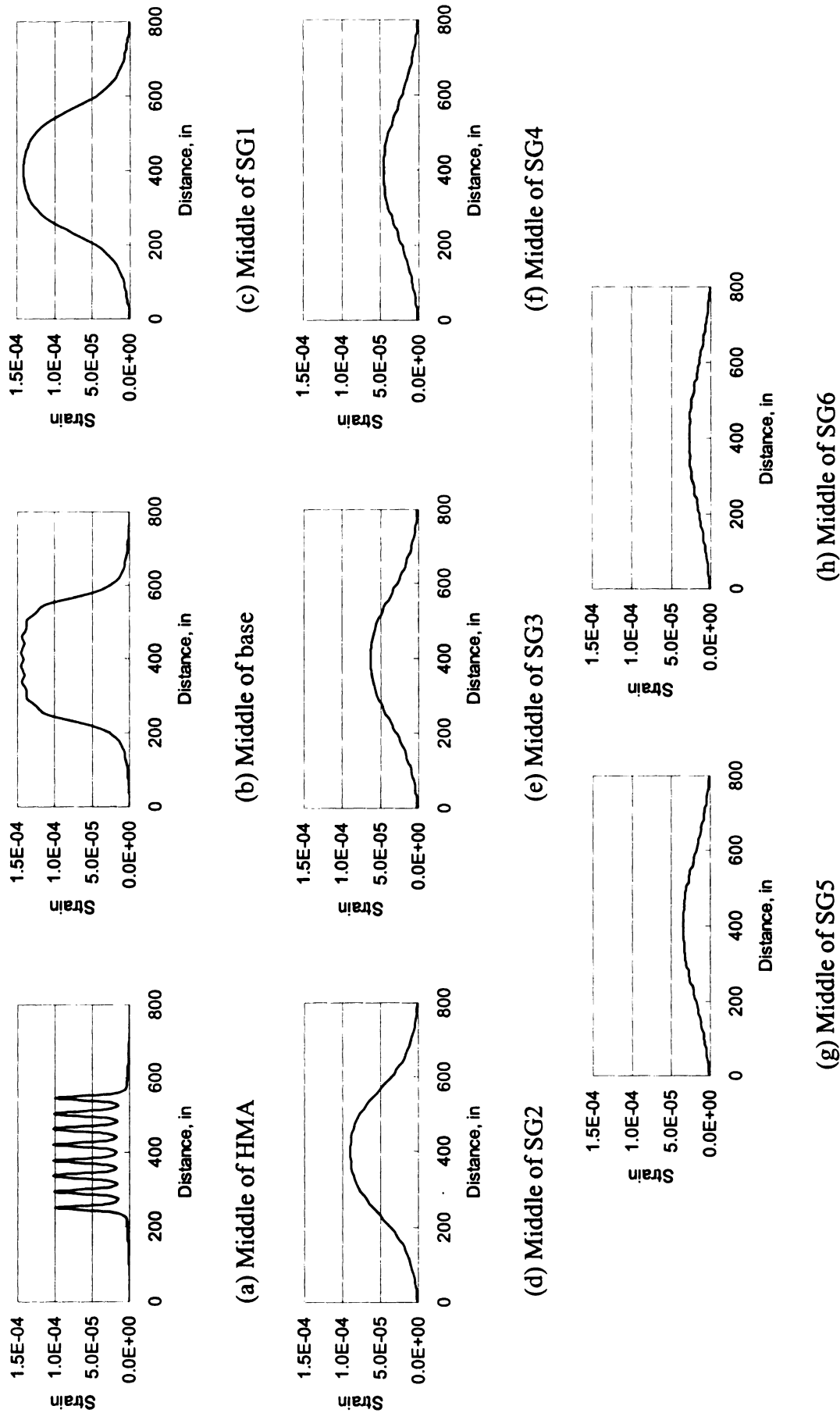


Figure 6-1 Vertical compression strain at the middle of each pavement layer due to an 8-axle group on thick pavement (profile 1)

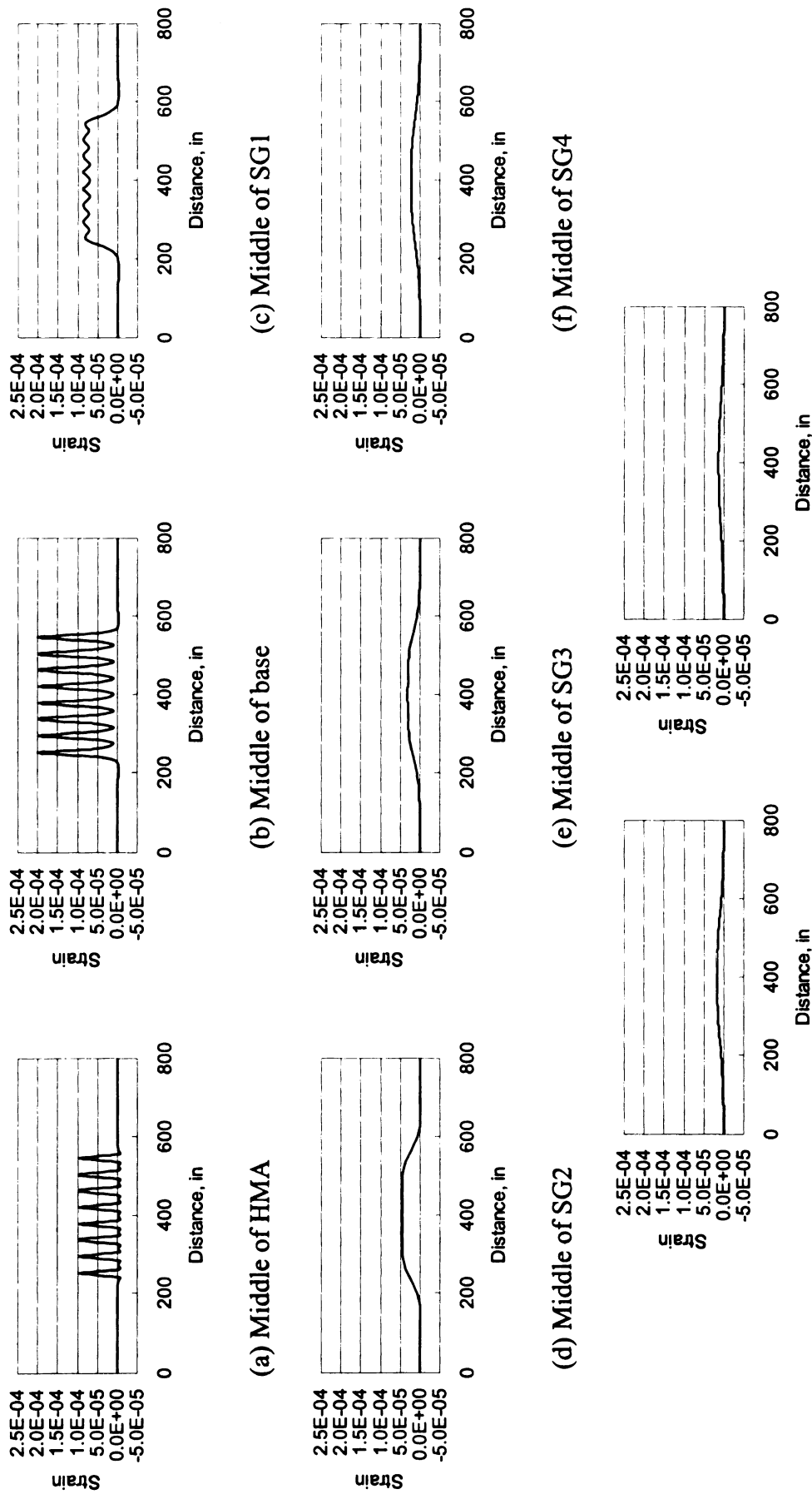


Figure 6-2 Vertical compression strain at the middle of each pavement layer due to an 8-axle group on thin pavement (profile 2)

6.3 RELATIVE COMPARISON OF RUTTING DAMAGE CAUSED BY MULTIPLE AXLES

The calibrated mechanistic-empirical rutting model (Chapter 4), along with the laboratory results (Chapter 5) make it possible to mechanistically compare the resulting rutting damage due to different axle and truck configurations for specific pavement profiles.

6.3.1 Calibrated mechanistic-empirical rutting model

In Chapter 4, The VESYS rutting model was calibrated using field data from the SPS-1 experiment. The calibrated rutting model is utilized in this mechanistic analysis to compare the resulting rutting (HMA, base, and subgrade) from different axle and truck configurations for different pavement profiles (Table 6-1). The calibrated rutting model is as follows:

$$\rho_p = h_{AC} \frac{\mu_{AC}}{1-\alpha_{AC}} \left(\sum_{i=1}^K (n_i)^{1-\alpha_{AC}} (\varepsilon_{ei,AC}) \right) + h_{base} \frac{\mu_{base}}{1-\alpha_{base}} \left(\sum_{i=1}^K (n_i)^{1-\alpha_{base}} (\varepsilon_{ei,base}) \right) + h_{SG} \frac{\mu_{SG}}{1-\alpha_{SG}} \left(\sum_{i=1}^K (n_i)^{1-\alpha_{SG}} (\varepsilon_{ei,SG}) \right) \quad (6-1)$$

where:

- ρ_p = total cumulative rut depth (in the same units as the layer thickness),
- i = subscript indicating axle group,
- K = number of axle group,
- h = layer thickness for HMA layer, combined base layer, and subgrade layer, respectively,
- n = number of load applications,
- ε_e = compression vertical elastic strain at the middle of the layers,
- μ = permanent deformation parameter representing the constant of proportionality between plastic and elastic strain, and
- α = permanent deformation parameter indicating the rate of decrease in rutting as the number of load applications increases.

The permanent deformation parameters for the two cross-sections were calculated from the developed regression equations in Chapter 4 (Equations 4-24, 4-25, 4-27, 4-28, 4-29, and 4-30). It should be noted that the pavement layer thicknesses and moduli shown in Table 6-1 were inputs for these equations, whereas all other variables were assumed at the mean values of the range used to develop the regression equations as shown in Tables 4-10, 4-14, and 4-18. Table 6-2 shows the calculated permanent deformation parameters for these cross-sections.

Table 6-2 Calculated permanent deformation parameters

	α_{HMA}	μ_{HMA}	α_{base}	μ_{base}	α_{SG}	μ_{SG}
Cross-Section 1	0.702	0.537	0.741	0.134	0.873	0.010
Cross-Section 2	0.594	0.271	0.716	0.129	0.910	0.037

As noted in Figure 6-1, the 8-axle responses (vertical compression elastic strain) at the middle of the HMA layer have lower interaction levels, whereas the interaction level increases with depth until the 8-axle response becomes one, wide pulse at deeper sub-layers. To study the effect of the response pulse duration and the interaction on rutting calculation for different axle and truck configurations, the strain value in the calibrated rutting model is employed in two different procedures: 1) sum the rutting damage due to only the strain values underneath each axle within an axle group, and 2) sum the rutting damage due to the strain values underneath the axles (similar to previous) and also include strain values outside the axle group (at the same intervals) until the strain becomes negligible. A diagram illustrating these two procedures for calculating rutting damage due to an 8-axle group is shown in Figure 6-3. The rutting due to one

million repetitions of different axle and truck configurations were calculated using both procedures for each layer for both cross-sections.

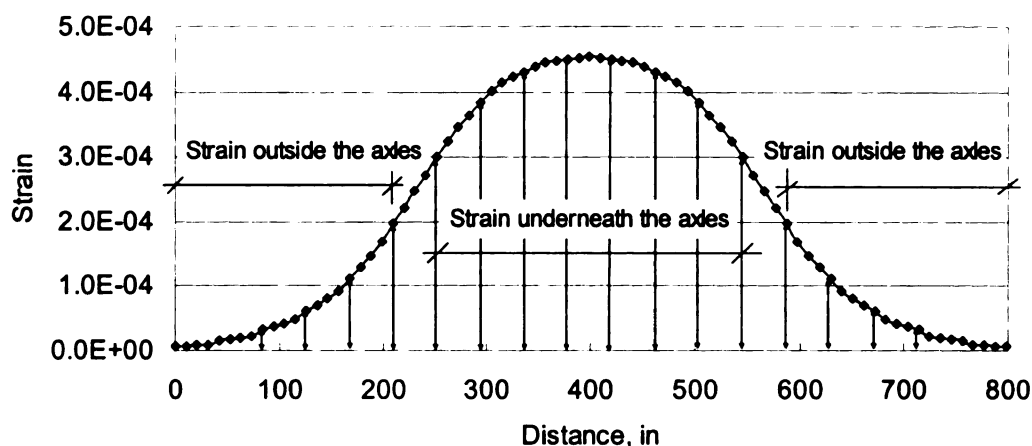


Figure 6-3 Strain values underneath and outside the axle group

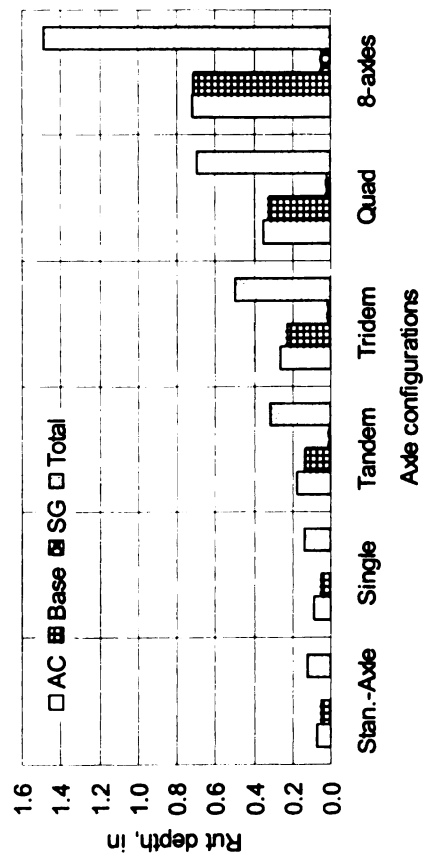
6.4 RESULTS AND DISCUSSION

The calibrated mechanistic-empirical rutting model (Equation 6-1) is employed to calculate the layer rutting for both thick and thin pavement sections. Figures 6-4 to 6-7 show the per-layer and total rut depth due to one million repetitions for different axle and truck configurations using both procedures. The calculated rutting for the individual layers as well as the total was normalized to the rutting due to a single axle (axle and truck factors) to study the relative effect of these axle and truck configurations on pavement rutting damage.

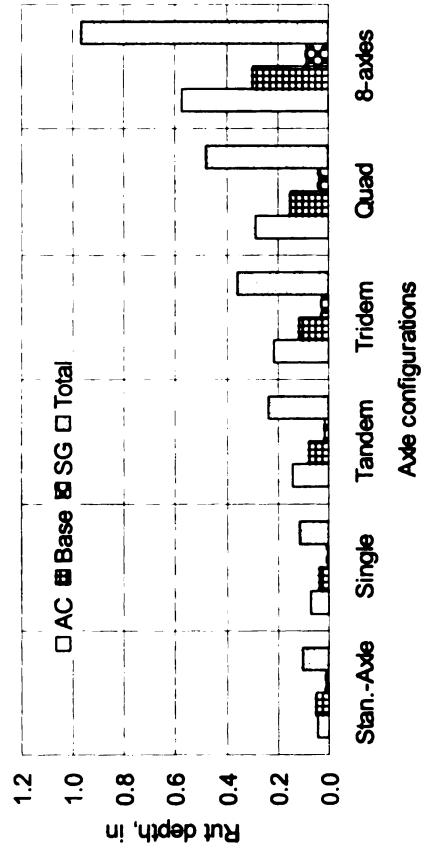
The results show that when there is no strain interaction between axles, both procedures for calculating the rut depth show rutting damage proportional to the number of axles. This is the case for HMA layer of cross-section 1 and HMA and base layers of cross-section 2. On the other hand, when there is strain interaction between the axles, the first procedure (accounting only for the strain values under the axles) shows that the

multiple axles are more damaging relative to the same number of single axles (Figures 6-4, c and d (axles) and Figures 6-5, c and d (trucks)). This result is due to the fact that procedure 1 ignores the strains outside the axles and the effect of these strain values becomes more severe at higher levels of interaction. Yet, since unaccounted for strain values still result in rutting damage, it is not logical to ignore strain values outside the axles, as shown in Figure 6-3. Calculating the rut depth by accounting for all strain values (strain underneath and outside the axles) shows that whether there is strain interaction or not, the axle and truck factors are proportional to the number of axles. The results of procedure 2 indicate that the interaction in the sub-layers is not important and does not impose additional relative rutting damage. These results can be further confirmed from the laboratory investigation of the HMA layer. Since interaction between pulses was not significant for the visco-elastic material (HMA layer) it will be even less significant for the granular sub-layers, as indicated by the mechanistic analysis in this study. This conclusion suggests that procedure 2 is more accurate than procedure 1 for calculating the rut depth due to multiple axle and truck configurations.

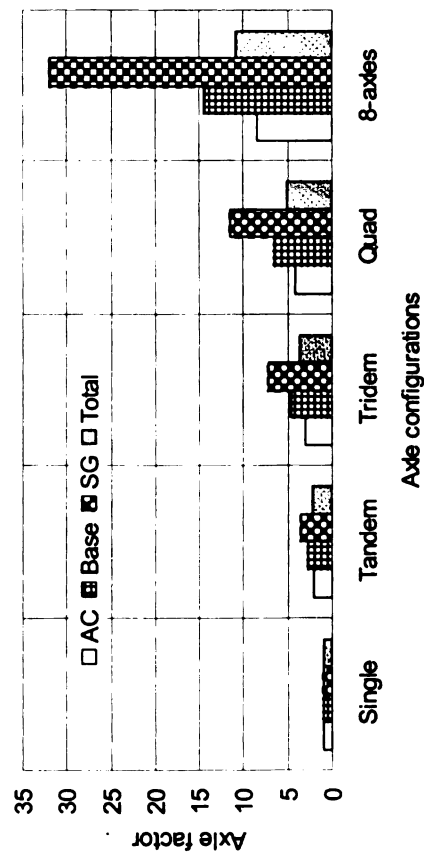
In a similar mechanistic analysis of the effect of heavy-vehicle characteristics on pavement response and performance, Gillespie *et al.*, 1993 calculated the rut depth for different truck configurations by integrating the influence function, which resulted in rutting damage that is proportional to the axle load. Though Gillespie's analyses include several truck configurations, the maximum axle group among all truck configurations was limited to tandem. Therefore, this current mechanistic analysis, laboratory experiment, and in-service pavement analysis extend these conclusions to a larger number of heavy axle and truck configurations.



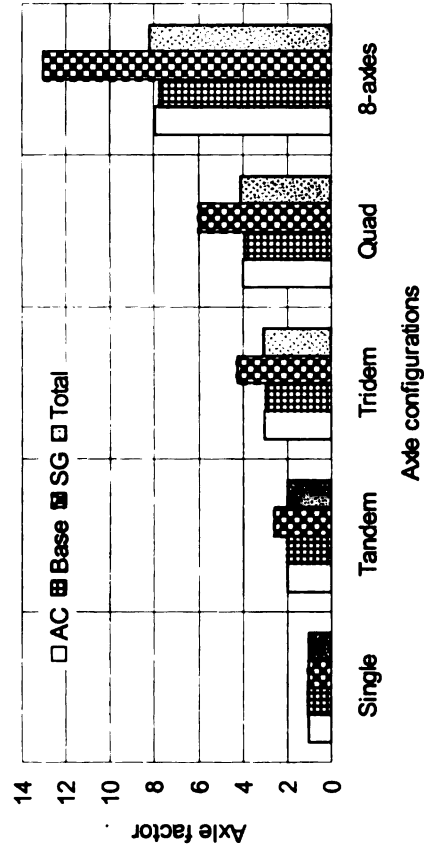
(a) Rut depth for section 1



(b) Rut depth for section 2

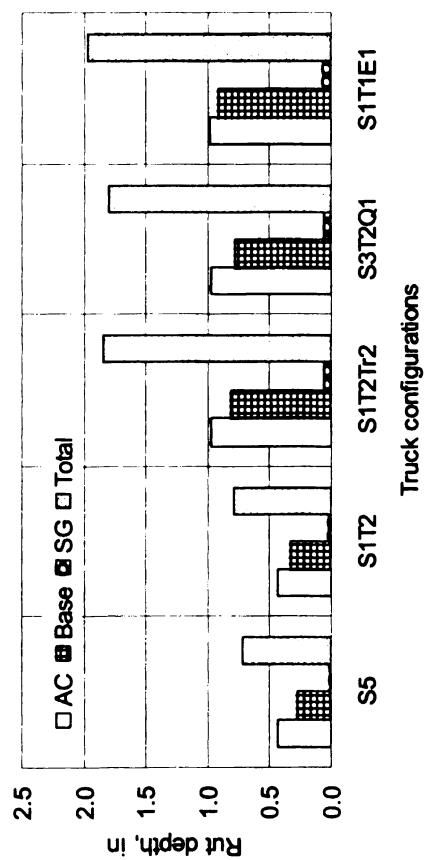


(c) Axle factor for section 1

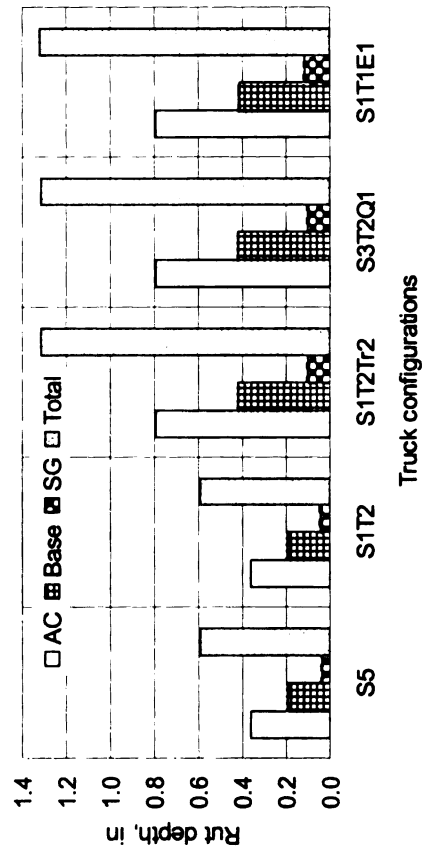


(d) Axle factor for section 2

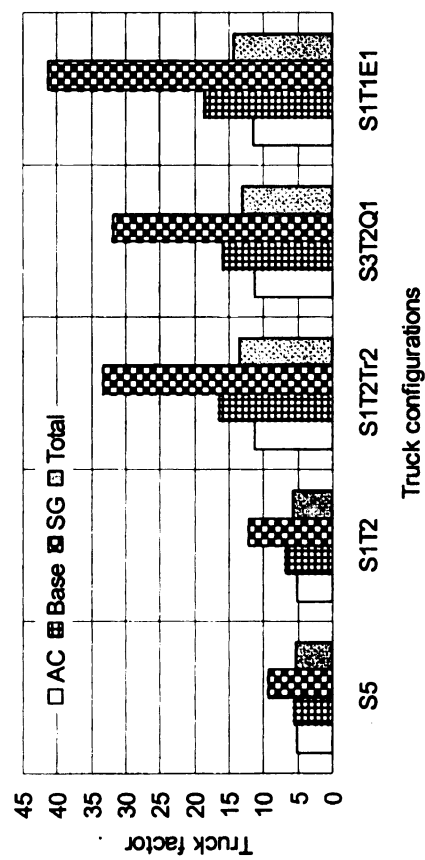
Figure 6-4 Rut depth for pavement layers and their axle factors at one million repetitions – procedure 1



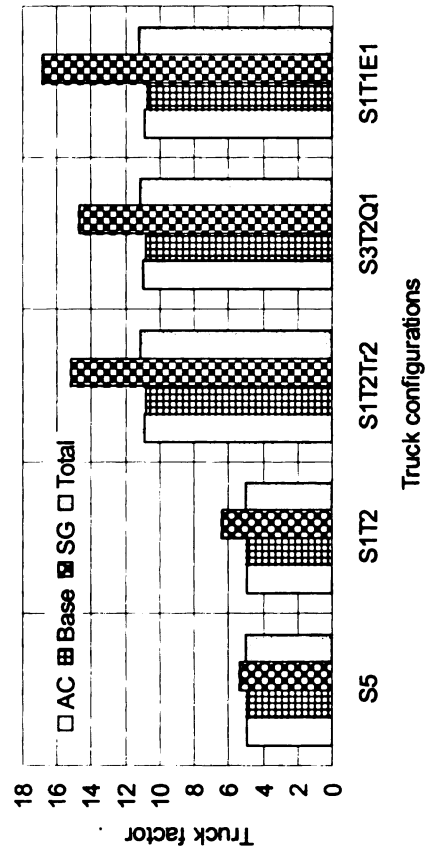
(a) Rut depth for section 1



(b) Rut depth for section 2

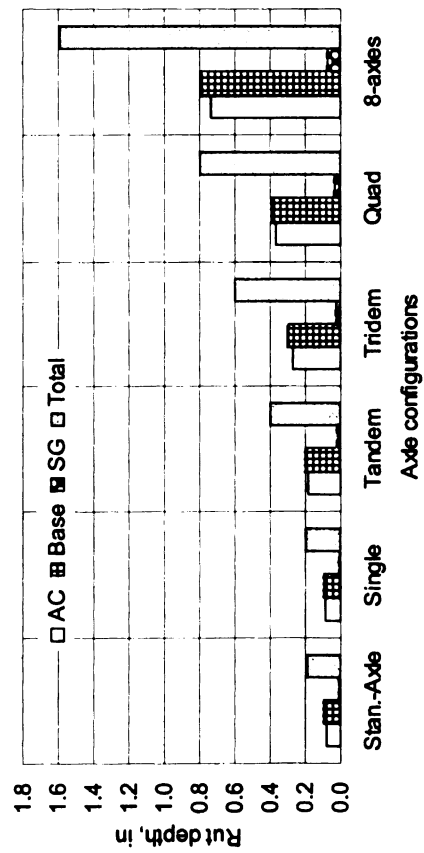


(c) Truck factor for section 1

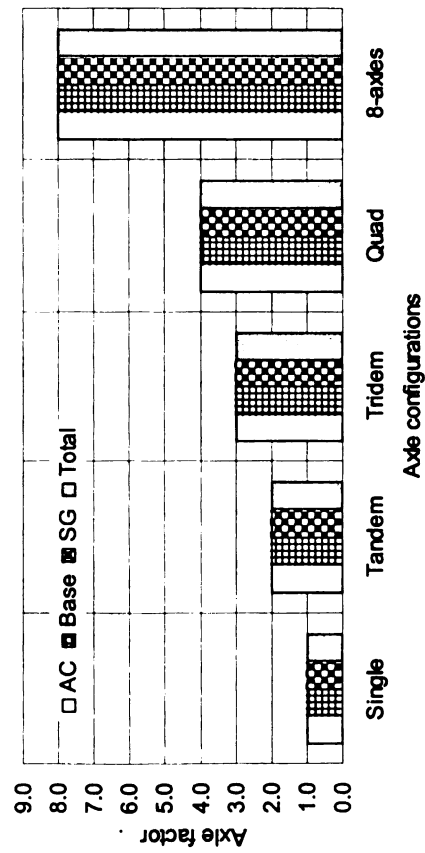


(d) Truck factor for section 2

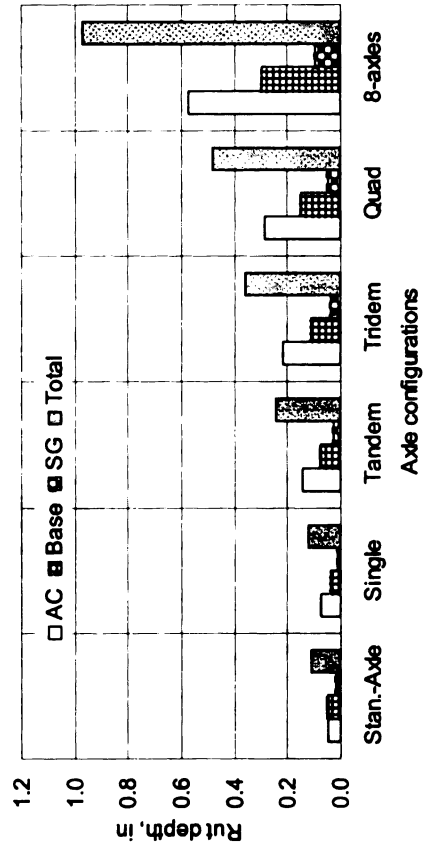
Figure 6-5 Rut depth for pavement layers and their truck factors at one million repetitions – procedure 1



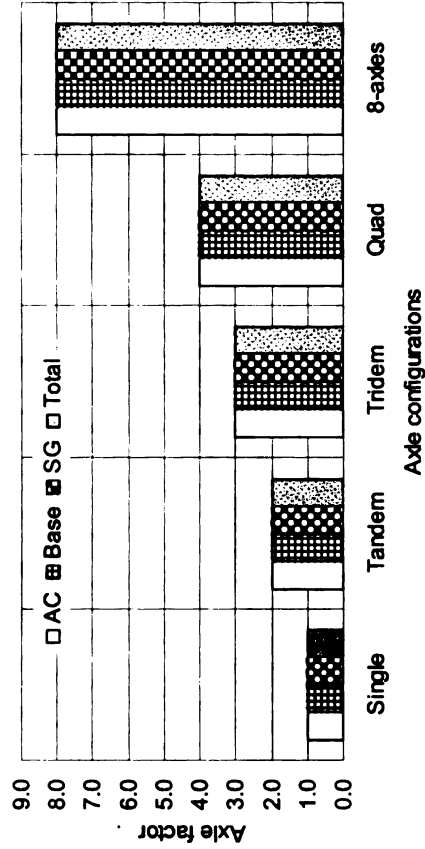
(a) Rut depth for section 1



(c) Axle factor for section 1

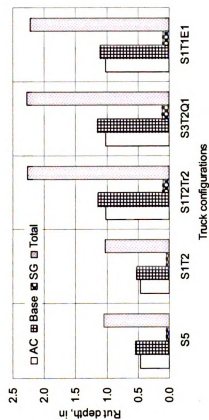


(b) Rut depth for section 2

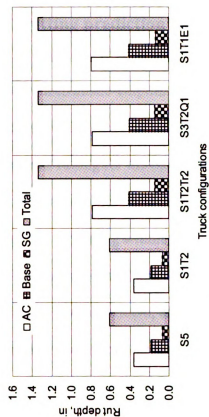


(d) Axle factor for section 2

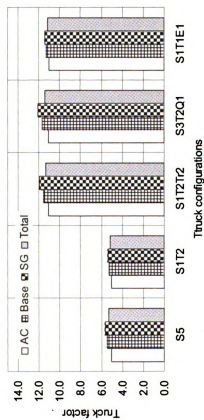
Figure 6-6 Rut depth for pavement layers and their axle factors at one million repetitions – procedure 2



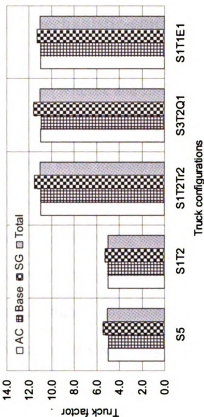
(a) Rut depth for section 1



(b) Rut depth for section 2



(c) Truck factor for section 1



(d) Truck factor for section 2

Figure 6-7 Rut depth for pavement layers and their truck factors at one million repetitions — procedure 2

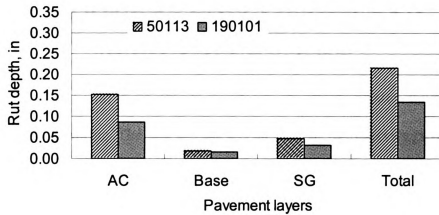
6.4.1 Rutting prediction using the new mechanistic-empirical design guide

The new mechanistic-empirical (ME) design guide (Witczak and El-basyouny, 2004) predicts several forms of distress, including rutting. In particular, the document discusses and predicts rutting for the individual layers as well as the total surface rutting. Unlike the VESYS rutting model, the ME software has two independent equations for predicting rutting: one for rutting within the HMA layer and one for rutting within granular materials (base/subbase) and the subgrade. Moreover, the program can handle trucks with single, tandem, tridem, and quad axle configurations. The rutting due to single and tandem axle configurations was calculated in the present study using the new design guide for a single SPS-1 section. The predicted rutting for each individual pavement layer and the total rutting were not proportional to the number of axles; that is, a tandem axle produced less than twice the rutting damage of a single axle. Figure 6-6 shows the rut depth and axle factor for tandem axles for two SPS-1 sections, thin (50113) and thick sections (190101). This prompted a further investigation of the methods and assumptions that were incorporated into the new ME guide. The two major concerns about the ME rutting models in the new design guide, and the solutions offered by the present study, are summarized below:

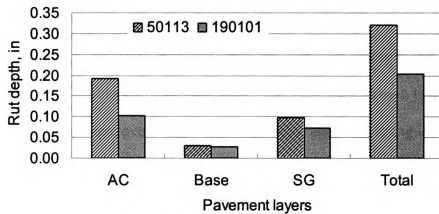
- Unlike the procedure described in the current study to calibrate the VESYS rutting model—linking the shape of the transverse surface profile to the layer rutting contributions—the ME guide research team bases layer rutting on an assumed and statistically idealized percentage that is applied to all LTPP sections equally. In the ME guide document, it states that a lack of trench data makes

section-based layer contributions impossible to calculate. The resulting lack of variation on a section-by-section basis therefore becomes a matter of “practical,” rather than statistical significance. By including the transverse surface profile as a means of quantifying the layer contribution of each section to the total rutting, the gap between assuming an individual section’s layer contribution and calculating it has been bridged.

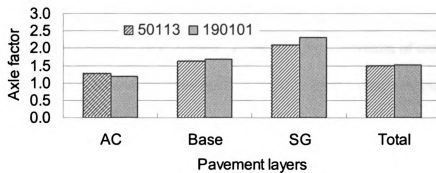
- The most significant drawback is that the ME guide model uses only the maximum strain value within a multiple axle group, as if the axle group can be quantitatively represented by the superposition of the many axles into a single, static pulse. However, this neglects the rutting damage due to those strain values outside the maximum; of which, there are many in a large multiple axle group. This, of course, can be partially accounted for in the calibration procedure, but this adjustment is highly artificial and not representative of the damage that occurs at an individual point in the pavement as the entire load (up to an 8-axle group) passes over. The present study attempted to validate the ME guide model, but found that, even with the calibration procedure adjustments, the predicted rutting damage is not proportional to the number of axles within a group. Therefore, the present study provides a more representative model for rutting prediction, based on the summation of rutting damage throughout the entirety of the passage of an axle group, not just the damage produced by the singular, maximum strain value.



(a) Rut depth due to single axles



(b) Rut depth due to tandem axles



(c) Tandem axle factor

Figure 6-8 Rut depth for single and tandem axles and tandem axle factor using new ME guide

CHAPTER 7 – CONCLUSIONS AND RECOMMENDATIONS

This study includes several approaches to investigate the effect of heavy, multiple axle trucks on pavement rutting. The first approach is an analysis of in-service pavement data from the State of Michigan to investigate the effect of multi-axle trucks on total pavement rutting damage (Chapter 3). The second approach is a laboratory experiment designed to simulate multiple axle and truck configurations and study their effects on hot mix asphalt concrete (HMA layer) rutting (Chapter 5). The third approach (Chapter 6) is the mechanistic analysis using the calibrated mechanistic-empirical rutting model (Chapter 4) and applying models developed in the laboratory. Though each approach is different in its methodology and design, overall agreement in results suggests a strong compatibility that will prove useful in further research. Such recommendations for future research and other conclusions from this work are the focus of this chapter.

7.1 CONCLUSIONS

Based on the field investigation of in-service pavement data, calibration of mechanistic-empirical rutting model, laboratory investigations, and the mechanistic analyses, the following conclusions are drawn:

- Truck traffic analysis shows that the percentage of the heavy, multiple axle trucks is less than 10%. Considering the increases in truck traffic and fuel prices, demands for heavier gross truck weight with larger axle groups direct the importance of this study toward policy-makers, as well as pavement designers.

- The analyses of in-service pavement rut data show that multiple-axle trucks (with higher gross vehicle weight) cause more rutting damage than single and tandem axle trucks.
- The common sense extension of the previous finding would be that the larger the multiple axle group, the more rutting damage the truck causes. However, laboratory results from this study indicate the opposite is the case. As the size of the largest axle group within a truck configuration increases, the relative rutting damage per axle caused by that truck decreases.
- In calibrating the VESYS rutting model, time-series, in-service pavement rut data was used from the SPS-1 experiment. This important methodological improvement over previous studies permits more accurate determination of the permanent deformation parameters (PDP) that have good agreement with results from accelerated loading facilities.
- Analyses of in-service pavement layer data for rutting contribution showed that, on average, total rutting breaks down as follows: 57% from HMA, 27% from base, and 16% from subgrade. These results show that the total system rutting is dependent upon more than just the subgrade layer. This is especially the case when considering the many new, and heavier axle and truck configurations.
- Prediction of permanent deformation parameters (α and μ) using layer-material properties, pavement layer cross-sections, and climatic conditions showed promising results for HMA and base layer predictions. However, due to the limitation of material properties data, the subgrade permanent deformation parameters showed poor predictions. Given the relatively small magnitude of the

subgrade layer contribution to the overall rutting and this reduced data availability, a decayed predictive ability is expected.

- The laboratory investigations indicate that rutting damage due to different axle configurations is approximately proportional to the number of axles within an axle group. In other words, rutting damage is proportional to the gross weight of the load.
- Calculating truck rutting damage by simply summing the vertical permanent deformation corresponding to of its constituent axle groups results in erroneous predictions. Using Miner's rule to determine truck rutting damage from its constituent axles does improve the prediction, although there are still variations among the damage values corresponding to different axle and truck configurations.
- Regardless of the truck or axle configuration, as well as the variable stress level and axle interaction within an axle group, the laboratory data in this study followed unique curves for each of the three permanent deformation models used: last peak strain, dissipated energy, and strain area. This result was for one particular HMA mix at one target air void percentage, but the excellent relationships show that this procedure can be used in the future for generating similarly unique curves to predict the lifetimes of other mixes.
- Quantifying pavement rut damage caused by multiple axles requires calibrations of the summation methods. In this study, the exponents for various summation methods were determined using laboratory-developed axle factors.

- The mechanistic analysis in this study confirms the laboratory findings related to the proportionality of axle and truck factors for the HMA layer. Moreover, it extends this same result into both the base and subgrade layers, which suggests no further laboratory experimentation is needed. This conclusion is based on the following logic. There was initial assumption about the importance of interaction between pulses in the pavement sub-layers. However, since the effect of interaction between pulses was not significant for the visco-elastic material (HMA layer), this interaction will be even less significant for the sub-layer, as indicated by the mechanistic analysis in this study.

7.2 RECOMMENDATIONS FOR FUTURE RESEARCH

Though this study successfully accomplished its main goals, there is always room to improve and expand knowledge.

- Permanent deformation parameters prediction analysis can be conducted again when there are more material properties available, such as *VTM*, *VMA*, and *VFA* for the HMA layer; compaction data (moisture content and dry density) and unconfined compression strength for the base layer; and more aggregate gradation information for all pavement layers.
- The same analysis procedures can be performed for ALFs where more data and more controlled environments are available.
- Further validation of the calibrated rutting model can be conducted using other data sets outside of the SPS-1 experiment, such as GPS-1 and ALFs.

- The rutting model was calibrated based on the calculated strain due to one ESAL; however, either validation or calibration can be done based on axle load spectra to eliminate the error due to converting the actual load to ESALs based on LEF.
- The rutting model was calibrated for conventional pavements (three layer system) and the amount of two layer system (full depth pavement) data was very small. So, similar procedures for full depth asphalt can be done wherever there are data for two layer pavement systems. Fortunately, the uniqueness problem will be less severe since there will be four PDPs instead of the six values in a three layer system.
- Future laboratory studies may focus on the effect of temperature and percent air void on laboratory axle and truck factors.
- Also, further laboratory studies may investigate the effect of axle group on rutting damage using Miner's rule and develop a nonlinear damage model that takes axle grouping within truck configurations into account.
- Though the developed dissipated energy and strain area models were for one HMA mixture, temperature, target air voids, similar to the calibrated rutting model, these two models can be calibrated using field data to use them universally.

APPENDIX

ANALYSIS OF FLEXIBLE PAVEMENT RUTTING FROM IN-SERVICE DATA

Table A-1 Sections information used in the field analysis of in-service rutting data

Control Section	Weigh station No.	Direction	Road	Year of latest improvement	Beginning mile post	Ending mile post	Project Length	Region	County	Direction
78022	73293	E-W	US-12	1999	7.351	11.984	4.633	Southwest	ST. Joseph	EB
54014	53095	N-S	US-131	1997	7.152	11.552	4.4	Grand	Mecosta	SB
54014	53095	N-S	US-131	2001	11.552	16.097	4.545	Grand	Mecosta	SB
59012	52491	N-S	US-131	1998	9.893	13.127	3.234	Grand	Montcalm	NB
59012	52495	N-S	US-131	1998	9.969	13.069	3.1	Grand	Montcalm	SB
69014	40491	N-S	I-75	2000	0.009	7.709	7.7	North	Otsego	NB
69014	40491	N-S	I-75	1994	7.709	13.1	5.391	North	Otsego	NB
69014	40495	N-S	I-75	2000	0.107	7.607	7.5	North	Otsego	SB
69014	40495	N-S	I-75	1997	7.607	8.707	1.1	North	Otsego	SB
69014	40495	N-S	I-75	1994	8.707	13.107	4.4	North	Otsego	SB
19033	50395	N-S	US-127	1995	8.453	13.543	5.09	University	Clinton	SB
18041	30493	E-W	M-61	1992	0	13.267	13.267	Bay	Clare	EB
18041	30493	E-W	M-61	1993	13.267	14.367	1.1	Bay	Clare	EB
18041	30497	E-W	M-61	1992	0.047	13.256	13.209	Bay	Clare	WB
18041	30497	E-W	M-61	1993	13.256	14.356	1.1	Bay	Clare	WB
72013		N-S	US127	1990	0	3	3	North	Roscommon	NB
72013		N-S	US127	1998	3	12.165	9.165	North	Roscommon	NB
72013		N-S	US127	1990	0.174	2.902	2.728	North	Roscommon	SB

Table A-1 Sections information used in the field analysis of in-service rutting data (cont.)

Control Section	Weight station No.	Direction	Road	Year of latest improvement	Beginning mile post	Ending mile post	Project Length	Region	County	Direction
72013		N-S	US127	1998	2.902	12.186	9.284	North	Roscommon	SB
25102	63093	E-W	M-57	1998	0	9.777	9.777	Bay	Genesee	EB
80041		E-W	M-43	1996	1.077	1.821	0.744	Southwest	Van Buren	EB
80041		E-W	M-43	1999	1.821	10.052	8.231	Southwest	Van Buren	EB
80041		E-W	M-43	1993	10.772	12.422	1.65	Southwest	Van Buren	EB
80041		E-W	M-43	1996	0.97	2.66	1.69	Southwest	Van Buren	WB
80041		E-W	M-43	1990	2.66	4.06	1.4	Southwest	Van Buren	WB
80041		E-W	M-43	1986	4.06	10.06	6	Southwest	Van Buren	WB
80041		E-W	M-43	1993	10.699	12.499	1.8	Southwest	Van Buren	WB
78022	73297	E-W	US-12	1977	7.789	11.691	3.902	Southwest	ST. Joseph	WB
67062	30493	E-W	M-61	1999	1	3.916	2.916	North	Osceola	EB
67062	30497	E-W	M-61	1992	0.937	3.911	2.974	North	Osceola	WB
16093	40491	N-S	I-75	1994	0	6.583	6.583	North	Cheboygan	NB
16093	40491	N-S	I-75	2000	6.583	14.937	8.354	North	Cheboygan	NB
16093	40495	N-S	I-75	1994	-0.074	6.591	6.665	North	Cheboygan	SB
16093	40495	N-S	I-75	2000	6.591	15.091	8.5	North	Cheboygan	SB
18034		N-S	US127	1996	5.938	8.038	2.1	Bay	Clare	NB
18034		N-S	US127	2001	8.038	12.162	4.124	Bay	Clare	NB
18034		N-S	US127	1996	5.916	7.974	2.058	Bay	Clare	SB

Table A-1 Sections information used in the field analysis of in-service rutting data (cont.)

Control Section	Weigh station No.	Direction	Road	Year of latest improvement	Beginning mile post	Ending mile post	Project Length	Region	County	Direction
18034		N-S	US127	2001	7.974	12.174	4.2	Bay	Clare	SB
54013	52491	N-S	US-131	1998	0	8.427	8.427	Grand	Mecosta	NB
54013	52495	N-S	US-131	1998	-0.049	8.452	8.501	Grand	Mecosta	SB
61075		N-S	US-31	1998	0.543	4.003	3.46	Grand	Muskegon	NB
61075		N-S	US-31	1998	0.452	3.961	3.509	Grand	Muskegon	SB
67016	53091	N-S	US-131	1996	0	5.534	5.534	North	Osceola	NB
67016	53095	N-S	US-131	1996	0.053	5.645	5.592	North	Osceola	SB
54014	53091	N-S	US-131	1997	7.177	11.677	4.5	Grand	Mecosta	NB
54014	53091	N-S	US-131	1998	11.677	16.216	4.539	Grand	Mecosta	NB
74062		E-W	M-46	1973	9.829	12.48	2.651	Bay	Sanilac	WB
74062		E-W	M-46	1970	13.389	18.952	5.563	Bay	Sanilac	WB
80042		E-W	M-43	1995	0	5.674	5.674	Southwest	Van Buren	EB
80042		E-W	M-43	1994	5.674	10.074	4.4	Southwest	Van Buren	EB
80042		E-W	M-43	1995	-0.075	6.704	6.779	Southwest	Van Buren	WB
80042		E-W	M-43	1994	6.704	10.004	3.3	Southwest	Van Buren	WB

Table A-2 Rutting and traffic information for pavement sections used in the field analysis of in-service rutting data

Control Section	Weight station No.	Rut depth, in	Year where rutting measured	age	Single and tandem axles	3, 4, 5, 6, 7, 8 axles	Trucks with single and tandem axles	Trucks with 3, 4, 5, 6, 7, and 8 axles	Truck class 6, 8, 9, 10, and 11	Truck class 13
78022	73293	0.461	2001	2	297790	6945	181808	6621	184690	9490
54014	53095	0.241	2001	4	2284138	150218	1082880	131326	953380	188340
54014	53095	0.230	2001	0	5710	376	2707	328	2383	471
59012	52491	0.223	2001	3	2432726	88596	1436009	79949	914325	134685
59012	52495	0.235	2001	3	2807098	100819	1474692	87091	905565	129210
69014	40491	0.169	2001	1	303813	36235	106992	32685	151840	64240
69014	40491	0.274	2001	7	2126689	253642	748946	228794	1062880	449680
69014	40495	0.184	2001	1	358761	32761	120698	29561	126655	70080
69014	40495	0.260	2001	4	1435045	131042	482792	118245	506620	280320
69014	40495	0.339	2001	7	2511329	229324	844885	206928	886585	490560
19033	50395	0.293	2001	6	3381790	243760	1500974	212140	1434450	483990
18041	30493	0.159	2000	8	323895	61656	193909	55341	154760	32120
18041	30493	0.181	2000	7	283408	53949	169670	48423	135415	28105
18041	30497	0.167	2000	8	718851	51594	548940	48237	134320	58400
18041	30497	0.188	2000	7	628995	45145	480322	42207	117530	51100
72013		0.220	2001	11	356761	32761	120698	29561	1059960	305140
72013		0.186	2001	3					289080	83220
72013		0.191	2001	11					915420	333245

Table A-2 Rutting and traffic information for pavement sections used in the field analysis of in-service rutting data (cont.)

Control Section	Weigh station No.	Rut depth, in	Year where rutting measured	age	Single and tandem axles	3, 4, 5, 6, 7, 8 axles	Trucks with single and tandem axles	Trucks with 3, 4, 5, 6, 7, and 8 axles	Truck class 6, 8, 9, 10, and 11	Truck class 13
72013		0.191	2001	3					249660	90885
25102	63093	0.142	2000	2	290669	16189	244916	12988	47450	15330
80041		0.123	2000	4					125560	5840
80041		0.069	2000	1					31390	1460
80041		0.110	2000	7					219730	10220
80041		0.069	2000	4					125560	7300
80041		0.037	2000	10					313900	18250
80041		0.075	2000	14					439460	25550
80041		0.126	2000	7					219730	12775
78022	73297	0.219	2001	24	3661203	92446	1918606	87123	2216280	113880
67062	30493	0.137	2000	1	40487	7707	24239	6918	19345	4015
67062	30497	0.139	2000	8	718851	51594	548940	48237	134320	58400
16093	40491	0.344	2001	7	2126689	253642	748946	228794	1062880	449680
16093	40491	0.174	2001	1	303813	36235	106992	32685	151840	64240
16093	40495	0.357	2001	7	2511329	229324	844885	206928	886585	490560
16093	40495	0.186	2001	1	358761	32761	120698	29561	126655	70080
18034		0.380	2001	5					481800	138700
18034		0.231	2001	0					964	277

Table A-2 Rutting and traffic information for pavement sections used in the field analysis of in-service rutting data (cont.)

Control Section	Weight station No.	Rut depth, in	Year where rutting measured	age	Single and tandem axles	3, 4, 5, 6, 7, 8 axles	Trucks with single and tandem axles	Trucks with 3, 4, 5, 6, 7, and 8 axles	Truck class 6, 8, 9, 10, and 11	Truck class 13
18034		0.324	2001	5					416100	151475
18034		0.258	2001	0					832	303
54013	52491	0.292	2001	3	2432726	88596	1436009	79949	914325	134685
54013	52495	0.361	2001	3	2807098	100819	1474692	87091	905565	129210
61075		0.233	2001	3					900090	147825
61075		0.217	2001	3					888045	158775
67016	53091	0.182	2001	5	2734984	167043	1270239	152330	1261075	222650
67016	53095	0.164	2001	5	2855173	187772	1353600	164157	1191725	235425
54014	53091	0.254	2001	4	2187987	133634	1016191	121864	1008860	178120
54014	53091	0.234	2001	3	1640990	100226	762143	91398	756645	133590
74062		0.310	2000	27					275940	147825
74062		0.090	2000	30					306600	164250
80042		0.102	2000	5					156950	7300
80042		0.090	2000	6					188340	8760
80042		0.111	2000	5					156950	9125
80042		0.073	2000	6					188340	10950

Table A-3 Effect of different truck/axle configurations on pavement DI

Axle/Truck Configurations	Independent variables	Simple linear regression			Multiple linear regression			Stepwise regression		
		β	P- value	R ²	β	P- value	R ²	β	P- value	R ²
Axle types	1 and 2	0.430	0.02	0.185	0.617	0.032	0.343	0.585	0.001	0.342
	3, 4, 5, 6, 7, and 8	0.265	0.164	0.070	-0.040	0.883		N/S*	NA	
Truck types	1 and 2	0.466	0.011	0.218	0.580	0.007	0.437	0.654	0.003	0.427
	3, 4, 5, 6, 7, and 8	0.272	0.154	0.074	0.122	0.540		N/S*	NA	
Truck classes	6, 8, 9, 10, and 11	0.272	0.048	0.074	0.340	0.090	0.092	0.301	0.028	0.091
	13	0.095	0.497	0.009	-0.053	0.790		N/S*	NA	

* N/S: not selected by model

Table A-4 Effect of Different Truck/Axle Configurations on Pavement RQI

Axle/Truck Configurations	Independent variables	Simple linear regression			Multiple linear regression			Stepwise regression		
		β	P- value	R ²	β	P- value	R ²	β	P- value	R ²
Axle types	1 and 2	0.129	0.502	0.017	1.019	0.0006	0.424	N/S*	NA	NA
	3, 4, 5, 6, 7, and 8	-0.264	0.166	0.069	-1.092	0.0003		N/S*	NA	
Truck types	1 and 2	0.318	0.093	0.101	0.796	0.00020	0.473	N/S*	NA	NA
	3, 4, 5, 6, 7, and 8	-0.268	0.159	0.072	-0.751	0.00037		N/S*	NA	
Truck classes	6, 8, 9, 10, and 11	-0.111	0.435	0.012	0.608	0.00356	0.314	0.608	0.00356	0.314
	13	-0.423	0.002	0.179	-0.909	0.00003		-0.909	0.00003	

*N/S: not selected by model

REFERENCES

- ARA, Inc., ERES Division (2004), "Guide for mechanistic- empirical design of new and rehabilitated pavement structures" NCHRP report No. 1-37A, appendix ii-1 and appendix gg-1.
- Aryes, M. Jr. (2002), "Unbound Material Rut Model Modification". Development of the 2002 Guide for the Design of New and Rehabilitated Pavement Structures. NCHRP 1-37A. Inter Team Technical Report.
- Ali, H. A., and S. D. Tayabji (2000), "Using transverse profile data to compute plastic deformation parameters for asphalt concrete pavements." *Transportation Research Record*(1716), pp 89-97.
- Ali, H. A., S. D Tayabji., and, F. La Torre (1998), "Calibration of mechanistic-empirical rutting model for in-service pavements." *Transportation Research Record*(1629), pp159-168.
- Allen, J.C. (2001), "Species-Habitat Relationships For The Breeding Birds of A Longleaf Pine Ecosystem" Master of Science in Ecology, Faculty of the Virginia Polytechnic Institute and State University.
- Belsley, D. A., Edwin Kuh, and Roy E. Welsch. (1980), *Regression diagnostics : identifying influential data and sources of collinearity*, New York : Wiley.
- Bonaquist, R. F. (1996), "Development and application of a comprehensive constitutive model for granular materials in flexible pavement structures." Ph. D. thesis, University of Maryland at Collage park.
- Bonaquist, R.F., D.W. Christensen, and William Stump (2003), "Simple Performance Tester for Superpave Mix Design: First-Article Development and Evaluation" NCHRP report 513, Transportation Research Board, Washington, D.C.
- Chatti, K., D. Lee., and T. Kim (2000) "Truck Damage Factors Using Dissipated Energy vs. Peak Strains" 6th International Symposium on Heavy Vehicle Weights and Dimensions. pp. 175-184. June 18-22.
- Chatti, K., H. Salama, and C. El Mohtar (2004), "Effect of heavy trucks with large axle groups on asphalt pavement damage" 8th International Symposium on Heavy Vehicle Weights and Dimensions, South Africa.
- Chatti, K., N. Buch, S. W. Haider, A. S. Pulipaka, R. W. Lyles, D. Gilliland, and P. Desaraju (2005), "LTPP Data Analysis: Influence of Design and Construction Features on the Response and Performance of New Flexible and Rigid Pavements," NCHRP report No. 20-50 [10/16].

- Chatti, K. and H. S. Lee (2004), "Evaluation of Strain and Energy Based Fatigue prediction Methods for Asphalt Pavement Subjected to Multiple Axle Loading" International Journal of Pavements, Vol. 3 No. 1& 2.
- Chatti, K. and El Mohtar, C. (2004), "Effect of Different Axle Configurations on Fatigue Life of Asphalt Concrete Mixture" Transportation Research Record, n 1891, p 121-130
- Chen, D.H., J. Bilyeu, T. Scullion, D. F. Lin, and F. Zhou, (2003), "Forensic Evaluation of Premature Failures of Texas Specific Pavement Study-1 Sections" ASCE Journal of Performance of Constructed Facilities, 2003, pp 67-74.
- Claussen, A. I. M., J. M. Edwards, P. Sommer, and P. Uge (1977), "Asphalt Pavement Design -The Shell Method." *Proceedings, 4th International Conference on the Structural Design of Asphalt Pavement*, 39-74.
- Datapave website <http://www.datapave.com/>
- Deen, C. Robert, Herbert F. Southgate, and Jesse G. Mayes (1980), "The Effect of Truck Design on Pavement Performance." Asphalt Paving Technology, Vol. 49, PP 606-632.
- Dillon, W. and M. Goldstein (1984), "Multivariate Analysis Method and Applications" John Wiley & Sons.
- El Mohtar, C. (2003), "The Effect of Different Axle Configurations on the Fatigue Life of an Asphalt Concrete Mixtures," MS., Michigan State University, E. Lansing MI 48824.
- Federal Highway Administration Website <http://fhwapap07.fhwa.dot.gov/vtris/>
- Fernando, E and, C. Bertrand (2002), "Application of profile data to detect localized roughness", Transportation Research Record, n 1813, 02-4050, p 55-61
- Gillespie, Thomas D., S. M. Karamihas, M. W. Sayers, and, D. Cebon (1993), "Effect s of Heavy-Vehicle Characteristics on Pavement Response and Performance." *NCHRP Report 353*, The University of Michigan, Transportation Research Institute, Ann Arbor, Michigan.
- Golub, G. H., M. Heath and, G. Wahba (1979), "Generalized Cross-Validation as a Method for Choosing a Good Ridge Parameter." *Technometrics*, Vol. 21 pp.215-223(No. 2), pp.215-223.
- Govind, S. (1988), "A dynamic Analysis of pavement systems to Determine a Damage Transform from Stress Fields." Ph.D. dissertation, Department of Civil Engineering, University of Texas at Austin, Austin, Tex.

- Hajek, J. J., and A. C. Agarwal (1990), "Influence of Axle Group Spacing on Pavement Damage" Transportation Research Record, No. 1286, pp. 138-149.
- Hanna, A.N., S.D. Tayabji, and J.S. Miller (1994), "SHRP-LTPP Specific Pavement Studies," Five-Year Report, Strategic Highway Research Program, National Research Council.
- Harold L. Von Quintus and Amy L. Simpson (2003), "Structural Factors for Flexible Pavements—Initial Evaluation of the SPS-1 Experiment" FHWA-RD-01-166.
- Harvey, John and Lorina Popescu (2000), "Rutting of Caltrans Asphalt Concrete and Asphalt- Rubber Hot Mix Under Different Wheels, Tires and Temperatures – Accelerated Pavement Testing Evaluation" Report Prepared for California Department of Transportation.
- Huang, Y. H., (1993), "Pavement analysis and design." Prentice Hall.
- Ilves, G. J., and Majidzadeh, K. (1991), "Reevaluation of the Methods for Calculation of Load Equivalency and Damage Ratios."
- Kenis, W. and W. Wang (1997), "Calibrating Mechanistic Flexible Pavement Rutting Model from Full Scale Accelerating Tests." *8th International conference on asphalt pavement*, Seattle, Washington, 663-672.
- Kim, H. B. (1999), "Framework for incorporating rutting prediction model in the reliability-based design of flexible pavements," Ph.D., Michigan State University, East Lansing.
- Kaloush, K.E and M. W. Witczak (2002), "Tertiary flow characteristics of asphalt mixtures", Journal of the Association of Asphalt Paving Technologists, Vol. 71, pp 249-280.
- Kaloush, K. E. and Witczak, M. W. (2000), "Development of a Permanent to Elastic Strain Ratio Model for Asphalt Mixtures" Development of the 2002 Guide for the Design of New and Rehabilitated Pavement Structures. NCHRP 1-37A. Inter Team Technical Report.
- Leahy, R.B. (1989), "Permanent Deformation Characteristics of Asphalt Concrete", Ph.D. Dissertation, University of Maryland, College Park.
- Leahy, R.B., E.T. Harrigan, and H. Von Quintus (1994), "Validation of Relationships Between Specification Properties and Performance" Report No. SHRP-A-409. Transportation Research Board, National Research Council, Washington, DC.

- Matthews, J. M., Monismith, C. L., and Craus, J. (1993), "Investigation of laboratory fatigue testing procedures for asphalt aggregate mixtures," *Journal of Transportation Engineering*, 119(4), 634-654.
- Miner, M. A. (1945), "Cumulative Damage in Fatigue," *Transactions of the ASME*, 67, A159-A164.
- Moavenzadeh, F., J. E. Soussou, H. K. Findakly, and B. Brademeyer (1974), "Synthesis for rational design of flexible pavement," *FH 11-776*, Federal Highway Administration.
- Monismith, C. L. (1994), "Fatigue Response of Asphalt-Aggregate Mixes. Strategic Highway Research Program," Project A-404, National Research Council.
- Monismith, C.L, J.T. Harvey, and F. Long, S. Weissman (2000), "Tests to Evaluate the Stiffness and Permanent Deformation Characteristics of Asphalt/Binder-Aggregate Mixes" Technical memorandum, TM-UCB PRC.
- Neter, J. and W. Wasserman (1996), "Applied Linear Statistical Models" Chicago: Irwin.
- Oh, B. Hwan (1991), "Cumulative Damage Theory of Concrete under Variable-Amplitude Fatigue Loadings." *ACI Materials Journal*, Vol. 88, No. 1.
- Park, Dong-Yeob (2000), "Effect of Temperature and Loading Time on the Stiffness Properties of HMAC in Flexible Pavements" Ph. D. thesis, Department of Civil and Environmental Engineering, Michigan State University, East Lansing Michigan.
- Qi, X. and M. W. Witczak (1998), "Time-Dependent Permanent Deformation Models for Asphaltic Mixtures" *Transportation Research Record*, No. 1639, pp. 83-93.
- Rao Tangella, S. C. S., J. Craus, J. A. Deacon, C. L. Monismith, (1990), "Summary Report on Fatigue Response of Asphalt Mixtures." SHRP Project A-003-A, University of California, Berkeley.
- Saraf, C. L., Ilves, G. J., and Majidzadeh, K (1995), "Effect of Heavy Vehicle Weight on Pavement Performance." *Road Transport Technology-4 Proceeding of the Fourth International Symposium on Heavy Vehicle Weights and Dimensions*.
- Schorsch, M. R. (2003) "Determining the causes of top-down cracks in bituminous pavements." Master Thesis, Department of Civil and Environmental Engineering, Michigan State University, East Lansing Michigan.
- Sebaaly, P. E., and Tabatabaee, N. (1992), "Effect of Tire Parameters on Pavement Damage and Load-Equivalency Factors." *Journal of Transportation Engineering*, 118(6), 805-819.

- Shook, J. F., F. N. Finn, M. W. Witczak, and C. L. Monismith (1982), "Thickness Design of Asphalt Pavement - The Asphalt Institute Method." *Proceedings, 5th International Conference on the Structural Design of Asphalt Pavement*, 17-44.
- Shigley, J. and Mischke, C. (1989), "Mechanical Engineering Design," 5th ed. p. 310. McGraw-Hill, Inc.
- Simpson, A. L., J. F. Daleiden, and W. O. Hadley (1995), " Rutting analysis from a different perspective" Transportation research record 1473, pp 9-16.
- Simpson A. L., J. B. Rauhut, P. R. Jordahl, E. Owusu-Antwi, M. I. Darter, R. Abroad, O. J. Pendleton, and Y. Lee (1994), "Sensitivity Analyses for Selected Pavement Distresses" SHRP report No. SHRP-P-393.
- Svasdisant, T. (2003), "Analysis of top-down cracking in rubblized and flexible pavements" Ph. D. thesis, Department of Civil and Environmental Engineering, Michigan State University, East Lansing Michigan.
- Ullidtz, P. (1987), "Pavement Analysis," Elsevier.
- Villiers, C., R. Roque, and B. Dietrich (2005), "Interpretation of Transverse Profiles to Determine the Source of Rutting within Asphalt Pavement System" 84th TRB Annual Meeting, January 9-13, TRB paper no: 05-1841.
- White, T. D., J. E. Haddock, A. J. T. Hand, and H. Fang (2002), "Contributions of Pavement Structural Layers to Rutting of Hot Mix Asphalt Pavements" NCHRP report No.468.
- Witczak, M. W., K. Kaloush, T. Pellinen, M. El-basyouny, and H. Von Quintus (2002), "Simple Performance Test for Superpave Mix Design" NCHRP report 465, National Academy Press, Washington, D.C.
- Witczak, M. W. and M. El-basyouny (2004), "Calibration of Permanent Deformation Models for Flexible Pavements" appendix gg-1 of guide for mechanistic-empirical design of new and rehabilitated pavement structures, ARA, inc., ERES division, 505 west University Avenue, Champaign, Illinois 61820
- Zhou, F. and Tom Scullion (2002), "VESYS5 Rutting Model Calibrations with Local Accelerated Pavement Test Data and Associated Implementation," Report No. FHWA/TX-03/9-1502-01-2

MICHIGAN STATE UNIVERSITY LIBRARIES



3 1293 02736 7782